UNIVERSITÀ DEGLI STUDI DI CATANIA
DIPARTIMENTO DI INGEGNERIA CIVILE E ARCHITETTURA

Dottorato di Ricerca in
"Valutazione e Mitigazione dei Rischi Urbani e Territoriali"
Ciclo XXXIV
Curriculum: Ingegneria strutturale e geotecnica

AN EQUIVALENT NON-UNIFORM INELASTIC BEAM-LIKE MODEL FOR THE SEISMIC VULNERABILITY ASSESSMENT OF BUILDINGS

Doctoral Thesis

PhD candidate
Ing. Ilaria Fiore

Supervisor:

Prof. Ing. Annalisa Greco

Co-Supervisors:

Prof. Ing. Salvatore Caddemi
Prof. Ing. Ivo Caliò

XXXIV cycle PhD coordinator:

Prof. Ing. Massimo Cuomo

Catania, 28th February 2022

PhD student

Ing. Ilaria Fiore

Supervisor

Prof. Ing. Annalisa Greco

Co-Supervisor

Prof. Ing. Salvatore Caddemi

Co-Supervisor

Prof. Ing. Ivo Caliò

SUMMARY

List of Tables

List of Figures

SECTION 1. **RESEARCH PROJECT**

1.1 INTRODUCTION: OBJECT, MOTIVATION, AIM, METHODOLOGY

1.1.1 MOTIVATION

Over the centuries, man has always tried to defend his buildings from the effects of earthquakes. With the advancement of technology and calculation tools, the estimation of the seismic vulnerability of structures and the consequent measures to make them more resistant have become objects of increasing interest.

The seismic risk affects a large number of territories across the globe, but some have tectonic geological conditions that make them more subject to seismic excitations. In particular, Italy is one of the countries in the Mediterranean area with the highest seismic risk, due to the frequency of occurrence of earthquakes that have historically affected its territory. Some of the past earthquakes occurred in Italy have reached a great intensity, resulting in a significant social and economic impact.

In relatively recent times, particularly destructive earthquakes occurred in Italy, among which we remember: Sicilia-Orientale 1693; Messina 1783; Messina 1908; Belice 1968; Friuli 1976; Irpinia 1980; L'Aquila 2009; Amatrice 2016; Santa Venerina 2018.

In the last 30 years, the National Seismic Network has recorded more than 190,000 seismic events in Italy and neighboring countries, most of which have not been felt by the population, but 45 earthquakes have reached a Richter M_L magnitude of 5.0 or greater. Although high-intensity earthquakes are less likely to occur, they could again affect our territory with devastating consequences.

Besides Italy, many other countries around the world have areas with a significant seismic risk and are characterised by the presence of buildings not designed to resist to earthquakes. An accurate assessment of the seismic risk of urban centres is therefore of considerable importance. Seismic risk is determined by a combination of hazard, vulnerability and exposure, and is directly related to damage that, depending on the type of seismicity, the strength of buildings and anthropization (nature, quality and quantity of goods exposed), can be expected in a given period of time.

A crucial aspect lies in the assessment of the seismic vulnerability of an existing building which can be performed by means of linear or non-linear models. Depending on the level of knowledge of the structure and on the type of analysis carried out, the adopted procedures, consistent with the technical regulation, can provide different results and therefore turn out to be not really objective.

The task is even more complicated if the seismic vulnerability assessment is extended to urban areas where a great number of buildings must be analysed and the interaction of aggregates of adjacent buildings can increase the overall vulnerability. There are many simplified methods which are used to assess the seismic vulnerability of an urban environment. Among all, the vulnerability maps are certainly the most widespread, since they allow to carry out a quick census of vulnerability of buildings thanks to the collection of data of the building itself and of

the territory operated by experts during in situ collection phases, allowing to keep track of the surveys themselves.
Another popular method is based on the Damage Probability Matrix, which returns an estimate of vulnerability in numeric form; in particular, it expresses the likelihood of a certain level of damage for each seismic intensity. The assessment of structural vulnerability by means of the Damage Probability Matrices evaluates the seismic behaviour of the buildings through the assignment of a certain structural type and then reworking the observed and detected data after a seismic event in statistical form. This method provides the seismic vulnerability as an estimation of the probability of occurrence of damage in buildings in terms of the intensity of the earthquake.
Such methods are useful for the seismic vulnerability assessment of urban areas, anyway due to their simplicity they do not provide accurate results on the individual building.
A reliable seismic vulnerability assessment of an individual building requires the adoption of an accurate numerical model and the knowledge of several data characterizing the structure. Different methods have been proposed in the scientific literature.
The “Is method” defines a seismic index *Is* of the structure [1, 2]. It is compared with a reference standard index *Is0* to determine whether the building is adequate to withstand a seismic event or not. The determination of this index is possible for buildings with no more than seven floors and requires a three-levels procedure with increasing depth and complexity.
The method proposed by Calvi [3] allows to determine the probability of reaching a certain level of damage (marked by fixed thresholds of limit states) for each class of identified buildings and for each level of contemplated seismic intensity. The method is designed to be used even without the need to carry out field surveys, referring only to databases. However, for the analytical study of the seismic behaviour of the structure, an 'equivalent' model properly characterised according to its typological class is adopted, over generalizing and not allowing to consider the differences due to the ductility of the system.
A reliable and accurate assessment of the seismic vulnerability of a building can also be provided in terms of probability of failure through the construction of its fragility curves which can be expressed as the probability of the building of reaching particular limit states in terms of the seismic intensity. The determination of the fragility curve is based on numerical simulations of the seismic response of the building, as a consequence the reliability of the results is directly related to the accuracy of the numerical models adopted for their evaluation. A reliable numerical model requires a deep knowledge and accuracy of the building data and engages a large computational burden thus limiting the possibility to perform a great number of numerical analyses, as required by the procedures for fragility curve determination. For this reason, this approach is usually applied only to buildings with particular strategic or historical value although its applicability, in principle, can be extended to the vulnerability assessment of all the existing buildings as a better alternative to index-based vulnerability assessment currently adopted for buildings.
The Capacity Spectrum Method and the N2 Method are based on a displacement approach for the analysis of non-linear behaviour of structures. They compare the displacement demand and the capacity of a structure, evaluated with a non-linear static analysis.
Non-linear static analysis is currently the most common approach for estimating the seismic vulnerability of existing buildings; it is now performed using accurate FEM models, however

requiring a high computational cost. Then, the seismic vulnerability is assessed by means of an equivalent SDOF system, thus oversimplifying the structural behaviour. Other equivalent models, richer than the SDOF one, could be considered in order to analyze the seismic behaviour of buildings. For example, in the last decades, attention has been given to simplified equivalent beam-like models, which have been adopted for an initial design of new buildings or for the reproduction of the behaviour of existing buildings.

1.1.2 RESEARCH PROBLEM AND AIM

A careful and accurate assessment of the building heritage in territories with high seismic risk would be desirable, but it represents a very difficult task and cannot be applied at a large scale. However, aiming at planning the needed actions for mitigating the seismic risk, expeditious seismic vulnerability assessment strategies allow to establish the priorities and to focus the accurate assessments on the more vulnerable structures.

At urban scale seismic vulnerability assessment strategies require fast and reliable tools available for the engineers. The use of oversimplified methods can provide misleading results and wrong decisions whose economic and social impact could be relevant. However, the analysis of real structures by means of simplified models is still of great importance in order to reduce the computational effort related to the so-called high-fidelity study of entire buildings performed by detailed FEM models able to predict the non-linear dynamic response of the structure subjected to earthquake loadings. Simplified but reliable models can allow to perform fast large-scale simulations and to identify the most vulnerable buildings within an urban area thus allowing the definition of planning strategies for seismic risk reduction.

The main goal of this study is to propose beam-like models that can be considered representative of the dynamic behaviour of buildings subjected to earthquake loadings. To this aim, a simplified model should be able to account for the non-uniform stiffness and strength distribution as well as the inelastic behaviour of the building along its height.

With this aim, this research proposes non-uniform beam-like models in linear and non-linear context which can be considered equivalent to spatial-framed buildings drastically simplifying the computational cost related to the need to perform linear and non-linear dynamic analysis for seismic vulnerability assessment of new and existing buildings (Figure 1.1).

Figure 1.1 - Building-beam equivalence

The simplified beam-like models already proposed in the scientific literature are conceived to reproduce planar [4, 5] or spatial frames [6] accounting for different beam models: shear only beam [7], Euler beam coupled with a shear only beam [8, 9, 10], Timoshenko beam [11, 12]. However, almost all the proposed beam-like models refer to uniform equivalent linear beams, with constant stiffness along the beam axis. Furthermore, the possible presence of eccentricity between the mass and stiffness centres is not taken into account by any of the models proposed in the literature, except in [13] where approximate formulas of vibration frequencies are provided in order to take into account the coupling between flexural and torsional modes in non-

symmetrical buildings, without, however, showing numerical examples. In addition, all the equivalent beam models already proposed in literature are based on the hypothesis of linear elastic behaviour.
Anyway, buildings do not have uniform strength and stiffness distribution along their height and are characterised by unsymmetrical plans, therefore it is extremely reductive to compare them to a uniform linear beam. Furthermore, buildings when subjected to moderate or high earthquake loadings exhibit a non-linear behaviour and this should be taken into account for the design of new buildings or the seismic vulnerability assessment of existing buildings. The oversimplified adoption of linear elastic behaviour is extremely reductive for a reliable assessment of the seismic vulnerability of real structures.
In view of the above considerations the main goals of this research can be summarized as follows:

- Provide a definition of a new linear beam-like model able to take into account the non-uniform stiffness distribution of buildings and the three-dimensional behaviour of the structure.
- Propose an inelastic beam-like model with non-uniform stiffness distribution able to represent the non-linear behaviour of buildings subjected to earthquakes.
- Adopt the simplified inelastic beam-like model for the seismic vulnerability assessment of new and existing buildings performed by means of the construction of reliable fragility curves. This procedure will provide, with a moderate computational effort, a more accurate measure of vulnerability assessment of existing buildings compared to index-based assessments methods.

1.1.3 METHODOLOGY

The presented study aims to propose a non-uniform beam-like model able to perform static and dynamic analyses of real structures with either the assumption of linear or non-linear behaviour. There are many advantages in the adoption of equivalent beam models, first of all the transition from a complex structure with a high number of degrees of freedom, computationally expensive, to a simple structure such as a continuous beam whose behaviour can be efficiently related to few degrees of freedom.

In this study, as a first step a new analytical linear model of an equivalent shear-torsional spatial beam was developed and implemented in a specific software through the MATLAB programming language, allowing the automatic construction of the model by defining only some initial data of the building.

A methodology for the choice and calibration of the equivalent beam has been proposed. The proposed equivalent beam is suitable for a simplified modeling of buildings which do not have uniform stiffness distribution along the height and are characterised by unsymmetrical plans, thus having eccentricity between the Mass Centre and the Stiffness Centre. By means of the definition of the characteristics of the equivalent beam, it has been possible to obtain, in a simplified way, the linear elastic response of buildings to earthquake excitations.

The analysis of the linear three-dimensional behaviour of the continuous beam, having infinite degrees of freedom, has been performed through a discretization strategy based on the Ritz method. This procedure allows a significant reduction of the degrees of freedom, making it much easier to perform static and dynamic analyses.

In order to test the proposed model, dynamic analyses have been performed on structurally complex buildings with simultaneous planar and vertical irregularities [14]. The obtained results have been validated through the comparison with those provided by a three-dimensional FEM model implemented in the software SAP2000.

As a further important step, the study has been extended to the definition of a beam-like model able to reproduce the complex inelastic behaviour of three-dimensional buildings subjected to earthquake loadings. The reason of such interest lies on the consideration that the analyses of inelastic beam models could provide a low-cost realistic simulation of the seismic response of existing buildings, taking into account the damage distribution at the different floors of the building.

A beam-like based equivalence strategy for multi-storey buildings is much more accurate for a low-cost evaluation of its non-linear response and provides several additional response data both in terms of capacity and demand if compared to the simplified approaches based on inelastic single degree of freedom dynamics.

In order to numerically identify appropriate non-linear constitutive law of the equivalent beam-like model, several calibration strategies of the inelastic beam have been investigated, validated and proposed. The most reliable strategy, which has been chosen for subsequent numerical applications, exploits the results related to non-linear static analyses performed on a full three-dimensional FEM model of the structure.

The effectiveness of the non-linear beam-like model to predict the non-linear behaviour of the corresponding building has been proved through several examples by conducting non-linear static and dynamic analyses performed on benchmark buildings.

In addition, a closed form solution for the static problem of a shear-torsional elastic beam in presence of curvature singularities due to the non-uniform stiffness distribution along the beam axis was determined. This solution was compared with the results obtained with the proposed equivalent beam model, confirming its validity. Furthermore, the closed form solution of the static problem allowed also to obtain the shape functions of a stepwise shear-torsional elastic beam. These shape functions can be adopted for the formulation of a displacement-based beam element with distributed plasticity, which can be used for the static non-linear analysis of the equivalent beam-like model.
The last achieved goal was crucial in the development of low cost strategy for the seismic vulnerability assessment of buildings by means of the construction of fragility curves.

The main contents of the thesis are briefly summarized in the following: in SECTION 1 a review on the simplified models of buildings has been first briefly discussed. Then, the beam-like models already presented in the scientific literature have been recalled. In SECTION 2 the new beam-like model proposed in this study has been described, considering the elastic and inelastic behaviour, and its use in the static and dynamic analyses. Particular attention has been focused on the calibration procedure for the definition of the beam-like model starting from the available data of the building. In SECTION 3 a brief description of the process adopted in this thesis for the construction of the fragility curves has been reported, while in SECTION 4 numerical applications of the equivalent beam-like model have been shown.

1.2 STATE OF THE ART ON SIMPLIFIED MODELS OF BUILDINGS

The evaluation of the dynamic response of multi-storey buildings, particularly when subjected to seismic loading, has represented one of the most important tasks of structural engineer researches in the last century and is still the objective of studies and improvements. The advancements in computational procedures and parallel processing of the last few years enhanced the accurate dynamic analysis and seismic vulnerability of multi-storey buildings. The analyses can be carried out at the building or urban level; simplified or high-fidelity models as well as approximate or sophisticated large-scale simulations are currently adopted. However, when analysing entire urban areas or when performing several simulations aiming at providing sufficient data for expressing probability failure maps, it is needed to balance accuracy and computational burden. It is in this context that beam-like models play an important role.

The analyses developed by means of 3D numerical models aim at providing an accurate representation of the main characteristics of the dynamic behaviour of real structures and, for this reason, must be detailed and based on reliable data. Therefore, an accurate evaluation of the dynamic response of a multi-storey building subjected to seismic excitation rigorously requires an adequate structural expertise and great computational burden. On the other hand, the need of a sufficiently accurate seismic vulnerability assessment of a large number of existing buildings on seismic areas, in particular at urban scale, stimulated a significantly increasing interest in simplified but sufficiently accurate models able to represent multi-storey buildings.

Since multi-storey buildings may exhibit a great number of degrees of freedom, especially if several deformability parameters of the structural members are taken into account, simplified Multi Degree Of Freedom (MDOF) models are usually taken into account. To this regard some models have been already presented in the scientific literature for the simulation of the linear as well as the non-linear dynamic response of multi-storey buildings. The most important goal of these simplified models is to reduce the number of degrees of freedom of the 3D model preserving the main features of its dynamic response.

A new and renovated interest has recently grown in beam-like models, which were introduced in the last century. Beam-like models, which are based on the equivalence of multi-level structures to flexural-shear coupling continuum beams, aim to simulate the dynamic behaviour of multi-level buildings by drastically reducing the computational burden. Several authors demonstrated interest in beam-like models and proposed suitable simplified approaches for the dynamic analysis of multi-storey structures.

1.2.1 Elastic beam-like models

In the following the elastic beam-like models proposed in literature from 1980, together with their use in practical applications, are briefly described.

With regard to high-rise buildings, the discretization of multi-floor frames with coupled beams was introduced by **Basu** in 1982 [15, 16], where a fixed-base multistorey building was idealized as an equivalent coupled shear wall connected in series to an equivalent frame. The coupled wall was modelled as a continuum of uniform properties and the frame as a uniform shear beam, and the solutions were obtained by treating the structure as a lumped parameter system. The proposed approach was limited to the principal three modes of vibrations for the in plane behaviour. The obtained modal features have been used in [17, 18] to evaluate the design forces of the building by means of seismic response spectra.

A similar approach has been used by **Stafford Smith et al.** in [19, 20] for the determination of the period of free vibration and the earthquake design forces of a building by means of equivalent coupled shear-flexure cantilevers. The stiffness of the equivalent beams is determined as a simple sum of the stiffness of the vertical members. The approach is limited to buildings with uniform properties along the height, with symmetrical plan and symmetrically loaded.

Iwan [21] and **Huang** [22] proposed a continuous uniform shear-beam model to predict elastic storey drift demand on structures due to near-field earthquake ground motions. Since they noticed that the continuous model more accurately predicts the inter-storey drifts than an equivalent SDOF system does, they suggested the use of a drift spectrum instead of the well-known response spectrum.

McCallen and Romstad proposed in [4, 23] a simple uniform continuum model for the analysis of lattice structures. The equivalence between the lattice structure and the continuum model was established in terms of deformation energies for three assumed global deformation modes (axial, shear, bending). The continuum model was then analysed in a traditional finite element approach. Geometrical non-linearities are accounted for through updated Lagrangian coordinate transformation for each continuum finite element.

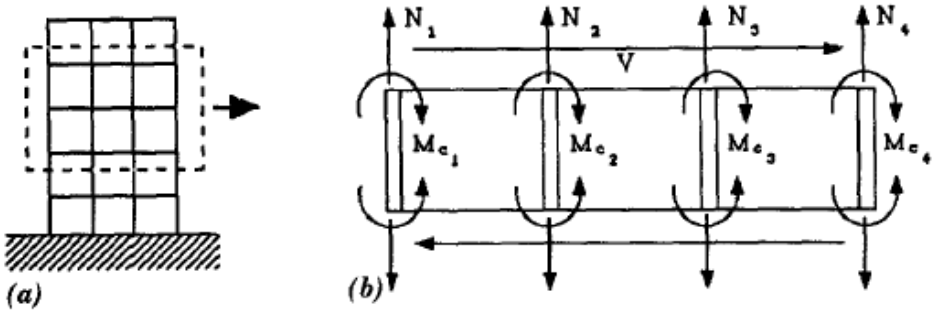

Figure 1.2 - Lattice stress resultants – Chajes, Romstad and McCallen [5]

In this model, the global curvature (and so the chord bending moment) is due to both shear and bending deformation:

$$M_c = EI_c\left(\frac{d^2v_s}{dx^2}+\frac{d^2v_b}{dx^2}\right) \tag{1.2.1}$$

If the longitudinal elements (chord) are stiff relative to the transverse elements (batten), the beam exhibits a global flexural behaviour and the curvature of the chords approaches the global curvature of the lattice; on the contrary, the beam behaves as a shear type one and the global curvature is due only to the shear strain energy. Intermediate cases can also be considered.

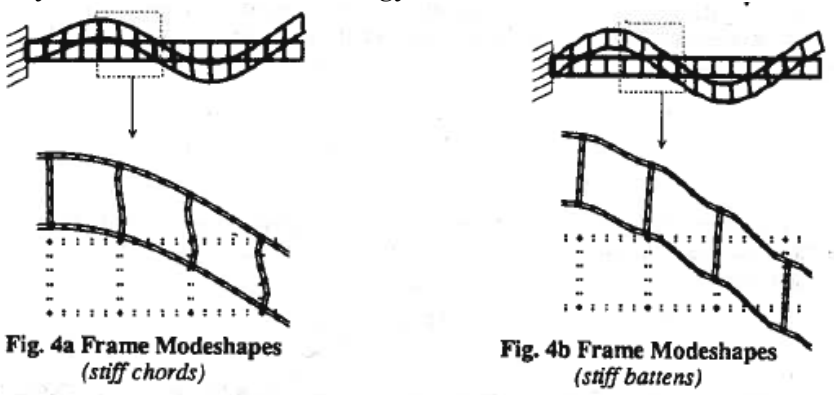

Figure 1.3 - Frame modeshapes – McCallen and Romstad [4]

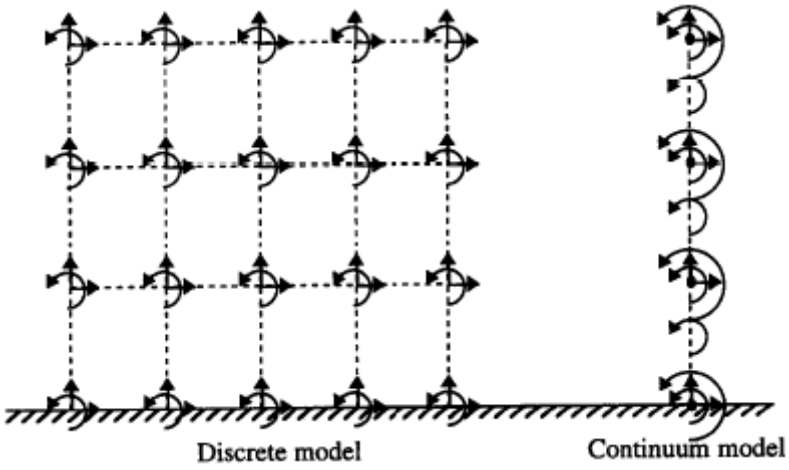

Figure 1.4 - Discrete and associate continuum models including global degrees of freedom – Chajes [24]

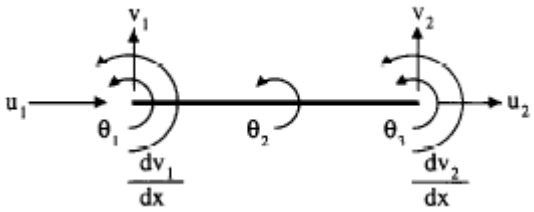

Figure 1.5 - Continuum finite element degrees of freedom – Chajes [24]

The translational and rotational inertias are lumped at the end or midpoint nodes of the finite elements of the discretised continuum.

The approach is extended to three-dimensional buildings with rigid floors. Therefore, the global model has only three degrees of freedoms, two orthogonal translations and one rotation at each floor level. By applying only horizontal forces, the rotational and axial degrees of freedom of the continuum can be condensed out. Later, the condensed continuum model of an individual frame can be transformed to global coordinates and added into the global stiffness.

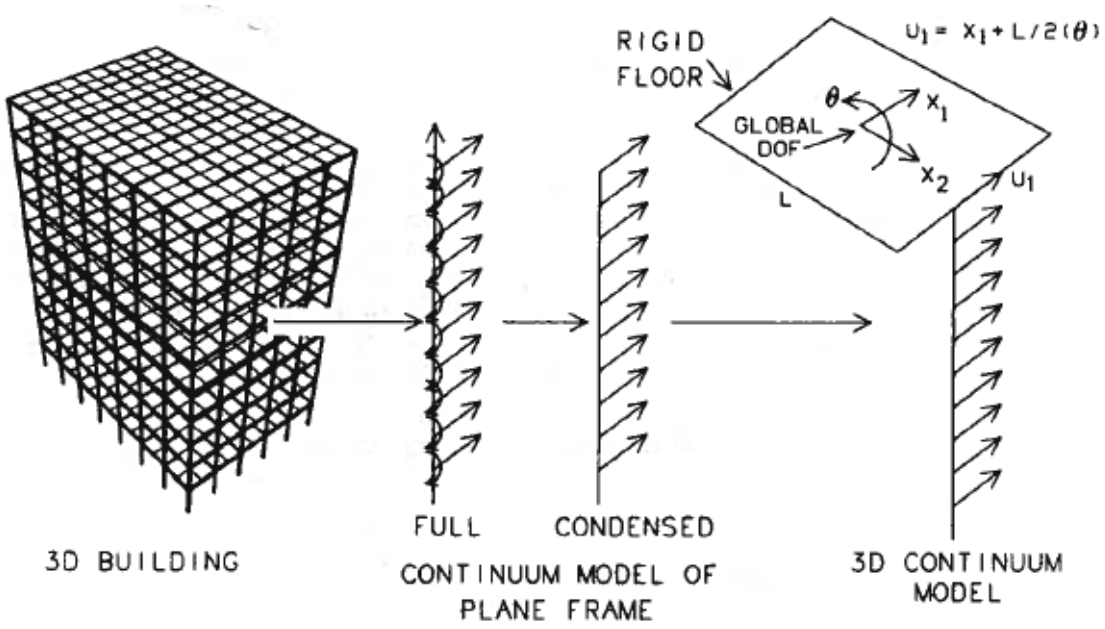

Figure 1.6 - Construction of a 3.D Building Model Using Continuum Models for Each Plane Frame – McCallen and Romstad [4]

The continuum is used for the free vibration analysis of planar frames or buildings with uniform stiffness distribution along the height and the results are shown in terms of natural frequencies and mode shapes.

In 1993 **Chajes** in [5] extended the approximate method proposed by McCallen and Romstad, based on the definition of the equivalent continuum model to replace the repetitive cells, for determining displacements and member forces in two-dimensional frames with reticular elements. In [24, 25] the equivalent continuum model was applied to predict the measured seismic response of two existing buildings (a reinforced concrete one and a steel one) during the Loma Prieta earthquake (using the continuum model discretized with a number of finite elements equal to the number of floors).

Later, an approximate method for estimating the maximum lateral displacement in multi-storey buildings, based on an equivalent uniform continuum model that linearly combines a flexural and a shear deformable cantilever beam (Figure 1.7), was introduced by **Miranda** in 1999 [26]. The lateral displacements of the building were given by the combination of shear and bending deformations and the seismic response was evaluated in terms of maximum roof displacement and maximum inter-storey drift ratio. Approximations on the dynamic response concern the assumption of uniform mass and stiffness along the height of the building and the consideration of the first mode of vibration only whose lateral displacements are given by a closed form solution of a static problem under a fixed load pattern. The formulation was successively generalised in [27, 28], where the limitation of uniform lateral stiffness distribution along the building was removed, assuming linear or parabolic variations. The uniform continuum model was subsequently used to find closed-form solutions capable of approximating the dynamic characteristics of the non-uniform buildings (for example mode shapes, periods and modal participation factors) [28]. An estimate of the ground acceleration request on the

structures that respond linearly to the seismic motions was determined in [29] for planar models, by considering up to the first three mode of vibration in the dynamic analysis.
In 2002 **Gulkan and Akkar** proposed a procedure to estimate the maximum ground storey and maximum interstorey drift of a building by means of the first-mode shape of a uniform shear beam [30]. In 2005 they modified the equivalent shear beam model in order to take into account the general moment resisting frame (MRF) behaviour of the structure by introducing some empirical coefficients into the maximum ground storey and interstorey drift expressions [31].
Later, Miranda and Akkar merged their studies and used the simplified continuous model of Miranda for the evaluation of generalised inter-storey drift spectrum in [32].

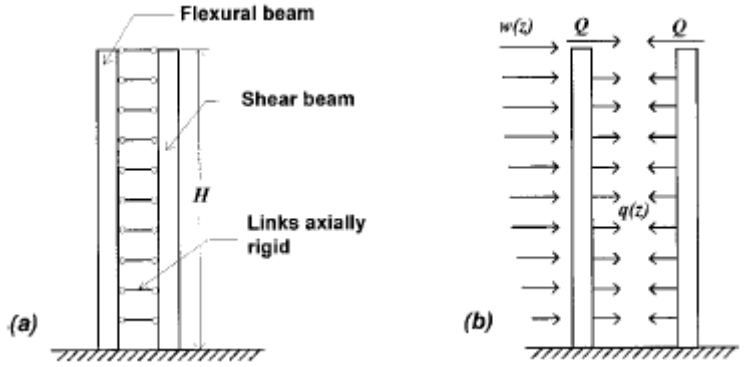

Figure 1.7 - (a) Simplified model of multi-storey building; (b) Interacting forces in the model – Miranda [26]

In 2000 **Wang et al.** proposed an approximate method to estimate the first two periods of vibration of multi-storey uniform buildings with asymmetrical plan [33]. The coupled natural frequencies of the multi-storey structure, due to the asymmetric distribution of the structural members with respect to the floor plan, have been expressed in terms of uncoupled lateral frequency, uncoupled fundamental torsional-to-lateral frequency ratio and the eccentricity ratio. However, this approach is valid only for proportionate structural systems whose centres of stiffness lie on a vertical line.

Kuang and Ng studied the modal analysis for coupled flexural-torsional vibration of asymmetric uniform tall buildings by means of an equivalent flexural-torsional cantilever, whose stiffness is determined as a simple sum of the stiffness of the vertical members [34, 35]. The equivalent beam can be coupled with a shear cantilever in order to take into account also the shear deformability. However, also further studies [36, 37] have been limited to the free vibration analysis only considering an equivalent Euler-Bernoulli beam or an equivalent shear cantilever, respectively.

In 2000 **Li et al.** in [38] studied the in-plane free vibration of tall buildings by means of an equivalent flexural multi-step cantilever beam with variably distributed stiffness, mass and axial loads according to a power or exponential law of variation. The approximated solution of this complex problem has been obtained using the exact solution of a one-step bar with variable cross-section together with the transfer matrix method. This approach was extended in [39] by

Rahgozar for an equivalent Timoshenko multi-step beam or in [40] for a sandwich beam, the latter defined according to Zalka, Potza and Kollar' approach described in the following.

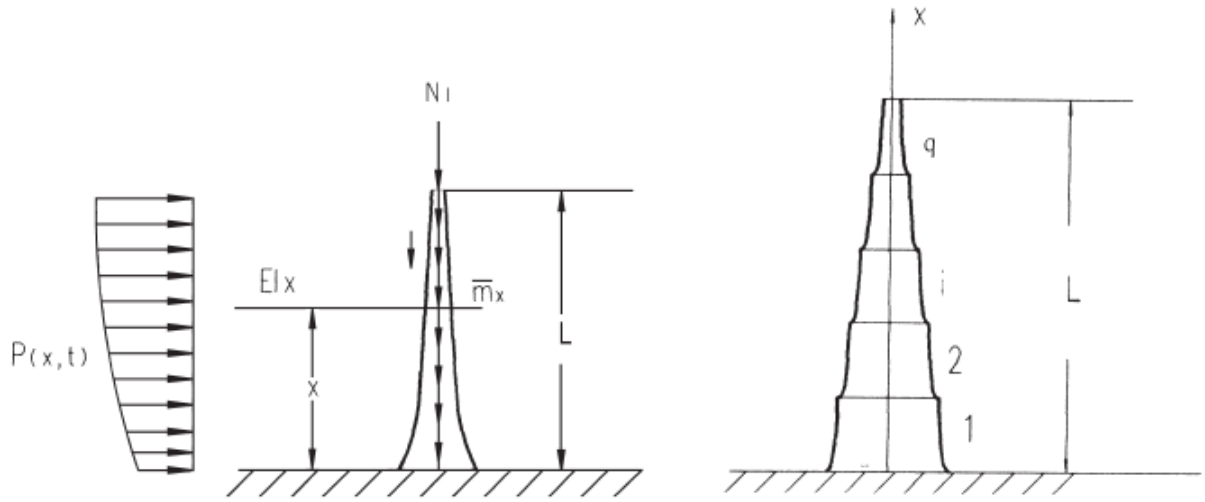

Figure 1.8 – A one-step bar with variable cross-section subjected to axial loads (right) and multi-step bar – Li [38]

Swaddiwudhipong et al. [41, 42] proposed a uniform shear-flexural cantilever for 3D free vibration analysis of frame-core wall buildings taking into account also the axial deformation. The solution in terms of natural frequencies and mode shapes is obtained using the Galerkin's technique, adopting an exponential shape function.

In 2008 **Khaloo and Khosravi** [43] used a combination of uniform shear and flexural cantilever beams to estimate the elastic structural response of a tall building. Extending the formulation proposed by Stafford Smith and Miranda, they investigated the multi-mode effects of tall buildings subjected to near-field ground motions, assuming the linearity of the system. The maximum inter-storey drift ratio spectra and its location along the height have been also calculated.

Applying the concept of an "equivalent column", **Zalka** proposed simple formulas in 2001 [13] for evaluating the natural three-dimensional frequencies of the buildings braced by frameworks, coupled shear-walls, shear-walls and cores. The method considered local bending of the single vertical elements, global bending of the frames/shear walls (associated with the axial deformation of the vertical elements) and shear deformations of the frames/shear walls. The pure torsional frequency is obtained by means of an analogy with respect to bending. Approximate formulas were provided to take into account the interaction between translational and torsional modes for non-symmetrical buildings. The equivalent column was applied for the analysis of regular buildings with double planar symmetry and in-plane rigid floors. The same author proposed approximated closed-form solutions for studying tall buildings subjected to uniformly distributed static horizontal loads for both symmetrical [44] and non-symmetrical [45] systems, in 2009 and 2014, respectively.

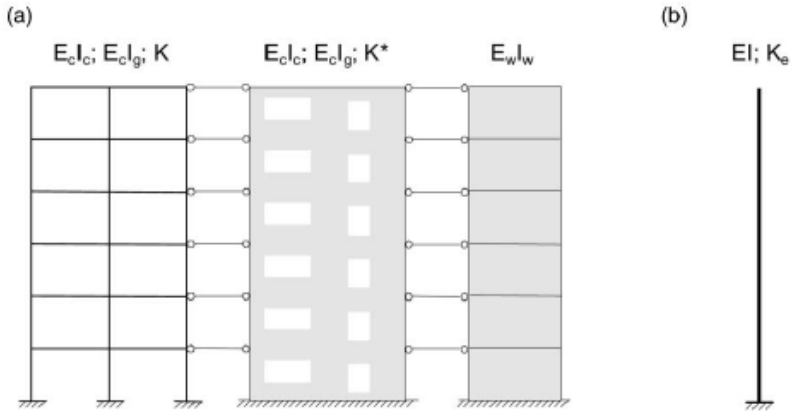

Figure 1.9 - Model for the lateral vibration analysis: (a) bracing system consisting of frames, coupled shear walls, shear walls and cores; (b) equivalent column. – Zalka [13]

- Shear stiffness

Global shear stiffness due to beams:
$$K_{bj} = \sum_{1}^{n-1} K_{b,i} = \sum_{1}^{n-1} \frac{12 E_b I_{b,i}}{l_i h} \tag{1.2.2}$$

With coupled shear walls modifies in:
$$K_{bj} = \sum_{1}^{n-1} \frac{6 E_b I_{b,i} \left[\left(l_i + s_i \right)^2 + \left(l_i + s_{i+1} \right)^2 \right]}{l_i^3 h \left[1 + 12 \left(\frac{\rho E_b I_{b,i}}{l_i^2 G_b A_{b,i}} \right) \right]} \tag{1.2.3}$$

Local shear stiffness due to columns:
$$K_{cj} = \sum_{1}^{n} K_{c,i} = \sum_{1}^{n} \frac{12 E_c I_{c,i}}{h^2} \tag{1.2.4}$$

The shear stiffness of the framework can be established by combining the two-part stiffness as:
$$K_j = \left(\frac{1}{K_{bj}} + \frac{1}{K_{cj}} \right)^{-1} = r_j K_{bj} \tag{1.2.5}$$

The fundamental frequency that is associated with the shear stiffness of the framework is:
$$f_{s',j}^2 = \frac{1}{\left(4H \right)^2} \frac{r_f^2 K_j}{m} \tag{1.2.6}$$

where m is the mass density per unit length and r_f is a reduction factor, which takes into account the fact that the mass of a building is not uniformly distributed over the height but is concentrated at floor levels.

- Flexural stiffness

Global bending stiffness due to the axial stiffness of the columns:
$$E_c I_{g,j} = E_c \sum_{1}^{n} A_{c,i} t_i^2 \tag{1.2.7}$$

The fundamental frequency that is associated with this stiffness is:
$$f_{g,j}^2 = \frac{0.313 r_f^2 E_c I_{g,j}}{H^4 m} \tag{1.2.8}$$

Since shear and flexural behaviour are often coupled, the vibration frequency should be:

$$\frac{1}{f_{s,j}^2}=\frac{1}{f_{s',j}^2}+\frac{1}{f_{g,j}^2} \tag{1.2.9}$$

Local bending stiffness due to columns: $E_c I_{c,j}=E_c\sum_1^n I_{c,i}$ (1.2.10)

The fundamental frequency that is associated with this stiffness is: $f_{b,j}^2=\dfrac{0.313 r_f^2 E_c I_{b,j}}{H^4 m}$ (1.2.11)

- Shear stiffness due to shear walls: $E_w I_{w,k}$ (1.2.12)

The fundamental frequency that is associated with this stiffness is: $f_{w,k}^2=\dfrac{0.313 r_f^2 E_w I_{w,k}}{H^4 m}$ (1.2.13)

- <u>Global stiffness of the equivalent column</u>: $EI=E_c I_c+E_w I_w=E_c\sum_1^f I_{c,j} r_j+E_w\sum_1^m I_{w,k}$ (1.2.14)

The fundamental frequency that is associated with this stiffness is:

$$f_b^2=f_f^2+f_w^2=\frac{0.313 r_f^2 EI}{H^4 m} \tag{1.2.15}$$

If higher frequencies are needed, the factor 0.313 should be replaced by 12.3 and 96.4, respectively, for the calculation of the second and third frequencies.

- <u>Global shear stiffness of the equivalent column</u>: $K_e=\sum_1^f s_j^2 K_j$ (1.2.16)

The fundamental frequency that is associated with this stiffness is: $f_s^2=\dfrac{1}{(4H)^2}\dfrac{r_f^2 K_e}{m}$ (1.2.17)

Considering the eigenvalues η, the lateral frequency is obtained from:

$$f=\sqrt{s f_b^2\left(\frac{\eta^2}{0.313}-\frac{k^2}{5}-1+\frac{1}{s}\right)+f_s^2} \tag{1.2.18}$$

- <u>Global torsional stiffness</u>: $(GJ)_e=\sum_1^M GJ_k+\sum_1^f\left[\left(K_{e,j}\right)_x y_j^2+\left(K_{e,j}\right)_y x_j^2\right]$ (1.2.19)

Making use of the flexural-torsional analogy, the fundamental frequency for pure torsional vibration is obtained:

$$f_\varphi=\sqrt{s_\varphi f_\omega^2\left(\frac{\eta_\varphi^2}{0.313}-\frac{k_\varphi^2}{5}-1+\frac{1}{s_\varphi}\right)+f_t^2} \tag{1.2.20}$$

with $f_\omega^2=\dfrac{0.313 r_f^2 EI_\omega}{i_p^2 H^4 m}$ and $f_t^2=\dfrac{1}{(4 i_p H)^2}\dfrac{r_f^2 (GJ)_e}{m}$.

When the Stiffness Centre does not coincide with the Mass Centre, flexural and torsional behaviour are coupled, and, once the Stiffness Centre has been determined, it is possible to find the frequencies of the building by means of a cubic equation which considers both flexural and torsional basic frequencies already determined.

In 2003, **Potzta e Kollar** [8] replaced the structures of the buildings with an equivalent uniform sandwich beam that was defined by three types of stiffness deriving from the resistant elements: global bending stiffness, local bending stiffness and shear stiffness. The deformation energy of the equivalent beam was deduced from the generalization of Timoshenko's theory [46] for spatial problems, introducing separate contributions between global flexural stiffness and shear stiffness, on one hand, and between global flexural stiffness and local flexural stiffness on the other. In any case, the shape of the displacements under sinusoidal horizontal loads had to be fixed (i.e., sinusoidal and cosinusoidal form) in order to obtain the replacement stiffness of the equivalent system, leaving the choice of a certain length (a sort of free length of element inflection) corresponding to the best equivalence. Using the obtained equivalent stiffness, an approximate expression was proposed for estimating the buckling load and the natural frequencies of symmetrical structures, while in unsymmetrical structures the lateral-torsional vibration modes were determined by an eigenvalue problem, assuming uniform mass distribution along the height. The model is applied to study doubly symmetrical or unsymmetrical buildings with uniform stiffness distribution along the height. The results are shown in terms of natural frequencies and buckling load of the structure. Later, **Tarjan and Kollar** applied the proposed model to estimate the basic internal forces [47]. Unfortunately, the procedure for calculating the stiffness of the equivalent model was rather complicated and not entirely automatic.

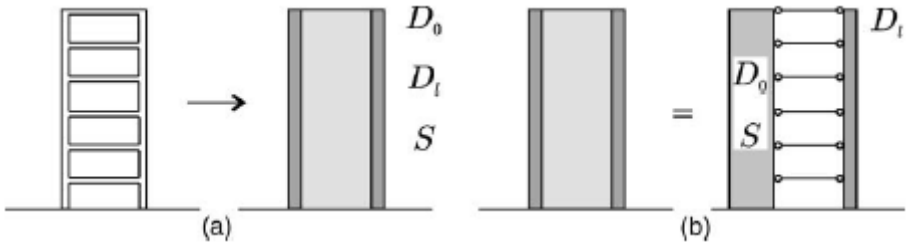

Figure 1.10 - Replacement beam of a frame (a), the sandwich beam is equivalent to a Timoshenko-beam supported by a beam with bending deformation only (b). – Potza and Kollar [8]

In order to study the dynamic response of tall buildings under wind loads, **Cluni** proposed two equivalent beam models [9]. Both equivalent beam models have uniform flexural and shear stiffness, linked together in series (Timoshenko beam) or in parallel. The equivalence criterion is based on the minimization of the difference of static and dynamic response features obtained by means of the equivalent beam and the FEM model. The mechanical parameters used to describe the beam can vary sensibly with respect to the real ones, but the main interest is to find an equivalent beam which can describe accurately the response of the slender building regardless of any physical meaning.

- In series stiffness cantilever beam

Free motion equation

$$\frac{\partial^4 v}{\partial z^4} + \frac{\mu \partial^2 v}{EJ \partial t^2} - \frac{\mu}{GK} \frac{\partial^4 v}{\partial z^2 \partial t^2} = 0 \qquad (1.2.21)$$

Solution

$$v(z,t) = \psi(z)\cos(\omega t + \phi)$$

$$\psi(z) = D_1\cos(k_1 z) + D_2\sin(k_1 z) + D_3\cosh(k_2 z) + D_4\sinh(k_2 z)$$

$$k_1 = \sqrt{-\frac{b}{2} + \frac{1}{2}\sqrt{b^2 - 4c}} \quad k_2 = \sqrt{\frac{b}{2} + \frac{1}{2}\sqrt{b^2 - 4c}} \tag{1.2.22}$$

$$b = \omega^2 \frac{\mu}{GK} \quad c = -\omega^2 \frac{\mu}{EJ}$$

- In parallel stiffness cantilever beam

Free motion equation

$$EI\frac{\partial^4 v}{\partial z^4} + \mu\frac{\partial^2 v}{\partial t^2} - GK\frac{\partial^2 v}{\partial z^2} = 0 \tag{1.2.23}$$

Solution

$$v(z,t) = \psi(z)\cos(\omega t + \phi)$$

$$\psi(z) = D_1\cos(k_1 z) + D_2\sin(k_1 z) + D_3\cosh(k_2 z) + D_4\sinh(k_2 z)$$

$$k_1 = \sqrt{-\frac{b}{2} + \frac{1}{2}\sqrt{b^2 - 4c}} \quad k_2 = \sqrt{\frac{b}{2} + \frac{1}{2}\sqrt{b^2 - 4c}} \tag{1.2.24}$$

$$b = -\frac{GK}{EJ} \quad c = -\omega^2 \frac{\mu}{EJ}$$

In 2020 the model was extended in order to describe the flexural, shear and torsional behaviour of uniform tall buildings with asymmetrical plant subjected to wind or earthquake loads [48]. In 2021 Cluni refined the definition of the equivalent beam model, adopting the procedure proposed by Potza and Kollar in the sandwich beam [49]. The mechanical and dynamic features of the equivalent 3D Timoshenko beam are first approximately evaluated by means of equivalence of the deformation energy between the equivalent sandwich beam and the sub-structures of the tall building, and then calibrated by minimizing a function which takes into account natural frequencies and static displacements. However, the model is not able to represent asymmetrical buildings. The results of the analyses performed on regular and symmetrical buildings with uniform stiffness distribution are shown in terms of natural frequencies and mode shapes and in terms of displacements under static or dynamic wind or earthquake loads.

In [50, 51] **Meftah et al.** proposed an approximate hand-method for seismic analysis of an asymmetric building structure having constant properties along its height and stiffened by a combination of shear-walls and thin-wall open section structures. The governing equations of free vibration of the equivalent flexural-torsional cantilever have been derived basing on the continuum method and D'Alembert principle, and the solution have been determined by applying the Galerkin's technique in [50] or an analytical method in [51]. Internal forces of the building subjected to an earthquake have been also derived using acceleration response spectrum and combining the modal responses by means of SRSS method.

In [52] and in [53] **Rafezy et al.** proposed a stepped shear-torsional cantilever model and a stepped Timoshenko cantilever model, respectively, for the calculation of the natural frequencies of asymmetric three-dimensional frame or wall-frame structures by means of the Wittrick-Williams's algorithm. Each beam segment can be representative of a number of uniform storeys variable from one to the total number of storeys of the building if it is uniform throughout its height. The stiffness of each beam segment has been calculated as the sum of the stiffness of each frame in the considered direction in the corresponding storeys. The equations of motion have been referred to each beam segment of the original, asymmetric, three-dimensional wall–frame structure. The entire original structure can then be modelled by assembling the substitute beams corresponding to each segment in the usual way.

In [12, 54], the Homogenization method of Periodic Discrete Media (HPDM) to repetitive reticular structures composed of interconnected elements (beams or plates) was adopted by **Boutin** with the purpose of deducing the modal characteristics of the repetitive framed buildings. The homogenized continuum model can be defined as a shear only beam, a Timoshenko beam or a Euler-Bernoulli beam and it provides the main structural characteristics. The first phase of the HPDM is the discretisation of the dynamic balance of the structure under harmonic vibrations, followed by the actual homogenisation procedure, through which a continuum model is elaborated from the discrete description. For the homogenization process, the scale parameter $\varepsilon = \frac{l_{cell}}{L}$ (size of the basic cell of the structure/characteristic size of deformation of the structure under vibrations) must be sufficiently small. For this reason, the method is limited to the first frequencies and mode shapes, having wavelengths much larger than cell size. In [55] the continuum model obtained by means of the HPDM was adopted for studying the local resonance in reticulated frames.

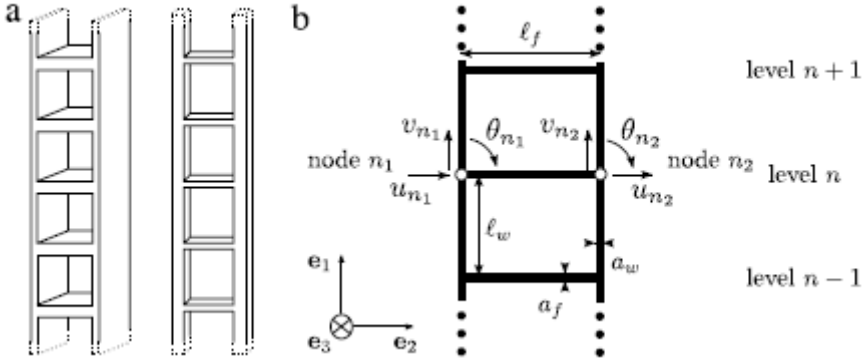

Figure 1.11 – (a) Example of structures studied by Boutin et al. and (b) equivalent continuum model – Boutin [55]

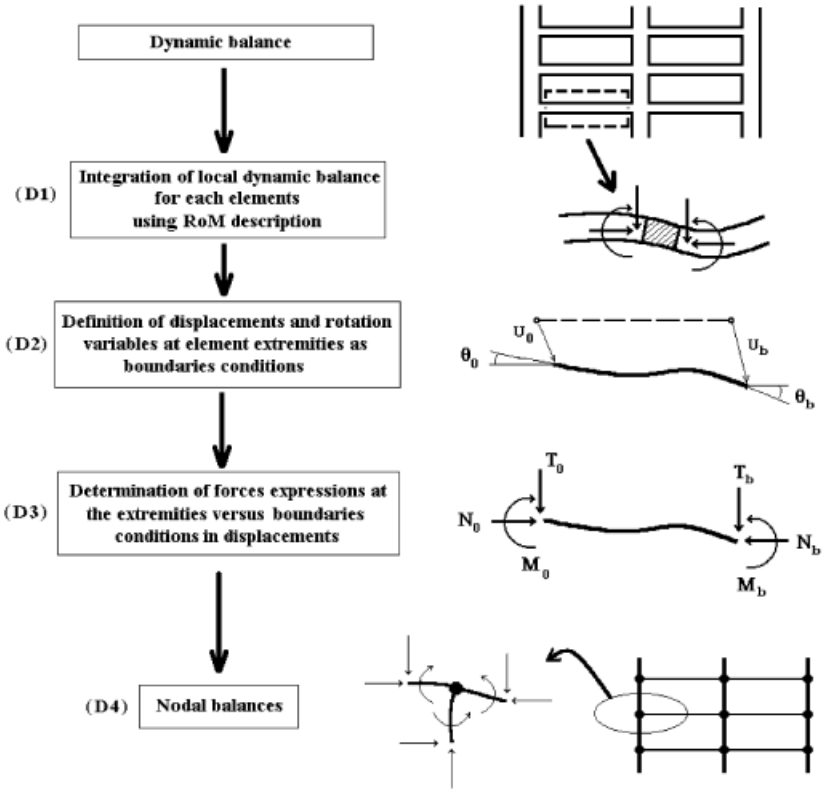

Figure 1.12 - The four steps of the discretisation process – Boutin [12]

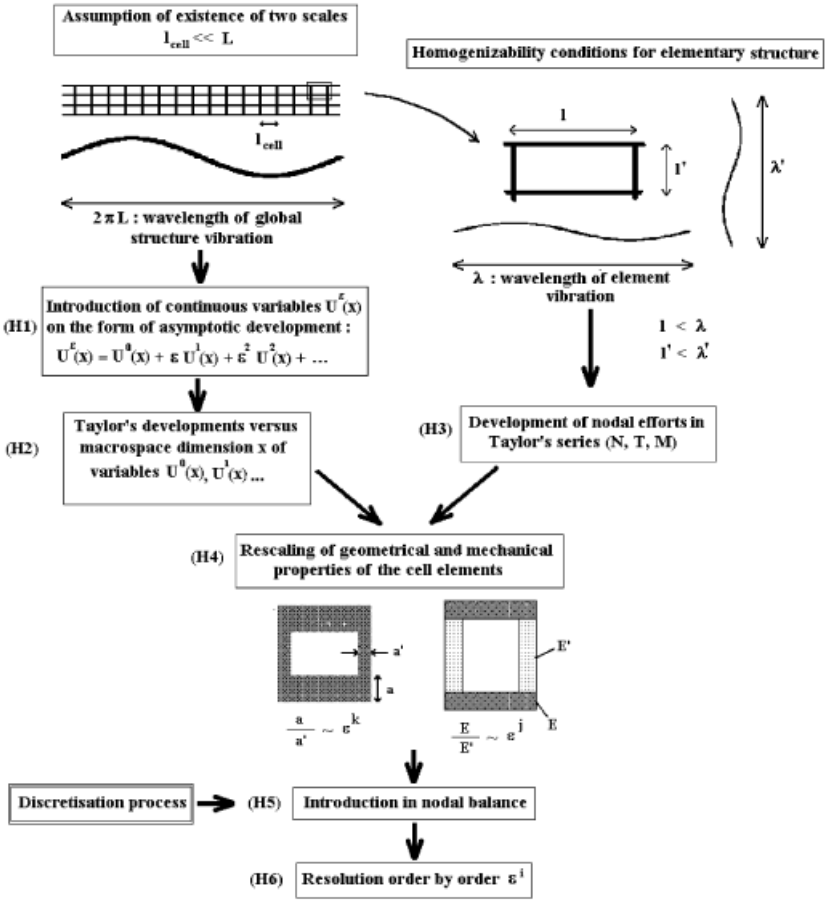

Figure 1.13 - The steps of the homogenization process– Boutin [12]

In 2010, basing the studies on previous research [56], **Rahgozar** proposed a continuum model for predicting the stress distribution and the displacement profile for a combined system of different structural elements, but only under specific load patterns [57]. The model consists of an equivalent uniform cantilever beam with flexural and shear deformability and rotational springs simulating the belt trusses. This model was applied to estimate the natural frequencies and mode shapes of the tall buildings [58, 59], obtaining acceptable errors if compared to Finite Element models.

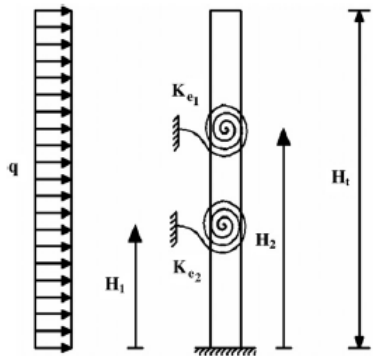

Figure 1.14 - Equivalent beam model – Rahgozar [58]

In 2013 **Carpinteri and Lacidogna** proposed an equivalent shear-torsional beam model for estimating the response of tall buildings under static horizontal loads in the initial design phase [60]. The equivalent shear beam has the stiffness of each inter-storey segment equal to the sum of stiffness of the columns of the corresponding floor and is subjected to elastic rotational springs simulating the stiffness of the floor slabs and to horizontal springs simulating the diagonal bracings. Therefore the model is able to consider a non-uniform stiffness distribution. Being N the number of floors of the building, the total number of degrees of freedom is 3N, two translations and one rotation for each floor. The results are shown in terms of displacements and internal forces due to static wind loads. In [61, 62] the model was extended in order to consider second order torsional effects (Vlasov's theory), allowing to compute also the natural frequencies and mode shapes of a uniform building by means of the equivalent beam with shear and torsional deformability.

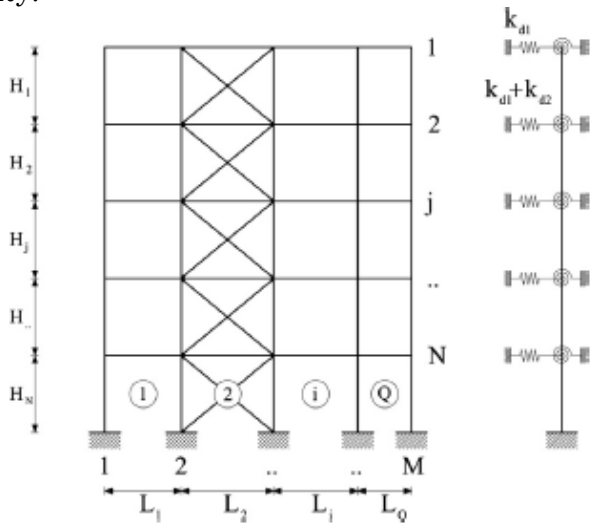

Figure 1.15 - Model of a braced frame equivalent to a shear wall – Carpinteri [60]

Bozdogan modelled a uniform building by means of an equivalent shear beam model, taking into account the axial deformability of structural elements by introducing a shear stiffness correction coefficient [10]. The coupled shear wall is modelled as a flexural beam. Mechanical and geometric characteristics are assumed uniform along the height of the building.

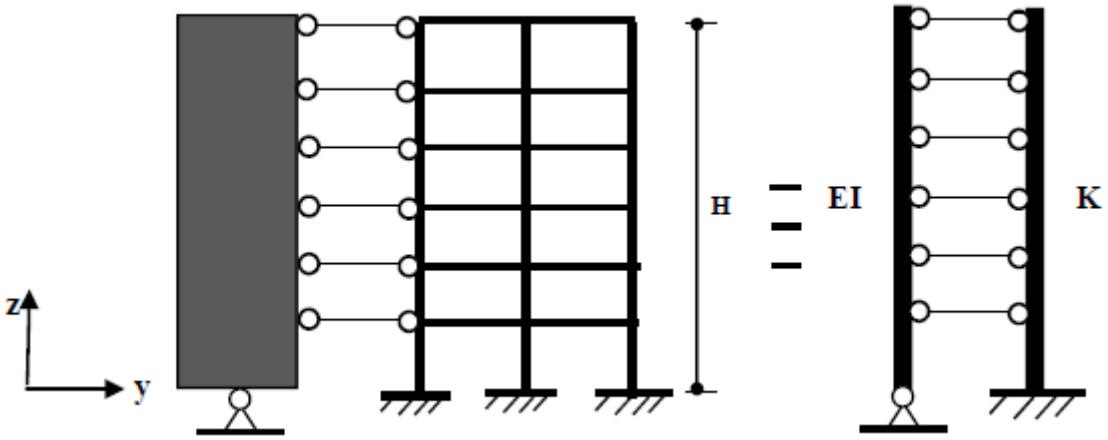

Figure 1.16 - Equivalent model of frame hinged shear wall structures – Bozdogan [10]

Shear stiffness of the equivalent beam can be expressed using Zalka's expressions [13]:

$$K = \frac{12}{h\left(\frac{1}{r}+\frac{1}{s}\right)} \qquad (1.2.25)$$

$$r = \sum_{i=1}^{p} \frac{EI_{bi}}{l_i} \qquad s = \sum_{i=1}^{q} \frac{EI_{ci}}{h}$$

Equation of motion is shown below:

$$EI\frac{\partial^4 y}{\partial z^4} - K\frac{\partial^2 y}{\partial z^2} + \frac{m}{h}\frac{\partial^2 y}{\partial t^2} = 0 \qquad (1.2.26)$$

Whose solution in dimensionless terms is:

$$A(\varepsilon) = c_1\cos(\beta_1\varepsilon) + c_2\sin(\beta_1\varepsilon) + c_3\cosh(\beta_2\varepsilon) + c_4\sinh(\beta_2\varepsilon)$$

$$\beta_1 = \sqrt{\sqrt{\left(\frac{k^4}{2}+\alpha\right)} - \frac{k^2}{2}} \qquad \beta_2 = \sqrt{\sqrt{\left(\frac{k^4}{2}+\alpha\right)} + \frac{k^2}{2}} \qquad (1.2.27)$$

By introducing the appropriate boundary conditions, natural frequencies and mode shapes of the equivalent beam can be determined. By means of the response spectra, it is possible to obtain maximum deflection, maximum relative displacement, maximum shear force and maximum bending moment of the system.

The proposed model was extended to beams with stiffness distribution which varies according to a fixed law along the height and with uniform mass distribution [63]. Equations of motion have been solved by means of the "differential transform method". Since only planar frames were considered, torsional problem has been neglected.

Later, starting from 2014, an equivalent beam model, deformable in shear and torsion and capable of approximately reproducing the dynamic behaviour of the three-dimensional shear-

type structures, was introduced by **Luongo** [64], and its aeroelastic instability to wind excitation has been analysed [6, 7]. The homogenization process id based on the equivalence of the strain energy of the building cell and of the corresponding beam segment. The model has been used for the modal analysis of periodic buildings with symmetrical and asymmetrical plans. The model has been adopted also in other papers in 2019 [65, 66], for studying the linear and non-linear elastic behaviour of periodic tower buildings under the assumption that the beam is internally constrained, so that it is capable of experiencing shear strains and torsion only. The elasto-geometric and inertial characteristics of the beam are directly identified from a discrete model of a three-dimensional frame, via a homogenization process. A more refined Timoshenko beam-like model suitable for the dynamic analysis of periodic buildings has been recently proposed [11]. The homogenization process is still based on the equivalence of the strain energy of the building cell, between two rigid floors with structural elements such as columns and shear walls, and of the corresponding beam segment. The results of the analyses performed on buildings with uniform stiffness distribution are shown in terms of natural frequencies and axial forces of the structural elements under static loads.

Ragni et al. [67] proposed a displacement-based method, particularly devoted to seismic design steel frames equipped with dissipative braces, by using an equivalent continuous beam-like model where flexural deformability and shear deformability are related respectively to columns and diagonals of the bracing system. The design method is appealing since analytical expressions of the required flexural and shear stiffness distributions are obtained and conveniently adopted in preliminary design of dissipative diagonal braces and columns of steel frames.

Crucial aspects of the proposed beam-like models already described, such as characteristics of the analysed buildings (out of plane deformability, spatial frames, non-uniform stiffness distribution, eccentricity between CM and CS, lumped or diffused mass) and the presence of the results in terms of dynamic response are reported in Table 1.1. The symbol √ indicates the presence of the hypothesis shown in the corresponding column into the beam-like model of the author in the corresponding row.

As this excursus shows, the definition of an equivalent beam was not always simple and immediate, especially in case of three-dimensional, torsional coupling behaviour. Furthermore, in scientific literature there are no equivalent models which evaluate the seismic response of non-uniform buildings with asymmetrical plans. This requirement is necessary in order to study existing irregular buildings.
The reduction of complex structural systems to equivalent beam models is still an open challenge of great interest.

Table 1.1 - Summary of the literature review about linear elastic beam-like models

Author	Shear beam	Flexural beam	Timoshenko's model	Out of plane floor deformability	Non-uniform stiffness	3D systems	CM≠CS	Distribuited and lumped masses	Modal analysis	Seismic response
Proposed model	√	-	-	√	√	√	√	√	√	√
Basu	√	√	-	-	-	-	-	-	√	-
Stafford Smith	√	√	-	-	-	-	-	-	√	-
Iwan and Huang	√	-	-	-	-	-	-	-	√	√
McCallen, Chajes	√	√	-	√	-	√	-	-	√	√
Miranda	√	√	-	-	√	-	-	-	√	√
Gulkan, Akkar	√	√	-	-	-	-	-	-	√	√
Wang	√	√	-	-	-	√	√	-	√	-
Kuang and Ng	√	√	-	-	-	√	√	-	√	-
Li, Rahgozar	-	√	√	-	√	-	-	-	√	-
Swaddiwudhipong	-	-	√	-	-	√	-	-	√	-
Khaloo, Khosravi	√	√	-	-	-	√	-	-	√	√
Zalka, Potzta, Kollar	√	√	-	√	-	√	√	-	√	-
Cluni	-	-	√	-	-	√	-	-	√	√
Meftah	-	√	-	-	-	-	√	-	√	√
Rafezy	√	-	√	-	√	√	√	-	√	-
Boutin	-	-	√	√	-	-	-	-	√	-
Rahgozar	-	-	√	-	-	-	-	-	√	-
Lacidogna	√	-	-	√	√	√	-	-	√	-
Bozdogan	√	√	-	-	√	-	-	-	√	-
Luongo	-	-	√	-	-	√	√	-	√	-
Ragni	-	-	√	-	√	√	-	-	-	-

All the above-mentioned papers focus exclusively on the linear dynamic behaviour of multi-storey buildings obtained by exploiting equivalent beam-like models. Nevertheless, as it is very well known, the dynamic response of real structures under seismic loads exhibits significant excursions into the plastic regime which cannot be taken into account by elastic models. In the following, the main simplified models which consider the non-linear behaviour of the building are discussed. First, equivalent inelastic Single Degree Of Freedom (SDOF) systems are treated; then, equivalent inelastic Multi Degree Of Freedom (MDOF) systems are shown, focusing on the inelastic beam-like models.

1.2.2 Inelastic SDOF models

Following a well-established procedure, consistent to actual seismic codes, the assessment of the seismic vulnerability of buildings is nowadays generally performed, rather than by means of non-linear dynamic analyses of detailed 3D FEM models, identifying the seismic demand of each building through the inelastic behaviour of a Single Degree Of Freedom (SDOF) system assumed equivalent to the 3D structural model.

The inelastic behaviour of equivalent SDOF oscillators is inferred by considering the results of non-linear static analyses performed on detailed 3D FEM models. Well-known examples of such procedure, computationally less demanding with respect to the dynamic non-linear analysis performed on 3D FEM model, are given by the N2 Method [68, 69, 70, 71, 72, 73, 74, 75, 76], the Capacity Spectrum Method (CSM) [77, 78], the Uncoupled Modal Response History Analysis (UMRHA) and the Modal Pushover Analysis (MPA) [79].

The N2 method was proposed by Fajfar in [68, 69, 70, 71, 72, 73] and consists in a non-linear procedure which intends to emphasize the evaluation of the non-linear (N) response of the multi-storey building by means of two (2) models: the 3D non-linear FEM model and the SDOF equivalent system. First, non-linear static analyses are performed by means of a 3D non-linear FEM model of the structure, considering distributions of external static loads which reflect somehow the mass distribution and the fundamental vibration modes of the structure. Then, the results, expressed in terms of capacity curves for several directions of the input, are considered for the definition of inelastic SDOF systems assumed to be representative of the non-linear global seismic behaviour of the building for each considered direction of the loading. Several International Technical Codes suggest similar procedures [80, 81, 82] inspired by the N2 method.

The Capacity Spectrum Method is a strategy similar to the N2 method, which also possesses the strong advantage to reduce the structure to a SDOF model thus facilitating the evaluation of the non-linear seismic response, by means of non-linear dynamic analyses, as well as the assessment of the seismic capacity of the entire structure based on elastic response and inelastic design spectra [77, 78].

Aiming at better exploiting the results obtained by 3D pushover analysis, some authors proposed different strategies for the assessment of the seismic response of the building. Few studies introduced some corrections to the original formulation of the N2 method [74, 75, 76], some included the contribution of more than one vibration mode [79], others considered the pushover analysis obtained by force distributions containing the contribution of different vibration modes [83], or else more computational demanding analysis based on adaptive force

distributions related to the evolution of the inelastic response of the building (adaptive pushover) [84].

In the following, the N2 method, the Capacity Spectrum Method, the Uncoupled Modal Response History Analysis and the Modal Pushover Analysis are described in detail. In particular, the evolution of the N2 method is exploited, through its first, second and basic formulation used nowadays in the technical codes, while some developments are treated in the extended formulation.

- *N2 method – first formulation [68, 69]*

The N2 method is a non-linear procedure for the seismic design of buildings whose name is inspired by the consideration that the method is based on the use of two different mathematical models (N2). In its initial formulation it has been proposed for structures oscillating predominantly in a single mode.

1) In the first step of the N2 procedure, a non-linear static analysis of the MDOF system under a monotonically increasing lateral load is performed. The most important result of the static analysis is the base shear – top displacement relationship. It enables the assessment of the three most important structural parameters: stiffness, strength, ductility. The relationship depends on the vertical distribution of the horizontal load. Uniform and inverted triangular distributions can be used.

2) In the second step, an equivalent SDOF system is defined, whose non-linear characteristics are based on the base shear - top displacement relationship obtained in the first step. A structure can, according to the well-known procedure of structural dynamics, be approximately transformed into an equivalent SDOF system by assuming a displacement shape $\underline{\phi}$ and a distribution of lateral resisting forces $\underline{\psi}$ which are constant during an earthquake.

The equation of motion for planar system subjected to a base acceleration $\ddot{u}_g(t)$ can be written in the form:

$$\mathbf{M}\cdot\ddot{\underline{U}}+\underline{P}=-\mathbf{M}\cdot\underline{1}\cdot\ddot{u}_g(t) \tag{1.2.28}$$

where $\underline{P}$ represents the restoring force vector (resistance of the structure). If the assumed shape $\underline{\phi}$ is taken to be the same as that resulting from the static application of the dynamic loads, then the distribution of lateral resisting forces $\underline{\psi}$ is equal to the distribution of lateral loads. By introducing:

$$\underline{U}=\underline{\phi}\cdot u \qquad \text{and} \qquad \underline{P}=\underline{\psi}\cdot p \tag{1.2.29}$$

by assuming concentrated masses m_t (a diagonal mass matrix) and by pre-multiplying by $\underline{\phi}^T$ the equation of motion (1.2.28) can be transformed into the form:

$$\sum m_i\phi_i\frac{\sum m_i\phi_i^2}{\sum m_i\phi_i}\ddot{u}+p\sum\phi_i\psi_i=-\left(\sum m_i\phi_i\right)\ddot{u}_g \tag{1.2.30}$$

or

$$m^*\ddot{u}^*+Q^*=-m^*\ddot{u}_g \tag{1.2.31}$$

Equation (1.2.31) represents the equation of motion for an equivalent SDOF system, where the constants are defined by:

$$m^*=\sum m_i\phi_i$$

$$Q^*=\frac{\sum\phi_i\psi_i}{\sum\psi_i}Q, \qquad Q=p\sum\psi_i \qquad (Q=\text{base shear}) \tag{1.2.32}$$

$$u^*=\frac{\sum m_i\phi_i^2}{\sum m_i\phi_i}u$$

Viscous damping can be included in Equation (1.2.31).

The $Q^* - u^*$ relationship of the SDOF system can be approximated by a tri-linear relationship for the sake of simplicity.

3) In the third step of N2 method, maximum displacements (and the corresponding ductility demand) are determined by carrying out non-linear dynamic analysis on the equivalent SDOF system. Dynamic analysis, in its simplest form, can also be performed by using inelastic response spectra. (There are some trial expressions to evaluate the maximum inelastic displacement from the response spectrum)
Some more details of the structural response (e.g. formation of plastic hinges, inelastic behaviour of structural elements, storey drifts, ductility demand in structural elements) can be obtained by following the inelastic static response of the MDOF model up to the maximum displacement determined by the non-linear dynamic analysis of the SDOF model.

The structural behaviour of a building during an earthquake can be evaluated by comparing ductility demand and supply. When using the N2 procedure, demand can be estimated by taking into account the results of the dynamic analysis of the equivalent SDOF system and of the static analysis of the MDOF system. The results are not very sensitive to the details of the equivalent SDOF system.
It should be emphasised that the N2 procedure generally yields unconservative results for shear forces along the whole height of the building.
If the first natural period of the structure is much larger than the predominant period of the ground motion, the higher mode effects may be important, therefore all quantities will be underestimated in the upper part of the structure if N2 method is used.
Additional research is needed to solve some particular problems in different phases of the method.

Extension of the method

In order to include the effect of cumulative damage, in the third step, in addition to the maximum displacement, the input energy imparted to the SDOF system is determined, which provides a very good estimate of the input energy for multi-storey buildings, unless the influence of the higher modes is important. The dissipated hysteretic energy E_H can be approximately distributed to the various elements of the MDOF system proportionally to the energy dissipated under monotonic static loading up to the maximum displacement. Finally, damage indices are computed at the component level:

$$DM = \frac{u}{u_u} + \beta \frac{E_H}{F_y u_u} \tag{1.2.33}$$

where DM is the damage index, u and u_u are the actual and ultimate displacements, respectively, F_y is the yield strength and β is a constant which depends on the structural characteristics.

- *N2 method – second formulation [70]*

The second formulation of the N2 method follows the same three steps of the first formulation. The main differences with respect to the first formulation are:
a) the hypothesis on the lateral resisting forces $\underline{P}$;
b) the linearization adopted for the force-displacement relationship of the SDOF system.

a) The vertical distribution of lateral resisting forces $\underline{P}$ is proportional to the assumed time-independent displacement shape $\underline{\phi}$ (normalized to the top displacement $\phi_n = 1$) by means of the diagonal mass matrix:

$$\underline{P} = \mathbf{M} \cdot \underline{\phi} \tag{1.2.34}$$

Therefore, the transformation of the MDOF system into the equivalent SDOF can be written in the form:

$$R^* = c \cdot R \tag{1.2.35}$$

where R^* represents the quantities in the equivalent SDOF system (force F^*, displacement D^* and hysteretic energy E_H^*) and R represents the corresponding quantities in the MDOF system (base shear V, top displacement D_t and hysteretic energy E_H). Constant c is defined as:

$$c = \frac{\underline{\phi}^T \mathbf{M} \underline{\phi}}{\underline{\phi}^T \mathbf{M} \underline{1}} = \frac{\sum m_i \phi_i^2}{\sum m_i \phi_i} \tag{1.2.36}$$

where m_i is the concentrated mass at the i-th storey. The value in the denominator represents the mass of the equivalent SDOF system $m^* = \sum m_i \phi_i$.

These expressions do not require the transformation of the elastic spectra.
Furthermore, the non-linear static analysis should be performed on the MDOF system under the increasing lateral loading $\underline{P}$. In this way, the vertical distribution of lateral loads in the pushover analysis corresponds to the distribution of inertia forces due to the assumed displacement shape.

b) The base shear – top displacement relationship of the MDOF system is transformed into a force-displacement relationship of the equivalent SDOF system. Then, for the force-displacement relationship of the SDOF system, an approximate bilinear relationship is used, in particular an elastic-plastic behaviour with positive hardening is adopted. Assuming this hypothesis, it is possible to define the seismic demand of the SDOF by means of the inelastic spectra, by determining the reduction factor R_μ and the corresponding displacement ductility demand μ.
Furthermore, in this version of the method, the damage index DM for each structural element is expressed as:

$$DM = \frac{\theta}{\theta_u} + \beta \frac{E_H}{M_y \theta_u} \tag{1.2.37}$$

where θ and θ_u are the actual and ultimate rotations, respectively, M_y is the yield moment and β is an empirical constant which depends on the structural characteristics.

- *N2 method – basic formulation used in technical codes [71, 72]*

The N2 method in its basic formulation consists of the following steps.

1) *Determine the base shear-top displacement relationship by a pushover analysis.*
It is assumed that the lateral force in the i-th storey is proportional to the component of the assumed displacement shape ϕ_i weighted by the storey mass m_i:

$$P_i = m_i \phi_i \tag{1.2.38}$$

Such distribution has a physical basis (inertia forces) and yields the simplest transformation from MDOF to SDOF systems. However, any other reasonable distribution can also be used. The distribution remains constant during the pushover analysis.

2) Transform the force-deformation relationship of the MDOF into that of an equivalent SDOF system.
The starting point is the equation of motion of a planar MDOF model that explicitly includes only lateral translational degrees of freedom:

$$\mathbf{M}\ddot{\underline{U}} + \underline{R} = -\mathbf{M}\underline{1}a \tag{1.2.39}$$

$\underline{U}$ and $\underline{R}$ are vectors representing displacements and internal forces, $\mathbf{M}$ is the diagonal mass matrix of the MDOF system and a represents the ground acceleration as a function of time. It will be assumed that the displacement shape $\underline{\phi}$ is constant, i.e. that it does not change during the structural response to ground motion. This is the basic and the most critical assumption within the procedure.
By introducing the assumptions $\underline{U} = \underline{\phi} D_t$ and $\underline{P} = \underline{R}$, and pre-multiplying Equation (1.2.39) by $\underline{\phi}^T$, the equation of motion of the SDOF system can be written as:

$$m^* \ddot{D}^* + F^* = -m^* a \tag{1.2.40}$$

where $m^* = \underline{\phi}^T \mathbf{M}\underline{1}$, D^* and F^* are, respectively, the mass, the displacement and the force of the equivalent SDOF system. Provided that the distribution of the lateral loading is defined by equation (1.2.38), the transformation of all quantities is performed by means of the equation:

$$Q = \Gamma Q^* \tag{1.2.41}$$

where Q^* represents the quantities in the equivalent SDOF system (force F^*, displacement D^* and hysteretic energy E_H^*, if needed), and Q represents the corresponding quantities in the MDOF system (base shear V, top displacement D_t and hysteretic energy E_H). The constant Γ is defined as:

$$\Gamma = \frac{\sum m_i \phi_i}{\sum m_i \phi_i^2} = \frac{\underline{\phi}^T \mathbf{M}\underline{1}}{\underline{\phi}^T \mathbf{M}\underline{\phi}} \tag{1.2.42}$$

It is usually called modal participation factor. Note that the assumed displacement shape $\underline{\phi}$ is normalized - the value at the top is equal to 1. Note also that any reasonable shape can be used for $\underline{\phi}$. Only in a special case $\underline{\phi}$ represents the first mode shape. The value in the numerator represents the mass of the equivalent SDOF system:

$$m^* = \sum m_i \phi_i \tag{1.2.43}$$

Note that the same constant Γ applies for the transformation of both displacements and forces. As a consequence, the force - displacement relationship determined for the MDOF system (the

V - D_t diagram) applies also to the equivalent SDOF system (the F^* - D^* diagram), provided that both force and displacement are divided by Γ.

3) *Idealize the force-displacement relationship of the equivalent SDOF system into an elastic-perfectly plastic form.*

In a regulatory document, some guidelines may be given [85, 86]. Note that the graphical procedure requires the post-yield stiffness equal to zero. This is because the reduction factor R_μ is defined as the ratio of the required elastic strength to the yield strength. The influence of moderate strain hardening is incorporated in the demand spectra.

The elastic period of the idealised bilinear system T^* can be determined as:

$$T^* = 2\pi\sqrt{\frac{m^* D_y^*}{F_y^*}} \tag{1.2.44}$$

where F_y^* and D_y^* are the yield strength and displacement, respectively.

If the forces in the force-displacement curve for the equivalent SDOF system are divided by the equivalent mass m^*, the acceleration-displacement relation (capacity curve) is obtained.

Finally, the capacity diagram in AD format is obtained by dividing the forces in the force-displacement diagram (F^* - D^*) by the equivalent mass m^*.

$$S_a = \frac{F^*}{m^*} \tag{1.2.45}$$

4) *Determine the seismic demand for the equivalent SDOF system.*

The intersection of the radial line corresponding to the elastic stiffness of the idealised bilinear system and the elastic demand spectrum (ADRS format) defines the strength required for the elastic behaviour and the corresponding elastic displacement demand.

In the following, the conservative assumption $T_0 = T_C$ has been used. If the elastic period T^* is larger than T_0, the inelastic displacement demand S_d is equal to the elastic one S_{de}. The ductility demand is equal to the reduction factor ($\mu = R_\mu$) and it can be obtained from the graph.

If T^* is smaller than T_0, the reduction factor R_μ is first determined as the ratio between the elastic acceleration S_{ae} and the yield acceleration S_{ay}, representing both the acceleration demand and the capacity of the inelastic system. The ductility demand is then calculated from:

$$\mu = \left(R_\mu - 1\right)\frac{T_0}{T^*} + 1 \tag{1.2.46}$$

The displacement demand is determined as:

$$D^* = S_d = \mu D_y^* \tag{1.2.47}$$

The inelastic demand in terms of accelerations and displacements corresponds to the intersection point of the capacity spectrum and the demand spectrum which corresponds to the ductility demand μ (ratio between the maximum displacement and the yield displacement).

Since the ductility μ has been determined, it is possible to define the corresponding demand inelastic spectrum.

For an inelastic SDOF system with a bilinear force-deformation relationship, the acceleration spectrum S_a and displacement spectrum S_d can be determined as:

$$S_a = \frac{S_{ae}}{R_\mu} \tag{1.2.48}$$

$$S_d = \frac{\mu}{R_\mu} S_{de} \tag{1.2.49}$$

The reduction factor R_μ-ductility μ relationship is expressed as:

$$R_\mu = (\mu - 1)\frac{T}{T_0} + 1 \qquad T \le T_0 \tag{1.2.50}$$

$$R_\mu = \mu \qquad T \ge T_0 \tag{1.2.51}$$

$$T_0 = 0.65\mu^{0.3} T_C \le T_C \tag{1.2.52}$$

An even simpler version (of R_μ spectra) can be obtained by fixing the transition period $T_0 = T_C$.

5) *Check performance at the expected maximum displacement.*
First, the displacement has to be transformed back from the SDOF (S_d) to the MDOF (D_t) system (Equation (1.2.41)). Then the performance at maximum displacement is evaluated on the global and local level. Nevertheless, only the displacement of the control point of the MDOF system, usually located at the top floor of the building and used for the V - D_t relationship determined in the pushover analysis, can be determined in any case.
The local seismic demand (e.g., story drifts, joint rotations) can be determined by a pushover analysis. Under monotonically increasing lateral loads with a fixed pattern (as in Step 1), the structure is pushed to its target top displacement D_t. The storey drifts are determined indirectly from the floor displacements obtained in the pushover analysis and corresponding to the displacement of the control point (top floor) equal to the target (maximum) displacement, assuming that the distribution of deformations throughout the structure in the static (pushover) analysis approximately corresponds to that which would be obtained in the dynamic analyses.

- *N2 method – extended formulation [74, 75, 76]*

The basic assumption used in pushover-based methods is that the structure vibrates predominantly in a single mode. This assumption is not always fulfilled, especially in the case of high-rise buildings and/or torsionally flexible plan-asymmetric buildings, and it may not detect the structural weaknesses which may be generated when the dynamic characteristics of the structure change after the formation of the first local plastic mechanism.
In [74, 75, 76] the N2 method has been extended in order to take into account torsional effects and higher mode effects in elevation. The extension is based on the assumption that the structure remains in the elastic range when vibrating in torsional or higher modes, and that the seismic demands in terms of displacements and storey drifts can be estimated as an envelope of demands determined by a basic pushover analysis, which does not take into account the torsional and higher mode effects, and normalized demands determined by a standard elastic modal analysis, which includes torsional and higher mode effects.

Plan-Asymmetric Building Structures

The steps of the extended N2 method taking into account torsional effect are as follows:

1) Perform pushover analyses by using a 3D mathematical model. Loading is applied at the mass centres, independently in two horizontal directions, in each direction with + and – sign. Determine the target displacement (displacement demand at CM at roof level) for each two horizontal directions (the larger value of two values, obtained for + and – sign).
2) Perform a linear modal analysis of the 3D mathematical model, independently for excitation in two horizontal directions (each one CQC or SRSS rule) and combine the results according to the SRSS rule.
3) Determine the correction factors c_T to be applied to the relevant results of pushover analyses. The correction factor is defined as the ratio between the normalised roof displacement obtained by elastic modal analysis and by pushover analysis. The normalized roof displacement is the roof displacement at an arbitrary location divided by the roof displacement at the CM. If the normalised roof displacement obtained by elastic modal analysis is smaller than 1, take 1. Correction factors are defined for each horizontal direction separately. The same values of c_T apply to the displacements and storey drifts. Note that the correction factor depends on the location of the element in the plan. It is assumed that the c_T factors are independent of the elevation of the structure, so the same c_T can be used for the adjustment of the pushover results at any storey in elevation.
4) Multiply all relevant quantities obtained by pushover analyses with appropriate correction factors. For example, in a perimeter frame parallel to the X-axis, all quantities are multiplied with the correction factor determined with pushover results obtained for loading in the X-direction and for the location of this frame. The relevant quantities are, for example, deformations for the ductile elements which are expected to yield and the stresses for brittle elements which are expected to remain in the elastic range.

The results obtained by this procedure are influenced both by the nonlinear static (pushover) and the elastic dynamic analysis. Displacement demand (amplitude and the distribution along

the height) at the mass centres is determined by the usual N2 method, which is based on pushover analysis. The amplification of demand due to torsion is determined by elastic dynamic analysis, while reduction of demand due to torsion is not taken into account.

Higher mode effects

As already pointed out, the N2 method is based on the very restrictive assumption that the structure vibrates predominantly in a single mode (a time-independent displacement shape). Thus, this method is in principle inaccurate for structures where higher mode effects are significant, and it may not detect the structural weaknesses which may be generated when the structure's dynamic characteristics change after the formation of the first local plastic mechanism.
The N2 method has been extended in order to take into account higher mode effects in elevation. It is worth remembering that the extension of the N2 method to plan-asymmetric buildings, where torsional influences are important, was made by assuming that the torsional influences in the inelastic range are the same as in the elastic range. The torsional influences are determined by the standard elastic modal analysis. They are applied in terms of correction factors, which are used for the adjustment of results obtained by the usual pushover analysis. Practically the same idea has been used for the extension of the N2 method to medium- and high-rise buildings, where higher mode effects are important along the elevation of the structure. It is assumed that the structure remains in the elastic range when vibrating in higher modes, and that the seismic demands can be estimated as an envelope of demands determined by a basic pushover analysis, which does not take into account the higher mode effects, and normalized demands determined by an elastic modal analysis, which includes higher mode effects. Typically, the pushover analysis controls the behaviour of those parts of the structure where the major plastic deformations occur, whereas the elastic analysis determines seismic demand at those parts where the higher mode effects are important. Due to the similarity of the approaches, basically the same procedure as in the case of torsion can be applied. The influence of higher modes is determined by standard elastic modal analysis and used for the adjustment of the results obtained by the usual pushover analysis. The proposed procedures (for taking into account higher mode effects in plan and in elevation) are consistent and compatible. Both effects can be considered simultaneously by two sets of correction factors.

In order to predict the structural response for a building with a non-negligible effect of higher modes along the elevation, the following procedure can be applied:

1) Perform the basic N2 analysis. The basic N2 analysis consists of a pushover analysis of an MDOF structural model, a bilinear idealization of the pushover curve and the transformation to an equivalent SDOF model, the determination of the displacement demand of the SDOF system by using inelastic response spectrum, and the transformation of the displacement demand from the SDOF to the MDOF system. Loading is applied at the mass centres (CM), independently in each of the two horizontal directions, in each direction with the + and − sign. The target displacement (the displacement demand at the CM at roof

level) is determined for each of the two horizontal directions (the larger value of the two values, obtained for the + and − sign). It is assumed that the effects of higher modes on the displacement demand (target roof displacement) are negligible. Seismic demand for all relevant quantities is represented by the results of the pushover analysis at the target roof displacement.

2) Perform the standard elastic modal analysis of the MDOF model independently for excitation in two horizontal directions, considering all relevant modes (using the CQC or SRSS rule), and combine the results for both directions according to the SRSS rule. Determine storey drifts (and displacement, if necessary) for each storey. Normalize the results in such a way that the top displacement (at the CM) is equal to the target top displacement.

3) Determine the envelope of the results obtained in Step 1 and 2.

   (3a) For each storey, determine the correction factors c_{HM}, which are defined as the ratio between the results (normalised storey drifts and displacements) obtained by elastic modal analysis (Step 2) and the results obtained by pushover analysis (Step 1). If the ratio is larger than 1.0, the correction factor c_{HM} is equal to this ratio, otherwise it amounts to 1.0. Note that the correction factors for displacement are small and can be neglected in most practical applications. The correction factors for storey drifts are important. One correction factor is determined for each storey in the two horizontal directions.
   (3b) The resulting storey drifts (and displacements, if necessary) are obtained by multiplying the results determined in Step 1 with the corresponding correction factors c_{HM}. Different values of c_{HM} apply to the displacements and storey drifts.

4) Determine other local quantities. The resulting correction factors for storey drifts c_{HM} apply to all local deformation quantities (e.g. rotations).

Nevertheless, although taking into account higher modes effects, the extended N2 method still neglects the inelastic behaviour of the structure when vibrating in higher modes, thus probably leading to an inaccurate assessment of the structural behaviour.

Plan-Asymmetric Building Structures and Higher mode effects

Higher mode effects in plan and in elevation can be considered simultaneously by two sets of correction factors, one for displacements (in plan) and the other for storey drifts (along the elevation).

1) Same Step 1 of Higher mode effects;

2) Same Step 2 of Higher mode effects;

3) Determine the seismic demand by using the results obtained in steps 1 and 2. This can be achieved by applying two sets of correction factors, one for displacements (in plan) and the other for storey drifts (along the elevation). The set determined for displacements (in plan) also applies to the storey drifts. So, the resulting correction factor for the storey drift in a

particular storey, and at a particular position in the plan, is obtained as a product of two correction factors. The correction factors are defined for each horizontal direction separately. They are applied to the relevant results of the pushover analyses. The correction factor for displacements due to torsion is defined as in Step 3 of Plan-Asymmetric Building Structures, while the correction factor for storey drifts due to higher mode effects in elevation is defined as in Step 3 of Higher mode effects.

4) The resulting correction factors for storey drifts (obtained as a product of two correction factors c_{HM} and c_T as described above) apply to all local deformation quantities (e.g. total joint rotations consisting of both elastic and plastic part) determined by pushover analysis and corresponding to the target displacements.

- *Capacity Spectrum Method [77]*

The Capacity Spectrum Method is a graphical procedure which compares the capacity of the structure to resist to lateral forces to the demand of earthquake ground motion on the structure. The fundamental steps of the procedure are described in the following.

1) *Capacity curve*: Estimate or calculate the capacity curve in terms of lateral roof displacement Δ_R and total lateral force at the base of the building V by performing a non-linear static analysis. Different distributions of horizontal forces can be used for the pushover analysis, such as the ones considered in the standard code procedure or alternatively distributed forces calibrated as masses times accelerations proportional to the first mode shape of the elastic model of the structure.

2) *Dynamic characteristics*: Estimate or calculate modal vibrational characteristics of the structure such as periods of vibration, mode shapes, modal participation factors, and effective modal mass ratios.

The effective mass ratio is: $\alpha = \dfrac{\left(\sum m_x \varphi_x\right)^2}{\sum m_x \sum m_x \varphi_x^2}$

The roof participation factor is: $PF\varphi_R = \dfrac{\sum m_x \varphi_x}{\sum m_x \varphi_x^2}\varphi_R$

where m_x is the lumped floor mass and φ_x is the mode shape.

3) *Capacity spectrum*: Convert the $V - \Delta_R$ capacity curve to a $S_a - S_d$ capacity spectrum by using the dynamic characteristics to represent the structure as a single degree of freedom structure. The spectral set of coordinates $S_a - S_d$ are given by: $S_a = \dfrac{V}{\alpha M g}$, $S_d = \dfrac{\Delta_R}{PF\varphi_R}$, where M is the total mass of the structure.

The secant period at each point along the curve can be calculated as: $T = 2\pi\left(\dfrac{S_a}{S_d g}\right)^{1/2}$.

After the capacity spectrum has been plotted, it is useful to approximate the force-displacement diagram with an equivalent bilinear capacity representation that establishes an effective yield point and an effective peak inelastic limit.

4) *Demand of earthquake - Response spectra*: Obtain or calculate linear elastic response spectra for several levels of damping, including the 5-percent damped spectrum. Higher damped response spectra are used to represent inelastic response spectra to account for hysteretic non-linear response of the structure.

5) *Graphical solution*: Plot capacity spectrum and family of damped response spectra together on an ADRS (acceleration-displacement response spectra) format. The intersection of the capacity spectrum with the appropriately damped response spectrum represents the estimated

inelastic demand of the earthquake on the structure. Finally, the displacement has to be transformed back from the SDOF to the MDOF system.

The CSM is applicable to a variety of uses such as a rapid evaluation technique for a large inventory of buildings, a design verification procedure for new construction of individual buildings, an evaluation procedure for an existing structure to identify damage states, and a procedure to correlate damage states of buildings to amplitudes of ground motion. However, the equivalence of the building with a SDOF system and the use of elastic demand spectra lead to an excessive simplification of the structure, which does not allow to exploit its complex inelastic behaviour.

- *Uncoupled Modal Response History Analysis and Modal Pushover Analysis [79]*

The Capacity Spectrum Method and the N2 method are based on the assumption that the response is controlled by the fundamental mode and that the mode shape remains unchanged after the structure yields. Obviously, after the structure yields, both assumptions are approximate. To overcome these limitations, several researchers have proposed adaptive force distributions [84] that attempt to follow more closely the time-variant distributions of inertia forces. While these adaptive force distributions may provide better estimates of seismic demands, they are conceptually complicated and computationally demanding for routine application in structural engineering practice. Therefore, an improved pushover analysis procedure has been developed, the Modal Pushover Analysis (MPA) [79]. The differential equations governing the response of an inelastic multistorey building to horizontal earthquake ground motion $\ddot{u}_g(t)$ are as follows:

$$\mathbf{M}\underline{\ddot{\mathbf{u}}}(t)+\mathbf{C_D}\underline{\dot{\mathbf{u}}}(t)+\mathbf{f_S}\left(\underline{\mathbf{u}}(t),\operatorname{sign}\underline{\dot{\mathbf{u}}}(t)\right)=-\mathbf{M}\underline{\mathbf{i}}\ddot{u}_g(t) \tag{1.2.53}$$

where $\mathbf{M}$ and $\mathbf{C_D}$ are the diagonal mass matrix and damping matrix of the MDOF system, respectively, $\underline{\mathbf{i}}$ denotes the spatial distribution of the load, $\ddot{u}_g(t)$ represents the earthquake ground motion and $\mathbf{f_S}$ is the vector of the lateral internal restoring forces. Expansion of the displacements of the inelastic system in terms of the natural vibration modes of the corresponding linear system leads to:

$$\underline{\mathbf{u}}(t)=\sum_{n=1}^{N}\underline{\boldsymbol{\psi}}_n q_n(t) \tag{1.2.54}$$

where $\underline{\boldsymbol{\psi}}_n$ is the nth mode of vibration of the linear system. Substituting Equation (1.2.54) in Equation (1.2.53), pre-multiplying by $\underline{\boldsymbol{\psi}}_n^T$ and using the mass- and classical damping-orthogonality property of modes, give:

$$\ddot{q}_n(t)+2\xi_n\omega_n\dot{q}_n(t)+\frac{F_{sn}(t)}{M_n}=-\Gamma_n\ddot{u}_g(t) \tag{1.2.55}$$

where ω_n is the nth natural frequency, ξ_n is the nth modal damping ratio and the resisting force, which depends on all modal coordinates $q_n(t)$, is given by:

$$F_{sn}(t)=F_{sn}\left(\underline{\mathbf{q}}(t),\operatorname{sign}\underline{\dot{\mathbf{q}}}(t)\right)=\underline{\boldsymbol{\psi}}_n^T\mathbf{f_S}\left(\underline{\mathbf{u}}(t),\operatorname{sign}\underline{\dot{\mathbf{u}}}(t)\right) \tag{1.2.56}$$

Equation (1.2.56) implies coupling of modal coordinates because of the yielding of the structure. Neglecting the coupling of the N equations in modal coordinates is the basic and most critical assumption of the UMRHA and MPA methods. Therefore, $F_{sn}(t)$ depends only on one modal coordinate $q_n(t)$, thus leading to the uncoupled equation of motion of the equivalent inelastic SDOF systems represented by Equation (1.2.55) divided by Γ:

$$\ddot{D}_n(t)+2\xi_n\omega_n\dot{D}_n(t)+\frac{F_{sn}(t)}{L_n}=-\ddot{u}_g(t) \tag{1.2.57}$$

where $D_n=q_n/\Gamma$, $L_n=\Gamma\cdot M_n$ and:

$$F_{sn}(t)=F_{sn}\left(q_n(t),\operatorname{sign}\dot{q}_n(t)\right)=\underline{\boldsymbol{\psi}}_n^T\mathbf{f_S}\left(\underline{\mathbf{u}}_n(t),\operatorname{sign}\underline{\dot{\mathbf{u}}}_n(t)\right) \tag{1.2.58}$$

Therefore, in the UMRHA and MPA methods the seismic demand due to individual terms in the modal expansion of the effective earthquake forces is determined as described in the following. The force-displacement non-linear relationship of each equivalent nth SDOF system is

determined by means of the base shear - roof displacement curve of the MDOF system, which is developed from a pushover analysis using the inertia force distribution corresponding to the nth mode. This pushover curve is idealized as a bilinear force - deformation relationship for the nth-mode inelastic SDOF system (with vibration properties in the linear range that are the same as those of the nth-mode elastic SDOF system). The peak deformation of this SDOF system, determined by non-linear response history analysis (solving Equation (1.2.57)) or from the inelastic response or design spectrum, for UMRHA and MPA respectively, and then multiplied by Γ, is used to determine the target value of roof displacement at which the nth-seismic response is determined by the pushover analysis. An estimate of the total seismic demand on inelastic MDOF systems is provided by the sum or the SRSS combination rule, for UMRHA and MPA respectively, of these 'modal' demands due to the first two or three terms of the expansion, each one obtained by means of an equivalent inelastic SDOF. The superposition of the results, however, is valid only for linear elastic systems.

1.2.3 Considerations about the adoption of SDOF Models

As already pointed out, nowadays the seismic vulnerability assessment of buildings is fulfilled by means of the adoption of equivalent SDOF systems. Although SDOF based approaches allow to obtain an easy and synthetic evaluation of the seismic performance of the building, in several cases they do not reflect the real inelastic behaviour of the entire structure. For the latter reason the high computational cost, related to the development of a non-linear static analysis on a detailed 3D model of the entire building, cannot always be considered fully justified on account of the successive interpretation of the results on the full model according to a seismic demand based on the inelastic response of a SDOF system.

The basic hypothesis of the equivalent SDOF system-based approaches is that the structure vibrates predominantly according to a single mode. However, in the case of high-rise or irregular buildings the higher modes effects cannot be neglected. For this reason, some researchers have extended the SDOF-based procedures in order to overcome this limitation by combining the fundamental mode effect and the elastic or inelastic contribution due to higher modes [75, 76, 79, 83, 84], as briefly described in the previous paragraphs. In order to account somehow of the real structural vibration modes, all the latter procedures share, as a common feature, the particular attention to the external load distribution used to generate the capacity curves. However, since all these methods in the final step rely on the definition of a SDOF system, the accuracy gained in virtue of the additional processed information might be spoiled by the roughness implied by the drastic reduction of degrees of freedom. In fact, they are affected by limitations, which do not reflect the real inelastic behaviour of the structure, such as, for example, the application of the superposition principle to inelastic responses as well as the evaluation of global displacements only, converted into local displacements (i.e. inter-storey drifts) by generalizing the along height distribution of the static capacity curve.

Several additional issues related to the seismic assessment procedures based on SDOF equivalent systems are detailed addressed in [87]. Some drawbacks are associated to the correct definition of the cyclic response of the SDOF equivalent system entitled to represent the complex response of the entire structure. This is particularly true for masonry structures whose cyclic behaviour is strongly related to the collapse mechanism and is generally affected by loss of strength and ductility [88] during the earthquake response. Further issues are related to the inability of SDOF systems to account for partial collapse mechanism, often related to the contribution of higher modes or triggered by geometrical irregularities, unless these have been correctly identified by the considered pushover analyses.

To the author's opinion, the drawbacks of the procedure, rather than related to the use of pushover analyses, are due to the oversimplified enforced equivalence with a SDOF system. Hence in order to better exploit the great deal of information relevant to the non-linear structural behaviour, obtained from a pushover analysis for a prescribed distribution of forces in a certain direction, the equivalent non-linear system should be endowed with additional degrees of freedom as proposed in the present study.

1.2.4 Inelastic MDOF models

In view of the promising results achieved by equivalent MDOF systems for the evaluation of the linear dynamic behaviour of multi-storey buildings, it is the author's belief that the extension of MDOF and beam-like models to embed the inelastic structural behaviour may introduce significant improvements in the assessment of seismic vulnerability of buildings.
Along this line, and in order to overcome the limitations implied by SDOF models, some simplified inelastic equivalent MDOF models have been proposed in the literature.

Lai et al. [89] in 1992 proposed a multi-rigid-body model with material non-linearity for the earthquake response analysis of shear-type structures. The model assumes that structural deformation concentrates totally on the nodes of the rigid elements. A damper and a spring are attached at each joint, and the stiffness of the spring incorporates the material non-linearities in accordance with each storey. The chosen non-linear models of restoring forces are bi-linear type and tri-linear degrading type. No further details were provided for the calibration strategy.

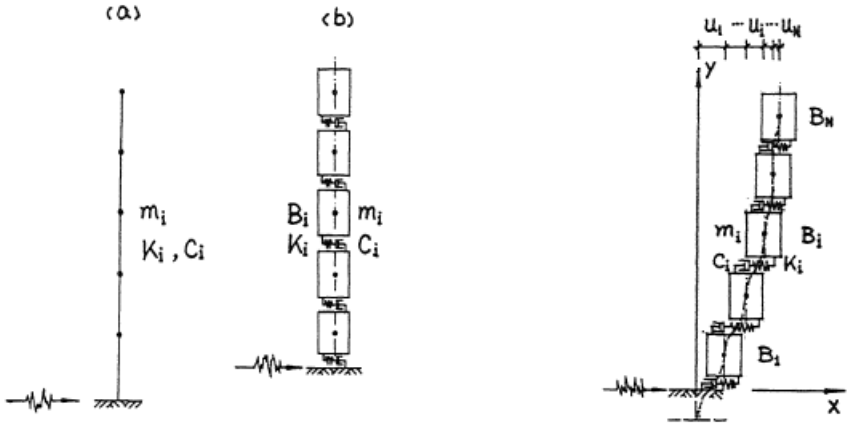

Figure 1.17 – From left to right: Shear-type model; multi-rigid-body discrete model; displacements of the shear-type structure described by multi-rigid-body model – Lai [89]

Hajirasouliha and Doostan [90] in 2010 proposed an equivalent shear-frame specifically devoted to the non-linear dynamic analysis of multi-storey planar braced steel frames. In the latter work the calibration of the inelastic mechanical properties of each inter-storey of the equivalent MDOF shear-frame system is conducted by means of a pushover analysis performed on the full-model frame structure. The inter-storey non-linear force-displacement relationship has been replaced with an idealized bilinear relationship to calculate the nominal storey stiffness and the effective yield strength of each storey (i.e. based on an energy equivalence among the two curves and assuming the nominal storey stiffness as the secant stiffness calculated at a storey shear force equal to 60% of the effective yield strength). Although pushover analyses are performed under different lateral load patterns, Hajirasouliha et al. [90] detected no relevant differences on the storey mechanical properties as the lateral load distribution changes. The model has been also adopted to investigate the seismic performance of multi-storey shear buildings considering soil-structure interaction [91].

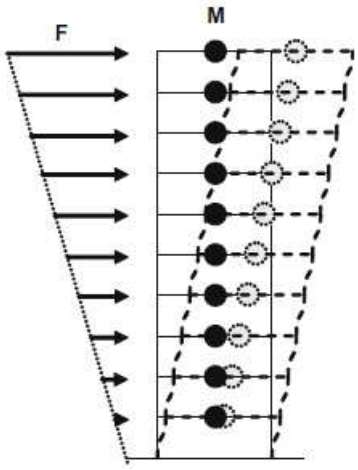

Figure 1.18 - Shear-frame model – Hajirasouliha [90]

Among the equivalent MDOF models, the fish-bone model (generic frame), first presented by **Nakashima et al.** [92] in 2002, is adopted for the seismic analysis of steel moment resisting frames. It consists of a single column with beams at every floor level extending halfway towards an adjacent column with a roller supporting each beam at midspan. The inelastic behaviour is taken into account by means of plastic hinges located at the ends of each member, representing the sum of the effects of the plastic hinges of the original frame in the corresponding position. Further applications on damage assessment of buildings by means of the fish-bone model can be found in [93]. The fish-bone model has been developed by several researches in order to take into account the flexural deformation of moment frames due to the axial elongation and contraction of columns in [94], also considering tall buildings or irregular frames such as braced frames and/or moment resisting frames with non-regular span-length in [95] and it has been also improved for the seismic analysis of reinforced concrete frames into the substitute frame model [96] and the improved fish-bone model [97].

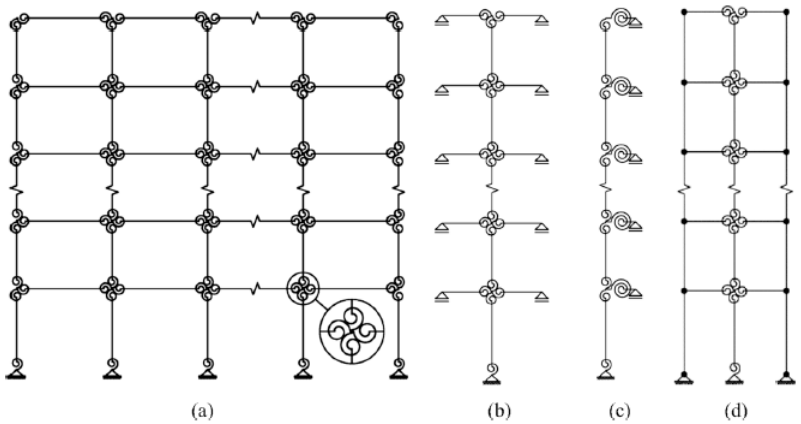

Figure 1.19 - (a) Frame building (b) fish-bone model (c) generic frame model (d) modified fish-bone model – Soleimani [96]

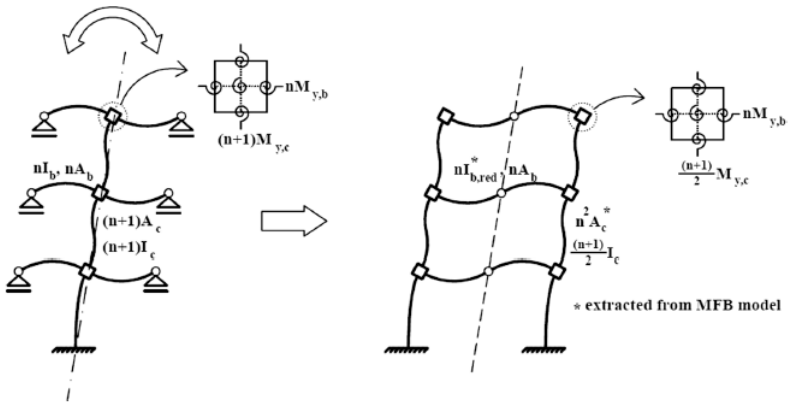

Figure 1.20 - Fish-bone model (left) and substitute frame model (right) - Soleimani [96]

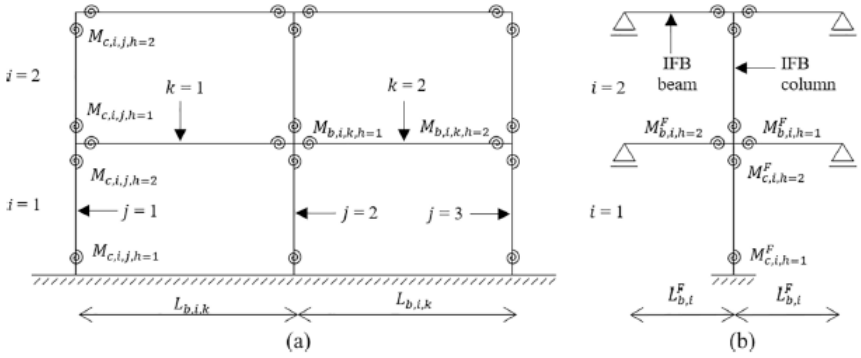

Figure 1.21 - (a) Frame building (b) improved fish-bone model – Jamsek [97]

Inelastic beam-like models

With regard to the extension of the already mentioned elastic beam-like models, modelling of the inelastic behaviour of buildings by means of inelastic beam-like models have been also investigated in the literature.

McCallen, Romstad and Chajes in [98, 99, 100] updated the elastic continuum model (discussed above) in order to consider also material non-linearities. They assumed that the structural elements of the lattice (which is a repetitive reticular structure) were characterised by the Ozdemir model elasto-platic behaviour with kinematic hardening [101] and derived the instantaneous stiffness matrix of the continuum finite element. The inelastic continuum model was adopted for predicting the static and dynamic non-linear analysis of planar lattice frames.

Gicev and Trifunac [102] analysed horizontal shear deformations in a 1-D building supported by a half-space and excited by a vertically propagating shear wave. The 1-D structure was characterised by elasto-plastic material properties.

Kuang and Huang [103] modelled a wall-frame structure with uniform stiffness as an equivalent continuum system consisting of a combination of a flexural cantilever and a shear cantilever. The model is based on the equivalent continuum system proposed by Miranda et al., but it is discretized by one flexural and one shear deformation elements at each storey, as shown in Figure 1.22. Furthermore, in the proposed model the deformation compatibility constraints

are set at the floor levels where the storey mass is lumped. In this case, a bilinear hysteretic model is used for the material properties of flexural and shear cantilevers.

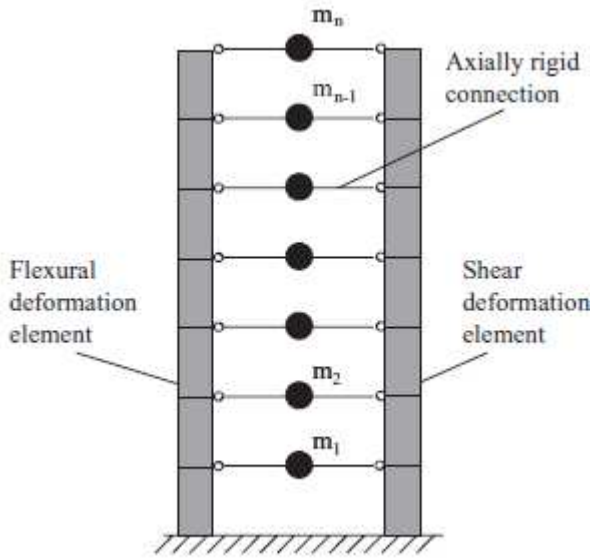

Figure 1.22 – Mass distribution, flexural and shear deformation elements and floor links in the proposed model - Kuang and Huang [103]

In the beam-like models, coupling shear and bending deformation already proposed in the literature, no attention on the shear locking effect has been paid. In the Kuang and Huang's work these contributions have been considered separately, however this separation can introduce further difficulties in the calibration strategies if the model has to be considered equivalent to a building structure. With reference to the spatial behaviour, further potential problems may arise coupling shear and torsional deformation fields.

SECTION 2. **THE PROPOSED BEAM-LIKE MODEL**

In this section, the proposed beam-like model is introduced. The main purpose of this research is to propose a simplified model considered representative of the dynamic behaviour of building structures both in linear and non-linear context. In this section an inhomogeneous three-dimensional beam-like model is introduced with the aim to establish a satisfactory equivalence with the linear or non-linear dynamic response provided by a three-dimensional FEM model of the building.

Firstly, the elastic behaviour is addressed and discussed, then an inelastic beam-like model is proposed and described by exploiting the non-linear behaviour.

The proposed non-uniform elastic beam-like model is able to take into account two different irregularities. In particular, this model is suitable for the schematization of real buildings that do not have a uniform mass and stiffness distribution along their height and are characterised by unsymmetrical plans. The equation of motion of the proposed beam-like model is derived through the application of Hamilton's principle. The linear dynamic behaviour of the non-uniform beam-like element is then evaluated by discretizing the continuous model according to a Rayleigh–Ritz approach based on an appropriate number of modal shapes of a uniform beam having only shear and torsional deformability.

Successively, an equivalent non-uniform inelastic beam-like model for the evaluation of the non-linear dynamic response of multi-storey buildings is presented. The non-linear and inhomogeneous model is characterised by a number of degrees of freedom equal to the number of floors and is capable to predict the non-linear dynamic response of an entire building adopting an opportune calibration based on the results of pushover analyses performed in certain directions for prescribed distribution of forces. As better specified in the following, the inelastic beam-like model aims at representing the non-linear behaviour of the building along a specific loading direction. The non-linear model, therefore, is defined as plane beam, nevertheless it is able to represent irregular buildings since it takes into account the spatial behaviour of the structure being calibrated on the base of a spatial pushover analysis.

The equivalent non-uniform inelastic beam-like model can be studied following two different approaches. The first approach considers a FE discretization of the equivalent beam, where each beam element represents an inter-storey of the building, as described in Par. 2.2. The second approach discretizes the equivalent beam according to a different displacement-based strategy that considers the exact static displacement function of a multi-stepped shear beam, as described in Par. 2.3.

2.1 NON-UNIFORM SHEAR-TORSIONAL BEAM-LIKE MODEL WITH PLANAR ECCENTRICITY – LINEAR ELASTIC BEHAVIOUR

The proposed model consists of a 3D shear-torsional cantilever beam able to reproduce the dynamic behaviour of multi-storey buildings. The equivalent beam has non-uniform stepwise cross-section, in order to correctly reproduce a multi-storey building with non-uniform stiffness distribution due to the decreasing column cross sections along the height and the presence of infills. Furthermore, planar irregularities due to the unsymmetrical distribution of the columns

or shear walls can be taken into account. This kind of irregularity must be properly considered since it induces eccentricity between the Stiffness Centre and the Mass Centre, thus causing unneglectable torsional effects. Each portion of the beam represents a building inter-storey, whose shear and torsional stiffness are initially approximately evaluated according to a geometrical consistent reference model. Stiffness contributions due to beams and floors of the building can be neglected (rigid floor hypothesis) or considered by means of appropriate stiffness reduction coefficients, as it will be shown later. When computing inertia forces, floor masses and gravity loads are supposed lumped at the floor level, while column masses are considered distributed along the beam-like axis or concentrated at the floor levels. Once the beam-like model of the entire building is defined, it can be calibrated on a reduced number of modal properties of the building itself.

The governing equations of both the static and dynamic responses are derived by means of the Hamilton's principle.

In order to evaluate the response of the equivalent beam by considering a limited number of degrees of freedom, an original Rayleigh-Ritz discretization based on an appropriate number of mode shapes of a uniform cantilever beam having only shear and torsional deformability is adopted.

Firstly, the equations of motion of the beam-like model in the generalised space are derived through the application of Hamilton's principle. Successively, the eigen problem, related to the evaluation of natural frequencies and mode shapes, is solved. Finally, the responses of the beam-like subjected to static or earthquake loads are evaluated.

2.1.1 Kinematics of the beam-like model

The proposed beam-like model is conceived for establishing an equivalence with 3D structures (Figure 2.1a) by means of a spatial beam element (Figure 2.1d). With reference to the k-th storey of the building, shown in Figure 2.1d, in the X,Y plane the Mass Centre (CM) and the Stiffness Centre (CS) will be assumed as not coincident, thus inducing a torsional behaviour of the structure. It is worth noting that, at each floor, the CM point is placed on the global vertical axis Z and, consequently, the CS coordinates coincide with the CS-CM eccentricity $\left(e_{x,k}, e_{y,k}\right)$. Each k-th building inter-storey (Figure 2.1b) is modelled by means of an equivalent beam segment having the same height h_k, uniform stiffness properties, uniform distributed masses $m_{x,k}, m_{y,k}$ and second order moment $I_{0,k}$. Concentrated values for the masses $M_{x,k}, M_{y,k}$ as well as the second order moment $\overline{I}_{0,k}$ are applied at the end of each beam segment in order to simulate the presence of beam and floor masses and applied loadings (Figure 2.1c).

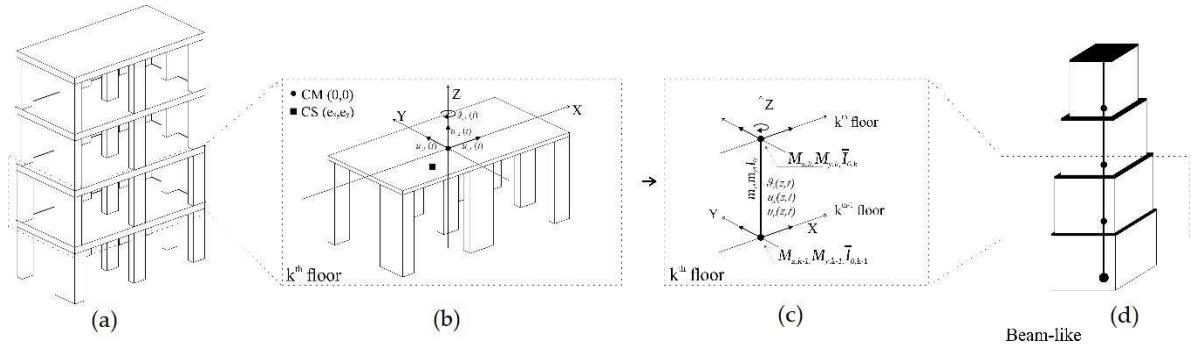

Figure 2.1 - (a) 3D structure (b) generic *k*-th inter-storey (c) equivalent beam segment (d) beam-like model

According to the assumed hypothesis of rigid floors, very often adopted in the literature, the end of each column, which has the coordinates $\left(x_{i,k}, y_{i,k}\right)$ at each k-th floor level, has the following displacement components:

$$u_{xi,k}\left(t\right) = u_{x,k}\left(t\right) + \vartheta_{z,k}\left(t\right) y_{i,k} \tag{2.1.1}$$

$$u_{yi,k}\left(t\right) = u_{y,k}\left(t\right) - \vartheta_{z,k}\left(t\right) x_{i,k} \tag{2.1.2}$$

where $u_{x,k}\left(t\right), u_{y,k}\left(t\right), \vartheta_{z,k}\left(t\right)$ are the displacement components and the rotation of the CM of the k-th floor level.

It is worth noting that displacements in X and Y directions and axis rotation of the equivalent beam are continuous functions of the abscissa z, denoted as $u_x\left(z,t\right), u_y\left(z,t\right), \vartheta_z\left(z,t\right)$.

The complete non-uniform beam-like model is obtained by the sequence of all the beam segments with uniform properties, as shown in Figure 2.1d.

2.1.2 The inter-storey shear and torsional stiffness

The equivalent beam shear stiffness in the two principal directions, denoted as $\hat{R}_{x,k}, \hat{R}_{y,k}$, and the torsional stiffness, denoted as $\hat{C}_k$, are obtained for the k-th segment by considering the contributes of all n_E columns of the k-th inter-storey of the building whose base points have planar coordinates $\left(x_{i,k}, y_{i,k}\right)$. The adopted inter-storey stiffness values are:

$$\hat{R}_{x,k} = \sum_{i=1}^{n_E} R_{xi,k} \tag{2.1.3a}$$

$$\hat{R}_{y,k} = \sum_{i=1}^{n_E} R_{yi,k} \tag{2.1.3b}$$

$$\hat{C}_k = \left(\sum_{i=1}^{n_E} C_{i,k} + \sum_{i=1}^{n_E} R_{xi,k}\, y_{i,k}^2 + \sum_{i=1}^{n_E} R_{yi,k}\, x_{i,k}^2 \right) \tag{2.1.3c}$$

If a shear type behaviour can be assumed, the flexural and torsional stiffness of each column can be expressed as:

$$R_{xi,k} = \frac{12EJ_{yi,k}}{h_k^3} \qquad R_{yi,k} = \frac{12EJ_{xi,k}}{h_k^3} \qquad C_{i,k} = \frac{GJ_{zi,k}}{h_k} \tag{2.1.4}$$

where E and G are Young modulus and shear modulus respectively, $J_{xi,k}$ and $J_{yi,k}$ the moment of inertia with respect to X and Y axes, $J_{zi,k}$ the rotational inertia moment with respect to Z axis of the i-th column of the k-th inter-storey.
The CS coordinates for the k-th segment are:

$$e_{x,k} = \frac{\sum_{i=1}^{N_E} R_{yi,k} x_{i,k}}{\hat{R}_{y,k}} \qquad e_{y,k} = \frac{\sum_{i=1}^{N_E} R_{xi,k} y_{i,k}}{\hat{R}_{x,k}} \tag{2.1.5}$$

In order to take into account the unknown or not properly identified structural properties (floor out-of-plane deformability, beam-column stiffness ratio and uncertainty on the position of the Stiffness Centre at each floor), three correction coefficients are introduced. These coefficients, denoted as k_x, k_y, k_c, are used to better calibrate the shear stiffness along the X and Y directions and the torsional one that are listed in Equations (2.1.3). The actual stiffness values are therefore provided by the following expressions:

$$R_{x,k} = k_x \hat{R}_{x,k} \qquad R_{y,k} = k_y \hat{R}_{y,k} \qquad C_k = k_c \hat{C}_k \tag{2.1.6}$$

In the following, each of these coefficients is assumed to have the same value in all the inter-storeys and is evaluated by means of an iterative optimization procedure described in Par. 2.1.7. Following this linear calibration strategy, the stiffness ratio between the floor remains the same as the initial one, defined according to the geometry of the building.
The choice of using the same correction coefficients for all the inter-storeys is justified by the need of mantaining the calibration procedure as simple and fast as possible. In fact, the assumption of different correction coefficients for each inter-storey would lead to a more complicated mathematical problem requiring at least as many input data as the number of coefficients. The adopted use of three correction coefficients will require, instead, the knowledge of only the first three modal characteristics of the building, as better specified in the following. Furthermore, in the case of different correction coefficient for each inter-storey, the mathematical problem would require the application of some constraints in order to avoid solutions not consistent with the actual stiffness distribution along the height of the building (for example for a regular building inter-storey stiffness at the lower floors smaller than the one at the higher floors).
Future developments of the study may be related to a better definition of different calibration coefficients at each inter-storey.

2.1.3 Rayleigh-Ritz discretization and Hamilton's principle

In order to evaluate the response of the non-uniform equivalent beam by introducing a limited number of degrees of freedom, a Rayleigh-Ritz discretization was performed. The discretization is based on the choice of an appropriate N number of mode shapes of a uniform shear cantilever beam, as displacement shape functions of the non-uniform beam, defined as follows:

$$\psi_m(\zeta) = \sin\left(\frac{\pi}{2}(2m-1)\zeta\right) \qquad m = 1, 2, ..., \infty \tag{2.1.7}$$

where $\zeta = z/h$ is the dimensionless abscissa of the beam, z the along-axis abscissa and h the beam length.
The introduced displacement components can be expressed as the sum of each shape function contribution as follows:

$$u_x(\zeta,t) = \sum_{i=1}^{N} \psi_i(\zeta) q_{i_x}(t) = \sum_{i=1}^{N} \psi_i q_{i_x} \tag{2.1.8a}$$

$$u_y(\zeta,t) = \sum_{i=1}^{N} \psi_i(\zeta) q_{i_y}(t) = \sum_{i=1}^{N} \psi_i q_{i_y} \tag{2.1.8b}$$

$$\vartheta_z(\zeta,t) = \sum_{i=1}^{N} \psi_i(\zeta) q_{i_\vartheta}(t) = \sum_{i=1}^{N} \psi_i q_{i_\vartheta} \tag{2.1.8c}$$

$q_{i_x}(t), q_{i_y}(t), q_{i_\vartheta}(t)$ being the generalised i-th coordinates along the X, Y, ϑ directions, which represent the contribution of the single shape function to the total response.
For the evaluation of the seismic response of the building, displacements $u_{gx}(t) = u_x(\zeta = 0, t), u_{gy}(t) = u_y(\zeta = 0, t)$ at the base of the beam $(\zeta = 0)$ have been introduced in the formulation in order to take into account seismic excitations. However, also the static response of the building has been calculated considering transversal loads applied along the height with assumed distributions. The governing equations of the static and dynamic problem of the multi-stepped beam in the generalised space are derived through the application of Hamilton's principle.

$$\int_{t_0}^{t_1} \left[\delta(T - U) + \delta W_{NC} \right] dt = 0 \qquad \forall t_0, t_1 \tag{2.1.9}$$

Firstly, the case of the static problem, which involves the contribution of the elastic energy and the work associated with the non-conservative forces, is considered. Secondly, the dynamic problem of the beam subjected to base motion is taken into account. Non-conservative forces, related to the viscous damping forces, are not considered in the following since for simplicity a classical damping model is assumed and, as a consequence, the damping will be introduced as modal damping ratios in the reduced modal space. Since the adopted beam model has only shear deformability, it does not account for second order geometrical effects and a geometric stiffness matrix is not introduced.
In the present formulation, primes and dots denote differentiation with respect to the normalized abscissa ζ and time t, respectively.

2.1.4 Static problem

The governing equations of the static problem of the beam-like model in the generalised space are derived through the application of Hamilton's principle, which in this case can be reduced to the contribution of the elastic energy U and the work associated with the non-conservative forces W_{NC} only, as follows:

$$\int_{t_0}^{t_1}\left[-\delta U+\delta W_{NC}\right]dt=0 \qquad \forall t_0,t_1 \qquad \rightarrow \qquad \delta U=\delta W_{NC} \tag{2.1.10}$$

The Rayleigh-Ritz discretization introduced in Paragraph 2.1.3 is performed.
According to the beam-like shear-torsional behaviour, the elastic energy U is given as follows:

$$\begin{aligned} U=&\left(\frac{1}{2}\frac{1}{h}\sum_{k=1}^{N_f}GA_{x,k}\int_{\zeta_{k-1}}^{\zeta_k}\left[\sum_{i=1}^{N}\psi'_i(\zeta)q_{i_x}(t)+e_{y,k}\sum_{i=1}^{N}\psi'_i(\zeta)q_{i_\vartheta}(t)\right]^2 d\zeta+\right.\\ &+\frac{1}{2}\frac{1}{h}\sum_{k=1}^{N_f}GA_{y,k}\int_{\zeta_{k-1}}^{\zeta_k}\left[\sum_{i=1}^{N}\psi'_i(\zeta)q_{i_y}(t)-e_{x,k}\sum_{i=1}^{N}\psi'_i(\zeta)q_{i_\vartheta}(t)\right]^2 d\zeta+\\ &\left.+\frac{1}{2}\frac{1}{h}\sum_{k=1}^{N_f}GJ_{z,k}\int_{\zeta_{k-1}}^{\zeta_k}\left[\sum_{i=1}^{N}\psi'_i(\zeta)q_{i_\vartheta}(t)\right]^2 d\zeta\right) \end{aligned} \tag{2.1.11}$$

where N_f is the number of floors, $GA_{x,k}, GA_{y,k}, GJ_{z,k}$ represent the shear and torsional stiffness, constant for each k-th beam segment, that can be computed in accordance with the equivalent beam model adopted as follows:

$$GA_{x,k}=R_{x,k}\cdot h_k \tag{2.1.12a}$$

$$GA_{y,k}=R_{y,k}\cdot h_k \tag{2.1.12b}$$

$$GJ_{z,k}=C_k\cdot h_k \tag{2.1.12c}$$

Lumped horizontal forces $F_{x,k}, F_{y,k}$ with eccentricity $\left(\overline{e}_{x,k}, \overline{e}_{y,k}\right)$ with respect to CM and torsional moment $M_{\vartheta,k}$ are considered acting at the k-th floor level.
The work associated with the non-conservative forces W_{NC} is:

$$\begin{aligned} W_{NC}=&\sum_{k=1}^{N_f}F_{x,k}\left[\sum_{i=1}^{N}\psi_i(\zeta=\frac{z_k}{h})q_{i_x}+\overline{e}_y\sum_{i=1}^{N}\psi_i(\zeta=\frac{z_k}{h})q_{i_\vartheta}\right]+\\ &+\sum_{k=1}^{N_f}F_{y,k}\left[\sum_{i=1}^{N}\psi_i(\zeta=\frac{z_k}{h})q_{i_y}-\overline{e}_x\sum_{i=1}^{N}\psi_i(\zeta=\frac{z_k}{h})q_{i_\vartheta}\right]+\\ &+\sum_{k=1}^{N_f}M_{\vartheta,k}\left[\sum_{i=1}^{N}\psi_i(\zeta=\frac{z_k}{h})q_{i_\vartheta}\right] \end{aligned} \tag{2.1.13}$$

Introducing Equations (2.1.11) and (2.1.13) in Hamilton's principle leads to the following expression:

$$\frac{1}{h}\sum_{k=1}^{N_f} GA_{x,k}\int_{\zeta_{k-1}}^{\zeta_k}\sum_{i=1}^{N}\sum_{j=1}^{N}\psi'_i(\zeta)\psi'_j(\zeta)\,d\zeta\,q_{i_x}\delta q_{j_x}+\frac{1}{h}\sum_{k=1}^{N_f} e_{y,k}GA_{x,k}\int_{\zeta_{k-1}}^{\zeta_k}\sum_{i=1}^{N}\sum_{j=1}^{N}\psi'_i(\zeta)\psi'_j(\zeta)\,d\zeta\,q_{i_\vartheta}\delta q_{j_x}+$$

$$+\frac{1}{h}\sum_{k=1}^{N_f} e_{y,k}GA_{x,k}\int_{\zeta_{k-1}}^{\zeta_k}\sum_{i=1}^{N}\sum_{j=1}^{N}\psi'_i(\zeta)\psi'_j(\zeta)\,d\zeta\,q_{i_x}\delta q_{j_\vartheta}+\frac{1}{h}\sum_{k=1}^{N_f} GA_{y,k}\int_{\zeta_{k-1}}^{\zeta_k}\sum_{i=1}^{N}\sum_{j=1}^{N}\psi'_i(\zeta)\psi'_j(\zeta)\,d\zeta\,q_{i_y}\delta q_{j_y}+$$

$$-\frac{1}{h}\sum_{k=1}^{N_f} e_{x,k}GA_{y,k}\int_{\zeta_{k-1}}^{\zeta_k}\sum_{i=1}^{N}\sum_{j=1}^{N}\psi'_i(\zeta)\psi'_j(\zeta)\,d\zeta\,q_{i_\vartheta}\delta q_{j_y}-\frac{1}{h}\sum_{k=1}^{N_f} e_{x,k}GA_{y,k}\int_{\zeta_{k-1}}^{\zeta_k}\sum_{i=1}^{N}\sum_{j=1}^{N}\psi'_i(\zeta)\psi'_j(\zeta)\,d\zeta\,q_{iy}\delta q_{j_\vartheta}+$$

$$+\frac{1}{h}\sum_{k=1}^{N_f} GJ_{z,k}\int_{\zeta_{k-1}}^{\zeta_k}\sum_{i=1}^{N}\sum_{j=1}^{N}\psi'_i(\zeta)\psi'_j(\zeta)\,d\zeta\,q_{i_\vartheta}\delta q_{j_\vartheta}+\frac{1}{h}\sum_{k=1}^{N_f} e_{y,k}^2GA_{x,k}\int_{\zeta_{k-1}}^{\zeta_k}\sum_{i=1}^{N}\sum_{j=1}^{N}\psi'_i(\zeta)\psi'_j(\zeta)\,d\zeta\,q_{i_\vartheta}\delta q_{j_\vartheta}+$$

$$+\frac{1}{h}\sum_{k=1}^{N_f} e_{x,k}^2GA_{y,k}\int_{\zeta_{k-1}}^{\zeta_k}\sum_{i=1}^{N}\sum_{j=1}^{N}\psi'_i(\zeta)\psi'_j(\zeta)\,d\zeta\,q_{i_\vartheta}\delta q_{j_\vartheta}=$$

$$=\sum_{k=1}^{N_f} F_{x,k}\sum_{j=1}^{N}\psi_{j,k}\delta q_{j_x}+\sum_{k=1}^{N_f} F_{x,k}\bar{e}_y\sum_{j=1}^{N}\psi_{j,k}\delta q_{j_\vartheta}+$$

$$+\sum_{k=1}^{N_f} F_{y,k}\sum_{j=1}^{N}\psi_{j,k}\delta q_{j_y}+\sum_{k=1}^{N_f} F_{y,k}\left(-\bar{e}_x\right)\sum_{j=1}^{N}\psi_{j,k}\delta q_{j_\vartheta}+\sum_{k=1}^{N_f} M_{\vartheta,k}\sum_{j=1}^{N}\psi_{j,k}\delta q_{j_\vartheta}$$

$$\forall\,\delta q_{j_x},\delta q_{j_y},\delta q_{j_\vartheta} \tag{2.1.14}$$

The mathematical notation of Hamilton's principle can be simplified by omitting for convenience the dependency on ζ, and by rearranging all the terms in a more compact manner as follows:

$$\boldsymbol{\delta q}^T\mathbf{K}\mathbf{q}=\boldsymbol{\delta q}^T\mathbf{F} \qquad \forall\boldsymbol{\delta q} \tag{2.1.15}$$

leading to the governing equations of the static problem of the proposed equivalent multi-stepped beam in the generalised space in matrix notation as follows:

$$\mathbf{K}\mathbf{q}=\mathbf{F} \tag{2.1.16}$$

where $\mathbf{K}$ is the generalised Stiffness Matrix, $\mathbf{F}$ the load vector and $\mathbf{q}$ the vector of generalised coordinates:

$$\mathbf{K}=\begin{bmatrix}\mathbf{K}_x & & \mathbf{K}_{x\vartheta}\\ & \mathbf{K}_y & \mathbf{K}_{y\vartheta}\\ \mathbf{K}_{\vartheta x} & \mathbf{K}_{\vartheta y} & \mathbf{K}_\vartheta\end{bmatrix} \qquad \mathbf{F}=\begin{bmatrix}\mathbf{F}_x\\ \mathbf{F}_y\\ \mathbf{M}_\vartheta\end{bmatrix} \qquad \mathbf{q}=\begin{bmatrix}\mathbf{q}_x\\ \mathbf{q}_y\\ \mathbf{q}_\vartheta\end{bmatrix} \tag{2.1.17}$$

The expressions of the dimensionless terms of the stiffness matrix and of the load vector are shown below.

Generalised Stiffness Matrix.

$$\mathbf{K}_{j_x i_x} = \frac{1}{h}\sum_{k=1}^{N_f} GA_{x,k}\int_{\zeta_{k-1}}^{\zeta_k} \psi'_i \psi'_j \, d\zeta \tag{2.1.18a}$$

$$\mathbf{K}_{j_y i_y} = \frac{1}{h}\sum_{k=1}^{N_f} GA_{y,k}\int_{\zeta_{k-1}}^{\zeta_k} \psi'_i \psi'_j \, d\zeta \tag{2.1.18b}$$

$$\mathbf{K}_{j_\vartheta i_\vartheta} = \frac{1}{h}\sum_{k=1}^{N_f}\left(GJ_{z,k} + e_{y,k}^2 GA_{x,k} + e_{x,k}^2 GA_{y,k}\right)\int_{\zeta_{k-1}}^{\zeta_k} \psi'_i \psi'_j \, d\zeta \tag{2.1.18c}$$

$$\mathbf{K}_{j_x i_\vartheta} = \mathbf{K}_{j_\vartheta i_x} = \frac{1}{h}\sum_{k=1}^{N_f} e_{y,k} GA_{x,k}\int_{\zeta_{k-1}}^{\zeta_k} \psi'_i \psi'_j \, d\zeta \tag{2.1.18d}$$

$$\mathbf{K}_{j_y i_\vartheta} = \mathbf{K}_{j_\vartheta i_y} = -\frac{1}{h}\sum_{k=1}^{N_f} e_{x,k} GA_{y,k}\int_{\zeta_{k-1}}^{\zeta_k} \psi'_i \psi'_j \, d\zeta \tag{2.1.18e}$$

Load vector equivalent to the applied static forces.

$$\mathbf{F}_{j_x} = \sum_{k=1}^{N_f} F_{x,k}\psi_{j,k} \tag{2.1.19a}$$

$$\mathbf{F}_{j_y} = \sum_{k=1}^{N_f} F_{y,k}\psi_{j,k} \tag{2.1.19b}$$

$$\mathbf{M}_{j_\vartheta} = \sum_{k=1}^{N_f}\left(F_{x,k}\overline{e}_y - F_{y,k}\overline{e}_x + M_{\vartheta,k}\right)\psi_{j,k} \tag{2.1.19c}$$

2.1.5 Equations of motion

The equations of motion of the proposed beam-like model in the generalised space are derived through the application of Hamilton's principle.

The explicit expression of the kinetic energy T is given as follows:

$$\begin{aligned} T = \Bigg(& \frac{1}{2}h\sum_{k=1}^{N_f} m_{x,k}\int_{\zeta_{k-1}}^{\zeta_k}\left[\sum_{i=1}^{N}\psi_i(\zeta)\dot{q}_{i_x}(t) + \dot{u}_{gx}(t)\right]^2 d\zeta + \frac{1}{2}h\sum_{k=1}^{N_f} m_{y,k}\int_{\zeta_{k-1}}^{\zeta_k}\left[\sum_{i=1}^{N}\psi_i(\zeta)\dot{q}_{i_y}(t) + \dot{u}_{gy}(t)\right]^2 d\zeta + \\ & + \frac{1}{2}h\sum_{k=1}^{N_f} I_{o,k}\int_{\zeta_{k-1}}^{\zeta_k}\left[\sum_{i=1}^{N}\psi_i(\zeta)\dot{q}_{i_\vartheta}(t)\right]^2 d\zeta + \frac{1}{2}\sum_{k=1}^{N_f} M_{x,k}\left[\sum_{i=1}^{N}\psi_i(\zeta=\frac{z_k}{h})\dot{q}_{i_x}(t) + \dot{u}_{gx}(t)\right]^2 + \\ & + \frac{1}{2}\sum_{k=1}^{N_f} M_{y,k}\left[\sum_{i=1}^{N}\psi_i(\zeta=\frac{z_k}{h})\dot{q}_{i_y}(t) + \dot{u}_{gy}(t)\right]^2 + \frac{1}{2}\sum_{k=1}^{N_f}\overline{I}_{o,k}\left[\sum_{i=1}^{N}\psi_i(\zeta=\frac{z_k}{h})\dot{q}_{i_\vartheta}(t)\right]^2\Bigg) \end{aligned} \tag{2.1.20}$$

The expression of the elastic energy U is given by Equation (2.1.11).

Since the beam is subjected to earthquake base motion, no external loads are applied and, for the kinematic hypothesis of the shear-torsional beam model (therefore in absence of axial deformability of the columns), the work associated with the gravity loads is equal to zero. Structural damping is neglected and will be later introduced, in terms of modal damping ratios, in the uncoupled equations of motions.

The work associated with the non-conservative forces is equal to zero.

$$W_{NC} = 0 \tag{2.1.21}$$

Therefore, Hamilton's principle can be reduced to the contribution of the kinematic T and elastic U energy only, as follows:

$$\int_{t_0}^{t_1} \left[\delta \left(T - U \right) \right] dt = 0 \qquad \forall t_0, t_1 \tag{2.1.22}$$

In view of the above expressions of the kinetic and elastic energies, integrating by parts the kinematic terms in Hamilton's principle leads to the following expression:

$$\begin{aligned}
&\int_{t_0}^{t_1} \Bigg\{ h \sum_{k=1}^{N_f} m_{x,k} \int_{\zeta_{k-1}}^{\zeta_k} \sum_{i=1}^{N} \sum_{j=1}^{N} \psi_i(\zeta) \psi_j(\zeta) \, d\zeta \, \ddot{q}_{i_x}(t) \, \delta q_{j_x} + \sum_{k=1}^{N_f} M_{x,k} \sum_{i=1}^{N} \sum_{j=1}^{N} \psi_i(\zeta_k) \psi_j(\zeta_k) \ddot{q}_{i_x}(t) \, \delta q_{j_x} + \\
&+ h \sum_{k=1}^{N_f} m_{y,k} \int_{\zeta_{k-1}}^{\zeta_k} \sum_{i=1}^{N} \sum_{j=1}^{N} \psi_i(\zeta) \psi_j(\zeta) \, d\zeta \, \ddot{q}_{i_y}(t) \, \delta q_{j_y} + \sum_{k=1}^{N_f} M_{y,k} \sum_{i=1}^{N} \sum_{j=1}^{N} \psi_i(\zeta_k) \psi_j(\zeta_k) \ddot{q}_{i_y}(t) \, \delta q_{j_y} + \\
&+ h \sum_{k=1}^{N_f} I_{o,k} \int_{\zeta_{k-1}}^{\zeta_k} \sum_{i=1}^{N} \sum_{j=1}^{N} \psi_i(\zeta) \psi_j(\zeta) \, d\zeta \, \ddot{q}_{i_\vartheta}(t) \, \delta q_{j_\vartheta} + \sum_{k=1}^{N_f} \overline{I}_{o,k} \sum_{i=1}^{N} \sum_{j=1}^{N} \psi_i(\zeta_k) \psi_j(\zeta_k) \ddot{q}_{i_\vartheta}(t) \, \delta q_{j_\vartheta} + \\
&+ \frac{1}{h} \sum_{k=1}^{N_f} GA_{x,k} \int_{\zeta_{k-1}}^{\zeta_k} \sum_{i=1}^{N} \sum_{j=1}^{N} \psi'_i(\zeta) \psi'_j(\zeta) \, d\zeta \, q_{i_x}(t) \, \delta q_{j_x} + \frac{1}{h} \sum_{k=1}^{N_f} e_{y,k} GA_{x,k} \int_{\zeta_{k-1}}^{\zeta_k} \sum_{i=1}^{N} \sum_{j=1}^{N} \psi'_i(\zeta) \psi'_j(\zeta) \, d\zeta \, q_{i_\vartheta}(t) \, \delta q_{j_x} + \\
&+ \frac{1}{h} \sum_{k=1}^{N_f} e_{y,k} GA_{x,k} \int_{\zeta_{k-1}}^{\zeta_k} \sum_{i=1}^{N} \sum_{j=1}^{N} \psi'_i(\zeta) \psi'_j(\zeta) \, d\zeta \, q_{i_x}(t) \, \delta q_{j_\vartheta} + \frac{1}{h} \sum_{k=1}^{N_f} GA_{y,k} \int_{\zeta_{k-1}}^{\zeta_k} \sum_{i=1}^{N} \sum_{j=1}^{N} \psi'_i(\zeta) \psi'_j(\zeta) \, d\zeta \, q_{i_y}(t) \, \delta q_{j_y} + \\
&- \frac{1}{h} \sum_{k=1}^{N_f} e_{x,k} GA_{y,k} \int_{\zeta_{k-1}}^{\zeta_k} \sum_{i=1}^{N} \sum_{j=1}^{N} \psi'_i(\zeta) \psi'_j(\zeta) \, d\zeta \, q_{i_\vartheta}(t) \, \delta q_{j_y} - \frac{1}{h} \sum_{k=1}^{N_f} e_{x,k} GA_{y,k} \int_{\zeta_{k-1}}^{\zeta_k} \sum_{i=1}^{N} \sum_{j=1}^{N} \psi'_i(\zeta) \psi'_j(\zeta) \, d\zeta \, q_{iy}(t) \, \delta q_{j_\vartheta} + \\
&+ \frac{1}{h} \sum_{k=1}^{N_f} GJ_{z,k} \int_{\zeta_{k-1}}^{\zeta_k} \sum_{i=1}^{N} \sum_{j=1}^{N} \psi'_i(\zeta) \psi'_j(\zeta) \, d\zeta \, q_{i_\vartheta}(t) \, \delta q_{j_\vartheta} + \frac{1}{h} \sum_{k=1}^{N_f} e_{y,k}^2 GA_{x,k} \int_{\zeta_{k-1}}^{\zeta_k} \sum_{i=1}^{N} \sum_{j=1}^{N} \psi'_i(\zeta) \psi'_j(\zeta) \, d\zeta \, q_{i_\vartheta}(t) \, \delta q_{j_\vartheta} + \\
&+ \frac{1}{h} \sum_{k=1}^{N_f} e_{x,k}^2 GA_{y,k} \int_{\zeta_{k-1}}^{\zeta_k} \sum_{i=1}^{N} \sum_{j=1}^{N} \psi'_i(\zeta) \psi'_j(\zeta) \, d\zeta \, q_{i_\vartheta}(t) \, \delta q_{j_\vartheta} + \\
&+ \ddot{u}_{gx}(t) h \sum_{k=1}^{N_f} m_{x,k} \int_{\zeta_{k-1}}^{\zeta_k} \sum_{j=1}^{N} \psi_j(\zeta) \, d\zeta \, \delta q_{j_x} + \ddot{u}_{gx}(t) \sum_{k=1}^{N_f} M_{x,k} \sum_{j=1}^{N} \psi_j(\zeta_k) \, \delta q_{j_x} + \\
&+ \ddot{u}_{gy}(t) h \sum_{k=1}^{N_f} m_{y,k} \int_{\zeta_{k-1}}^{\zeta_k} \sum_{j=1}^{N} \psi_j(\zeta) \, d\zeta \, \delta q_{j_y} + \ddot{u}_{gy}(t) \sum_{k=1}^{N_f} M_{y,k} \sum_{j=1}^{N} \psi_j(\zeta_k) \, \delta q_{j_y} \Bigg\} dt = 0
\end{aligned}$$

$$\forall t_0, t_1, \delta q_{j_x}, \delta q_{j_y}, \delta q_{j_\vartheta} \tag{2.1.23}$$

where $j = 1, 2, \ldots N$ and $\zeta_k = \frac{z_k}{h}$.

The mathematical notation of Hamilton's principle can be simplified by omitting for convenience the dependency on t and ζ, and, furthermore, by rearranging all the terms in a more compact manner as follows:

$$\boldsymbol{\delta q}^T \mathbf{M}\ddot{\mathbf{q}} + \boldsymbol{\delta q}^T \mathbf{K}\mathbf{q} = \boldsymbol{\delta q}^T \mathbf{P} \qquad \forall \boldsymbol{\delta q} \tag{2.1.24}$$

leading to the equations of motion of the proposed equivalent multi-stepped beam in the generalised space in matrix notation as follows:

$$\mathbf{M}\ddot{\mathbf{q}} + \mathbf{K}\mathbf{q} = \mathbf{P} \tag{2.1.25}$$

where $\mathbf{M}$ is the generalised Mass Matrix, $\mathbf{K}$ the generalised Stiffness Matrix introduced in Paragraph 2.1.4, $\mathbf{P}$ the equivalent generalised load vector and $\mathbf{q}$ the vector of generalised coordinates:

$$\mathbf{M} = \begin{bmatrix} \mathbf{M}_x & & \\ & \mathbf{M}_y & \\ & & \mathbf{M}_\vartheta \end{bmatrix} \quad \mathbf{K} = \begin{bmatrix} \mathbf{K}_x & & \mathbf{K}_{x\vartheta} \\ & \mathbf{K}_y & \mathbf{K}_{y\vartheta} \\ \mathbf{K}_{\vartheta x} & \mathbf{K}_{\vartheta y} & \mathbf{K}_\vartheta \end{bmatrix} \quad \mathbf{P} = \begin{bmatrix} \mathbf{P}_x \\ \mathbf{P}_y \\ \mathbf{P}_\vartheta \end{bmatrix} \quad \mathbf{q} = \begin{bmatrix} \mathbf{q}_x \\ \mathbf{q}_y \\ \mathbf{q}_\vartheta \end{bmatrix} \tag{2.1.26}$$

The expressions of the dimensionless terms of the matrices are shown below.

Generalised Mass Matrix.

$$\mathbf{M}_{j_x i_x} = h \sum_{k=1}^{N_f} m_{x,k} \int_{\zeta_{k-1}}^{\zeta_k} \psi_i \psi_j d\zeta + \sum_{k=1}^{N_f} M_{x,k} \psi_{i,k} \psi_{j,k} \tag{2.1.27a}$$

$$\mathbf{M}_{j_y i_y} = h \sum_{k=1}^{N_f} m_{y,k} \int_{\zeta_{k-1}}^{\zeta_k} \psi_i \psi_j d\zeta + \sum_{k=1}^{N_f} M_{y,k} \psi_{i,k} \psi_{j,k} \tag{2.1.27b}$$

$$\mathbf{M}_{j_\vartheta i_\vartheta} = h \sum_{k=1}^{N_f} I_{0,k} \int_{\zeta_{k-1}}^{\zeta_k} \psi_i \psi_j d\zeta + \sum_{k=1}^{N_f} \bar{I}_{o,k} \psi_{i,k} \psi_{j,k} \tag{2.1.27c}$$

Load vector equivalent to the seismic excitation.

$$\mathbf{P}_{j_x} = -\ddot{u}_{gx} h \sum_{k=1}^{N_f} m_{x,k} \int_{\zeta_{k-1}}^{\zeta_k} \psi_j d\zeta - \ddot{u}_{gx} \sum_{k=1}^{N_f} M_{x,k} \psi_{j,k} \tag{2.1.28a}$$

$$\mathbf{P}_{j_y} = -\ddot{u}_{gy} h \sum_{k=1}^{N_f} m_{y,k} \int_{\zeta_{k-1}}^{\zeta_k} \psi_j d\zeta - \ddot{u}_{gy} \sum_{k=1}^{N_f} M_{y,k} \psi_{j,k} \tag{2.1.28b}$$

$$\mathbf{P}_{j_\vartheta} = 0 \tag{2.1.28c}$$

where $\psi_{i,k}$ is the shape function evaluated at the floor level with abscissa z_k.

2.1.6 Eigen-problem

The modes of vibration in the generalised space, denoted as $\hat{\boldsymbol{\psi}}$, and the natural frequencies ω of the equivalent beam are obtained solving the following generalised eigen-problem:

$$\left[\mathbf{K} - \omega^2 \mathbf{M}\right] \hat{\boldsymbol{\psi}} = \mathbf{0} \tag{2.1.29}$$

where $\mathbf{M}$ and $\mathbf{K}$ are the Stiffness and Mass Matrices already seen in the previous paragraphs. Consequently, the mode shapes in the geometric space can be obtained by means of Equations (2.1.8), where the N displacement shape functions of a uniform beam, of the type given in Equation (2.1.7), are considered. Consequently, the j-th mode shape in the geometric space of

the equivalent non-uniform multi-stepped beam, denoted as vector function $\boldsymbol{\varphi}_j(\zeta)$, is obtained, in view of Equations (2.1.8), by multiplying each displacement shape function of the uniform beam $\psi_i(\zeta)$, $i=1,2,...,N$, considered for the discretization, times the corresponding eigen-vector components.

$$\varphi_{u,j}(\zeta)=\psi_1(\zeta)\hat{\psi}_{1_x j}+\psi_2(\zeta)\hat{\psi}_{2_x j}+\ldots+\psi_N(\zeta)\hat{\psi}_{N_x j} \tag{2.1.30a}$$

$$\varphi_{v,j}(\zeta)=\psi_1(\zeta)\hat{\psi}_{1_y j}+\psi_2(\zeta)\hat{\psi}_{2_y j}+\ldots+\psi_N(\zeta)\hat{\psi}_{N_y j} \tag{2.1.30b}$$

$$\varphi_{\vartheta,j}(\zeta)=\psi_1(\zeta)\hat{\psi}_{1_\vartheta j}+\psi_2(\zeta)\hat{\psi}_{2_\vartheta j}+\ldots+\psi_N(\zeta)\hat{\psi}_{N_\vartheta j} \tag{2.1.30c}$$

Equations (2.1.30) provide the three spatial components in the actual geometric space (Figure 2.1) of the j-th mode shape to be adopted to perform a suitable dynamic analysis of the equivalent non-uniform beam by means of a suitable modal superposition procedure, as shown later.

2.1.7 Shear and Torsional stiffness optimization

The correction coefficients k_x,k_y,k_c, introduced in Paragraph 2.1.2 in order to take into account all the unknown or improperly identified structural properties, are evaluated by means of an iterative procedure aiming at minimizing the following objective function:

$$O\left(k_x,k_y,k_c\right)=\underbrace{\sqrt{\sum_{j=1}^{n}\left(\frac{\omega_j\left(k_x,k_y,k_c\right)-\tilde{\omega}_j}{\tilde{\omega}_j}\right)^2}}_{frequencies}+\underbrace{\beta\left[1-\frac{\boldsymbol{\varphi}\cdot\tilde{\boldsymbol{\varphi}}^T}{\sqrt{\left(\boldsymbol{\varphi}\cdot\boldsymbol{\varphi}^T\right)\left(\tilde{\boldsymbol{\varphi}}\cdot\tilde{\boldsymbol{\varphi}}^T\right)}}\right]}_{\text{mod}\,al\ shapes} \tag{2.1.31}$$

where $n<3N$, being N the number of inter-storeys, and β a Boolean parameter.

The objective function O, dependent on the three correction coefficients k_x,k_y,k_c, represents a measure of the deviation with respect to target values of a given number n of natural frequencies ω_j and mode shapes $\boldsymbol{\varphi}_{j;k}$, collected in the modal displacement vector $\boldsymbol{\varphi}=\left[\boldsymbol{\varphi}_{1;k}\quad\boldsymbol{\varphi}_{2;k}\quad\ldots\quad\boldsymbol{\varphi}_{j;k}\quad\ldots\quad\boldsymbol{\varphi}_{n;k}\right]$, where $\boldsymbol{\varphi}_{j;k}=\left[\varphi_{u,j}(\zeta_k;k_x,k_y,k_c)\quad\varphi_{v,j}(\zeta_k;k_x,k_y,k_c)\right]$ is evaluated at suitably chosen m floor levels of dimensionless abscissa ζ_k, $k=1,...,m$ by means of the beam-like model. At each step of the iterative optimization procedure, the modal parameters are calculated by solving the eigen-problem in Equation (2.1.29) of the non-uniform equivalent beam by assuming trial values of the stiffness coefficients k_x,k_y,k_c. It is worth noting that the eigen-properties of the non-uniform beam-like model are strictly dependent on the values of the correction coefficients k_x,k_y,k_c. The target values, denoted with a superimposed tilde "~", represent the objective values which can be obtained by a three-dimensional FEM model of the building, if available, but can also be obtained by means of dynamic identification methods performed on real building without the need to develop a FEM model. In the applications reported in the following, these values will be obtained numerically by means of reference detailed linear FEM models.

Correction coefficients are assumed to vary into the range [0.1 1]. The choice of the upper bound of the range rises from the consideration that, since the considered beam exhibits only shear deformation, it is reasonably stiffer than the FEM model. The presence of out-of-plane floor deformability and flexural stiffness of the real structure leads to the identification of stiffness correction coefficients for the beam-like model lower than one. On the other hand, the lower bound has been chosen assuming that, since the initial shear and torsional stiffness of the beam-like have been defined according to the geometry of the building, a variation higher than 90% is not realistic. The parameter β is set equal to 0 for buildings with only one stiffness irregularity (either planar or vertical), equal to 1 on the other case. In the last case, indeed, because of the structural complexity, it is necessary to consider also the modes of vibration in the objective function in order to obtain reliable values of the correction coefficients through the optimization process.
The problem of the amount of data available to conduct a reliable calibration is of significant importance, particularly when a large scale real investigation has to be conducted. With this regard the present study intended to explore and provide a first insight into the performance of the proposed procedure based on the availability of a minimum amount of data. In particular, the minimum number of eigen-properties required to accurately evaluate the stiffness of the equivalent beam has been chosen after several numerical analyses.
The influence of the amount of data on the problem is also crucial for the unicity of the solution. With this regard, it is the case to state that, since the objective function cannot be explicitly formulated, the study of the unicity of the solution is a complex mathematical task. In addition, the adopted numerical optimization procedure may provide different solutions (intended at local minima) in accordance with the trial initial values adopted for the correction coefficients. To further explore this aspect, as explained before, the values of the three stiffness correction coefficients have been bounded in the range [0.1 1] and for each analysed building the minimization procedure has been implemented by testing different trial initial values of the correction factors. Then the stiffness correction coefficients associated to the lower value of the objective function have been selected. This procedure does not claim to assure the unicity of the solution in terms of stiffness correction coefficients however it provides the accuracy of different selected solutions.

2.1.8 Static response

Once Equation (2.1.16) has been solved, the static deflection of the beam-like model in the geometric space can be obtained by means of Equations (2.1.8).

2.1.9 Dynamic response

The dynamic response of the beam-like model subjected to external loading, in the generalised space, can be expressed as a combination of $S \le 3N$ modes of vibration multiplied by the time-dependent functions $z_j(t)$:

$$\mathbf{q}(t) = \sum_{j=1}^{S} \hat{\boldsymbol{\psi}}_j \cdot z_j(t) \tag{2.1.32}$$

where S indicates the number of modes of vibration. Substitution of Equation (2.1.32) into the equations of motion (2.1.25) leads to:

$$\mathbf{M}\sum_{j=1}^{S}\hat{\boldsymbol{\psi}}_j\cdot\ddot{z}_j(t)+\mathbf{K}\sum_{j=1}^{S}\hat{\boldsymbol{\psi}}_j\cdot z_j(t)=\mathbf{P} \tag{2.1.33}$$

Furthermore, in view of the orthogonality conditions of the vibration modes, Equation (2.1.33) provides:

$$\underbrace{\hat{\boldsymbol{\psi}}_j^T\mathbf{M}\hat{\boldsymbol{\psi}}_j}_{M_{mod,j}}\cdot\ddot{z}_j(t)+\underbrace{\hat{\boldsymbol{\psi}}_j^T\mathbf{K}\hat{\boldsymbol{\psi}}_j}_{K_{mod,j}}\cdot z_j(t)=\underbrace{\hat{\boldsymbol{\psi}}_j^T\mathbf{P}}_{P_{mod,j}} \tag{2.1.34}$$

So, the equations of motion are simplified as follows:

$$M_{mod,j}\cdot\ddot{z}_j(t)+C_{mod,j}\cdot\dot{z}_j(t)+K_{mod,j}\cdot z_j(t)=P_{mod,j} \tag{2.1.35}$$

It is worth noting that the terms $C_{mod,j}$ are representative of the generalised modal damping for all the modes of vibration and are related to the corresponding modal damping ratios as follows: $\frac{C_{mod,j}}{M_{mod,j}}=2\xi_j\omega_j$.

Lastly, the dynamic response in the geometric space is obtained by means of the following expressions:

$$u_x(z,t)=\sum_{j=1}^{S}\sum_{i=1}^{N}\psi_i(z)\hat{\psi}_{i_x j}\cdot z_j(t) \tag{2.1.36a}$$

$$u_y(z,t)=\sum_{j=1}^{S}\sum_{i=1}^{N}\psi_i(z)\hat{\psi}_{i_y j}\cdot z_j(t) \tag{2.1.36b}$$

$$\vartheta(z,t)=\sum_{j=1}^{S}\sum_{i=1}^{N}\psi_i(z)\hat{\psi}_{i_\vartheta j}\cdot z_j(t) \tag{2.1.36c}$$

where N is the number of displacement shape functions adopted in the discretization and S is the number of modes of vibration used to compute the dynamic response.

2.2 NON-UNIFORM SHEAR-ONLY BEAM-LIKE MODEL –INELASTIC BEHAVIOUR

In order to take into account the global inelastic seismic response of multi-storey buildings, the inhomogeneous beam-like model, used in the previous section to characterize the linear elastic behaviour, must be substantially revisited for its extension to the non-linear context. With this purpose, in this section a new cantilever beam model, conceived to be representative of the inelastic response of a 3D framed building when subjected to a horizontal force distribution in a certain direction, is formulated. The proposed model is suitable to represent the inhomogeneous and the inelastic properties of the building along its height, which are assumed variable from one floor to the other. The inter-storey non-linear behaviour of the building is modelled considering a beam-like model with shear deformability only defined according to a suitable inelastic constitutive law. Since the beam-like model is intended to represent the non-linear behaviour of the building along a specific loading direction, the beam is defined as a plane model, able anyway to take into account the spatial behaviour of irregular buildings by means of a calibration procedure based on a non-linear analysis performed on a 3D FEM model. Figure 2.2 reports a qualitative scheme to emphasize the proposed beam-building equivalence. It is evident that the corresponding inelastic beam model will inherit a constitutive law that depends not only on the load direction but also on the adopted distribution of forces. Since the model is proposed for the assessment of the seismic response of the building, its calibration has been performed by means of the results of a pushover analysis along the considered direction under a suitable distribution of loads.

The mass distribution of the beam-like model is assumed to be consistent to the actual mass distribution of the 3D structural model, therefore it can be concentrated at the floor levels as well as, when required, distributed along the height. This latter mass distribution is preferable for modelling masonry structures or combined reinforced concrete masonry buildings, in which the actual mass distribution is spread along the height of the building and its concentration at the floor level does not well represent the actual distribution of inertia loads. In Figure 2.2.a the 3D model of a building with N_f floors together with the force resultant $F_{d,i}$ at i-th floor acting in direction d are reported. In Figure 2.2.b the proposed equivalent beam-like model suitable for the dynamic analysis of the building in direction d is qualitatively shown.

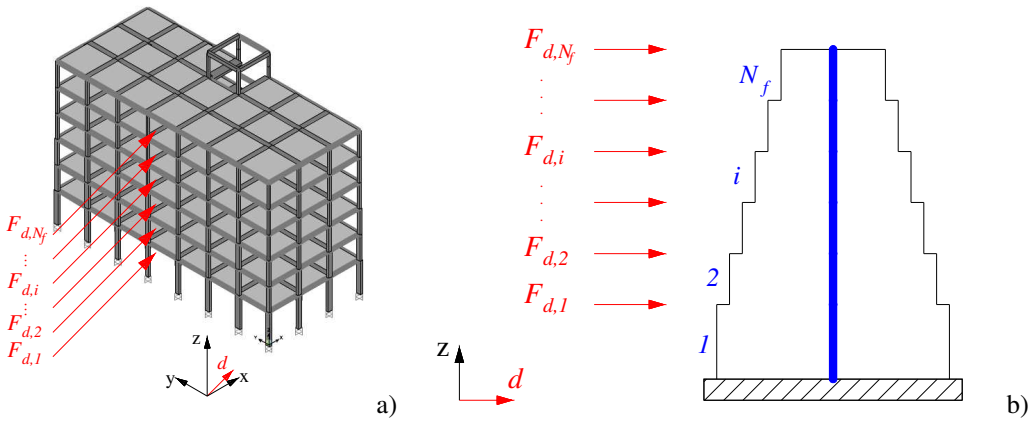

Figure 2.2 - a) 3D FEM model of the building and b) equivalent beam-like model along the considered direction

2.2.1 Considerations About Beam-Like and SDOF Models

As already pointed out, one of the main goals of the proposed inelastic beam-like model is to represent a more accurate and therefore promising alternative to the SDOF model nowadays used to assess the seismic vulnerability demands of multi-storey buildings. With this aim, in the present paragraph some considerations, concerning the comparison between the proposed model and the SDOF one, are formulated.

It has been already highlighted that the equivalent SDOF system-based approaches rely on the hypothesis that the structure vibrates predominantly with a single mode. This assumption is not always fulfilled, especially in the case of high-rise or irregular buildings. Some procedures have been employed in order to overcome this limitation by combining the fundamental mode effect and the elastic or inelastic contribution due to higher modes [75, 76, 79, 83, 84].

On the contrary, the proposed beam-like models are able to take into account the higher mode effects, since defined in order to be equivalent to the MDOF building system. As it has been proposed for the linear behaviour and will be shown in the following paragraphs for the inelastic response, the beam-like model stiffness distributions and degrees of freedom have been set with the aim to represent the dynamic behaviour of each floor of the building when subjected to earthquake loadings.

It is worth noting that the presence of floor degrees of freedom leads to the evaluation of all the floor displacements allowing the identification of partial failure mechanisms. This is not possible by using equivalent SDOF system-based approaches, since the displacement pattern obtained by means of the non-linear static analysis is inherited by the SDOF system [87].

The results reported in the following section show how the proposed inelastic beam-like model can be able to reproduce the non-linear static and dynamic behaviour of the building with sufficient accuracy drastically reducing the computational burden and, as a consequence, the required computational time. The low computational cost of the proposed beam-like model will allow to propose new seismic assessment numerical strategies alternative to those currently used partially based on the inelastic behaviour of SDOF model.

2.2.2 The inelastic beam-like model and its discretization

The beam-like model, represented in Figure 2.2, can be analysed as an inhomogeneous continuous beam model or it can be discretized according to finite element approach. The linear elastic beam-like model has been discretized according to a Rayleigh-Ritz strategy that allowed to limit the number of degrees of freedom required to obtain an accurate linear dynamic response of the model. With regard to the inelastic beam model, the need to achieve a reliable simulation of the inelastic response at the floor levels, where inelastic displacements tend to concentrate, suggests considering a discretization in which the beam element is divided into a number N_f of sub-beam shear deformable elements of length h_i equal to the inter-storey height. The characterization of the inelastic response of each i-th uniform beam sub-element can be defined by means of appropriate uniaxial inelastic constitutive laws, in terms of shear force T_i and inter-storey drift s_i. Figure 2.3.a and Figure 2.3.b summarise the equivalent shear beam-like model approach described so far.

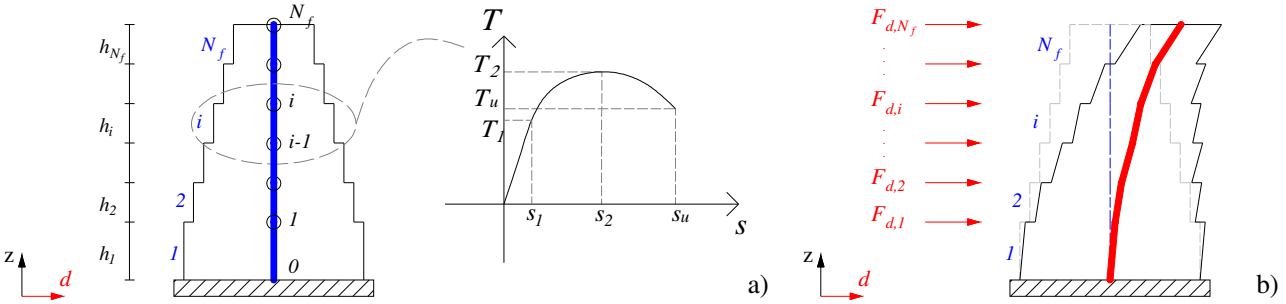

Figure 2.3 - a) Discretization of the equivalent beam-like model with non-linear constitutive law of the i-th sub-element and b) the deflection of the equivalent beam under the considered load distribution

Therefore, following a simple FEM discretization for simulating the inelastic response of the inhomogeneous shear beam, the axis of the proposed cantilever equivalent beam is divided into a number of segments representing the inter-storeys of the building. Each beam segment has the same length and constitutive law of the corresponding inter-storey of the building while the mass can generally be assumed to be concentrated at the floor level.

It is worth highlighting that, in view of the adopted inelastic calibration of the beam-like model, the equivalence concerns the static and dynamic responses of the building and the equivalent beam along a fixed direction, which may vary according to the direction of the applied loadings. Each floor of the building is represented by a node i, which coincides with the end of a beam segment.

Therefore, the equivalent beam, qualitatively shown in Figure 2.4.a, is defined by means of:

1. Nodes, numbered from bottom to top as shown in Figure 2.3.a, according to the reference global system d-z.
2. Initial and final nodes of each beam segment and its normalized vector t_i = [0 1] (shown in red in Figure 2.4.b) directed from the initial to the final node.

3. Characteristics of each beam segment, as shown in Figure 2.5: length, lumped mass on the final node, distributed mass, initial shear stiffness in direction d (R_{d0}) and the corresponding tangent stiffness (R_{dt}) useful for the non-linear behaviour.

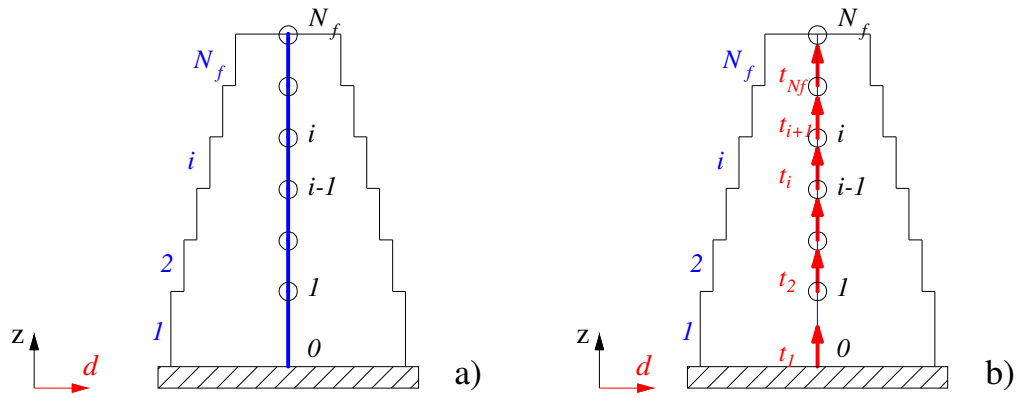

Figure 2.4 – a) Nodes and segments of the equivalent beam-like model and b) beam segment vectors

In Figure 2.5, in each i-th inter-storey m_i denotes the distributed mass, M_i the lumped mass, T_y and T_u the yielding and ultimate shear force, respectively, and s_y and s_u the yielding and ultimate inter-storey drifts, respectively.

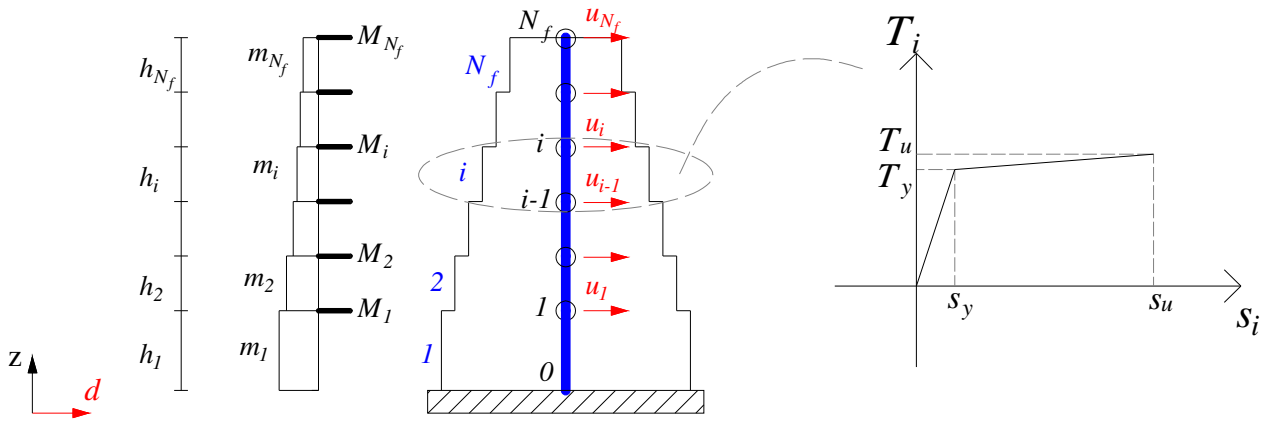

Figure 2.5 - Equivalent beam-like model with mass distribution, degrees of freedom u_i and assumed non-linear constitutive law of the i-th sub-element

According to the adopted discretization approach of the shear beam, it is necessary to define nodal displacements and nodal forces.
Nodal displacements are referred only to the non-constrained nodes (thus neglecting node 0). For node i the displacement components in the fixed direction d are denoted as u_i. The vector of nodal displacements can therefore be expressed as:

$$\mathbf{u} = \begin{bmatrix} u_1 \\ u_2 \\ \vdots \\ u_N \end{bmatrix} \tag{2.2.1}$$

where N is the total number of beam nodes corresponding to the number of floors.

The vector of the nodal forces, according to the vector of nodal displacement, is shown below:

$$\mathbf{F} = \begin{bmatrix} F_1 \\ F_2 \\ \vdots \\ F_N \end{bmatrix} \tag{2.2.2}$$

where F_i is the force applied to node i in the fixed direction d.
Different load distributions can be applied. The beam-like model can be subjected to a static force vector $\mathbf{F}$ according to the following relationships:

$$\mathbf{F} = \mathbf{M}\boldsymbol{\phi} \tag{2.2.3}$$

where $\boldsymbol{\phi}$ is the fixed displacement distribution and $\mathbf{M}$ is the diagonal mass matrix which considers lumped masses at the nodes due to the applied seismic masses.
In particular, the following three load distributions have been considered in the numerical applications:

a) mass proportional force distribution;
b) inverse triangular proportional force distribution;
c) force distribution associated with the fundamental natural mode.

As better highlighted in the subsequent section, alternatively, a displacement distribution can also be applied on the beam-like model. In particular, the following displacement distribution has been considered in the numerical applications:

d) displacement distribution proportional to the fundamental natural mode.

Adaptive force or displacement distributions can also be considered; however, in the present research, attention has been focused on invariant load or displacement distributions. As suggested by some technical codes, like for example Italian Code NTC – D.M. 17.01.2018, static forces equivalent to the inertia forces due to the seismic actions corresponding to a linear dynamic analysis can also be applied.
Alternatively, it is also possible to apply a user defined static force distribution.

The non-linear dynamic analysis is performed considering a seismic acceleration $\ddot{u}_g(t)$ applied at the base of the beam. Since there are only translational degrees of freedom, horizontal inertia forces can be computed as:

$$\mathbf{F}(t) = -\mathbf{M}\mathbf{i}\ddot{u}_g(t) \tag{2.2.4}$$

where $\mathbf{M}$ is the beam mass matrix and $\mathbf{i}$ the vector of load spatial distribution having unitary components according to the direction of the applied earthquake.
It is worth highlighting that, differently from Section 2.1 where the equations of motion for the linear elastic beam-like model are derived in terms of generalised coordinates q, in this section the equations of motion of the inelastic beam-like model are expressed in terms of floor displacements.

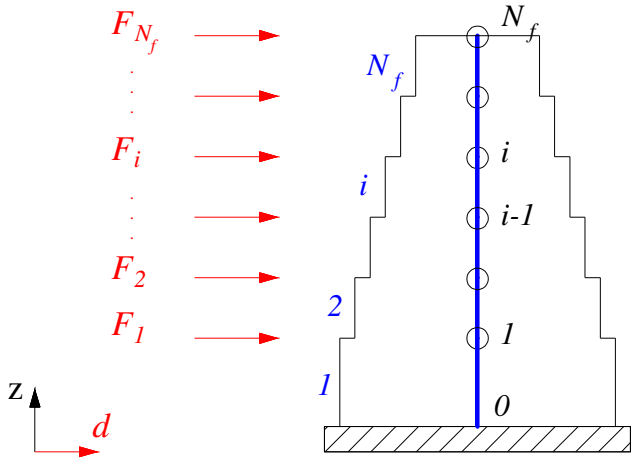

Figure 2.6 - Applied forces

The derivation of the stiffness, mass and damping matrices of the inelastic beam are reported in Appendix B.

2.2.3 The Calibration of the Inelastic Properties

As already pointed out, the proposed beam-like model is conceived to be representative of the inelastic response of the 3D building when subjected to a specific horizontal load distribution along a given direction. For this reason, the equivalence between the beam and the building is enforced by calibrating the inelastic beam model in order to predict the same pushover curve obtained by performing non-linear static analysis on the 3D FEM model. This result can be easily obtained reconstructing, according to a step by step procedure, the tangent shear stiffness of each inter-storey beam segment which provides the same inter-storey displacements of the full 3D FEM model. This inverse non-linear static identification procedure allows to obtain an inelastic beam-like model somehow equivalent to the more demanding 3D FEM model, although related to a specific direction and under a precise distribution of horizontal loadings. In particular, the inter-storey shear force is equal to the sum of the shear forces of the structural vertical elements (columns) of the considered inter-storey, while the displacement is due to the difference between the mean values of the displacements of the nodes situated at the top and at the bottom of the considered inter-storey. These values, collected for each step of the pushover analysis, allow to draw the non-linear "inter-storey capacity curve", which relates the shear force to the corresponding relative displacement.

Under this assumption, the proposed beam-like model can be considered as representative of the 3D structure, in the considered direction, both for the linear and non-linear behaviour.

In order to adopt this equivalent model for predicting the non-linear dynamic response of the entire building, when subjected to earthquake loading in the same direction, it is necessary to characterize the inter-storey cyclic behaviour to be associated to each segment of the inhomogeneous inelastic multi-stepped beam. For this latter reason, the non-linear inter-storey constitutive law, obtained by the above described calibration strategy, has been first substituted with a bilinear curve and then extended to a cyclic inelastic behaviour, in accordance with what proposed in the scientific literature for the SDOF equivalent system [68, 70]. In the present study the most adopted simplified strategy, based on the definition of a bilinear elasto-plastic model, generally adopted to define the equivalent SDOF models, is considered. The cyclic inelastic behaviour of each inter-storey is attributed to each uniform segment of the multi-stepped beam. In the numerical applications reported in the next section, an elasto-plastic behaviour with kinematic hardening, defined according to an energy equivalence criterion on the hysteresis loop, has been adopted. It is worth noting that the contribution of infill walls to the building strength and stiffness is disregarded, anyway it could be captured by the proposed model by performing a pushover analysis accounting for the non-linear contribution of these non-structural elements. In this latter case more complex constitutive laws could be needed if the low ductile and cyclic degrading behaviour of the masonry infills are considered in the FEM model. This further application, exploiting the capability of the beam-like model, will be the subject of future investigations.

In Figure 2.7.a-b an example of inter-storey capacity curve (in black) and the corresponding back-bone inelastic force-displacement response (in red) are reported, respectively.

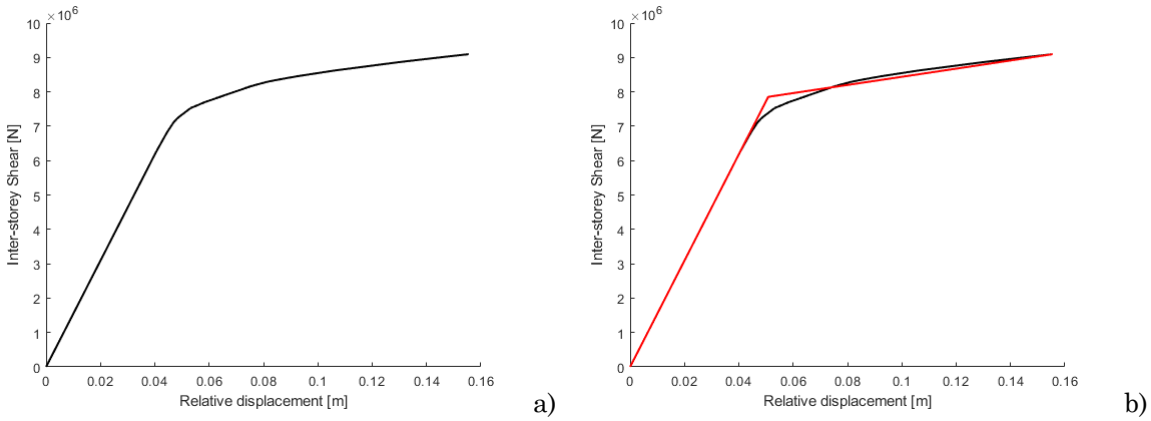

Figure 2.7 - a) An example of inter-storey capacity curve and b) the corresponding back-bone curve

If the considered building, subjected to a load distribution in a given direction, undergoes different inelastic responses according to the load versus, an asymmetric cyclic behaviour has to be considered, as reported in Figure 2.8.a, where R, R_T, F_Y indicate the elastic, post elastic stiffness and the yield force, respectively, while R', R'_T, F'_Y indicate the same quantities with the opposite sign loading.

Alternatively, if the capacity curve is not affected by the load versus, a simple symmetric elasto-plastic law with kinematic hardening can be considered (Figure 2.8.b).

Without loss of generality, for simplicity, a symmetric elasto-plastic law with kinematic hardening is considered in what follows.

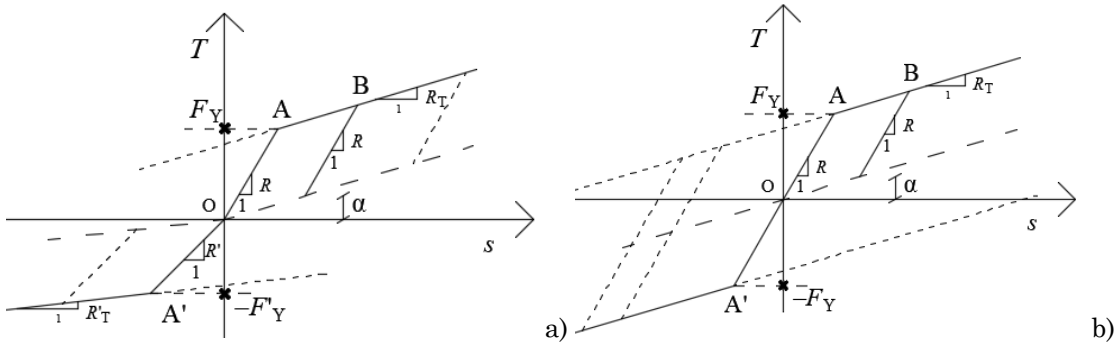

Figure 2.8 - Elasto-plastic force-displacement constitutive law with positive kinematic hardening: a) asymmetrical behaviour; b) symmetrical behaviour.

In some cases, it is not possible to determine a good correspondence between the inter-storey capacity curve obtained from the static non-linear analysis and a bilinear curve, especially when the inter-storey undergoes a softening behaviour. In order to define a more accurate simplified constitutive law for each segment of the equivalent beam-like model, a cyclic static non-linear analysis is performed on the FEM model and the cyclic non-linear inter-storey capacity curve is obtained as already described. The inter-storey simplified cyclic inelastic behaviour is finally defined according to an energy equivalence criterion on the hysteresis loop (which has been imposed by equating the areas inside the curves), as shown in Figure 2.9.

In general a symmetric elasto-plastic behaviour with kinematic hardening is adopted, while an elasto-perfectly plastic behaviour is considered if the inter-storey cyclic law shows a softening behaviour.

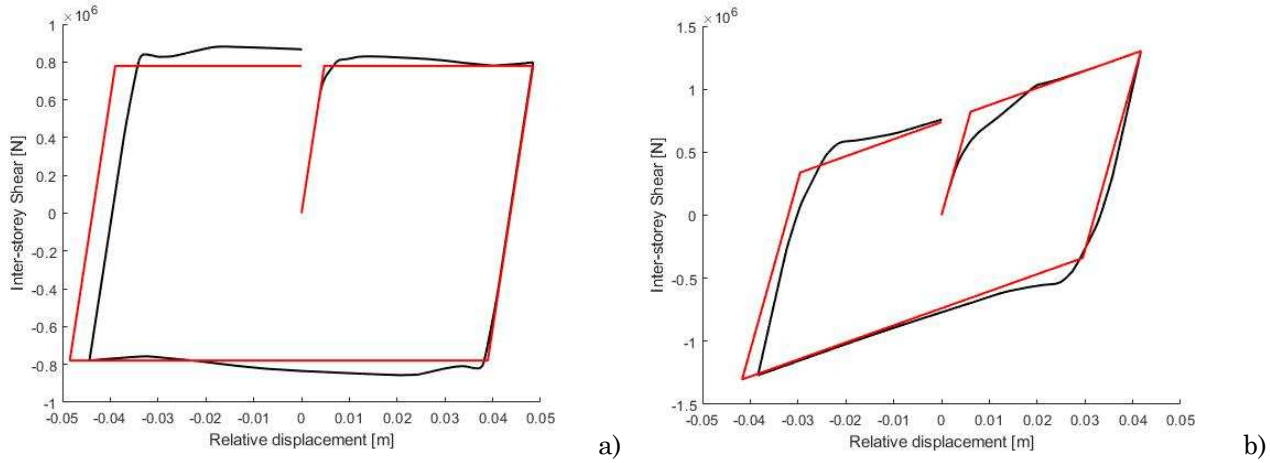

Figure 2.9 - An example of cyclic inter-storey capacity curve and the corresponding cyclic back-bone curve adopting a) a symmetric elasto-perfectly plastic behaviour or b) a symmetric elasto-plastic behaviour with kinematic hardening

The calibration of the equivalent inelastic beam-like model is performed considering the 3D building subjected to a precise distribution of horizontal loadings. However, the imposition of the force distribution could lead sometimes to obtain some inter-storey capacity curves not showing a non-linear behaviour if according to the distribution of forces the corresponding inter-storey elements do not exhibit an inelastic behaviour. However, the pushover analysis not necessarily provides the same damage distribution associated to a non-linear dynamic analysis and it is therefore needed to characterise a suitable non-linear constitutive law for each level of the building. For these reasons it has been also proposed a calibration strategy based on a pushover analysis associated to a specific displacement distribution on the building in order to exploit the non-linear behaviour of each inter-storey. In fact, in this case all the inter-storey drifts are forced to increase proportionally allowing to follow the inter-storey force-displacement relationships until a chosen ductility. Therefore, the choice of using a displacement distribution instead of a force distribution would be preferable.

Once the inelastic beam-like equivalent model has been defined, different numerical strategies can be adopted for the evaluation of the non-linear response under static and dynamic loadings, as described in the Appendices C and D.

2.3 ALTERNATIVE INELASTIC BEAM MODEL BASED ON GENERALISED FUNCTIONS

In this sub-section the inelastic beam model already proposed in sub-section 2.2 is discretized according to a different displacement based approach. In particular, the static response of multi-stepped linear shear-torsional beam is determined in closed form and successively used for discretizing the inelastic beam model.

2.3.1 The multi-stepped linear beam element

Beams with non-uniform stiffness distribution along their axis can be conveniently modelled as stepped. Although in the scientific literature closed form solutions for the static analysis of either Timoshenko or Euler stepped beams are available [104, 105], the case of shear-torsional beams has not been explicitly reported. A part of the study of the PhD course has therefore been devoted to the derivation of the closed form solution for static displacements of shear-torsional elastic stepped beams.

The well-known static governing equations of the shear-torsional beam with variable shear $G(z)A(z)$ and torsional $G(z)J_T(z)$ stiffness are written as follows:

- Equilibrium equations: $V^I = -\overline{p}(z) \qquad M_T{}^I = -\overline{t}(z)$ (2.3.1)
- Constitutive equations: $V = G(z)A(z)\gamma \qquad M_T = G(z)J_T(z)\theta^I(z)$ (2.3.2)
- Compatibility equation: $\gamma = v'(z)$ (2.3.3)

where $\overline{p}(z)$ is the transversal load, $\overline{t}(z)$ is the distributed torsional moment, $V(z)$ is the shear force, $M_T(z)$ is the torsional moment, $\gamma(z)$ is the shear strain, $v(z)$ is the transversal displacement, $\theta(z)$ is the torsional rotation.

Equations (2.3.1), (2.3.2), (2.3.3) can be combined to provide the following second order differential equations:

$$\left[G(z)A(z)v^I(z)\right]^I = -\overline{p}(z) \tag{2.3.4}$$

$$\left[G(z)J_T(z)\theta^I(z)\right]^I = -\overline{t}(z) \tag{2.3.5}$$

where, once again, the prime denotes differentiation with respect to z.

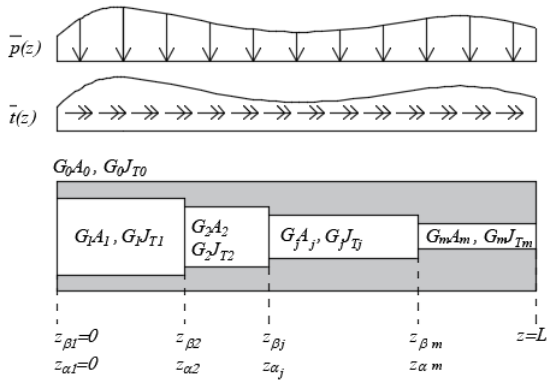

Figure 2.10 - Step-wise shear-torsional elastic beam

The shear $G(z)A(z)$ and torsional $G(z)J_T(z)$ stiffness, with m abrupt variations with respect to the reference values G_0A_0 and G_0J_{T0} respectively along the beam axis, can be expressed by means of the adoption of the Heaviside unit-step generalised function as follows:

$$G(z)A(z) = G_0A_0\left[1-\sum_{j=1}^{m}\left(\beta_j-\beta_{j-1}\right)U\left(z-z_{\beta_j}\right)\right] \tag{2.3.6}$$

$$G(z)J_T(z) = G_0J_{T0}\left[1-\sum_{j=1}^{m}\left(\alpha_j-\alpha_{j-1}\right)U\left(z-z_{\alpha_j}\right)\right] \tag{2.3.7}$$

where:

$$G_jA_j = G_0A_0\left[1-\beta_j\right] \quad \Rightarrow \quad \beta_j = 1-\frac{G_jA_j}{G_0A_0} \tag{2.3.8}$$

$$G_jJ_{Tj} = G_0J_{T0}\left[1-\alpha_j\right] \quad \Rightarrow \quad \alpha_j = 1-\frac{G_jJ_{Tj}}{G_0J_{T0}} \tag{2.3.9}$$

The parameters $\beta_j, j=1,...,m$ and $\alpha_j, j=1,...,m$ represent the shear and torsional stiffness jumps, while z_{β_j} and z_{α_j} are the relevant singularity positions, respectively.

Substituting Equation (2.3.6) into Equation (2.3.4) and Equation (2.3.7) into Equation (2.3.5), the following uncoupled differential equations governing the shear and torsional problems of the step-wise beam are obtained:

$$\left[G_0A_0\left(1-\sum_{j=1}^{m}\left(\beta_j-\beta_{j-1}\right)U\left(z-z_{\beta_j}\right)\right)v^I(z)\right]^I = -\overline{p}(z) \tag{2.3.10}$$

$$\left[G_0J_{T0}\left(1-\sum_{j=1}^{m}\left(\alpha_j-\alpha_{j-1}\right)U\left(z-z_{\alpha_j}\right)\right)\theta^I(z)\right]^I = -\overline{t}(z) \tag{2.3.11}$$

For simplicity, by considering the dimensionless coordinate $\xi = z/L$, the governing differential equations of the shear-torsional beam by accounting for the singularities introduced in Equations (2.3.6)-(2.3.7), take the following dimensionless form:

$$\left[\left(1-\sum_{j=1}^{m}\left(\beta_j-\beta_{j-1}\right)U\left(\xi-\xi_{\beta_j}\right)\right)u^I(\xi)\right]^I = -p(\xi) \tag{2.3.12}$$

$$\left[\left(1-\sum_{j=1}^{m}\left(\alpha_j-\alpha_{j-1}\right)U\left(\xi-\xi_{\alpha_j}\right)\right)\theta^I(\xi)\right]^I = -t(\xi) \tag{2.3.13}$$

where the normalized function $u(\xi)=\dfrac{v(\xi)}{L}$ and the normalized load parameters $p(\xi)=\dfrac{\overline{p}(\xi)L}{G_0A_0}$ and $t(\xi)=\dfrac{\overline{t}(\xi)L^2}{G_0J_{T0}}$ have been introduced.

Integration of Equations (2.3.12) - (2.3.13) leads to:

$$\left(1-\sum_{j=1}^{m}\left(\beta_j-\beta_{j-1}\right)U\left(\xi-\xi_{\beta_j}\right)\right)u^I(\xi) = -p^{[1]}(\xi)+C_2 \tag{2.3.14}$$

$$\left(1-\sum_{j=1}^{m}\left(\alpha_j-\alpha_{j-1}\right)U\left(\xi-\xi_{\alpha_j}\right)\right)\theta^I(\xi) = -t^{[1]}(\xi)+D_2 \tag{2.3.15}$$

where $p^{[k]}(\xi)$ and $t^{[k]}(\xi)$ indicate a primitive of order k of the relevant function.

Therefore, it is possible to obtain $u^I(\xi)$ and $\theta^I(\xi)$:

$$u^I(\xi)=\frac{-p^{[1]}(\xi)+C_2}{1-\sum_{j=1}^{m}\left(\beta_j-\beta_{j-1}\right)U\left(\xi-\xi_{\beta_j}\right)}=\left[-p^{[1]}(\xi)+C_2\right]\frac{1}{\left[1-\sum_{j=1}^{m}\left(\beta_j-\beta_{j-1}\right)U\left(\xi-\xi_{\beta_j}\right)\right]} \tag{2.3.16}$$

$$\theta^I(\xi)=\frac{-t^{[1]}(\xi)+D_2}{1-\sum_{j=1}^{m}\left(\alpha_j-\alpha_{j-1}\right)U\left(\xi-\xi_{\alpha_j}\right)}=\left[-t^{[1]}(\xi)+D_2\right]\frac{1}{\left[1-\sum_{j=1}^{m}\left(\alpha_j-\alpha_{j-1}\right)U\left(\xi-\xi_{\alpha_j}\right)\right]} \tag{2.3.17}$$

Making use of the properties of the Heaviside's function, Equations (2.3.16) – (2.3.17) can be rewritten as:

$$u^I(\xi)=\left[-p^{[1]}(\xi)+C_2\right]\left[1+\sum_{j=1}^{m}\beta^*{}_j\,U\left(\xi-\xi_{\beta_j}\right)\right] \tag{2.3.18}$$

$$\theta^I(\xi)=\left[-t^{[1]}(\xi)+D_2\right]\left[1+\sum_{j=1}^{m}\alpha^*{}_j\,U\left(\xi-\xi_{\alpha_j}\right)\right] \tag{2.3.19}$$

where: $\beta^*{}_j=\frac{\beta_j}{1-\beta_j}-\frac{\beta_{j-1}}{1-\beta_{j-1}}$, $\alpha^*{}_j=\frac{\alpha_j}{1-\alpha_j}-\frac{\alpha_{j-1}}{1-\alpha_{j-1}}$.

Integration of Equations (2.3.18) – (2.3.19) lead to:

$$u(\xi)=C_1+C_2\left[\xi+\sum_{j=1}^{m}\beta^*{}_j\left(\xi-\xi_{\beta_j}\right)U\left(\xi-\xi_{\beta_j}\right)\right]-p^{[2]}(\xi)-\sum_{j=1}^{m}\beta^*{}_j\left[p^{[2]}(\xi)-p^{[2]}\left(\xi_{\beta_j}\right)\right]U\left(\xi-\xi_{\beta_j}\right) \tag{2.3.20}$$

$$\theta(\xi)=D_1+D_2\left[\xi+\sum_{j=1}^{m}\alpha^*{}_j\left(\xi-\xi_{\alpha j}\right)U\left(\xi-\xi_{\alpha_j}\right)\right]-t^{[2]}(\xi)-\sum_{j=1}^{m}\alpha^*{}_j\left[t^{[2]}(\xi)-t^{[2]}(\xi_{\alpha_j})\right]U\left(\xi-\xi_{\alpha_j}\right) \tag{2.3.21}$$

Equations (2.3.20) – (2.3.21) can be rewritten as:

$$u(\xi)=C_1f_1(\xi)+C_2f_2(\xi)+f_3(\xi) \tag{2.3.22}$$

$$\theta(\xi)=D_1g_1(\xi)+D_2g_2(\xi)+g_3(\xi) \tag{2.3.23}$$

where:

$$f_1(\xi)=1 \tag{2.3.24a}$$

$$f_2(\xi)=\xi+\sum_{j=1}^{m}\beta^*{}_j\left(\xi-\xi_{\beta_j}\right)U\left(\xi-\xi_{\beta_j}\right) \tag{2.3.24b}$$

$$f_3(\xi)=-p^{[2]}(\xi)-\sum_{j=1}^{m}\beta^*{}_j\left[p^{[2]}(\xi)-p^{[2]}\left(\xi_{\beta_j}\right)\right]U\left(\xi-\xi_{\beta_j}\right) \tag{2.3.24c}$$

$$g_1(\xi)=1 \tag{2.3.24d}$$

$$g_2(\xi)=\xi+\sum_{j=1}^{m}\alpha^*{}_j\left(\xi-\xi_{\alpha_j}\right)U\left(\xi-\xi_{\alpha_j}\right) \tag{2.3.24e}$$

$$g_3(\xi)=-t^{[2]}(\xi)-\sum_{j=1}^{m}\alpha^*{}_j\left[t^{[2]}(\xi)-t^{[2]}\left(\xi_{\alpha_j}\right)\right]U\left(\xi-\xi_{\alpha_j}\right) \tag{2.3.24f}$$

The boundary conditions for a cantilever beam are shown in the following:

1) $u(\xi = 0) = 0$

2) $V(\xi = 0) = G_0 A_0 u^I(\xi = 0) = \int_0^L \overline{p}(z)dz = \int_0^1 \overline{p}(\xi) L d\xi \qquad \Rightarrow \qquad u^I(\xi = 0) = \int_0^1 p(\xi) d\xi$

3) $\theta(\xi = 0) = 0$

4) $M_T(\xi = 0) = G_0 J_{T0} \theta^I(\xi = 0) = \int_0^L \overline{t}(z)dz = \int_0^1 \overline{t}(\xi) L d\xi \qquad \Rightarrow \qquad \theta^I(\xi = 0) = \int_0^1 t(\xi) d\xi$

(2.3.25)

Thus, allowing to obtain the following constants:

1) $C_1 = 0$

2) $C_2 f_2^I(0) + f_3^I(0) = \int_0^1 p(\xi) d\xi \qquad \Rightarrow \qquad C_2 = \dfrac{\int_0^1 p(\xi) d\xi - f_3^I(0)}{f_2^I(0)} = \int_0^1 p(\xi) d\xi$

3) $D_1 = 0$

4) $D_2 g_2^I(0) + g_3^I(0) = \int_0^1 p(\xi) d\xi \qquad \Rightarrow \qquad D_2 = \dfrac{\int_0^1 t(\xi) d\xi - g_3^I(0)}{g_2^I(0)} = \int_0^1 t(\xi) d\xi$

(2.3.26)

In case the multi-stepped beam is subjected only to n_F concentrated forces $\overline{F}_r, r = 1, \ldots, n_F$, applied at the abscissae ξ_{F_r} with eccentricity e_r with respect to the centre of stiffness, the load terms become:

$$\overline{p}(z) = \sum_{r=1}^{nF} \overline{F}_r \delta(z - z_{F_r}) \tag{2.3.27}$$

$$\overline{p}(\xi) = \sum_{r=1}^{nF} \frac{\overline{F}_r \delta(\xi - \xi_{F_r})}{L} \qquad \Rightarrow \qquad p(\xi) = \frac{\overline{p}(\xi) L}{G_0 A_0} = \sum_{r=1}^{nF} \frac{\overline{F}_r \delta(\xi - \xi_{F_r})}{G_0 A_0} = \sum_{r=1}^{nF} F_r \delta(\xi - \xi_{F_r}) \tag{2.3.28}$$

$$\overline{t}(z) = \sum_{r=1}^{nF} \overline{F}_r e_r \delta(z - z_{F_r}) \tag{2.3.29}$$

$$\overline{t}(\xi) = \sum_{r=1}^{nF} \frac{\overline{F}_r e_r \delta(\xi - \xi_{F_r})}{L} \qquad \Rightarrow \qquad t(\xi) = \frac{\overline{t}(\xi) L^2}{G_0 J_{T0}} = \sum_{r=1}^{nF} \frac{\overline{F}_r e_r \delta(\xi - \xi_{F_r}) L}{G_0 J_{T0}} = \sum_{r=1}^{nF} T_r \delta(\xi - \xi_{F_r}) \tag{2.3.30}$$

where the property $\delta\left[L(\xi - \xi_i)\right] = \dfrac{\delta(\xi - \xi_i)}{L}$ of the Dirac's delta distribution has been exploited and the normalized loads $F_r = \dfrac{\overline{F}_r}{G_0 A_0}$ and $T_r = \dfrac{\overline{F}_r e_r}{G_0 J_{T0}} L$ have been introduced.

Further useful quantities are:

$$p^{[1]}(\xi) = \sum_{r=1}^{nF} F_r U(\xi - \xi_{F_r}) \tag{2.3.31 a}$$

$$p^{[2]}(\xi) = \sum_{r=1}^{nF} F_r (\xi - \xi_{F_r}) U(\xi - \xi_{F_r}) \tag{2.3.31b}$$

$$t^{[1]}(\xi) = \sum_{r=1}^{nF} T_r U(\xi - \xi_{F_r}) \tag{2.3.31c}$$

$$t^{[2]}(\xi) = \sum_{r=1}^{nF} T_r \left(\xi - \xi_{F_r}\right) U\left(\xi - \xi_{F_r}\right) \tag{2.3.31d}$$

In this case, the boundary conditions for a cantilever beam give the following constants:

1) $C_1 = 0$

2) $C_2 = \int_0^1 p(\xi) d\xi = \int_0^1 \sum_{r=1}^{nF} F_r \delta\left(\xi - \xi_{F_r}\right) d\xi = \sum_{r=1}^{nF} F_r$

3) $D_1 = 0$

4) $D_2 = \int_0^1 t(\xi) d\xi = \int_0^1 \sum_{r=1}^{nF} T_r \delta\left(\xi - \xi_{F_r}\right) d\xi = \sum_{r=1}^{nF} T_r$

(2.3.32)

2.3.2 Inelastic beam finite element

In this paragraph, by exploiting the closed form solution presented above, a displacement based beam element with distributed plasticity is formulated. Such an element is characterised by the capability of adapting its stiffness matrix by means of displacement shape functions enriched by generalised functions including the effect of plastic deformation occurrences on transversal displacements.

The displacement field along the span of the beam element is that consistent with the model adopted for the plastic deformation distribution and is also able to account for the presence of any external load distribution.

Lastly, the adoption of the below described beam finite element for the non-linear static analysis of the beam-like model will be shown.

Shape functions

Referring to the step-wise shear-torsional beam reported in Figure 2.11 in dimensionless coordinate (whose closed form solution has been determined in 2.3.1), the shape functions of the finite element are determined in the following.

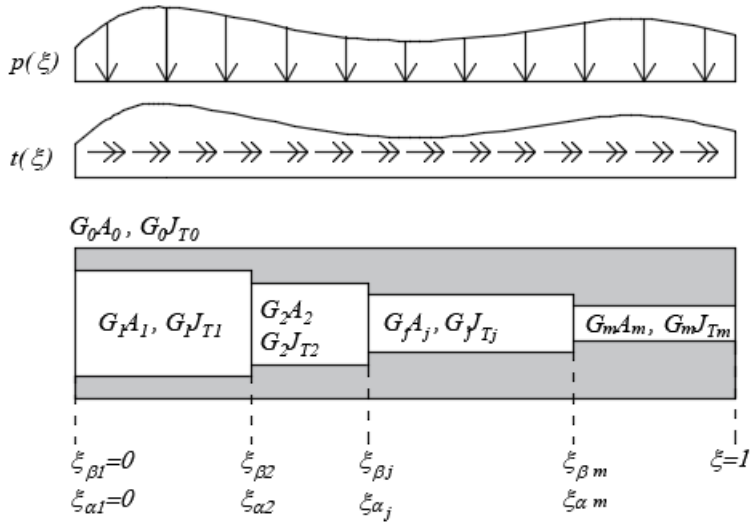

Figure 2.11 - Step-wise shear-torsional elastic beam in dimensionless coordinates

The degrees of freedom and the corresponding nodal forces of the step-wise shear-torsional beam finite element are shown in Figure 2.12.a and Figure 2.12.b respectively.

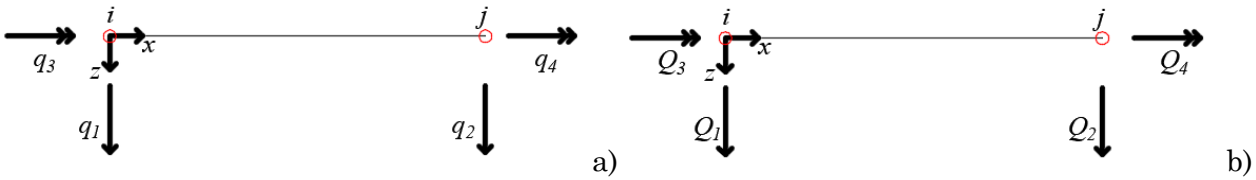

Figure 2.12 - a) Degrees of freedom and b) corresponding nodal forces of the finite element

The transversal displacement and the torsional rotation of the beam axis subjected to a distributed transversal load $p(\xi)$ and a distributed torsional moment $t(\xi)$ can be expressed as follows:

$$\begin{bmatrix} u(\xi,\boldsymbol{\xi}^{\mathbf{GA}},\boldsymbol{\beta}^*) \\ \theta(\xi,\boldsymbol{\xi}^{\mathbf{GJ}},\boldsymbol{\alpha}^*) \end{bmatrix} = \begin{bmatrix} N_1(\xi,\boldsymbol{\xi}^{\mathbf{GA}},\boldsymbol{\beta}^*) & N_2(\xi,\boldsymbol{\xi}^{\mathbf{GA}},\boldsymbol{\beta}^*) & 0 & 0 \\ 0 & 0 & N_3(\xi,\boldsymbol{\xi}^{\mathbf{GJ}},\boldsymbol{\alpha}^*) & N_4(\xi,\boldsymbol{\xi}^{\mathbf{GJ}},\boldsymbol{\alpha}^*) \end{bmatrix} \begin{bmatrix} q_1 \\ q_2 \\ q_3 \\ q_4 \end{bmatrix} +$$

$$+ \begin{bmatrix} u_p(\xi,\boldsymbol{\xi}^{\mathbf{GA}},\boldsymbol{\beta}^*) \\ \theta_p(\xi,\boldsymbol{\xi}^{\mathbf{GJ}},\boldsymbol{\alpha}^*) \end{bmatrix} =$$

$$= \mathbf{N}(\xi,\boldsymbol{\xi}^{\mathbf{GA,GJ}},\boldsymbol{\beta}^*,\boldsymbol{\alpha}^*)\cdot\mathbf{q}_e + \mathbf{u}_p(\xi,\boldsymbol{\xi}^{\mathbf{GA,GJ}},\boldsymbol{\beta}^*,\boldsymbol{\alpha}^*) \tag{2.3.33}$$

where $N_i(\xi,\boldsymbol{\xi}^{\mathbf{GA,GJ}},\boldsymbol{\beta}^*,\boldsymbol{\alpha}^*)$ $i=1,2,3,4$ denotes the shape function associated with the i-th degree of freedom, which can be collected into the matrix $\mathbf{N}(\xi,\boldsymbol{\xi}^{\mathbf{GA,GJ}},\boldsymbol{\beta}^*,\boldsymbol{\alpha}^*)$, $\mathbf{q}_e^T=\begin{bmatrix} q_1 & q_2 & q_3 & q_4 \end{bmatrix}$ denotes the degrees of freedom displacement vector and $\mathbf{u}_p(\xi,\boldsymbol{\xi}^{\mathbf{GA,GJ}},\boldsymbol{\beta}^*,\boldsymbol{\alpha}^*)$ the vector of the solution due to the contribution of external loads.

The shape functions can be derived by imposing unit displacements in the corresponding degrees of freedom in Equations (2.3.22) - (2.3.23) and neglecting the presence of external loads.

$$N_i(\xi,\boldsymbol{\xi}^{\mathbf{GA}},\boldsymbol{\beta}^*) = {}^iC_1 f_1(\xi) + {}^iC_2 f_2(\xi) \quad i=1,2 \tag{2.3.34}$$

$$N_i(\xi,\boldsymbol{\xi}^{\mathbf{GJ}},\boldsymbol{\alpha}^*) = {}^iD_1 g_1(\xi) + {}^iD_2 g_2(\xi) \quad i=3,4 \tag{2.3.35}$$

where:

$$\begin{aligned} &{}^1C_1 = 1; \qquad {}^1C_2 = -\frac{1}{f_2(1)}; \\ &{}^2C_1 = 0; \qquad {}^2C_2 = \frac{1}{f_2(1)}; \\ &{}^3D_1 = 1; \qquad {}^3D_2 = -\frac{1}{g_2(1)}; \\ &{}^4D_1 = 0; \qquad {}^4D_2 = \frac{1}{g_2(1)}. \end{aligned} \tag{2.3.36}$$

The components of the vector of the solution due to the contribution of external loads $\mathbf{u}_p(\xi,\boldsymbol{\xi}^{\mathbf{GA,GJ}},\boldsymbol{\beta}^*,\boldsymbol{\alpha}^*)$ can be derived by imposing zero displacements in all the degrees of freedom in Equations (2.3.22) - (2.3.23), respectively.

$$u_p(\xi,\boldsymbol{\xi}^{\mathbf{GA}},\boldsymbol{\beta}^*) = -f_3(0) f_1(\xi) + \frac{f_3(0)-f_3(1)}{f_2(1)} f_2(\xi) + f_3(\xi) \tag{2.3.37}$$

$$\theta_p(\xi,\boldsymbol{\xi}^{\mathbf{GJ}},\boldsymbol{\alpha}^*) = -g_3(0) g_1(\xi) + \frac{g_3(0)-g_3(1)}{g_2(1)} g_2(\xi) + g_3(\xi) \tag{2.3.38}$$

Using Equations (2.3.12) – (2.3.13), it is possible to express the shear force and the torsional moment along the beam axis:

$$\begin{bmatrix} T(\xi,\boldsymbol{\xi}^{\mathbf{GA}},\boldsymbol{\beta}^*) \\ M_T(\xi,\boldsymbol{\xi}^{\mathbf{GJ}},\boldsymbol{\alpha}^*) \end{bmatrix} = \mathbf{k}(\xi,\boldsymbol{\xi}^{\mathbf{GA,GJ}},\boldsymbol{\beta},\boldsymbol{\alpha})\cdot\begin{bmatrix} u^I(\xi,\boldsymbol{\xi}^{\mathbf{GA}},\boldsymbol{\beta}^*) \\ \theta^I(\xi,\boldsymbol{\xi}^{\mathbf{GJ}},\boldsymbol{\alpha}^*) \end{bmatrix} \tag{2.3.39}$$

where:

$$\begin{bmatrix} u^I(\xi,\boldsymbol{\xi}^{\mathbf{GA}},\boldsymbol{\beta}^*) \\ \theta^I(\xi,\boldsymbol{\xi}^{\mathbf{GJ}},\boldsymbol{\alpha}^*) \end{bmatrix} = \mathbf{B}(\xi,\boldsymbol{\xi}^{\mathbf{GA,GJ}},\boldsymbol{\beta}^*,\boldsymbol{\alpha}^*)\cdot\mathbf{q}_e + \begin{bmatrix} u_p^I(\xi,\boldsymbol{\xi}^{\mathbf{GA}},\boldsymbol{\beta}^*) \\ \theta_p^I(\xi,\boldsymbol{\xi}^{\mathbf{GJ}},\boldsymbol{\alpha}^*) \end{bmatrix} \tag{2.3.40}$$

$$\mathbf{B}(\xi,\boldsymbol{\xi}^{\mathbf{GA,GJ}},\boldsymbol{\beta}^*,\boldsymbol{\alpha}^*) = \begin{bmatrix} N_1^I(\xi,\boldsymbol{\xi}^{\mathbf{GA}},\boldsymbol{\beta}^*) & N_2^I(\xi,\boldsymbol{\xi}^{\mathbf{GA}},\boldsymbol{\beta}^*) & 0 & 0 \\ 0 & 0 & N_3^I(\xi,\boldsymbol{\xi}^{\mathbf{GJ}},\boldsymbol{\alpha}^*) & N_4^I(\xi,\boldsymbol{\xi}^{\mathbf{GJ}},\boldsymbol{\alpha}^*) \end{bmatrix} \tag{2.3.41}$$

$$\mathbf{k}(\xi,\boldsymbol{\xi}^{\mathbf{GA,GJ}},\boldsymbol{\beta},\boldsymbol{\alpha}) = \begin{bmatrix} 1-\sum_{j=1}^{m}\left(\beta_j-\beta_{j-1}\right)U\left(\xi-\xi_{\beta_j}\right) & 0 \\ 0 & 1-\sum_{j=1}^{m}\left(\alpha_j-\alpha_{j-1}\right)U\left(\xi-\xi_{\alpha_j}\right) \end{bmatrix} \tag{2.3.42}$$

The element stiffness matrix

The relationship between nodal displacements $\mathbf{q}_e$ and nodal forces $\mathbf{Q}_e^T = \begin{bmatrix} Q_1 & Q_2 & Q_3 & Q_4 \end{bmatrix}$ is ruled by the stiffness matrix $\mathbf{K_e}$ of the finite element, which can be obtained by means of the Principle of Virtual Work.

$$\mathbf{Q}_e^T\delta\mathbf{q}_e = \int_0^1 \mathbf{F}^T(\xi,\boldsymbol{\xi}^{\mathbf{GA,GJ}},\boldsymbol{\beta}^*,\boldsymbol{\alpha}^*)\cdot\delta\mathbf{u}^I(\xi,\boldsymbol{\xi}^{\mathbf{GA,GJ}},\boldsymbol{\beta}^*,\boldsymbol{\alpha}^*)d\xi \qquad \forall\delta\mathbf{q}_e,\forall\delta\mathbf{u}^I(\xi,\boldsymbol{\xi}^{\mathbf{GA,GJ}},\boldsymbol{\beta}^*,\boldsymbol{\alpha}^*) \tag{2.3.43}$$

where:

$$\mathbf{F}(\xi,\boldsymbol{\xi}^{\mathbf{GA,GJ}},\boldsymbol{\beta}^*,\boldsymbol{\alpha}^*) = \begin{bmatrix} T(\xi,\boldsymbol{\xi}^{\mathbf{GA}},\boldsymbol{\beta}^*) \\ M_T(\xi,\boldsymbol{\xi}^{\mathbf{GJ}},\boldsymbol{\alpha}^*) \end{bmatrix} \tag{2.3.44}$$

$$\mathbf{u}^I(\xi,\boldsymbol{\xi}^{\mathbf{GA,GJ}},\boldsymbol{\beta}^*,\boldsymbol{\alpha}^*) = \begin{bmatrix} u^I(\xi,\boldsymbol{\xi}^{\mathbf{GA}},\boldsymbol{\beta}^*) \\ \theta^I(\xi,\boldsymbol{\xi}^{\mathbf{GJ}},\boldsymbol{\alpha}^*) \end{bmatrix} \tag{2.3.45}$$

Substituting Equation (2.3.39) in Equation (2.3.43):

$$\mathbf{Q}_e^T\delta\mathbf{q}_e = \int_0^1 \mathbf{u}^{I,T}(\xi,\boldsymbol{\xi}^{\mathbf{GA,GJ}},\boldsymbol{\beta}^*,\boldsymbol{\alpha}^*)\cdot\mathbf{k}(\xi,\boldsymbol{\xi}^{\mathbf{GA,GJ}},\boldsymbol{\beta},\boldsymbol{\alpha})\cdot\delta\mathbf{u}^I(\xi,\boldsymbol{\xi}^{\mathbf{GA,GJ}},\boldsymbol{\beta}^*,\boldsymbol{\alpha}^*)d\xi \tag{2.3.46}$$
$$\forall\delta\mathbf{q}_e,\forall\delta\mathbf{u}^I(\xi,\boldsymbol{\xi}^{\mathbf{GA,GJ}},\boldsymbol{\beta}^*,\boldsymbol{\alpha}^*)$$

Substituting Equation (2.3.40), neglecting the contribution of the external load, in Equation (2.3.46):

$$\mathbf{Q}_e^T\delta\mathbf{q}_e = \mathbf{q}_e^T\cdot\int_0^1 \mathbf{B}^T(\xi,\boldsymbol{\xi}^{\mathbf{GA,GJ}},\boldsymbol{\beta}^*,\boldsymbol{\alpha}^*)\cdot\mathbf{k}(\xi,\boldsymbol{\xi}^{\mathbf{GA,GJ}},\boldsymbol{\beta},\boldsymbol{\alpha})\cdot\mathbf{B}(\xi,\boldsymbol{\xi}^{\mathbf{GA,GJ}},\boldsymbol{\beta}^*,\boldsymbol{\alpha}^*)d\xi\cdot\delta\mathbf{q}_e \qquad \forall\delta\mathbf{q}_e \tag{2.3.47}$$

Equation (2.3.47) allows to obtain the relationship between nodal displacements $\mathbf{q}_e$ and nodal forces $\mathbf{Q}_e$:

$$\mathbf{Q}_e = \mathbf{K_e}(\boldsymbol{\xi}^{\mathbf{GA,GJ}},\boldsymbol{\beta},\boldsymbol{\alpha},\boldsymbol{\beta}^*,\boldsymbol{\alpha}^*)\cdot\mathbf{q}_e \tag{2.3.48}$$

Where the stiffness matrix of the finite element is defined as:

$$\mathbf{K_e}(\boldsymbol{\xi}^{\mathbf{GA,GJ}},\boldsymbol{\beta},\boldsymbol{\alpha},\boldsymbol{\beta}^*,\boldsymbol{\alpha}^*) = \int_0^1 \mathbf{B}^T(\xi,\boldsymbol{\xi}^{\mathbf{GA,GJ}},\boldsymbol{\beta}^*,\boldsymbol{\alpha}^*)\cdot\mathbf{k}(\xi,\boldsymbol{\xi}^{\mathbf{GA,GJ}},\boldsymbol{\beta},\boldsymbol{\alpha})\cdot\mathbf{B}(\xi,\boldsymbol{\xi}^{\mathbf{GA,GJ}},\boldsymbol{\beta}^*,\boldsymbol{\alpha}^*)d\xi \tag{2.3.49}$$

Integrals can be solved in closed form due to the simple adopted shear-torsional only beam model. In particular, the G Points are representative of the beam segments with length w_j, as shown in Figure 2.13. Therefore, the singularity positions can be expressed as $\xi_{\beta j} = \sum_{n=1}^{j-1} w_n$.

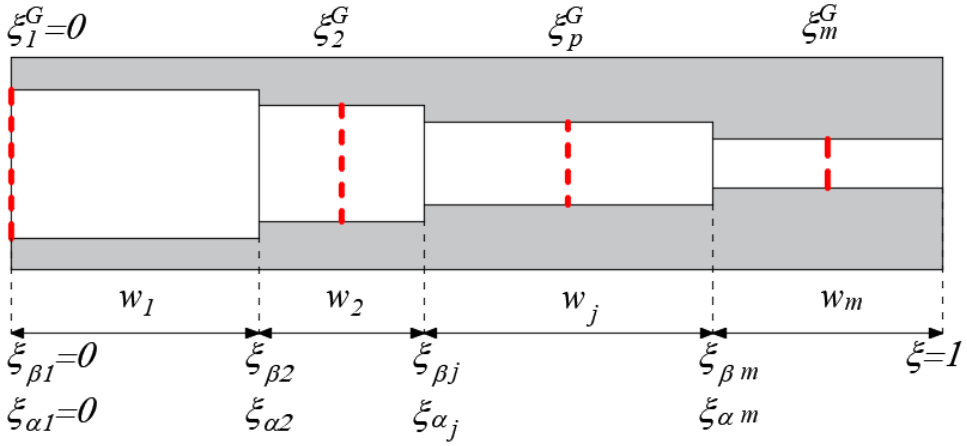

Figure 2.13 - Finite element subdivision

The stiffness matrix can be evaluated as follows:

$$\mathbf{K_e}(\boldsymbol{\xi}^{\mathbf{GA,GJ}},\boldsymbol{\beta},\boldsymbol{\alpha},\boldsymbol{\beta}^*,\boldsymbol{\alpha}^*) \approx \sum_{p=1}^{m} \mathbf{B}^T(\xi_p^G,\boldsymbol{\xi}^{\mathbf{GA,GJ}},\boldsymbol{\beta}^*,\boldsymbol{\alpha}^*)\cdot\mathbf{k}(\xi_p^G,\boldsymbol{\xi}^{\mathbf{GA,GJ}},\boldsymbol{\beta},\boldsymbol{\alpha})\cdot\mathbf{B}(\xi_p^G,\boldsymbol{\xi}^{\mathbf{GA,GJ}},\boldsymbol{\beta}^*,\boldsymbol{\alpha}^*)w_p \tag{2.3.50}$$

The nodal resisting forces and the nodal forces equivalent to the external load

Applying again the Principle of Virtual Work, it is possible to compute the nodal forces equivalent to the resisting forces. Substituting Equation (2.3.40), neglecting the contribution of the external load, in Equation (2.3.43), it is possible to obtain:

$$\mathbf{Q}_e^T\delta\mathbf{q}_e = \int_0^1 \mathbf{F}^T(\xi,\boldsymbol{\xi}^{\mathbf{GA,GJ}},\boldsymbol{\beta}^*,\boldsymbol{\alpha}^*)\cdot\mathbf{B}(\xi,\boldsymbol{\xi}^{\mathbf{GA,GJ}},\boldsymbol{\beta}^*,\boldsymbol{\alpha}^*)d\xi\cdot\delta\mathbf{q}_e \qquad \forall\delta\mathbf{q}_e \tag{2.3.51}$$

Or:

$$\mathbf{Q}_e(\boldsymbol{\xi}^{\mathbf{GA,GJ}},\boldsymbol{\beta}^*,\boldsymbol{\alpha}^*) = \int_0^1 \mathbf{B}^T(\xi,\boldsymbol{\xi}^{\mathbf{GA,GJ}},\boldsymbol{\beta}^*,\boldsymbol{\alpha}^*)\cdot\mathbf{F}(\xi,\boldsymbol{\xi}^{\mathbf{GA,GJ}},\boldsymbol{\beta}^*,\boldsymbol{\alpha}^*)d\xi \tag{2.3.52}$$

Analogously to the stiffness matrix, the vector of the nodal resisting forces can be evaluated by means of the following closed form solution:

$$\mathbf{Q}_e(\boldsymbol{\xi}^{\mathbf{GA,GJ}},\boldsymbol{\beta}^*,\boldsymbol{\alpha}^*) \approx \sum_{p=1}^{m} \mathbf{B}^T(\xi_p^G,\boldsymbol{\xi}^{\mathbf{GA,GJ}},\boldsymbol{\beta}^*,\boldsymbol{\alpha}^*)\cdot\mathbf{F}(\xi_p^G,\boldsymbol{\xi}^{\mathbf{GA,GJ}},\boldsymbol{\beta}^*,\boldsymbol{\alpha}^*)w_p \tag{2.3.53}$$

Applying the Principle of Virtual Work, it is possible to obtain the vector of the nodal forces equivalent to the external load:

$$\mathbf{P}_e^T\delta\mathbf{q}_e = \int_0^1 \mathbf{f}^T(\xi)\cdot\delta\mathbf{u}(\xi,\boldsymbol{\xi}^{\mathbf{GA,GJ}},\boldsymbol{\beta}^*,\boldsymbol{\alpha}^*)d\xi \qquad \forall\mathbf{u}(\xi,\boldsymbol{\xi}^{\mathbf{GA,GJ}},\boldsymbol{\beta}^*,\boldsymbol{\alpha}^*) \tag{2.3.54}$$

where:

$$\mathbf{f}(\xi)=\begin{bmatrix} p(\xi) \\ t(\xi) \end{bmatrix} \tag{2.3.55}$$

$$\mathbf{u}(\xi,\boldsymbol{\xi}^{\mathbf{GA,GJ}},\boldsymbol{\beta}^*,\boldsymbol{\alpha}^*)=\begin{bmatrix} u(\xi,\boldsymbol{\xi}^{\mathbf{GA}},\boldsymbol{\beta}^*) \\ \theta(\xi,\boldsymbol{\xi}^{\mathbf{GJ}},\boldsymbol{\alpha}^*) \end{bmatrix} \tag{2.3.56}$$

Substituting Equation (2.3.33) , neglecting the contribution of the external load, in Equation (2.3.54), it is possible to obtain:

$$\mathbf{P}_e^T\delta\mathbf{q}_e=\int_0^1\mathbf{f}^T(\xi)\cdot\mathbf{N}(\xi,\boldsymbol{\xi}^{\mathbf{GA,GJ}},\boldsymbol{\beta}^*,\boldsymbol{\alpha}^*)d\xi\cdot\delta\mathbf{q}_e \qquad \forall\delta\mathbf{q}_e \tag{2.3.57}$$

Therefore, the vector of the nodal forces equivalent to the external load is:

$$\mathbf{P}_e(\boldsymbol{\xi}^{\mathbf{GA,GJ}},\boldsymbol{\beta}^*,\boldsymbol{\alpha}^*)=\int_0^1\mathbf{N}^T(\xi,\boldsymbol{\xi}^{\mathbf{GA,GJ}},\boldsymbol{\beta}^*,\boldsymbol{\alpha}^*)\cdot\mathbf{f}(\xi)d\xi \tag{2.3.58}$$

As before, it can be evaluated by means of the following closed form solution:

$$\mathbf{P}_e(\boldsymbol{\xi}^{\mathbf{GA,GJ}},\boldsymbol{\beta}^*,\boldsymbol{\alpha}^*)\approx\sum_{p=1}^{m}\mathbf{N}^T(\xi_p^G,\boldsymbol{\xi}^{\mathbf{GA,GJ}},\boldsymbol{\beta}^*,\boldsymbol{\alpha}^*)\cdot\mathbf{f}(\xi_p^G)w_p \tag{2.3.59}$$

In case the multi-stepped beam element is subjected only to n_F concentrated forces $\bar{F}_r, r=1,\ldots,n_F$, applied at the abscissae ξ_{F_r} with eccentricity e_r, the load terms become:

$$p(\xi)=\sum_{r=1}^{nF}F_r\delta\left(\xi-\xi_{F_r}\right) \qquad \text{where } F_r=\frac{\bar{F}_r}{G_0A_0} \tag{2.3.60}$$

$$t(\xi)=\sum_{r=1}^{nF}T_r\delta\left(\xi-\xi_{F_r}\right) \qquad \text{where } T_r=\frac{\bar{F}_re_r}{G_0J_{T0}}L \tag{2.3.61}$$

$$\begin{aligned}\mathbf{P}_e(\boldsymbol{\xi}^{\mathbf{GA,GJ}},\boldsymbol{\beta}^*,\boldsymbol{\alpha}^*)&=\int_0^1\mathbf{N}^T(\xi,\boldsymbol{\xi}^{\mathbf{GA,GJ}},\boldsymbol{\beta}^*,\boldsymbol{\alpha}^*)\cdot\begin{bmatrix}\sum_{r=1}^{nF}F_r\delta\left(\xi-\xi_{F_r}\right)\\ \sum_{r=1}^{nF}T_r\delta\left(\xi-\xi_{F_r}\right)\end{bmatrix}d\xi=\\ &=\sum_{r=1}^{nF}\int_0^1\mathbf{N}^T(\xi,\boldsymbol{\xi}^{\mathbf{GA,GJ}},\boldsymbol{\beta}^*,\boldsymbol{\alpha}^*)\delta\left(\xi-\xi_{F_r}\right)d\xi\cdot\begin{bmatrix}F_r\\T_r\end{bmatrix}=\\ &=\sum_{r=1}^{nF}\mathbf{N}^T(\xi_{F_r},\boldsymbol{\xi}^{\mathbf{GA,GJ}},\boldsymbol{\beta}^*,\boldsymbol{\alpha}^*)U\left(1-\xi_{F_r}\right)\cdot\begin{bmatrix}F_r\\T_r\end{bmatrix}\end{aligned} \tag{2.3.62}$$

Useful quantities:

$$f_1^I(\xi)=0$$

$$f_2^I(\xi)=1+\sum_{j=1}^{m}\beta^*{}_jU\left(\xi-\xi_{\beta_j}\right)$$

$$f_3^I(\xi)=-p^{[1]}(\xi)-\sum_{j=1}^{m}\beta^*{}_jp^{[1]}(\xi)U\left(\xi-\xi_{\beta_j}\right)$$

$$g_1^I(\xi)=0$$

$$g_2^I(\xi)=1+\sum_{j=1}^{m}\alpha^*{}_jU\left(\xi-\xi_{\alpha_j}\right)$$

$$g_3^I(\xi) = -t^{[1]}(\xi) - \sum_{j=1}^{m} \alpha^*{}_j \, t^{[1]}(\xi) U\left(\xi - \xi_{\alpha_j}\right)$$

$$u_p^I(\xi, \boldsymbol{\xi}^{\mathbf{GA}}, \boldsymbol{\beta}^*) = -f_3(0) f_1^I(\xi) + \frac{f_3(0) - f_3(1)}{f_2(1)} f_2^I(\xi) + f_3^I(\xi)$$

$$\theta_p^I(\xi, \boldsymbol{\xi}^{\mathbf{GJ}}, \boldsymbol{\alpha}^*) = -g_3(0) g_1^I(\xi) + \frac{g_3(0) - g_3(1)}{g_2(1)} g_2^I(\xi) + g_3^I(\xi)$$

$$N_i^I(\xi, \boldsymbol{\xi}^{\mathbf{GA}}, \boldsymbol{\beta}^*) = {}^iC_1 f_1^I(\xi) + {}^iC_2 f_2^I(\xi) \quad i = 1,2$$

$$N_i^I(\xi, \boldsymbol{\xi}^{\mathbf{GJ}}, \boldsymbol{\alpha}^*) = {}^iD_1 g_1^I(\xi) + {}^iD_2 g_2^I(\xi) \quad i = 3,4$$

where:

$${}^1C_1 = 1; \qquad {}^1C_2 = -\frac{1}{f_2(1)};$$

$${}^2C_1 = 0; \qquad {}^2C_2 = \frac{1}{f_2(1)};$$

$${}^3D_1 = 1; \qquad {}^3D_2 = -\frac{1}{g_2(1)};$$

$${}^4D_1 = 0; \qquad {}^4D_2 = \frac{1}{g_2(1)}.$$

Graphical representation of the shape functions

The shape functions of the step-wise shear-torsional beam finite element are able to reproduce correctly the static deflection of a multi-stepped beam, even in presence of localisation of plastic deformations at a storey. Of course, the shape functions depend on the stiffness jumps β_j and α_j of each beam segment. In case of uniform beam segments, the shape functions are equal to the shape functions of a uniform shear-torsional beam element.

In order to provide a graphical representation of these shape functions, a beam finite element with length equal to 6 m has been considered. The beam finite element has been divided into 6 uniform segments of equal length, as reported in Figure 2.14. Three case studies, which assume different steel section profiles in each uniform beam segment as reported in Table 2.1, are analysed. The adopted shear modulus is G = 80769 MPa.

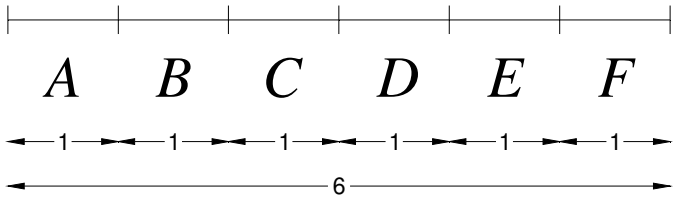

Figure 2.14 - Investigated beam finite element

Table 2.1 - Adopted section profiles for each beam segment

Beam segment	Case 1 Uniform	Case 2 Step-wise	Case 3 Soft-segment
	Profile	**Profile**	**Profile**
A	HE 240 A	HE 240 A	HE 240 A
B	HE 240 A	HE 240 A	HE 240 A
C	HE 240 A	HE 180 A	HE 120 A
D	HE 240 A	HE 180 A	HE 240 A
E	HE 240 A	HE 120 A	HE 240 A
F	HE 240 A	HE 120 A	HE 240 A

Table 2.2 - Profile areas

Profile	Area 10^{-4} [m2]
HE 240 A	76.8
HE 180 A	45.3
HE 120 A	25.3

In Figure 2.15 the two shape functions for the shear behaviour have been reported for each case study: Uniform beam element (blue), Step-wise beam element with decreasing size of the section profile (red) and beam element with segment C having smaller cross section than the others (soft-segment, green). The torsional shape functions have similar graphical representation.

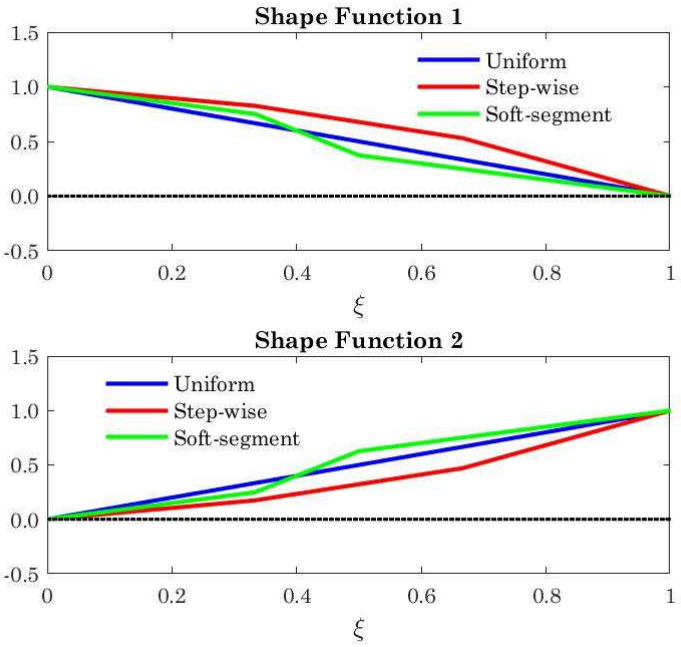

Figure 2.15 - Shear shape functions of a step-wise beam element

Inelastic beam finite element for the beam-like model

In this paragraph, the step-wise shear-torsional beam finite element is adopted for the static non-linear analysis of the inelastic beam-like model.

A unique step-wise shear-torsional beam finite element is adopted for the entire beam-like model, each beam finite element segment with uniform stiffness corresponding to an inter-storey building. In particular, the singularities positions ξ_{β_j} and ξ_{α_j} coincide with the floor levels.

For the sake of simplicity, the chosen G points represent control sections of the beam segments where the plastic constitutive laws are usually integrated according to a discrete incremental approach. In this case, the G points are assumed to be coincident with the central position of each uniform finite element segment, except for the first beam segment where the G point is located at the initial end. Therefore, the constitutive law of each beam segment is assumed to be equal to the constitutive law of the corresponding inter-storey and the total number of beam segments is equal to the number of inter-storeys of the building. The terms w_j are the dimensionless length of the uniform beam segments.

According to the classical Newton–Raphson approach for the solution of non-linear incremental problems in the context of holonomic plasticity in each time step, an incremental iterative procedure is followed. Initially, the parameters β_j and α_j represent the shear and torsional stiffness jumps with respect to the reference values G_0A_0 and G_0J_{T0},respectively, along the beam axis. In the generic step of the incremental integration procedure in presence of plastic occurrences, the parameters β_j and α_j have to be updated according to the current internal force-relative displacement state and the inter-storey constitutive law.

In Figure 2.16 the beam-like model with m beam segments (and control sections) is depicted. The dimensionless length of the uniform beam segments and the positions of the G points are indicated with w_j and ξ_j^G, respectively.

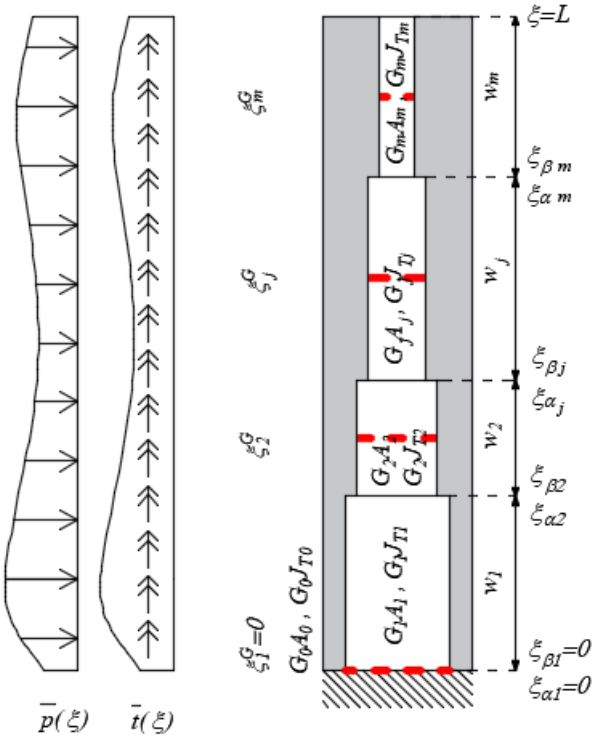

Figure 2.16 - Beam-like model according to the proposed inelastic finite element

SECTION 3. THE ADOPTION OF THE BEAM-LIKE MODEL FOR SEISMIC ASSESSMENT OF BUILDINGS

Nowadays the seismic vulnerability assessment of new and existing buildings is one of the most important tasks focused by researchers. The link between the seismic hazard and the effects on the built environment can be established by means of fragility curves. In this section, a brief description of fragility curves and their construction process is reported. These curves can be evaluated either by means of a complete FEM non-linear model of the building or a low-cost beam-like model. In the numerical section it will be emphasized how the proposed beam-like model can be very useful for the seismic assessment of existing buildings. In fact, it will be shown that analytical fragility functions can be estimated by performing non-linear dynamic analyses on the equivalent beam-like model drastically reducing the required computational effort but still maintaining a high level of accuracy.

3.1 FRAGILITY CURVES

A fragility function specifies the probability of collapse, or some other limit states of interest, of a structure as a function of some ground motion intensity measure (*IM*). The term collapse refers in general to the achievement of a fixed threshold (*DT*) by the chosen Damage Parameter (*DP*). Therefore, in the following the probability of collapse is used to refer to the probability of reaching a limit state of interest.

The *IM* of the ground motion should describe its main intensity characteristics and may be related to time-history, to energy-content or to spectral components. It could be represented by different parameters such as the Peak Ground Acceleration (PGA), the spectral acceleration corresponding to the first period of vibration of the structure (Sa(T)), the Housner Intensity (SI_H), the Energy density (Iv), the strong motion time duration (t_D), etc. While, on the other hand, the *DP* should be a simple output of the structural analyses. Displacement of the top floor, inter-storey drifts ratio or floor accelerations can be chosen for example as Damage Parameters. In Figure 3.1 an example of fragility function for a hypothetic building has been reported. It clearly shows the probability of collapse for a fixed *IM* level. For example, for a ground motion with *IM* = 0.75, the probability of collapse of the building is about 80%.

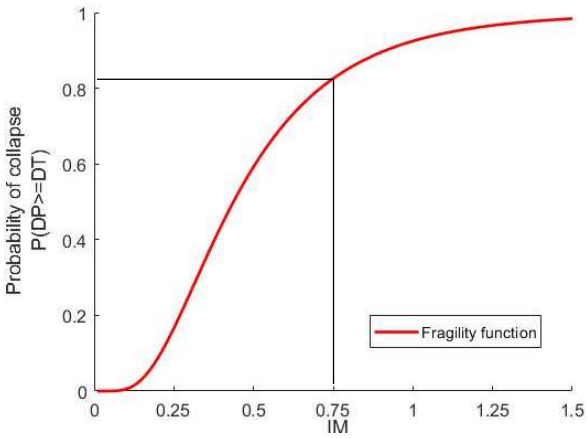

Figure 3.1 - Example of a fragility function

The fragility curves have been estimated following the Baker statistical procedure, reported in [106] and briefly described in the following.

Two different approaches can be used for the evaluation of the fragility curves: the first follows the incremental dynamic analysis (IDA) procedure, while the second follows the multiple stripe analysis (MSA) procedure. In the IDA a suite of ground motions is repeatedly scaled in order to find the *IM* level at which each ground motion causes collapse. In the MSA the analysis is performed at a specified set of *IM* levels, each of which has a unique ground motion set. The second one allows to reduce the number of non-linear dynamic analyses to be performed for different ground motions at varying intensity levels.

A lognormal cumulative distribution function is often used to define a fragility function:

$$P(C|IM = x) = \Phi\left(\frac{\ln(x) - \mu}{\sigma}\right) \tag{3.1.1}$$

where $P(C|IM = x)$ is the probability that a ground motion with $IM=x$ will cause the structure to collapse, $\Phi(\ )$ is the standard cumulative distribution function (CDF), μ is the median of the fragility function ($\ln IM$), σ is the standard deviation of $\ln IM$. Calibration of Equation (3.1.1) for a given structure requires estimating μ and σ from structural analysis results. Their estimated values will be denoted as $\hat{\mu}$ and $\hat{\sigma}$ in the following.

There are two common statistical approaches for estimating parameters from data. The *method of moments* finds parameters such that the resulting distribution has the same moments (e.g. the mean and standard deviation) of the sample moments of the observed data. The *maximum likelihood method* finds the parameters such that the resulting distribution has the highest likelihood of having produced the observed data.

In the following, appropriate methods for estimating parameter values for the fragility function that are consistent with the data collected as results of the IDA or MSA are briefly described.

Incremental Dynamic Analysis

Incremental dynamic analysis involves scaling each ground motion in an opportune range until it causes the collapse of the structure [107]. This process produces a set of *IM* values associated with the collapse limit state for each ground motion, as illustrated in Figure 3.2a. For a given $IM=x$, the probability of collapse can be estimated as the cumulative frequency of the analyses reaching collapse at a level lower than x.

These probabilities are referred to as an empirical cumulative distribution function, and are illustrated in Figure 3.2b. Fragility function parameters can be estimated from this data by taking logarithms of each ground motion's *IM* value associated with onset of collapse, and computing their mean and standard deviation [108]:

$$\hat{\mu} = \frac{1}{n}\sum_{i=1}^{n} \ln IM_i \tag{3.1.2}$$

$$\hat{\sigma} = \sqrt{\frac{1}{n-1}\sum_{i=1}^{n} \left(\ln IM_i - \hat{\mu}\right)^2} \tag{3.1.3}$$

where n is the number of ground motions considered, and IM_i is the *IM* value associated with onset of collapse for the i-th ground motion. This is a method of moment estimators, as μ and σ are the mean and standard deviation, respectively, of the lognormal distribution representing the *IM* values. The mean and standard deviation, or moments, of the distribution are estimated

using the sample moments from a set of data. A fragility function fitted using this approach is shown in Figure 3.2b.

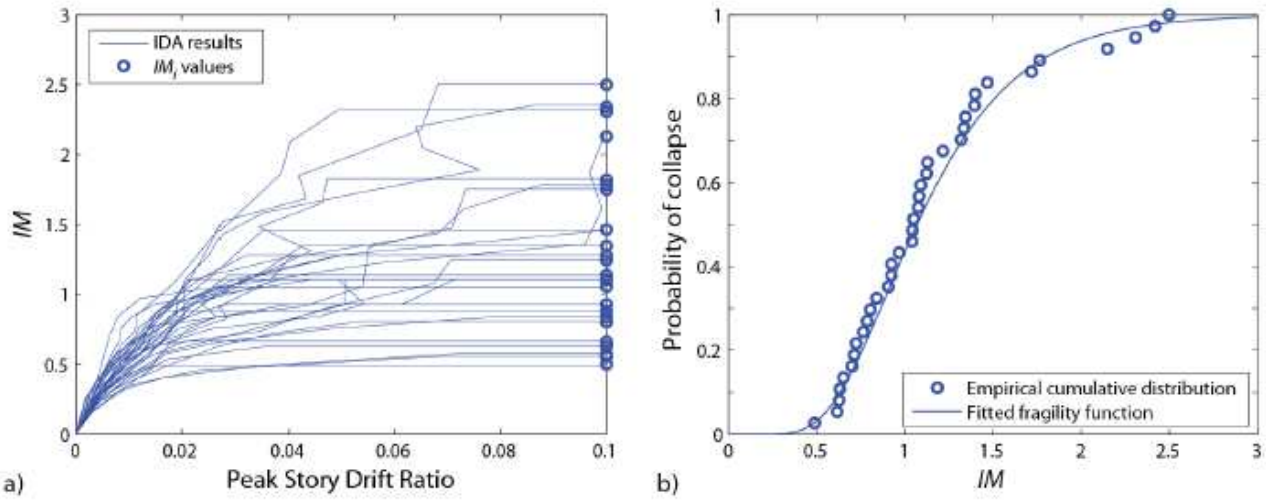

Figure 3.2 - a) Example IDA results, used to identify *IM* values associated with collapse for each ground motion; b) observed fractions of collapse as a function of *IM*, and a fragility function estimated using equations (3.1.2) and (3.1.3) - [106]

Truncated Incremental Dynamic Analysis

In the incremental dynamic analysis some ground motions may need to be scaled to large *IM* values in order to produce collapse; this procedure raises several concerns which are illustrated in the following. First of all, in order to observe collapse, many structural analyses have to be performed with increasing *IM* levels, therefore it is computationally expensive. Second, the large-*IM* results are less practically relevant, as the fragility function values at large-*IM* levels are less interesting than the values corresponding to small-*IM* levels. Furthermore, scaling typical moderate-*IM* ground motions up to extreme *IM* levels is not an accurate way to represent earthquakes of such large-*IM* levels [109].

A different strategy has been proposed in [106] in order to overcome these limitations. In particular, incremental dynamic analysis is performed only up to a level, IM_{max}, above which no further non-linear dynamic analyses are performed. Illustrative results from this type of analysis are shown in Figure 3.3a. Therefore, if n ground motions are used in the analysis, there will in general be m ground motions that caused collapse at *IM* levels lower that IM_{max} and n-m ground motions that did not cause collapse prior to the analysis being stopped.

The data collected in this type of analysis cannot be used to estimate the fragility function parameters by using Equations (3.1.2)-(3.1.3). However, it is possible to estimate μ and σ by using the maximum likelihood method to compute the likelihood of observing the data obtained in the analysis.

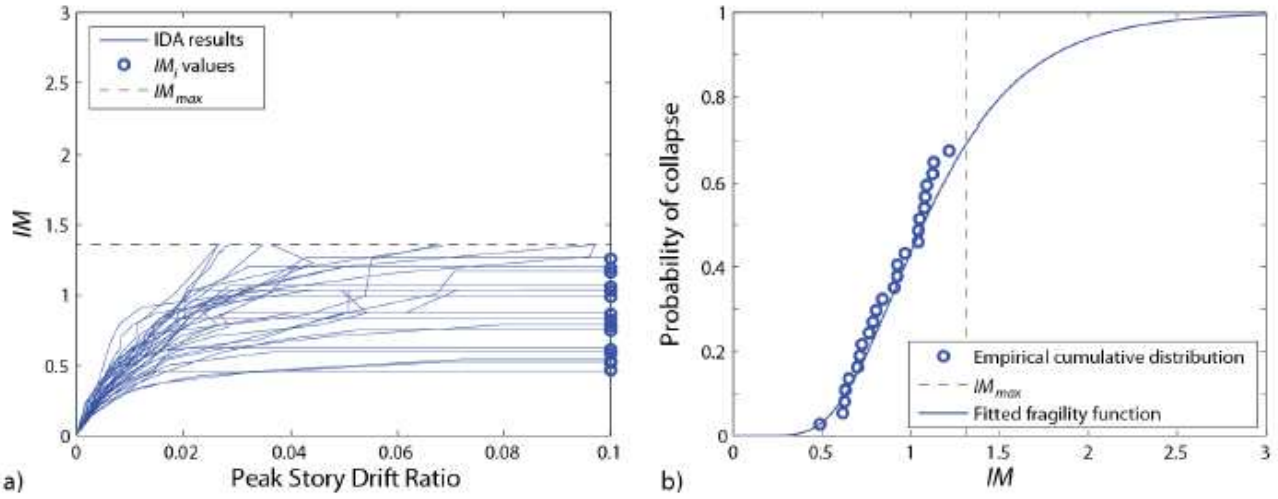

Figure 3.3 - a) Example truncated IDA analysis results; b) observed fractions of collapse as a function of *IM*, and a fragility function estimated using equation (3.1.7) - [106]

The *IM* values at collapse (IM_i) for the m ground motions causing collapse are known. Assuming Equation (3.1.1) for the definition of the fragility function, the likelihood that an arbitrary ground motion with IM_i causes collapse is given by the lognormal distribution probability density function (PDF):

$$\text{Likelihood} = \phi\left(\frac{\ln(IM_i)-\mu}{\sigma}\right) \tag{3.1.4}$$

where $\phi(\ )$ denotes the standard normal distribution PDF. The n-m ground motions that did not cause collapse at IM_{max} are called censored data, since it is possible to know only that the corresponding IM_i are greater than IM_{max}. The likelihood that a given ground motion can be scaled to IM_{max} without causing collapse is the probability that the corresponding IM_i is greater than IM_{max}:

$$\text{Likelihood} = 1-\Phi\left(\frac{\ln(IM_{\max})-\mu}{\sigma}\right) \tag{3.1.5}$$

Assuming that the IM_i value for each ground motion is independent, the likelihood of the entire observed data set is the product of the individual likelihoods:

$$\text{Likelihood} = \left(\prod_{i=1}^{m}\phi\left(\frac{\ln(IM_i)-\mu}{\sigma}\right)\right)\left(1-\Phi\left(\frac{\ln(IM_{\max})-\mu}{\sigma}\right)\right)^{n-m} \tag{3.1.6}$$

where $\prod$ denotes a product over i values from 1 to m (corresponding to the m ground motions that caused collapse at *IM* levels lower than IM_{max}). Maximizing this Likelihood Equation, the fragility function parameters can be estimated. It is mathematically equivalent and numerically easier to maximize the logarithm of the likelihood function:

$$\{\hat{\mu},\hat{\sigma}\} = \arg\max_{\mu,\sigma}\left\{\sum_{i=1}^{m}\ln\phi\left(\frac{\ln(IM_i)-\mu}{\sigma}\right)+(n-m)\ln\left[1-\Phi\left(\frac{\ln(IM_{\max})-\mu}{\sigma}\right)\right]\right\} \tag{3.1.7}$$

A fragility function obtained using this Equation is shown in Figure 3.3b. It is worth noting that in the special case where all the n ground motions cause collapse at *IM* values lower than IM_{max}, the solution of Equation (3.1.7) is equivalent to the Equations (3.1.2)-(3.1.3), except that the "*n-1*" in Equation (3.1.3) is an "*n*" in Equation (3.1.7). furthermore, the normal distribution PDF

and CDF in Equation (3.1.7) can be replaced with the PDF and CDF of another distribution type, in order to fit a fragility function for some other distributions.

Multiple Stripe Analysis

The fragility functions can be estimated with a different approach than IDA, by using the Multiple Stripe Analysis, where the structural analyses are performed at a discrete set of *IM* levels and different ground motions are used at each *IM* level. Following this approach, the analysis need not to be performed up to *IM* amplitudes where all ground motions cause collapse. An example of MSA results is shown in Figure 3.4a. Due to the differing ground motions used at each *IM* level, strictly increasing fractions of collapse with increasing *IM* level may not be observed, even though it is expected that the true probability of collapse is increasing with *IM*. With this type of data, it is not possible to estimate the fragility function parameters by using the approaches described above, because the IM_i values associated with the onset of collapse for a given ground motion are unknown. Instead, the structural analysis results provide the fraction of ground motions that cause collapse at each *IM* level. The appropriate fitting technique for this type of data is to use the method of maximum likelihood, briefly described in the following.

At each intensity level $IM=x_j$, the dynamic analyses produce some number of collapses out of a total number of ground motions. Assuming that observation of collapse or no-collapse from each ground motion is independent on the observations from other ground motions, the probability of observing z_j collapses out of n_j ground motions with $IM=x_j$ is given by the binomial distribution:

$$P\left(z_j \text{ collapses in } n_j \text{ ground motions}\right) = \binom{n_j}{z_j} p_j^{z_j} \left(1-p_j\right)^{n_j-z_j} \tag{3.1.8}$$

where p_j is the probability that a ground motion with $IM=x_j$ will cause collapse of the structure. The goal is to identify the fragility function that will predict p_j, and the maximum likelihood approach identifies the fragility function that gives the highest probability of observing the collapse data obtained from dynamic analyses. The likelihood of the entire data set is obtained by the product of the binomial probabilities (Equation (3.1.8)) at each *IM* level:

$$\text{Likelihood} = \prod_{j=1}^{m} \binom{n_j}{z_j} p_j^{z_j} \left(1-p_j\right)^{n_j-z_j} \tag{3.1.9}$$

where m is the number of *IM* levels. Substituting Equation (3.1.1) in p_j, it is possible making explicit the fragility function parameters in the likelihood function:

$$\text{Likelihood} = \prod_{j=1}^{m} \binom{n_j}{z_j} \left(\Phi\left(\frac{\ln(x_j)-\mu}{\sigma}\right)\right)^{z_j} \left(1-\Phi\left(\frac{\ln(x_j)-\mu}{\sigma}\right)\right)^{n_j-z_j} \tag{3.1.10}$$

Estimates of the fragility function parameters are obtained by maximizing this likelihood function. It is equivalent and numerically easier to maximize the logarithm of the likelihood function:

$$\{\hat{\mu},\hat{\sigma}\} = \arg\max_{\mu,\sigma} \sum_{j=1}^{m} \left\{ \ln\binom{n_j}{z_j} + z_j \ln\Phi\left(\frac{\ln(x_j)-\mu}{\sigma}\right) + \left(n_j-z_j\right)\ln\left(1-\Phi\left(\frac{\ln(x_j)-\mu}{\sigma}\right)\right)\right\} \tag{3.1.11}$$

A fragility function obtained using this approach is plotted in Figure 3.4b.

Equation (3.1.11) has been obtained using a lognormal cumulative distribution function for the fragility function, but other functions can be substituted without changing the fitting approach. It is worth noting that this formulation does not require multiple observations at each *IM* level of interest (i.e. n_i can equal 1). This makes it useful, for example, when fitting a fragility function using unscaled ground motions, each having unique *IM* amplitude.

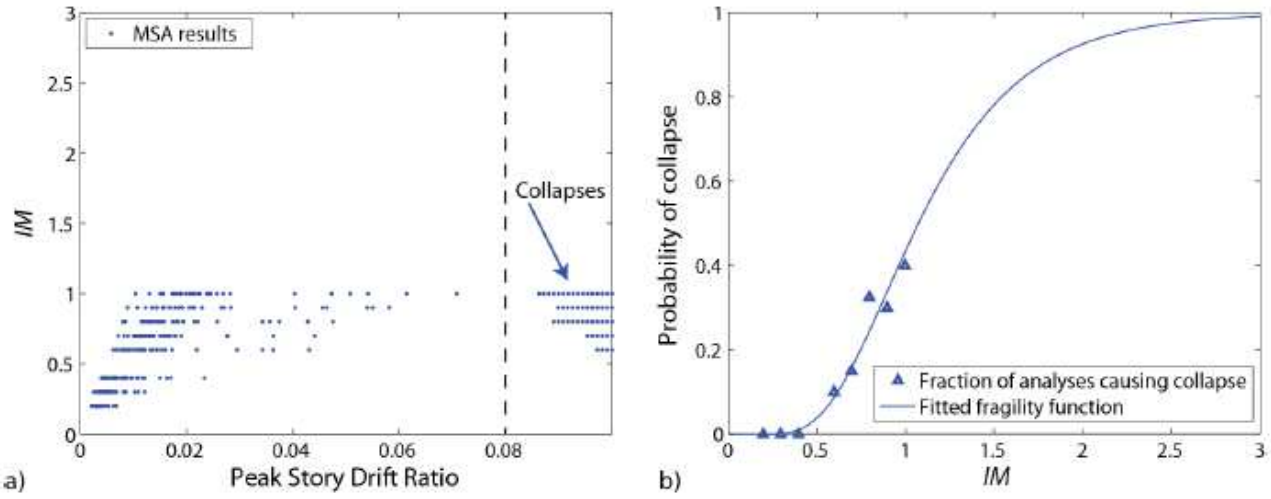

Figure 3.4 - a) Example MSA analysis results. Analyses causing collapse are plotted at Peak Storey Drift Ratios greater than 0.08, and are offset from each other to aid in visualizing the number of collapses; b) observed fractions of collapse as a function of *IM*, and a fragility function estimated using equation (3.1.11) - [106]

SECTION 4. **NUMERICAL APPLICATIONS**

In this section, the reliability of the beam-like model has been investigated by performing structural analyses on two benchmarks. The first case study is a multi-storey RC frame denoted as "Edificio Catania", while the second one is the well-known SAC9 building already considered in the scientific literature. In the following, the "Edificio Catania" has been first presented, then static and dynamic analyses have been performed by means of both its equivalent elastic and inelastic beam-like models. Fragility curves for this building have been also obtained by using the equivalent inelastic beam-like model.
Finally, the inelastic beam-like model has been used for the static and dynamic non-linear analyses of the SAC9 building.

4.1 CASE STUDY 1: EDIFICIO CATANIA

In order to apply the proposed procedure to real structures, a multi-storey RC frame representative of residential buildings designed to resist only gravity loads has been considered. The considered building has been chosen as benchmark, characterised by different number of storeys, within an extensive survey focused on multi-storey RC buildings built in Catania, Italy, before the introduction of the seismic code [110, 111, 112].
The building here considered has 6 storeys, each one having inter-storey height equal to 3.3 m except the first storey which has an inter-storey height equal to 4.3 m. The dimensions of the cross sections of the beams on the edge were assumed to be 30 × 50 cm^2, while all the remaining beams have a 110 × 23 cm^2 size. The columns were assumed fully fixed at the base. A reduction along the height of the building in the column cross-section has been introduced as shown in Figure 4.2. The material properties were characterised by a Young's modulus of 29962 MPa, a Poisson ratio equal to 0.2 and a mass density of 25 kN/m^3.

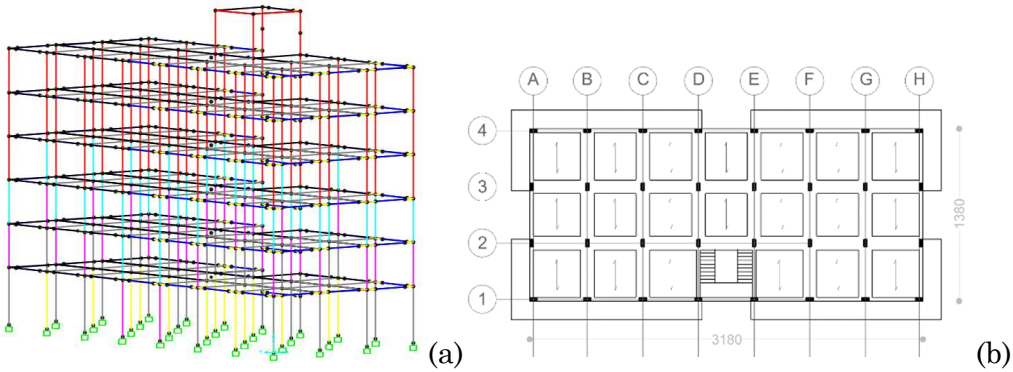

Figure 4.1 - 3D FEM model (a) and plan of the building (b)

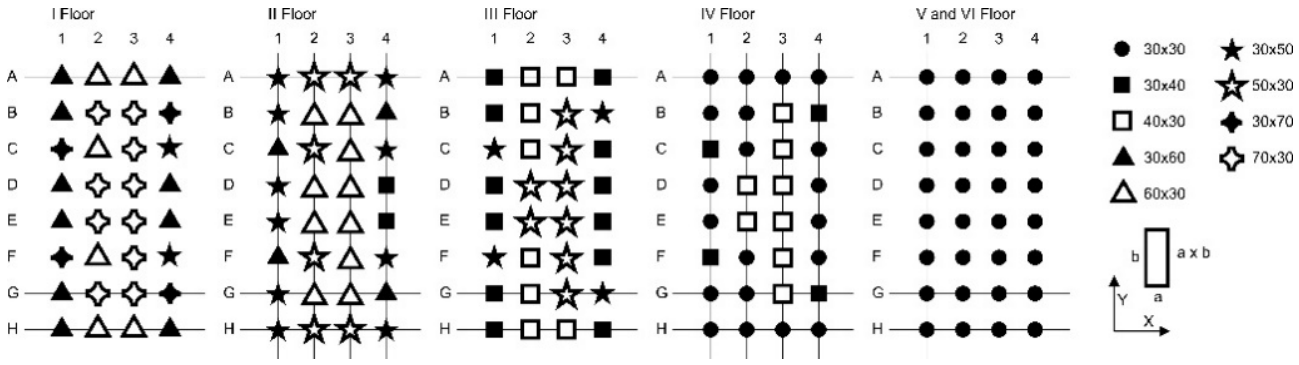

Figure 4.2 - Cross sections of the columns

The floors haven't been modelled, but they are reported as uniformly distributed area loads according to Table 4.1. The loads referring to the balcony and the stairs have been reported as uniformly distributed line loads according to Table 4.2 and Figure 4.3. Floor diaphragms have been also introduced.

Table 4.1 - Area loads

	Gk [kN/m^2]	**Qk** [kN/m^2]
1°-2°-3°-4°-5° FLOOR	6,25	2
TOP FLOOR	5,25	2
BALCONY	4,60	4
STAIRS	7,87	4

Table 4.2 - Line loads

	Gk [kN/m]	**Qk** [kN/m]	**Gk_tamp** [kN/m]
EDGE BEAMS - Balcony	6,89	6,00	5,67
EDGE BEAMS - Balcony – Top floor	6,89	6,00	2,84
STAIRS BEAMS	17,71	9	

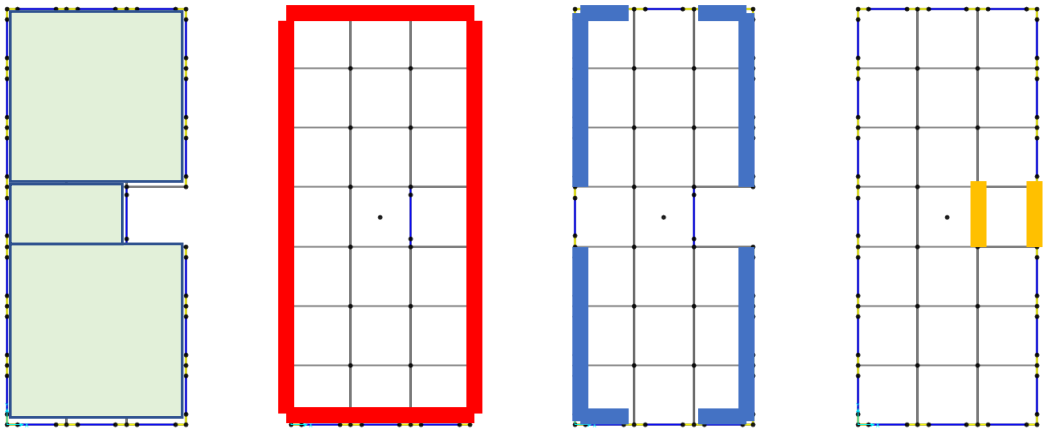

Figure 4.3 - From left to right: area, infill, balcony and stairs applied load position

4.2 CASE STUDY 1: BEAM LIKE MODEL - LINEAR ELASTIC BEHAVIOUR

In this paragraph the linear elastic behaviour of the considered building has been studied by means of the elastic beam-like model.

First, the calibration procedure was performed. Then the proposed multi-stepped beam was adopted for simulating the static and dynamic behaviour of the building and the results, in terms of static and seismic response, were compared to those obtained by means of a conventional 3D FEM model developed with SAP2000 v.23 [113].

The static displacements of the nodes at each floor have been evaluated by considering a uniform and an inverse triangular force distribution. The forces in the FEM and in the beam-like models are applied to the center of gravity (centroid) of each floor of the building, separately in the x and y directions. The values of the applied forces from the bottom to the top floor in the two load conditions are assumed as follows:

a) [100 100 100 100 100 100] kN;

b) [20.67 36.54 52.40 68.27 84.13 100] kN.

Aiming at simulating representative seismic inputs that may occur on the Italian peninsula, linear dynamic analyses were performed by considering, in the x and y directions, two real seismic records [114] that occurred in Santa Venerina (2018) and L'Aquila (2009), plotted, respectively, in Figure 4.4a-b. Some characteristic data of the two records (PGA, PGV, PGD, distance for epicentre) are reported in Table 4.3. In all the time-histories, constant modal damping ratios $\xi_j = 0.05$, for all considered modes, were assumed.

Table 4.3 - Records adopted in numerical simulation

Record	State	Date	Hour	Mw	Dist. (km)	PGA (cm/s²)	PGV (cm/s)	PGD (cm)	Lat. (°)	Long. (°)
Santa Venerina	Italy	2018-12-26	02:19:17	4.9	6.9	−547.932 (E)	37.128 (E)	5.696 (E)	37.644	15.116
L'Aquila	Italy	2009-04-06	01:32:40	6.1	4.9	644.246 (E)	−42.720 (N)	6.789 (E)	42.342	13.380

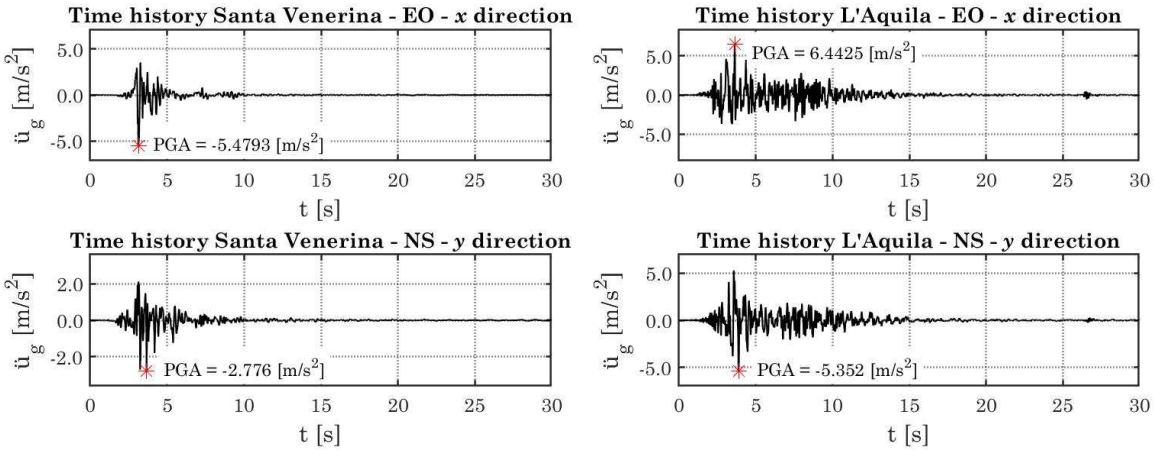

(**a**) (**b**)

Figure 4.4 - Accelerograms of (a) Santa Venerina (2018) and (b) L'Aquila (2009).

4.2.1 Calibration procedure

Aiming to numerically compare, for the considered building, the modal shapes that have been obtained by means of the beam-like and the FEM models, a consistency indicator is needed. The Modal Assurance Criterion (MAC) is here used calculating the following matrix elements:

$$MAC_{ij} = \frac{\left(\boldsymbol{\varphi}_{i,BL} \cdot \boldsymbol{\varphi}_{j,FEM}^{T}\right)^{2}}{\left(\boldsymbol{\varphi}_{i,BL} \cdot \boldsymbol{\varphi}_{i,BL}^{T}\right)\left(\boldsymbol{\varphi}_{j,FEM} \cdot \boldsymbol{\varphi}_{j,FEM}^{T}\right)} \tag{4.2.1}$$

where each term of the MAC matrix is bounded between 0 and 1.
Taking into account the orthogonality properties of the modes of vibration, a perfect coincidence between the modal shapes in the two models would provide a diagonal unitary matrix. Therefore, values close to 1 in the main diagonal of the matrix indicate a good correspondence of the modal shapes, while low values indicate that the modes are not consistent [115].

With reference to the number of eigen-properties required to accurately evaluate the stiffness of the equivalent beam, after some numerical analyses it has been verified that in this case it is sufficient to consider the first three frequencies and the corresponding mode shapes. Namely, in the optimization problem of the stiffness coefficients, for the considered building, due to the contemporary presence of the considered irregularities (in the horizontal and in the vertical distribution of stiffness), besides the first three frequencies, the mode shape displacements at the top floor of the first three modes of vibration have been taken into account in Eq. (2.1.31).

The validity of the latter statement has been proved by evaluating the stiffness correction coefficients for the equivalent beam like model either by including or neglecting the modal shapes in the objective function ($\beta = 1$ and $\beta = 0$, respectively). The corresponding modes of vibration of the beam-like and FEM models have then been numerically compared by means of the MAC.
For the analysed building the MAC_A and MAC_B matrices ($\beta = 1$ and $\beta = 0$, respectively) assume the following expressions:

$$\text{MAC\_A} = \begin{array}{c} \\ \varphi_{1,BL} \\ \varphi_{2,BL} \\ \varphi_{3,BL} \end{array} \begin{array}{c} \begin{array}{ccc} \varphi_{1,FEM} & \varphi_{2,FEM} & \varphi_{3,FEM} \end{array} \\ \begin{bmatrix} 0.9958 & 0 & 0 \\ 0 & 0.9976 & 0.0905 \\ 0 & 0.1223 & 0.9952 \end{bmatrix} \end{array} \tag{4.2.2}$$

$$\text{MAC\_B} = \begin{array}{c} \\ \varphi_{1,BL} \\ \varphi_{2,BL} \\ \varphi_{3,BL} \end{array} \begin{array}{c} \begin{array}{ccc} \varphi_{1,FEM} & \varphi_{2,FEM} & \varphi_{3,FEM} \end{array} \\ \begin{bmatrix} 0.9958 & 0 & 0 \\ 0 & 0.3345 & 0.9128 \\ 0 & 0.5783 & 0.1382 \end{bmatrix} \end{array} \tag{4.2.3}$$

The observation of the two MAC matrices clearly shows that the addition of the modal shapes in the objective function provides a more precise correspondence between the modes of vibration of the beam-like and the FEM models and consequently increases the accuracy in the evaluation of the dynamic response by means of the proposed procedure.

Numerical analyses on the appropriate number of shape functions to be used in the Rayleigh-Ritz discretization in order to obtain an accurate seismic response have been previously carried

out. It is possible to show that the increase in the number of Rayleigh-Ritz components (mode shapes of a uniform shear cantilever beam) allows to reduce the differences with respect to the results obtained through the FEM model. In this case, the number of shape functions adopted in the Rayleigh-Ritz discretization is equal to 10.

For the considered building, the minimization of the objective function provided the following values for the stiffness correction coefficients: $k_x = 0.36111$; $k_y = 0.54568$; $k_c = 0.41421$, assumed uniform along the height of the equivalent beam.
Table 4.4, Figure 4.5 and Table 4.5 compare three periods, modal shapes and modal participating masses, respectively, calculated through the FEM approach to those obtained by means of the proposed beam like model. The geometry of the building is reconstructed simply by assuming a rigid diaphragm behaviour at the floor levels.

Table 4.4 - Modal periods comparison

Type	Mode 1	Mode 2	Mode 3
FEM	1.458 s	1.278 s	1.213 s
Proposed beam-like model	1.458 s	1.251 s	1.236 s

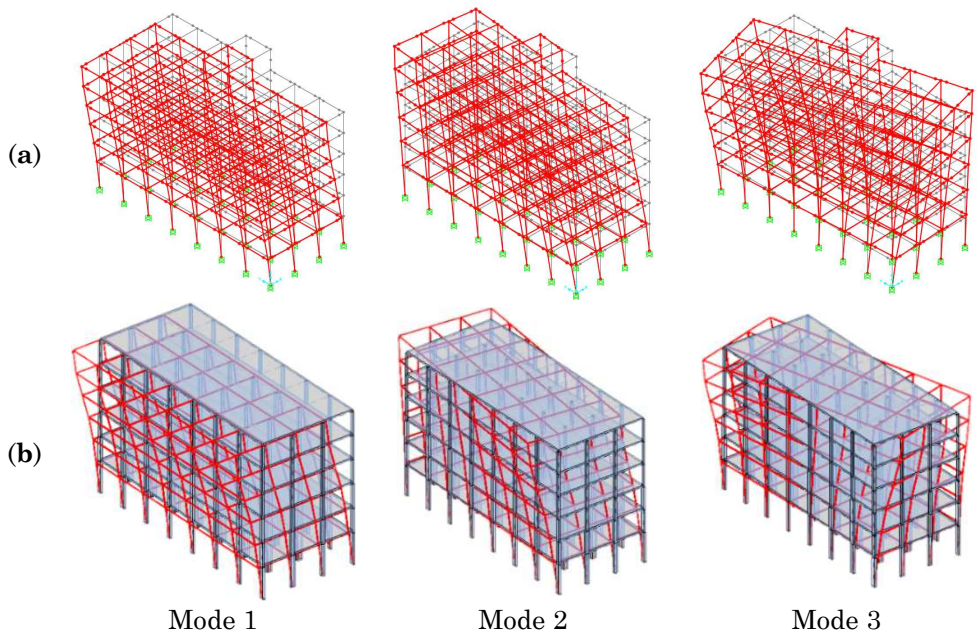

Figure 4.5 - Modal shapes comparison between the (a) FEM and (b) beam-like models

Table 4.5 - Modal participating masses comparison

Mode1	UX	UY	RZ
FEM	79%	0%	0%
Proposed beam-like model	76.3%	0%	0%
Mode2	**UX**	**UY**	**RZ**
FEM	0%	69%	11%
Proposed beam-like model	0%	69.1%	9.0%
Mode3	**UX**	**UY**	**RZ**
FEM	0%	11%	68%
Proposed beam-like model	0%	9.2%	66.6%

As it can be observed from Figure 4.5, Table 4.4 and Table 4.5, there is very good agreement between the results obtained from the beam-like model and those related to the 3D FEM model, for all the modal properties related to the first two translational modes and to the third torsional one.

4.2.2 Static response

The static displacements of the beam-like model have been obtained by means of the two different approaches presented in 2.1.8 and in 2.3.1, respectively. The first one considers the described Rayleigh-Ritz discretization of the multi-stepped beam and evaluates the static displacements by means of the construction of the stiffness matrix. The second approach is based on a closed form solution of the considered multi-stepped beam appropriately derived.
The reliability of the beam-like model has been evaluated by comparing the static displacements in the x and y directions of some control points located at the upper left and the lower right corners of each floor (nodes A.4 and H.1 whose positions in plan are shown in Figure 4.1b).
The figures show the displacements in the x and y directions for the beam-like model obtained by means of the Rayleigh-Ritz approach (red line), the closed form solution (blue line) and the ones obtained on the FEM model of the building (black line). The results plotted in Figure 4.6 and Figure 4.7 clearly show the accuracy of both the proposed discretization approaches for the evaluation of the linear static response of the considered building.

a)

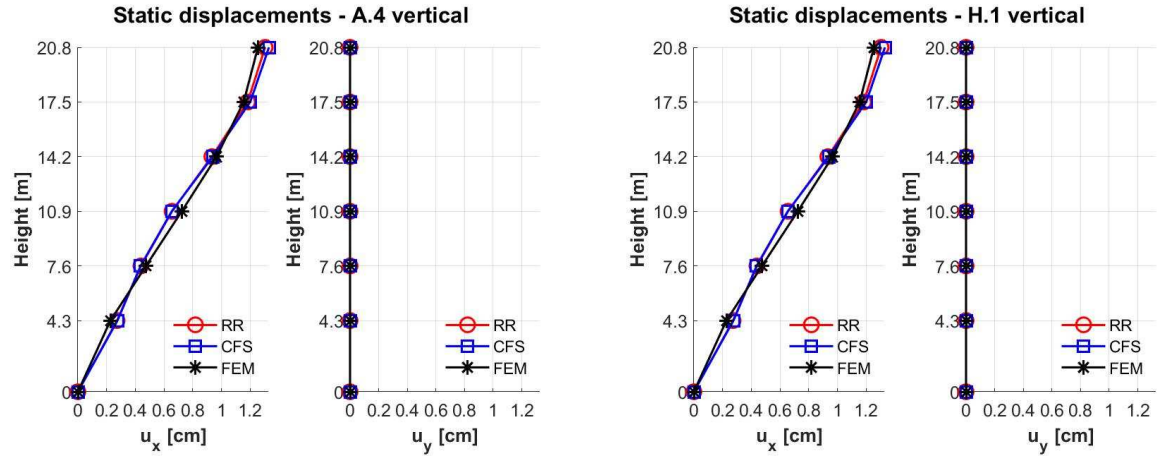

b)

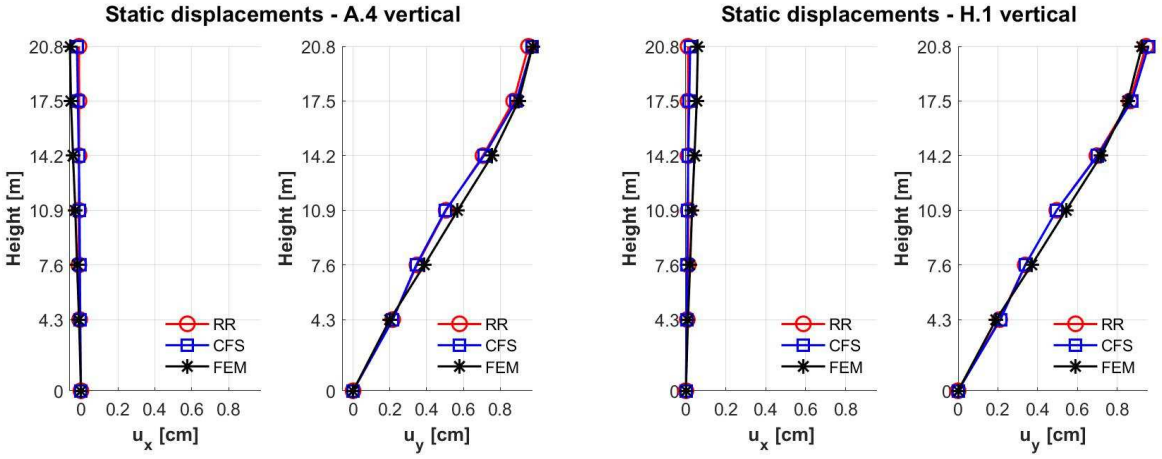

Figure 4.6 - Static displacements in x and y direction for uniform force distribution applied in a) x and b) y direction. Red line: Multi-stepped equivalent beam with Rayleigh-Ritz discretization. Blue line: Closed form solution for the equivalent beam multi-stepped beam. Black line: FEM model of the building

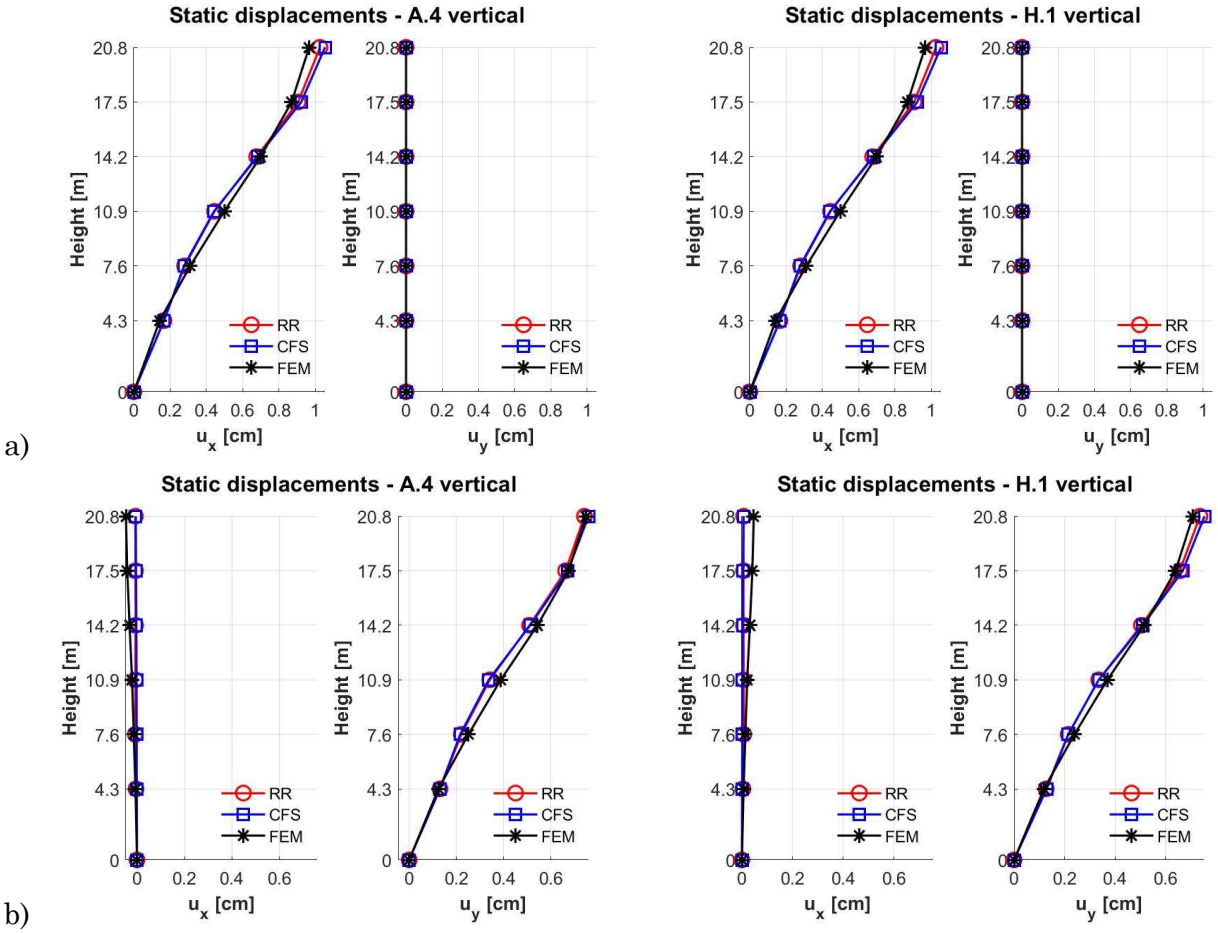

Figure 4.7 - Static displacements in x and y direction for inverse triangular force distribution applied in a) x and b) y direction. Red line: Multi-stepped equivalent beam with Rayleigh-Ritz discretization. Blue line: Closed form solution for the equivalent beam multi-stepped beam. Black line: FEM model of the building

4.2.3 Dynamic response

The dynamic response of the beam-like model has been obtained by means of the approach presented in 2.1.9, which considers the described Rayleigh-Ritz discretization of the multi-stepped beam.

The reliability of the beam-like model has been evaluated by comparing the time histories of the x and y displacements and accelerations of some control points.

For the sake of brevity, in the following only the results related to two control points located at the upper left and the lower right corners of each floor are reported (nodes A.4 and H.1 in Figure 4.1b). These control points have been chosen in order to highlight possible non negligible torsional effects. Furthermore, the maximum displacements of the same corners located at each floor and the maximum inter-storey drifts were calculated.

Figure 4.8 and Figure 4.9 report the displacement time histories of the control points at each floor in both the x and y directions, calculated by means of the beam-like (red-line) and FEM (black line) models during the considered seismic excitations. In particular Figure 4.8 and Figure 4.9 report, respectively, the x and y displacements due to the Santa Venerina and L'Aquila earthquake loading.

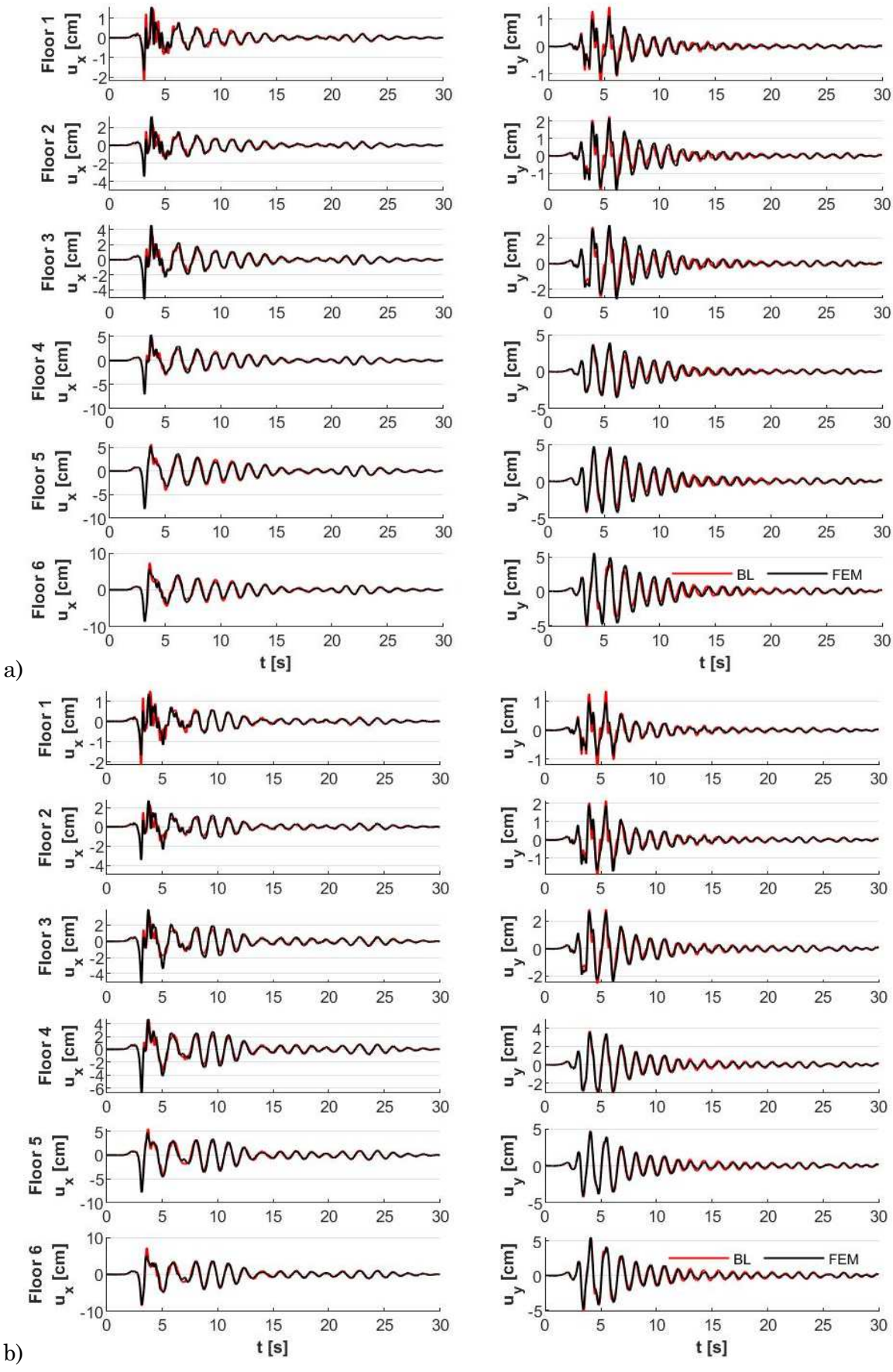

Figure 4.8 - Displacement time histories along the *x* and *y* direction for the control points a) A.4 and b) H.1 at each floor for Santa Venerina earthquake.

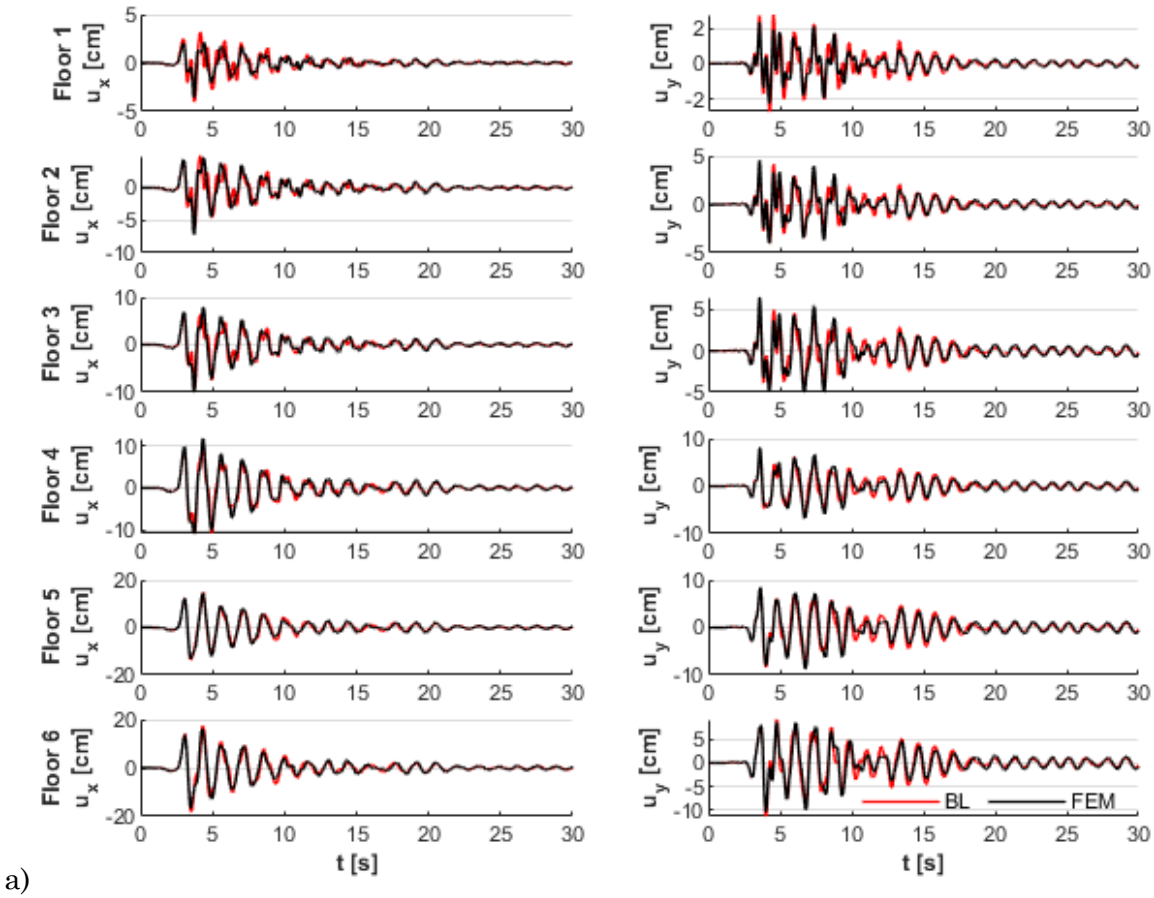

a)

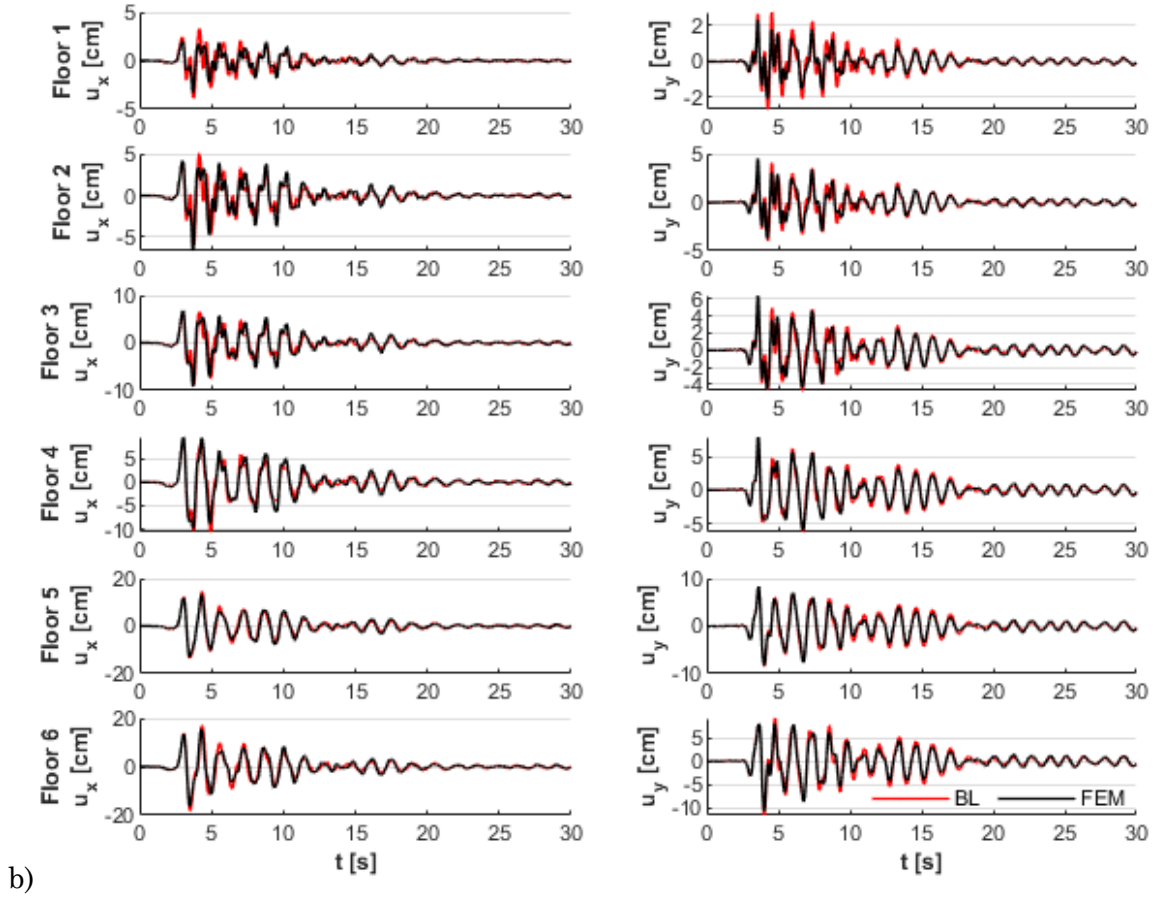

b)

Figure 4.9 - Displacement time histories along the x and y direction for the control points a) A.4 and b) H.1 at each floor for L'Aquila earthquake.

Figure 4.10 reports the floor rotation time history, calculated at each floor by means of the beam-like (red-line) and FEM (black line) models during the considered seismic excitations. In particular Figure 4.10 a-b report, respectively, the top floor rotation due to the Santa Venerina and L'Aquila earthquake loading. It can be observed that the values of the floor rotations are very small, as a consequence the differences between the beam-like and the FEM models can be considered negligible since do not provide significant displacements.

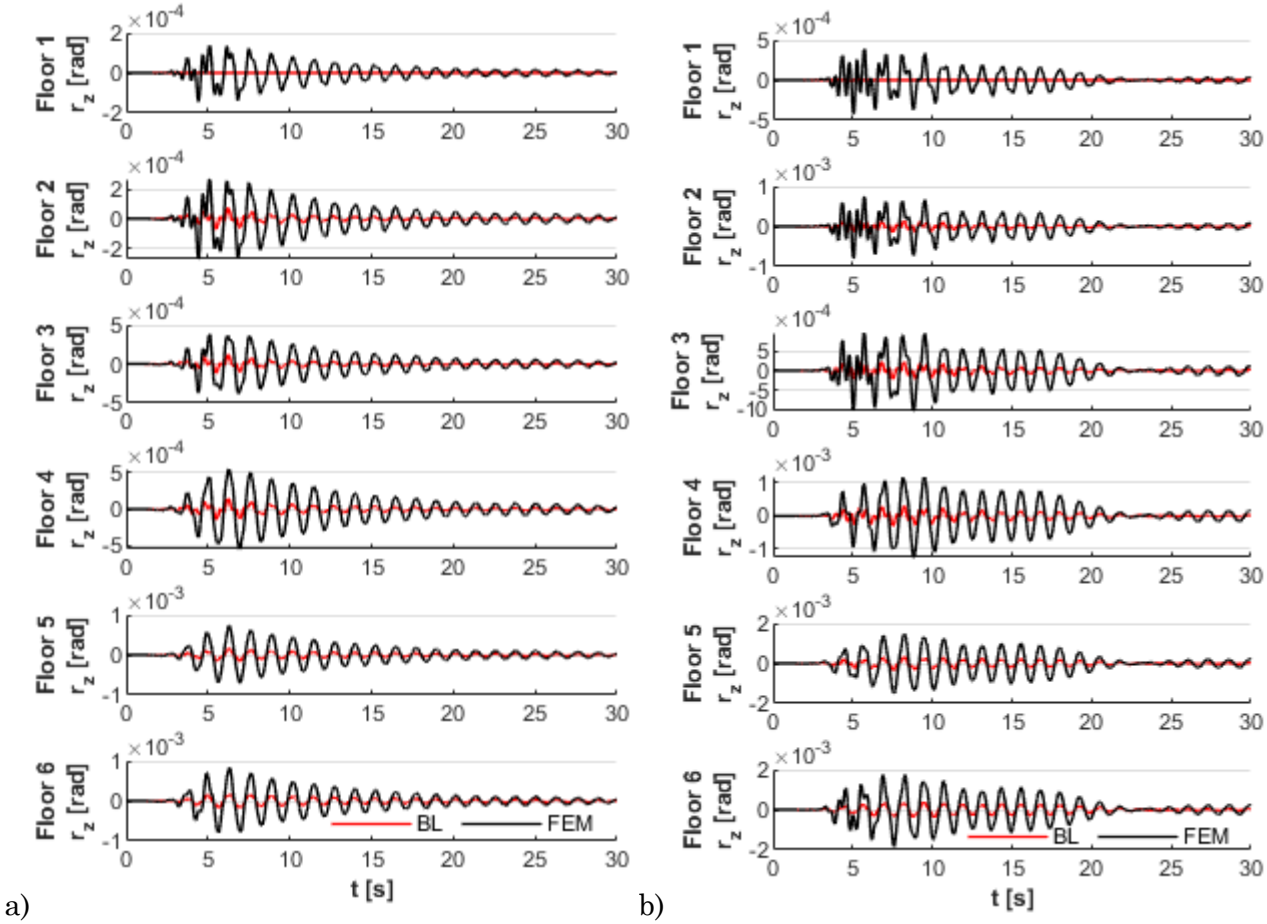

Figure 4.10 - Top floor rotation time history for a) Santa Venerina and b) L'Aquila earthquake.

Figure 4.11 and Figure 4.12 report the acceleration time histories of the control points in both the *x* and *y* directions, calculated by means of the beam-like (red-line) and FEM (black line) models during the considered seismic excitations. In particular Figure 4.11 and Figure 4.12 report, respectively, the *x* and *y* accelerations due to the Santa Venerina and L'Aquila earthquake loading.

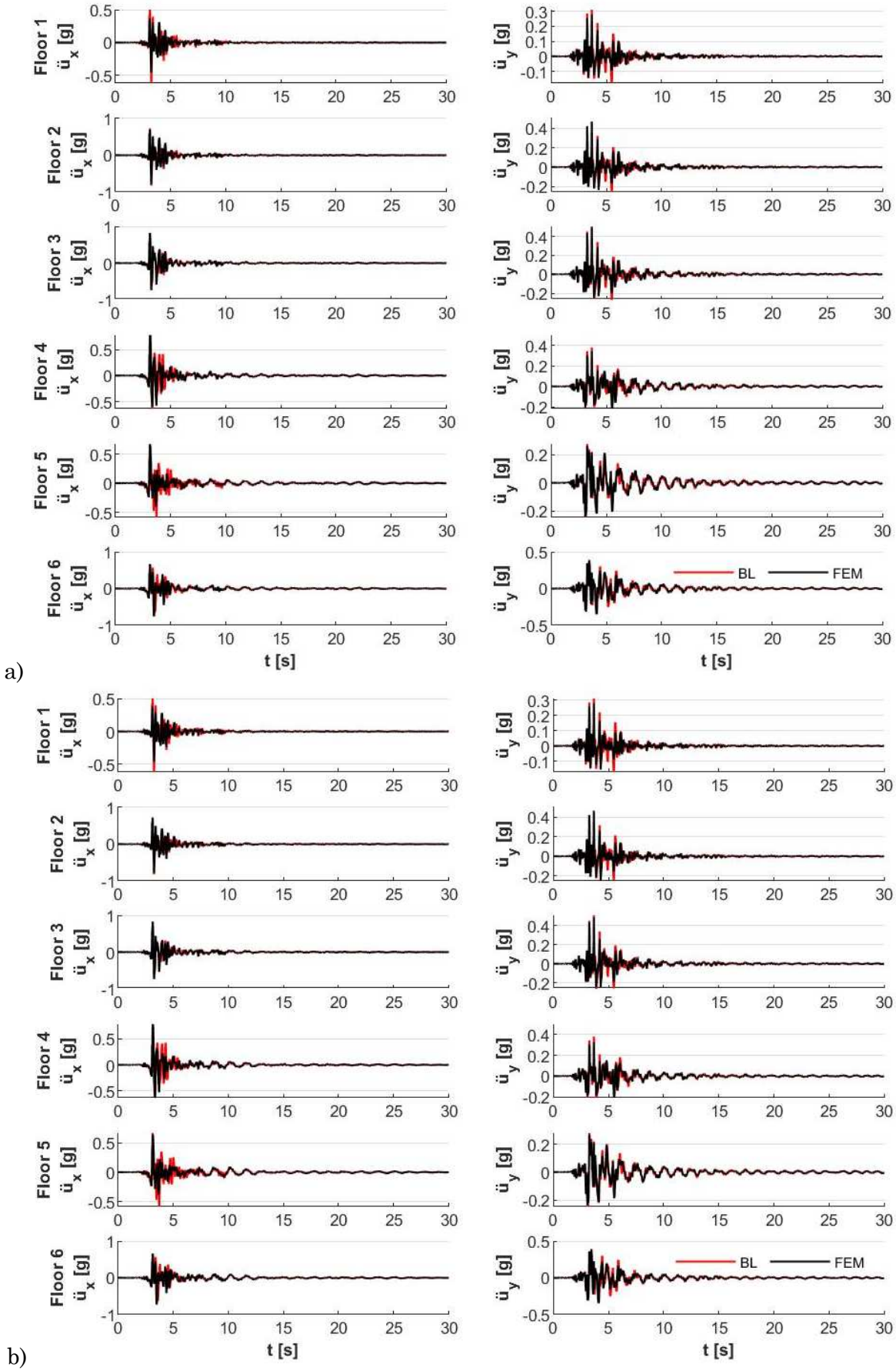

Figure 4.11 - Acceleration time histories along the *x* and *y* direction for the control points a) A.4 and b) H.1 at each floor for Santa Venerina earthquake.

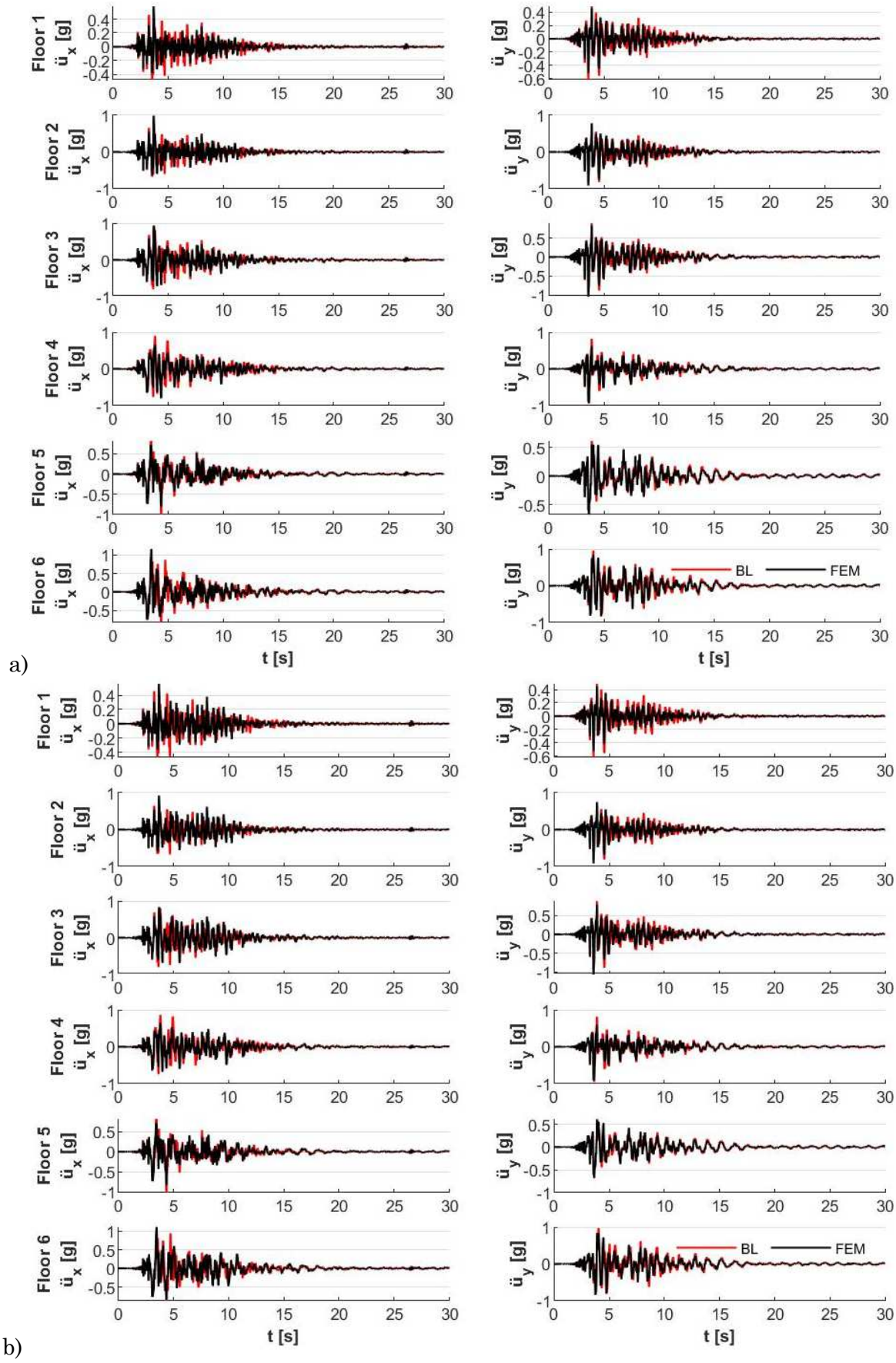

Figure 4.12 - Acceleration time histories along the *x* and *y* direction for the control points a) A.4 and b) H.1 at each floor for L'Aquila earthquake.

Once again, it must be remarked how the proposed approach is able to correctly reproduce the time history of any chosen point on the building. Finally, as it can be observed in Figure 4.13-Figure 4.14 and Figure 4.15-Figure 4.16 respectively, also the maximum displacements and inter-storey drifts normalised by the storey height of the same corners located at each floor, calculated by means of the beam-like model, give very accurate results.

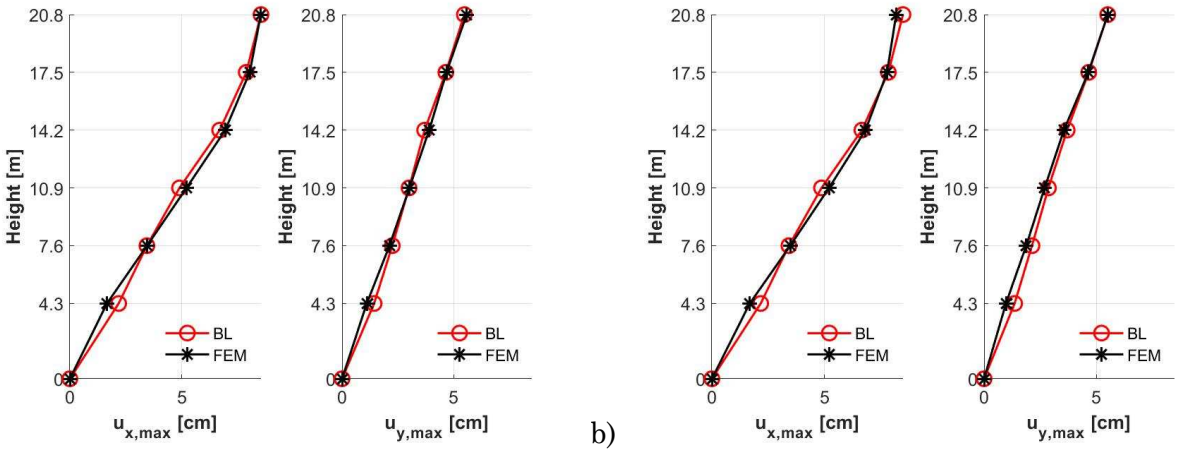

Figure 4.13 - Maximum floor displacements for the control points a) A.4 and b) H.1 at each floor in the Santa Venerina earthquake.

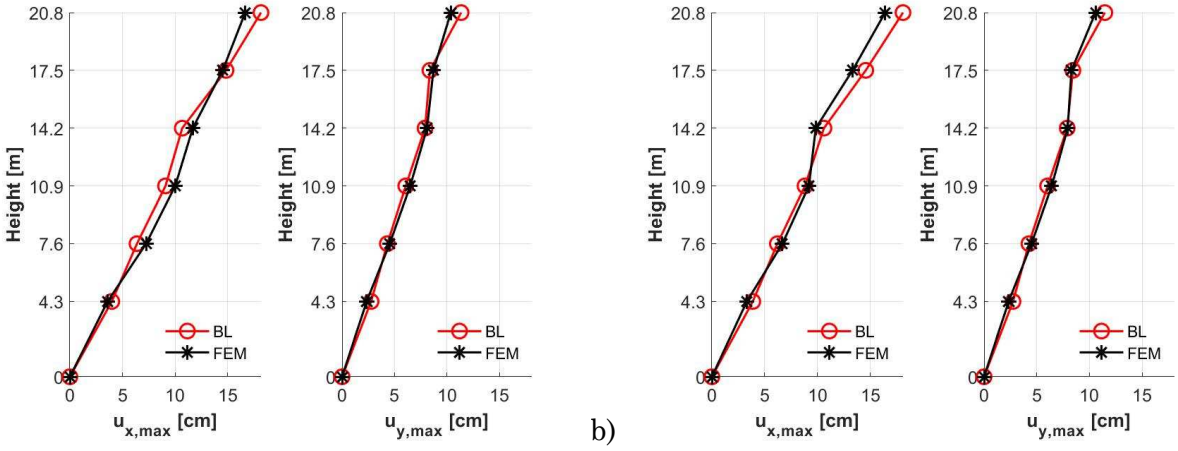

Figure 4.14 - Maximum floor displacements for the control points a) A.4 and b) H.1 at each floor in the L'Aquila earthquake.

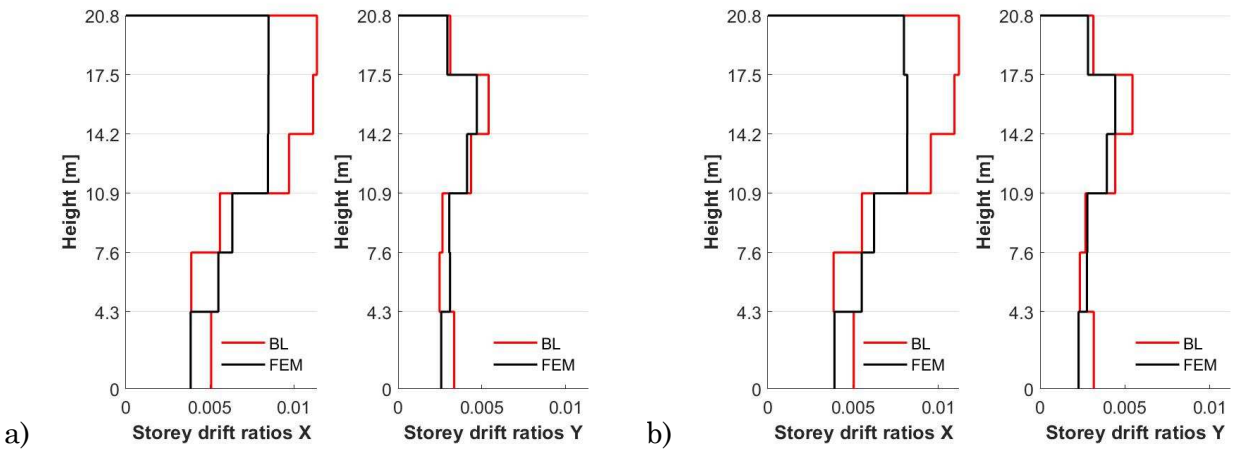

Figure 4.15 - Maximum inter-storey drifts normalised by the storey height for the control points a) A.4 and b) H.1 in the Santa Venerina earthquake.

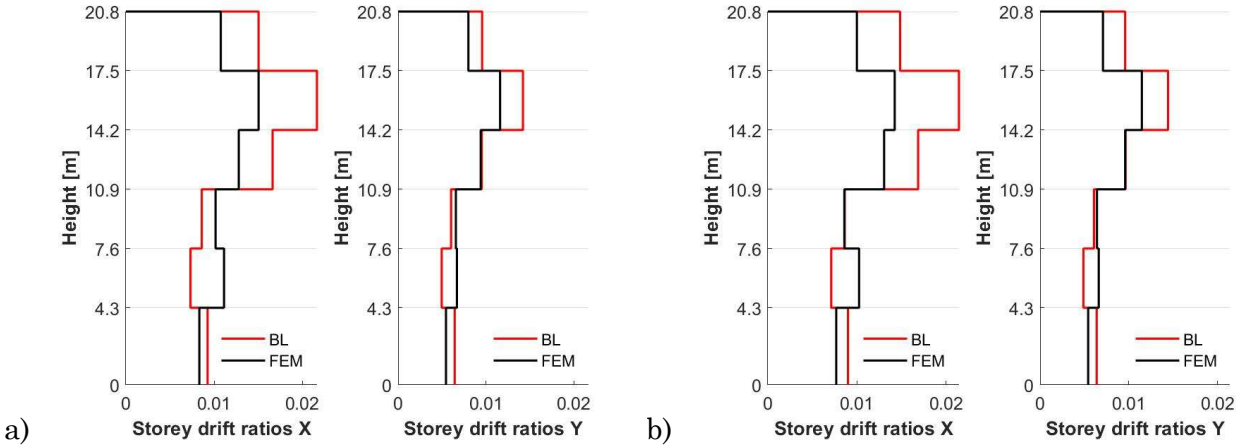

Figure 4.16 - Maximum inter-storey drifts normalised by the storey height for the control points a) A.4 and b) H.1 in the L'Aquila earthquake.

4.3 CASE STUDY 1: BEAM LIKE MODEL - INELASTIC BEHAVIOUR

In this chapter the non-linear behaviour of the "Edificio Catania" has been studied by means of the inelastic beam-like model presented in paragraph 2.2.
The non-linear static and dynamic analyses on a FEM model of the building have been performed using the software SAP2000 v.23 [113]. The global non-linear behaviour of the structure has been modelled by introducing plastic hinges at the ends of all the structural elements (beams and columns). In particular, P-M2-M3 hinges have been used for columns and M3 hinges for beams, where shear failure has been neglected, according to the idealized flexural hinge criteria.
First, the calibration procedure, already described in paragraph 2.2.3, was performed. Then the proposed multi-stepped beam was adopted for simulating the static and dynamic inelastic behaviour of the building and the results, in terms of static and seismic response, were compared to those obtained by means of the conventional 3D FEM model.
Since the capacity curves depend on the applied distribution of forces, different loading patterns have been taken into account in order to investigate the corresponding differences in predicting the inelastic responses, as better specified in the following.
The complete FEM and the beam-like models of the building have been subjected to a static force vector $\mathbf{F}_b$ according to the following relationships:

$$\mathbf{F}_b = \mathbf{M}_b \boldsymbol{\phi} \tag{4.2.4}$$

where $\boldsymbol{\phi}$ is the fixed displacement distribution and $\mathbf{M}_b$ is the diagonal mass matrix which considers lumped masses at the nodes due to the applied seismic masses.
In particular, the following three force distributions have been considered in the numerical applications:

a) mass proportional force distribution (Figure 4.17a-Figure 4.18a);
b) inverse triangular proportional force distribution (Figure 4.17b-Figure 4.18b);
c) force distribution associated with the fundamental natural mode (Figure 4.17c-Figure 4.18c).

The forces in the FEM and in the beam-like models are applied to the center of gravity (centroid) of each floor of the building, separately in the *x* and *y* directions. The values of the applied forces from the bottom to the top floor in the three load conditions are assumed as shown in Figure 4.17 and Figure 4.18.

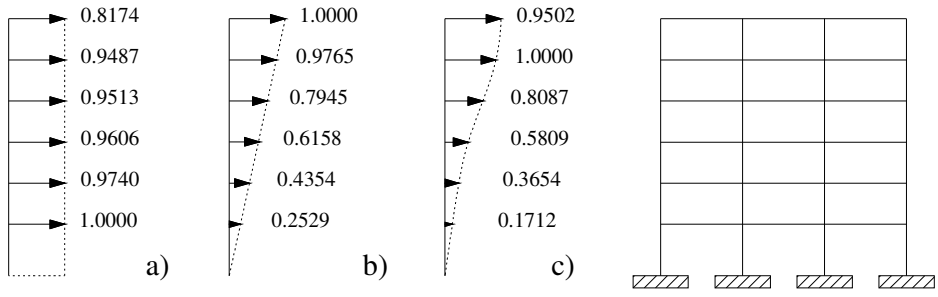

Figure 4.17 - Lateral force distribution types in *x* direction: a) Mass proportional, b) inverse triangular mass proportional and c) associated with fundamental mode.

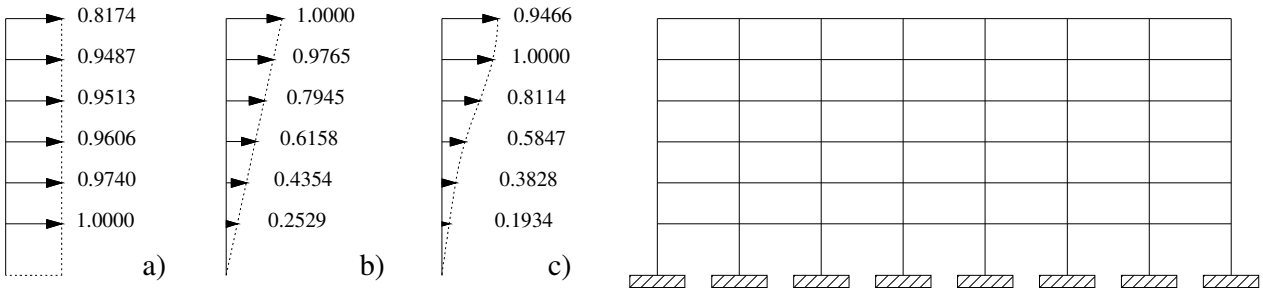

Figure 4.18 - Lateral force distribution types in *y* direction: a) Mass proportional, b) inverse triangular mass proportional and c) associated with fundamental mode.

Aiming to simulate representative seismic inputs that may occur on the Italian peninsula, non-linear dynamic analyses were performed by considering the two real seismic records in the *x* and *y* directions that occurred in Santa Venerina (2018) and L'Aquila (2009), already presented in 4.2 for the linear dynamic analyses.

4.3.1 Calibration procedure

The results of the non-linear static analysis performed on the FEM model with displacement control have been reported in terms of inter-storey capacity curves for the three described load distributions (a, b, c) in Figure 4.19 and Figure 4.20 in the *x* and *y* directions, respectively.

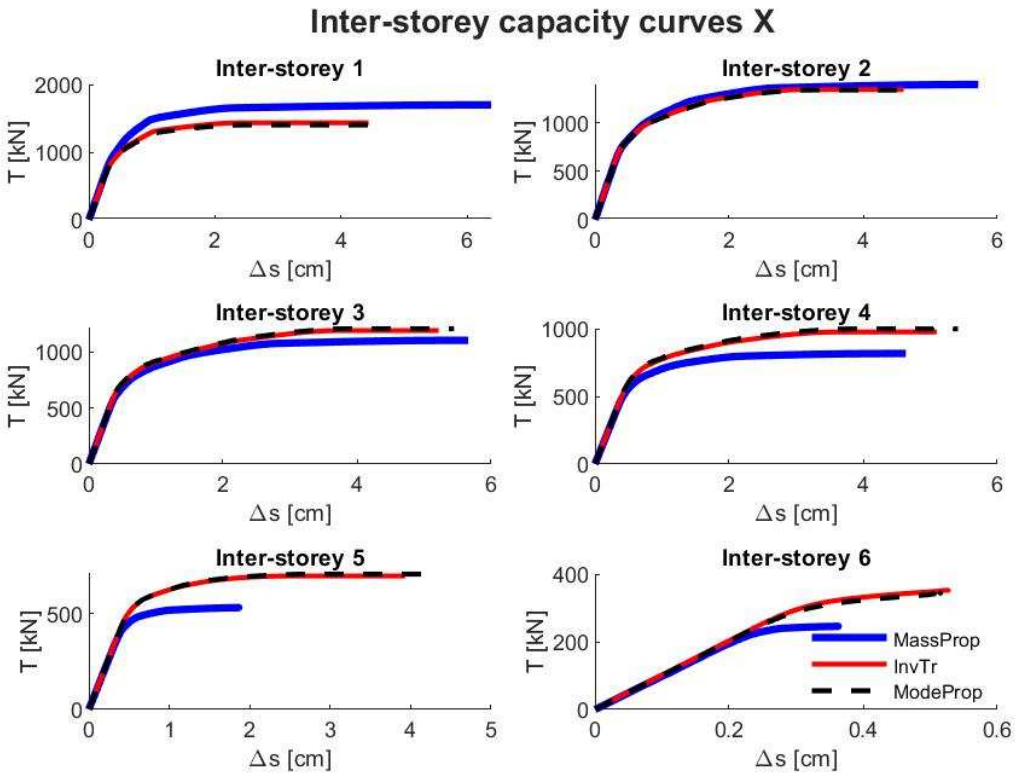

Figure 4.19 - Inter-storey capacity curves in *x* direction for load distribution a (blue), b (red) and c (black)

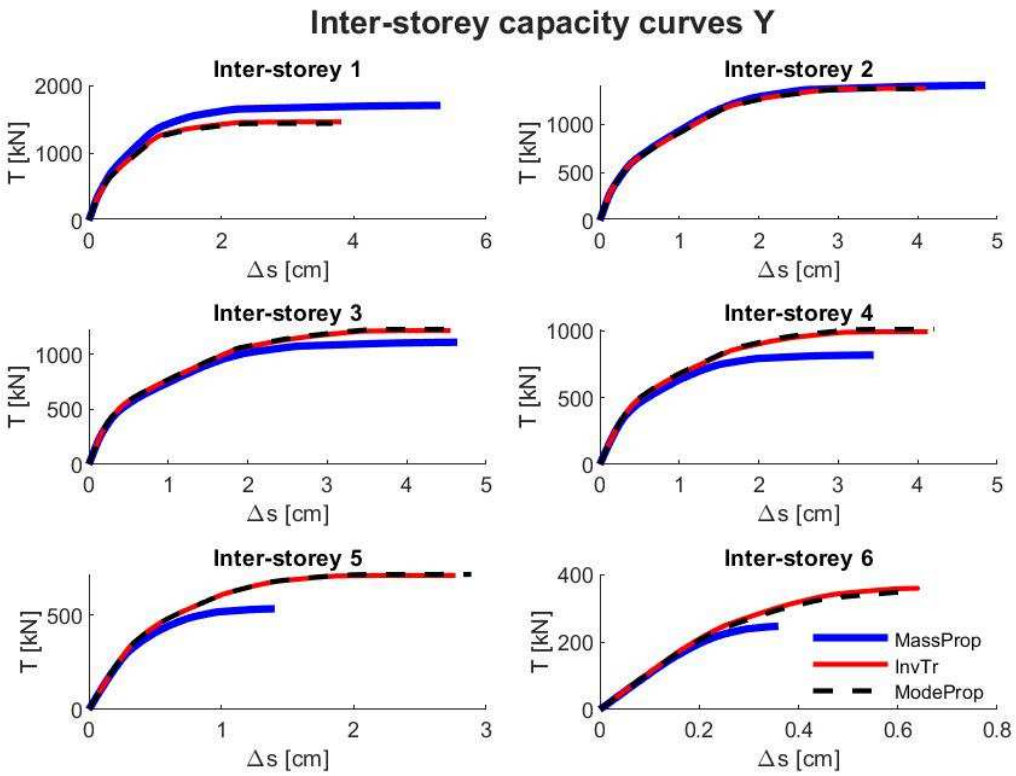

Figure 4.20 - Inter-storey capacity curves in *y* direction for load distribution a (blue), b (red) and c (black)

Some further analyses have been performed in order to study with more accuracy the non-linear behaviour of the considered building. In particular, a static non-linear analysis has been performed on the FEM model with displacement control by applying a displacement distribution equal to the fundamental natural mode in the considered direction, reported in Figure 4.21. Also in this case, the results in terms of inter-storey capacity curves have been compared to the ones obtained by applying the first two load distributions (a, b) in Figure 4.22 and Figure 4.23 in the *x* and *y* directions, respectively. This displacement distribution will be denoted as d) and compared to the previous load distributions a-b-c in the following.

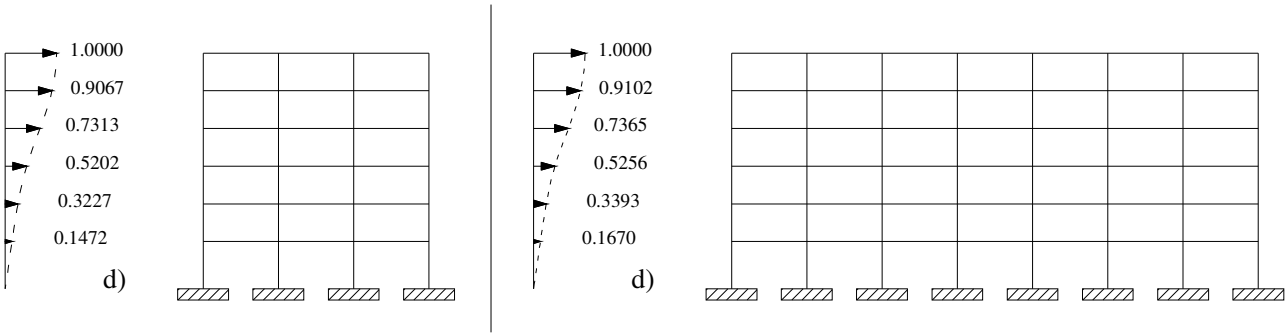

Figure 4.21 - Lateral displacement distribution type, equal to the fundamental mode in *x* (left) and *y* (right) directions.

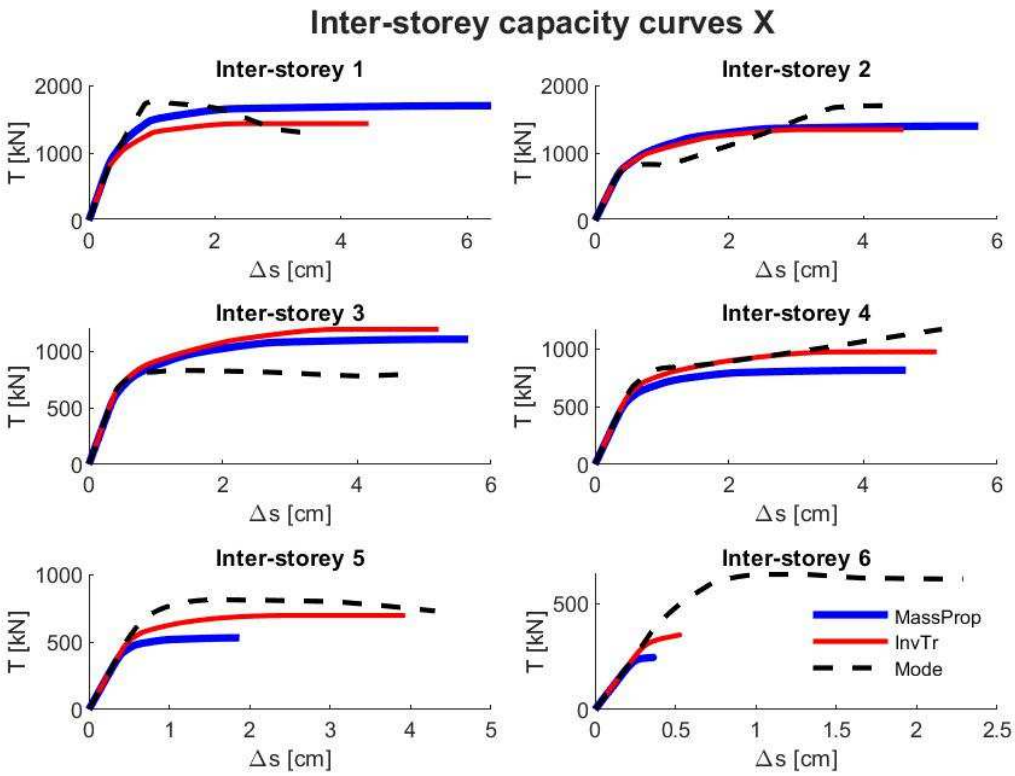

Figure 4.22 - Inter-storey capacity curves in *x* direction for load distribution a (blue), b (red) and displacement distribution d (black)

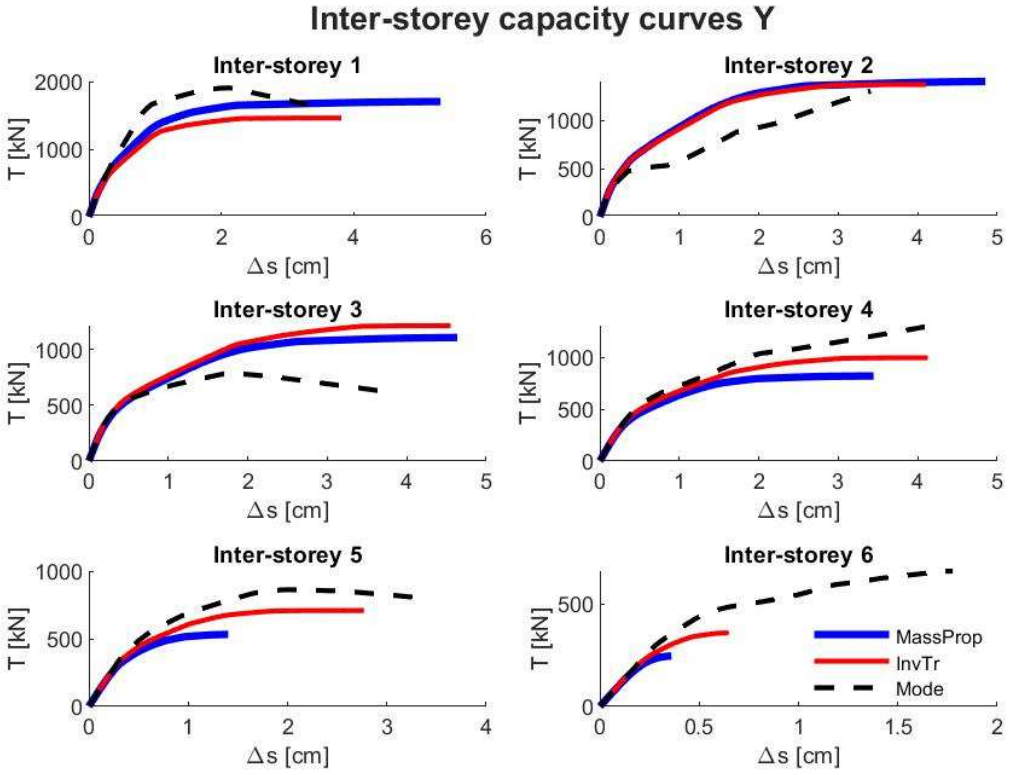

Figure 4.23 - Inter-storey capacity curves in *y* direction for load distribution a (blue), b (red) and displacement distribution d (black)

The beam-like model has been calibrated by following the procedure described in paragraph 2.2.3. As first step, the inelastic inter-storey responses, reported in Figure 4.19 and Figure 4.20, have been considered for the calibration of the inelastic multi-stepped beam. As second step, the obtained inter-storey capacity curves have been transformed into equivalent bilinear elasto-plastic force-displacement laws with positive kinematic hardening. The equivalence has been obtained by imposing the equality between the areas below the non-linear and bilinear capacity curves and assuming as initial inter-storey stiffness the tangent to the origin of the inter-storey capacity curve. With regard to the curves reported in black in Figure 4.22 and Figure 4.23 obtained by applying a displacement distribution, the equivalence has been obtained by imposing an energy equivalence criterion on the hysteresis loop and still assuming as initial inter-storey stiffness the tangent to the origin of the inter-storey capacity curve. It is worth remembering that in general a symmetric elasto-plastic behaviour with kinematic hardening is adopted, while an elasto-perfectly plastic behaviour is adopted if the inter-storey force-displacement law shows a softening behaviour.
The stiffness values of each beam segment, assumed as initial stiffness in the successive non-linear analyses, are reported in Table 4.6; the latter data, together with the mass distribution, allow to define the linear elastic behaviour of each beam-like model associated with each load or displacement distribution. In Table 4.7 and Table 4.8 the inelastic limits and the hardening parameters for each beam segment are reported, respectively. No limits of the ductile behaviour have been considered since the limits of ductility have been checked a posteriori.
The above described identified parameters are sufficient for the characterization of the non-linear response of the beam-like model.

Table 4.6 - Initial stiffness of each beam segment associated with each different load and displacement distribution

Beam segment	Height h [m]	Initial stiffness R [N/m] · 10^8							
		Force dist. a)		Force dist. b)		Force dist. c)		Displ. dist. d)	
		x	y	x	y	x	y	x	y
1	4.30	2.659	2.779	2.549	2.690	2.532	2.664	2.540	2.765
2	3.30	2.027	2.264	2.034	2.282	2.033	2.286	2.027	2.209
3	3.30	1.591	1.832	1.630	1.863	1.646	1.853	1.639	1.853
4	3.30	1.237	1.326	1.258	1.339	1.263	1.358	1.253	1.351
5	3.30	1.055	1.141	1.085	1.157	1.086	1.160	1.086	1.160
6	3.30	0.980	1.055	1.019	1.098	1.008	1.084	1.011	1.095

Table 4.7 - Yielding force of each beam segment associated with each different load and displacement distribution

Beam segment	Height h [m]	Yielding force F_y [N] · 10^5							
		Force dist. a)		Force dist. b)		Force dist. c)		Displ. dist. d)	
		x	y	x	y	x	y	x	y
1	4.30	15.609	14.360	13.167	11.990	12.907	11.748	18.458	16.835
2	3.30	12.240	10.651	11.553	9.909	11.569	9.820	6.827	5.644
3	3.30	9.675	8.335	10.098	8.654	10.253	8.705	7.793	8.637
4	3.30	7.390	6.425	8.523	7.464	8.727	7.565	7.521	8.209
5	3.30	4.922	4.208	6.467	5.846	6.550	5.906	7.914	9.111
6	3.30	2.316	2.056	3.075	2.804	2.953	2.679	5.782	6.975

Table 4.8 - Hardening parameter of each beam segment associated with each different load and displacement distribution

Beam segment	Height h [m]	Post yielding stiffness R_T [N/m] · 10^6							
		Force dist. a)		Force dist. b)		Force dist. c)		Displ. dist. d)	
		x	y	x	y	x	y	x	y
1	4.30	2.371	5.586	3.018	7.759	2.757	8.067	-	-
2	3.30	3.398	7.700	4.722	10.364	4.390	10.653	26.249	23.448
3	3.30	2.725	6.586	3.974	8.554	3.796	8.708	-	-
4	3.30	1.918	5.966	2.795	6.938	2.658	7.003	9.163	13.532
5	3.30	2.737	10.794	1.475	5.471	1.372	5.181	-	-
6	3.30	10.903	24.765	19.853	20.345	21.823	21.300	-	1.699

Four bilinear relationships have been defined, each one representing the monotonic or cyclic inelastic inter-storey response of the building subjected to the considered force or displacement distribution. In Figure 4.24 and Figure 4.25 the inter-storey inelastic equivalent force-displacement laws in x and y directions, relative to the mode proportional force distribution, are reported as an example, while in Figure 4.26 and Figure 4.27 the inter-storey inelastic equivalent hysteresis loops due to force-displacement laws, relative to the modal displacement distribution analyses, are reported. In particular, the inter-storey capacity curves or hysteresis loops (in black), the corresponding Back-Bone curves of the bilinear force-displacement laws (in red) and the extended Back-Bone curves without limits of the ductile behaviour (dashed in red) have been reported in each figure.

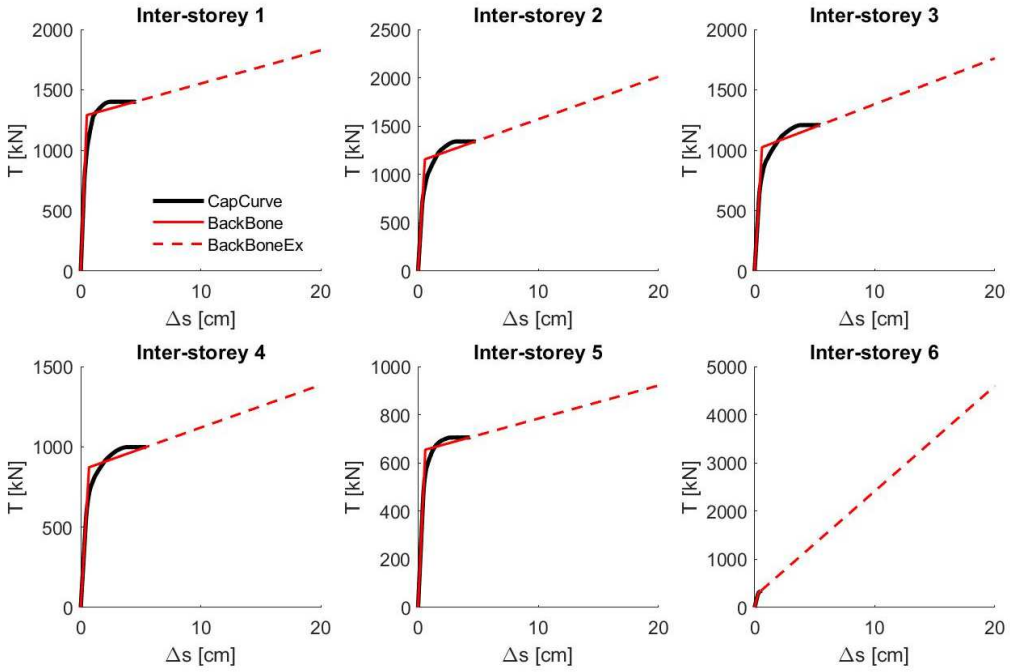

Figure 4.24 - Inter-storey capacity curves (CapCurve in black), the corresponding Back-Bone curves (red) and the extended Back-Bone without limits of the ductile behaviour (BackBoneEx dashed in red) for mode proportional analysis in x direction

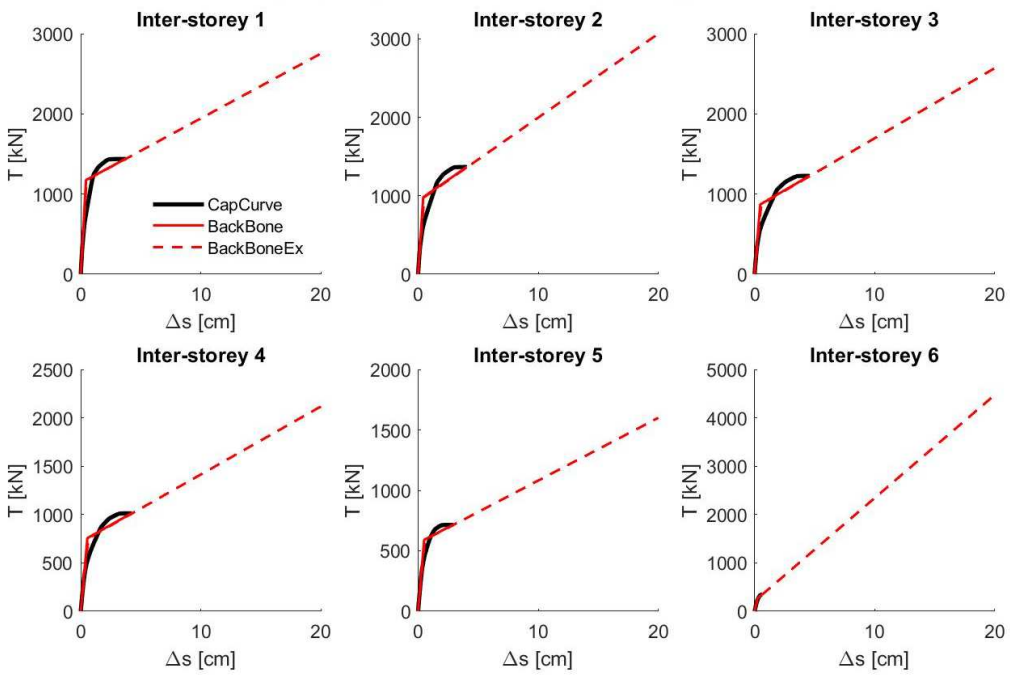

Figure 4.25 - Inter-storey capacity curves (CapCurve in black), the corresponding Back-Bone curves (red) and the extended Back-Bone without limits of the ductile behaviour (BackBoneEx dashed in red) for mode proportional analysis in *y* direction

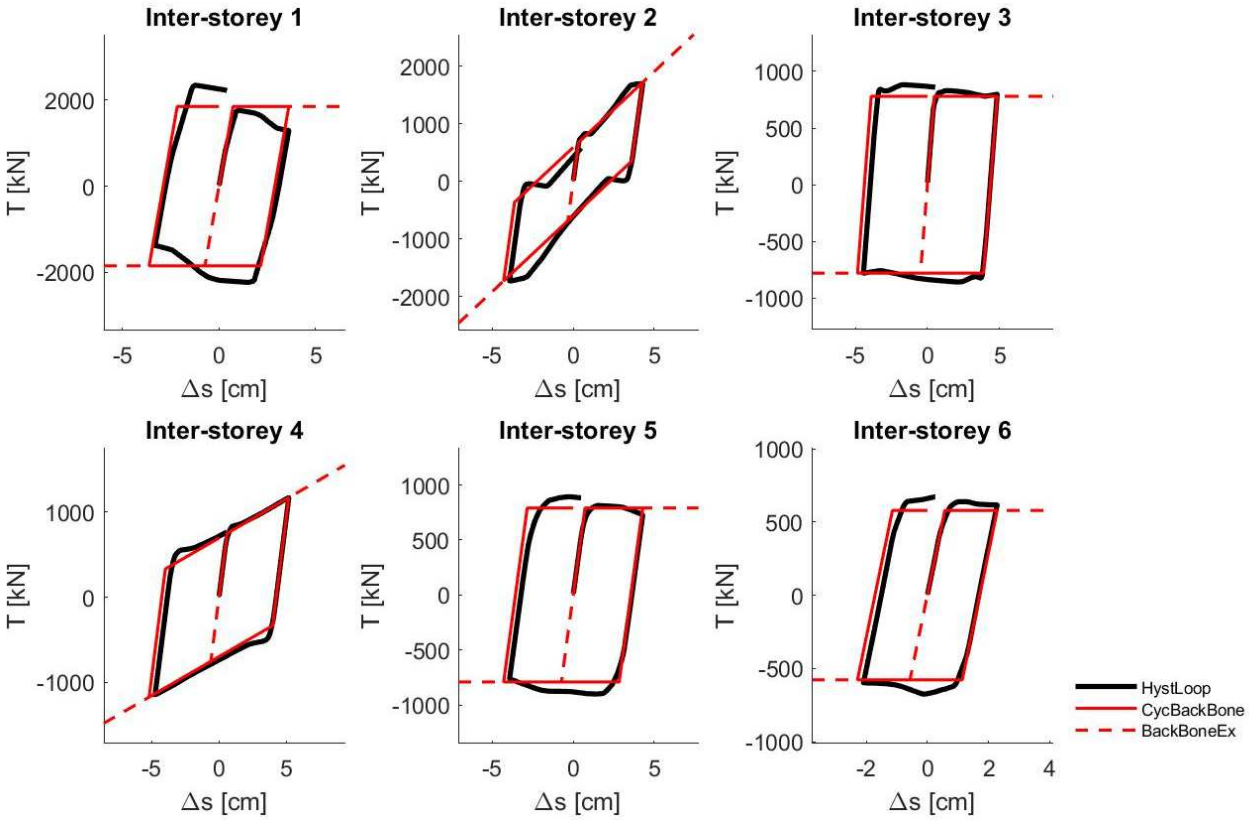

Figure 4.26 - Inter-storey hysteresis loops (HystLoop in black), the corresponding cyclic Back-Bone curves (red) and the extended Back-Bone without limits of the ductile behaviour (BackBoneEx dashed in red) for modal displacement distribution analysis in *x* direction

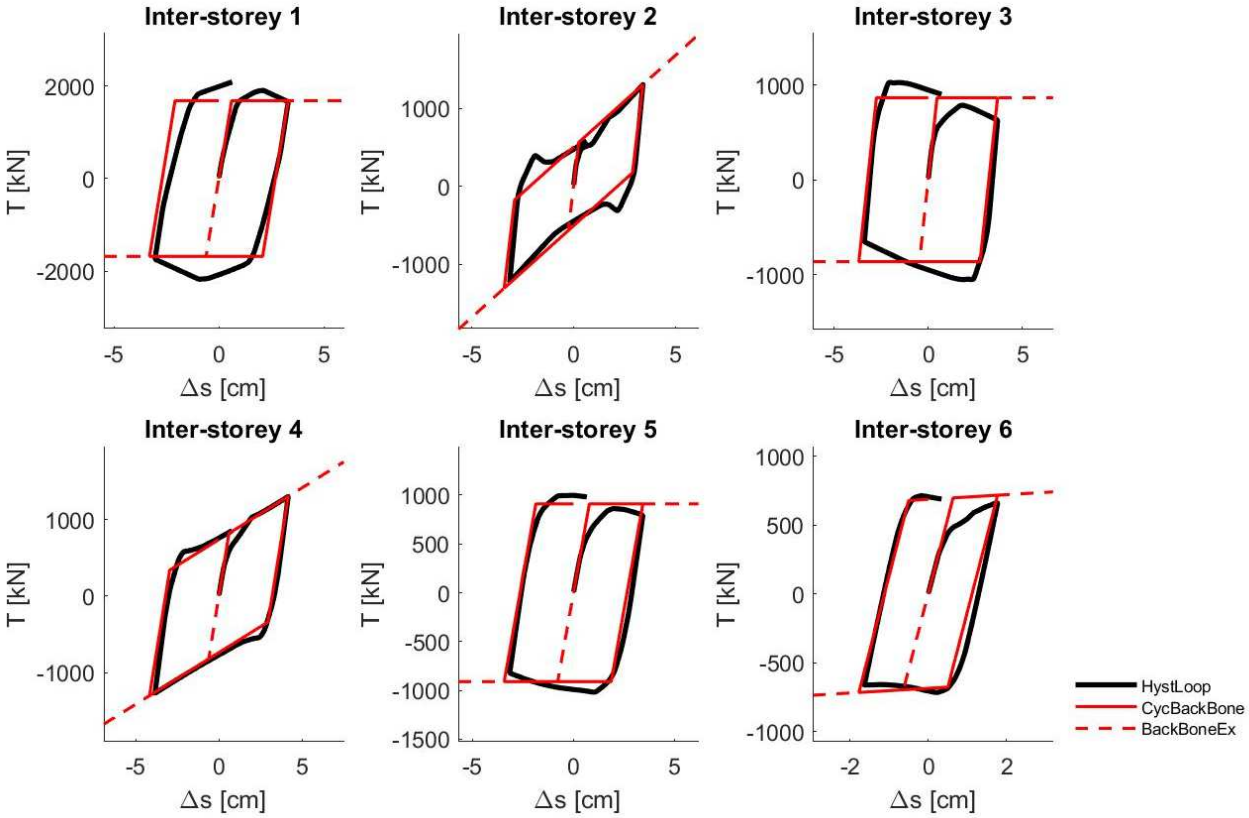

Figure 4.27 - Inter-storey hysteresis loops (HystLoop in black), the corresponding cyclic Back-Bone curves (red) and the extended Back-Bone without limits of the ductile behaviour (BackBoneEx dashed in red) for modal displacement distribution analysis in *y* direction

4.3.2 Non-linear static response

Once each inter-storey non-linear behaviour has been defined, it is possible to perform non-linear pushover analyses by making use of the beam-like model.

The non-linear pushover analyses of the equivalent beam model take into account load distributions equal to the above described initial force or displacement distributions (a, b, c, d) adopted for the FEM model. The forces are applied on the beam axis at the floor level and are proportionally increased until conventional values of 0.25 m or 0.2 m top displacements are obtained, respectively in *x* and *y* directions. The displacements are also applied on the beam axis at the floor level and are proportionally increased or decreased in order to obtain a closed cyclic capacity curve.

In the case of applied force distributions, the Newton-Raphson iterative procedure, presented in Appendix C.1, has been used in order to evaluate the response of the beam-like model to the static non-linear loading process. Instead in the case of applied displacement distributions, the procedure presented in Appendix C.5 has been implemented.

For each load distribution and for each considered direction, the capacity curves representative of the global behaviour of the building have been retrieved by considering the above described beam-like models. In Figure 4.28a-d and Figure 4.29a-d the comparisons between the global capacity curves, obtained by means of the FEM and the beam-like models, are reported showing

a satisfactory agreement. The differences arise from the simplified assumption on the inter-storey constitutive laws adopted for the beam-like model.

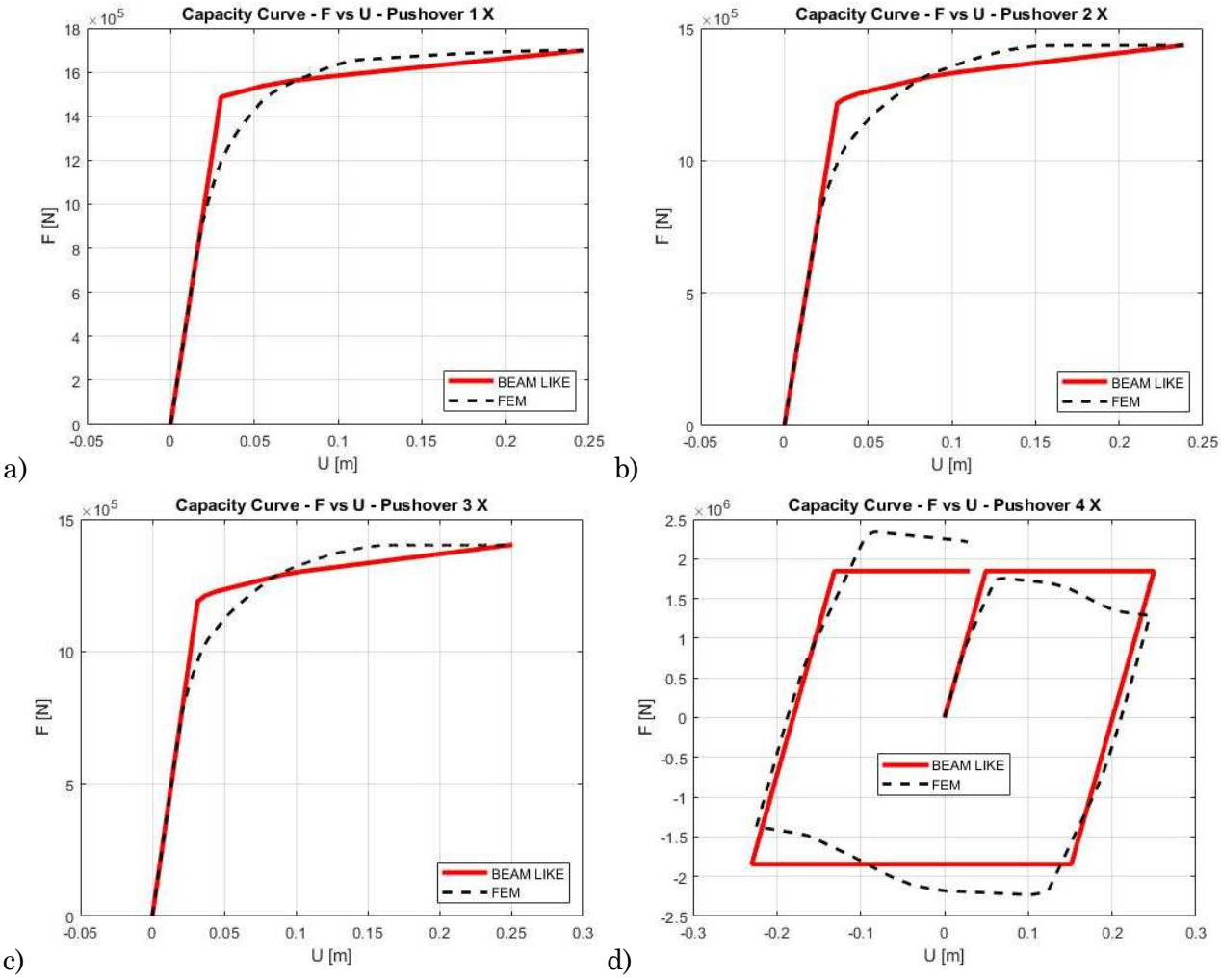

Figure 4.28 - Capacity curves in *x* direction for a) Mass proportional force distribution; b) Inverse triangular force distribution; c) Fundamental natural mode force distribution; d) Fundamental natural mode displacement distribution

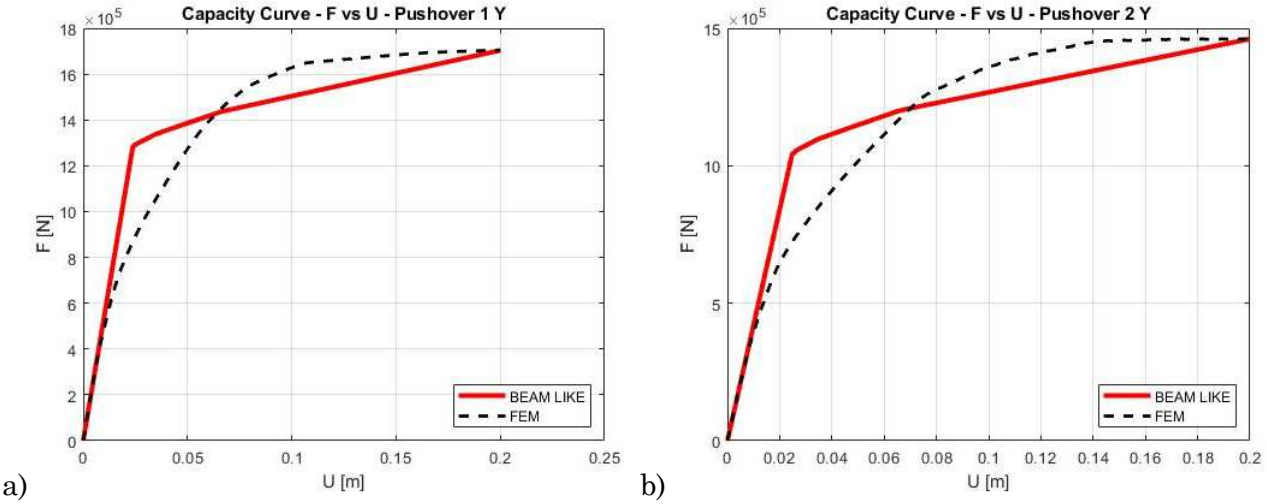

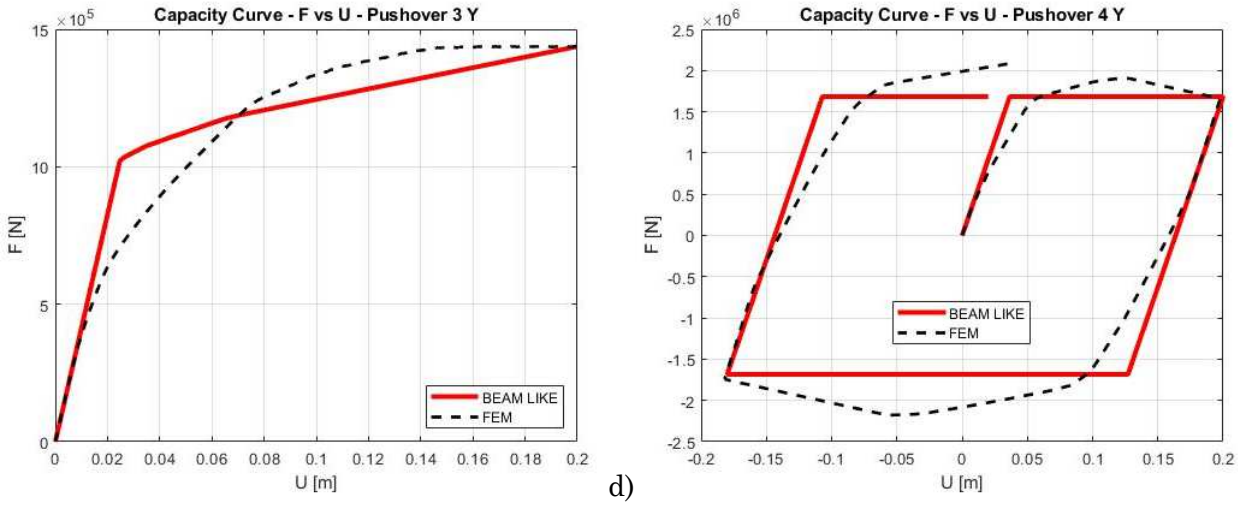

c) d)

Figure 4.29 - Capacity curves in *y* direction for a) Mass proportional force distribution; b) Inverse triangular force distribution; c) Fundamental natural mode force distribution; d) Fundamental natural mode displacement distribution

The latter comparisons confirm the ability of the beam-like model to reproduce accurately the non-linear static response of the building even if the inter-storey force-displacement relationships has been replaced by equivalent bilinear inelastic behaviour with kinematic hardening or by equivalent elasto-perfectly plastic behaviour.
In the following sub-section, the beam-like model is adopted to predict the non-linear dynamic response of the considered building by means of non-linear dynamic analyses.

4.3.3 Non-linear dynamic response

The dynamic response of the beam-like model was obtained by means of the approach presented in Appendix D.
For each seismic record, four dynamic analyses have been performed both in direction *x* and *y*, each one assuming the inter-storey shear-displacement relationship corresponding to load or displacement distribution a), b), c) or d). The damping matrix $\mathbf{C}$ has been obtained by setting the modal damping ratio equal to 5% for all the vibration modes (six as the number of degrees of freedom) of the beam-like model.
The reliability of the non-linear dynamic response of the beam-like model was evaluated by comparing the time histories of the displacements of the centre of gravity at each floor in the considered direction. For simplicity, no limits have been considered in the available ductility at each floor level. In the FEM model, the displacements of the centre of gravity have been calculated as the mean values of the four corner nodes of the same floor.
Figure 4.30.a-b and Figure 4.31.a-b report the time histories, expressed in terms of floor level displacements, for the four beam-like models in *x* and *y* directions for Santa Venerina e L'Aquila earthquakes, respectively, compared to the results of the FEM model.

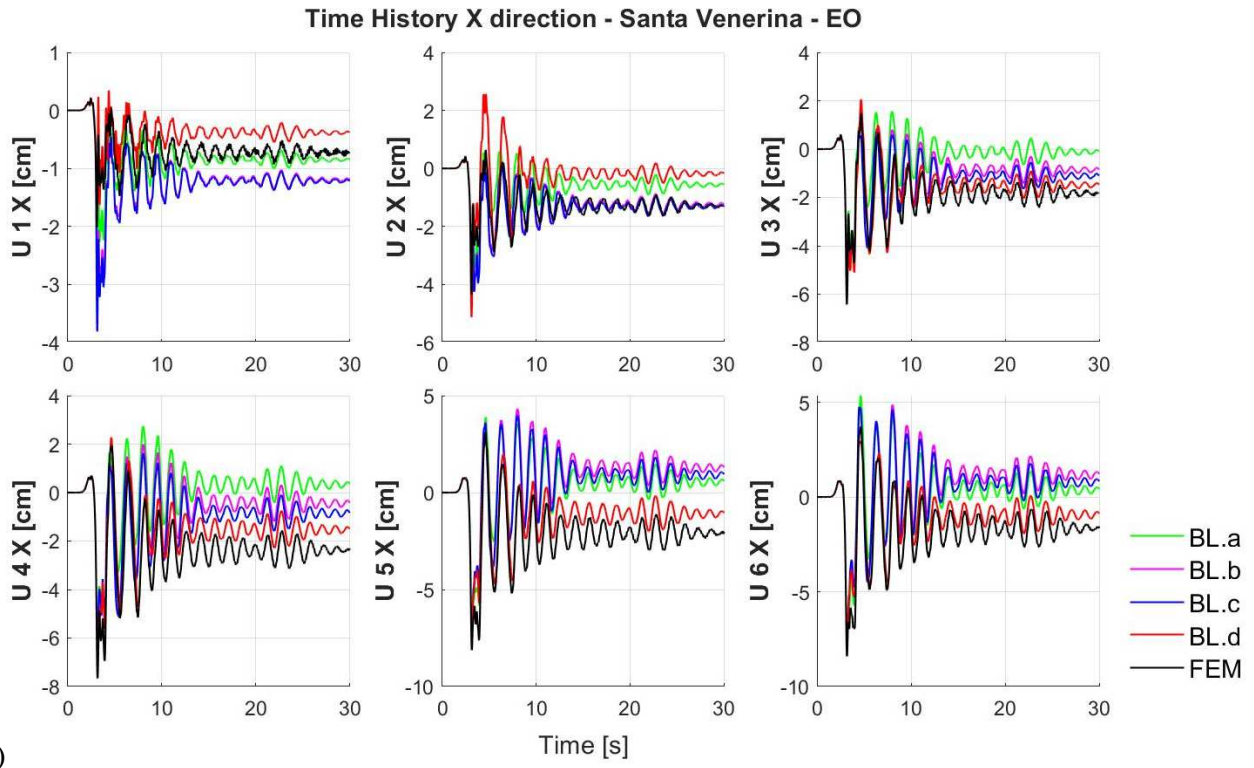

a)

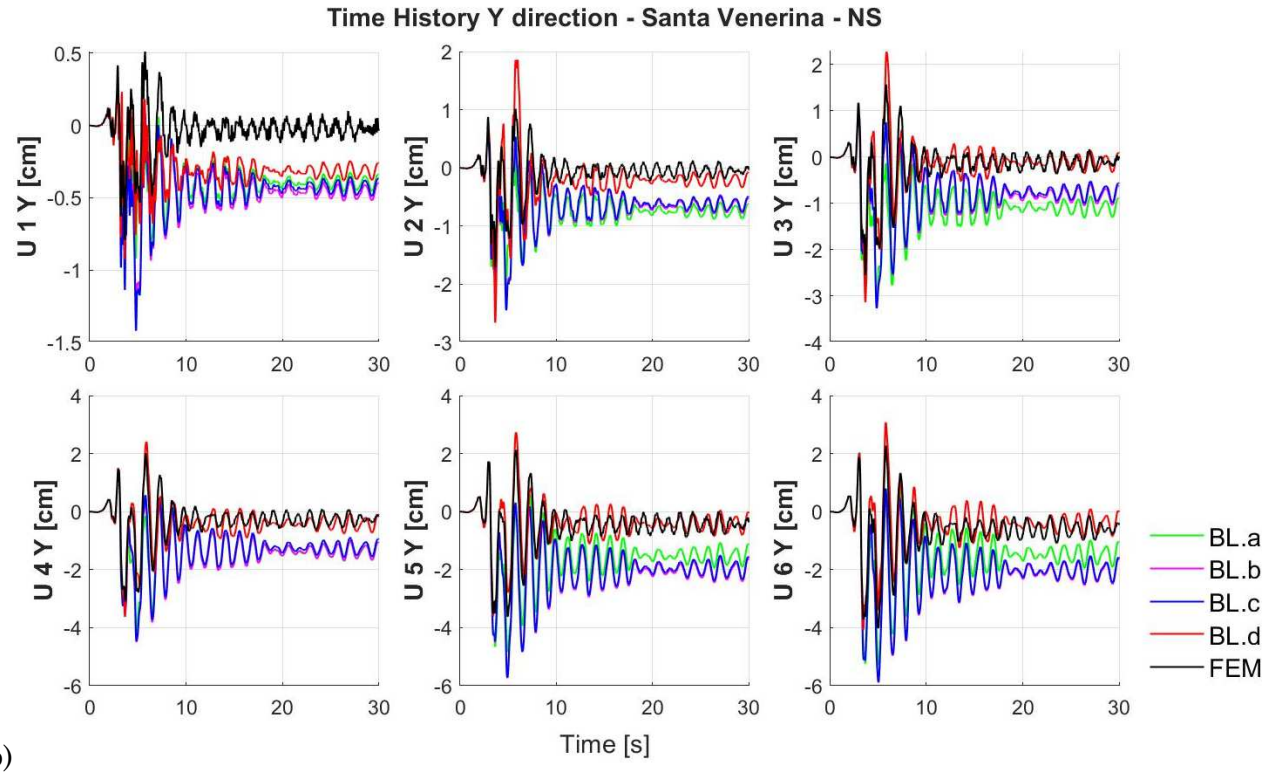

b)

Figure 4.30 - Dynamic response to Santa Venerina earthquake with constitutive law of the Beam-Like model associated with mass proportional (BL.a), inverse triangular (BL.b), mode proportional (BL.c) force distributions and mode displacement distribution (BL.d) in a) *x* and b) *y* directions

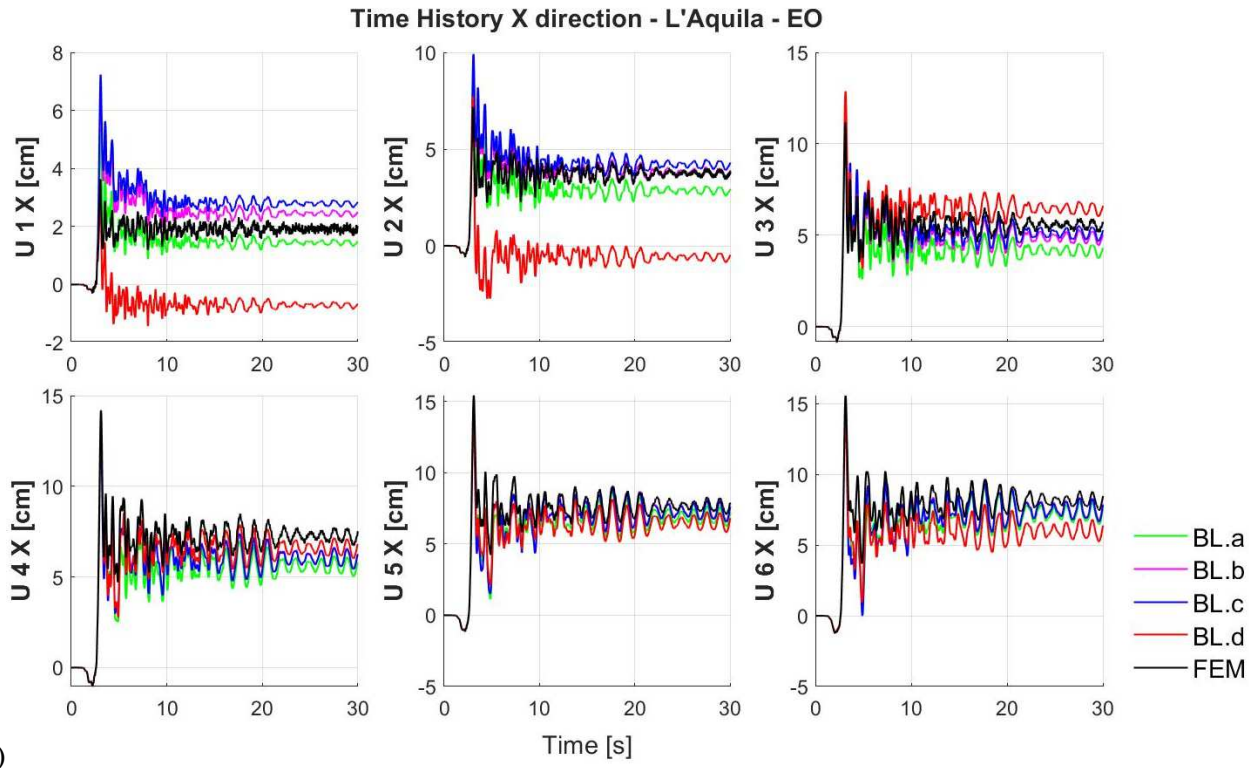

a)

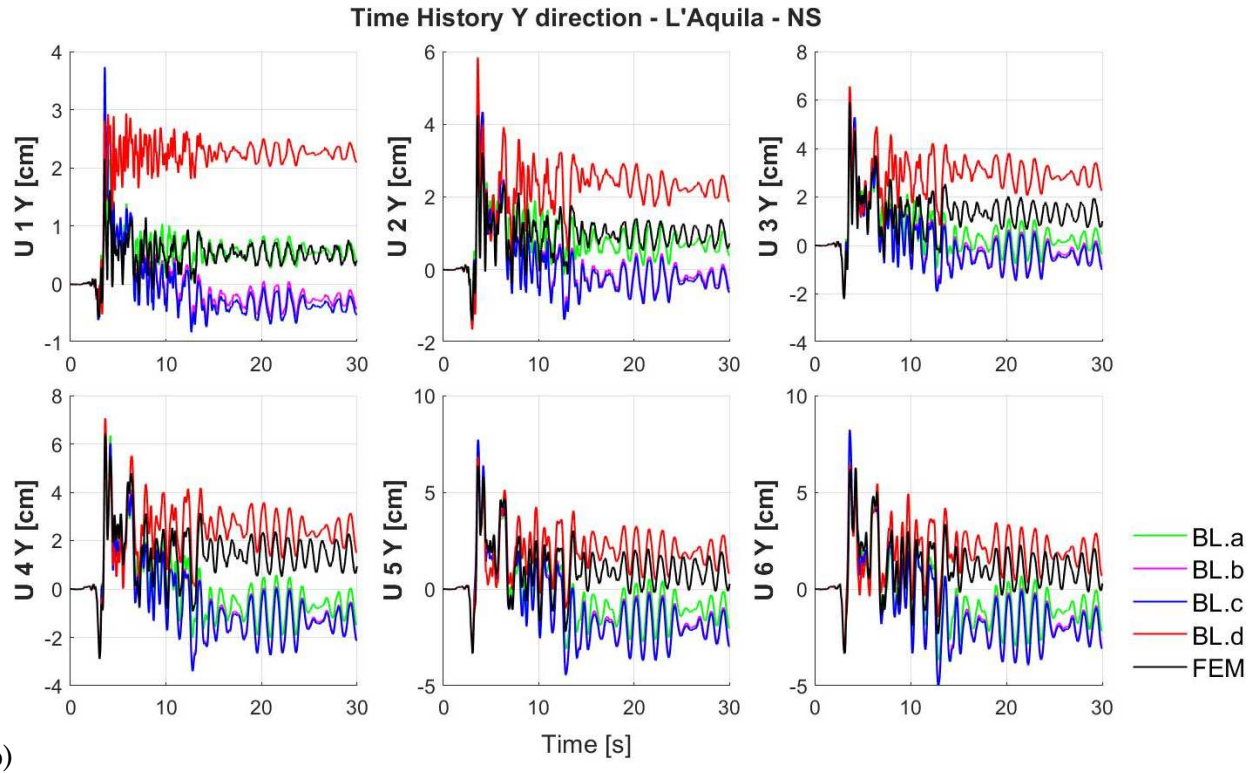

b)

Figure 4.31 - Dynamic response to L'Aquila earthquake with constitutive law of the Beam-Like model associated with mass proportional (BL.a), inverse triangular (BL.b), mode proportional (BL.c) force distributions and mode displacement distribution (BL.d) in a) *x* and b) *y* directions

The results show that all the proposed inelastic beam models are able to reproduce the non-linear dynamic behaviour of the entire building with a good accuracy. Some differences in terms of residual displacements can be observed with reference to the different distribution of force adopted for the calibration of the beam-like model. However, in terms of maximum displacement all the models are comparable.
Differently from the analyses based on the equivalent SDOF system, it is worth noting that the beam-like model allows to compute the non-linear dynamic response at each floor level without introducing any kinematic constraint.
The proposed beam-like model allows to reduce drastically the computational burden being related to a beam-like model characterised by a number of degrees of freedom equal to the number of floors, independently on the complexity of the full FEM model. In fact, the computational time required by the beam-like model for each dynamic non-linear analysis is about 60 times lower than the one required by a FEM model.

4.3.4 Beam-like model versus N2 approach

Aiming at comparing the beam-like model with another simplified approach proposed in the literature, the obtained results for the analysed structure have been compared with those provided by the SDOF-based N2 method proposed by Fajfar [71, 72].
The inter-storey drifts provided by the N2 method have been retrieved by the 3D FEM model capacity curve. Precisely, the displacement distributions associated to the ultimate displacement, corresponding to the target point, obtained on the equivalent SDOF system, have been identified. This procedure has been applied for each of the three previously described force distributions (mass proportional, inverse triangular, mode proportional). The definition of the equivalent SDOF system has been obtained according to the bilinearization procedure suggested in the Eurocode 8 [86]. The main characteristics of the equivalent SDOF system (conventional notation has been used) are reported in Table 4.9.
The seismic demand for the equivalent SDOF system has been calculated by means of non-linear dynamic analyses, which were performed in *x* and *y* directions by considering the Santa Venerina and L'Aquila ground motions, already used in the previous paragraph. Consistently to the previously performed analyses, a damping ratio equal to 5% has been assumed.

Table 4.9 - Characteristics of equivalent SDOF system

Characteristic	Force distribution a)		Force distribution b)		Force distribution c)	
	x	***y***	***x***	***y***	***x***	***y***
m* [kg]·10^6	2.68	2.68	1.60	1.60	1.60	1.62
Γ	1.00	1.00	1.39	1.39	1.33	1.33
T* [s]	1.88	2.05	1.63	1.79	1.67	1.83
F_y* [kN] ·10^3	1.70	1.70	1.03	1.05	1.06	1.08
s_y* [cm]	5.64	6.74	4.38	5.37	4.68	5.66

The displacement time history of the top floor Centre of Mass (CM) of the building, assumed as control point in accordance with the N2 method and obtained by means of the N2 equivalent SDOF system, has been compared to: *i*) the top node displacement of the equivalent beam-like model and *ii*) to the FEM displacement time history of the top floor of the building. Furthermore,

the maximum floor displacements, as well as the maximum inter-storey drifts, have been compared.
The results of the dynamic analyses for each adopted force distribution a), b) and c) in the pushover analysis are shown in Figure 4.32a-d, Figure 4.33 a-d, Figure 4.34 a-d, respectively. Furthermore, since the N2 method can be applied only by performing a static non-linear analysis on the structure with a prefixed force distribution, the results of the dynamic analyses for the displacement distribution d) in the pushover analysis have been compared to the results of the N2 method obtained by considering the force distribution c) in Figure 4.35 a-d. The percentage errors, with respect to FEM results, on the maximum floor displacements and storey drifts have been reported in Figure 4.36 a-d, Figure 4.37 a-d, Figure 4.38 a-d, Figure 4.39 a-d.
The figures show that the beam-like model is able to well reproduce the time histories of the top floor obtained with the FEM model, while the N2 method overestimates the amplitude of the displacement of the top floor. With regard to the maximum floor displacements, the N2 and the beam-like model are both in accordance with the FEM results, especially when adopting a force-displacement inter-storey constitutive law associated with modal displacement distribution d) (Figure 4.39 a-d).
From these figures it can be noticed that the maximum inter-storey drifts obtained by means of the beam-like model seem to overestimate the corresponding values obtained by means of the FEM model. However, these values overcome the inter-storey drifts which correspond to a collapse mechanism of the considered building and these results are not realistic since they have been evaluated considering the maximum values of the whole time history while the collapse can be achieved in the first few instants of time. Therefore, in the next paragraph, the collapse floor mechanism of the considered building will be investigated. It is worth highlighting that this study will be devoted to the beam-like and the FEM models only, since the inter-storey drifts time histories that could be obtained using the N2 method are all proportional being constrained by only one degree of freedom.

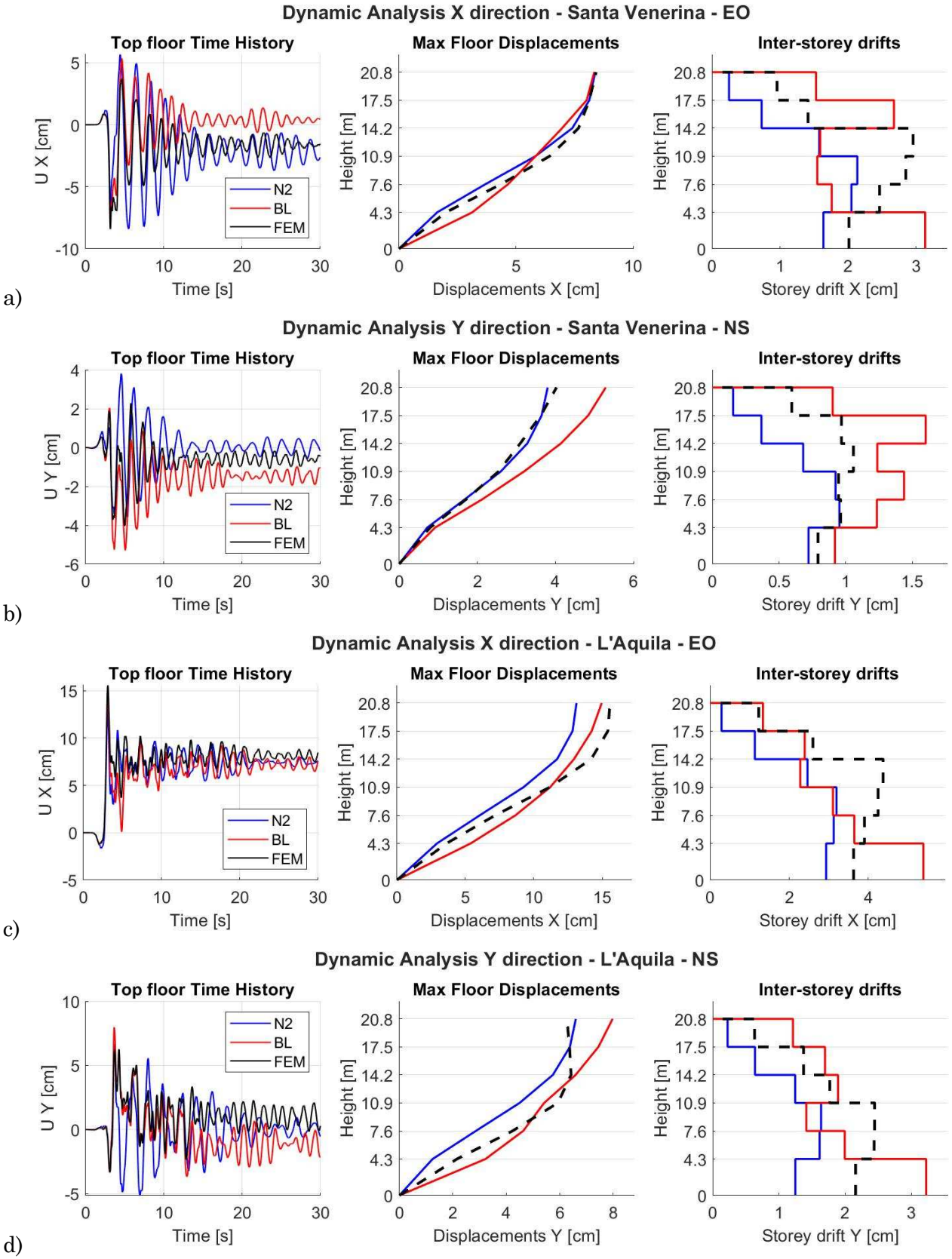

Figure 4.32 - Top displacement time history, maximum floor displacements and inter-storey drifts under Santa Venerina earthquake in a) *x* and b) *y* directions and L'Aquila earthquake in c) *x* and d) *y* directions with non-linear beam-like and N2 SDOF models associated with mass proportional force distribution

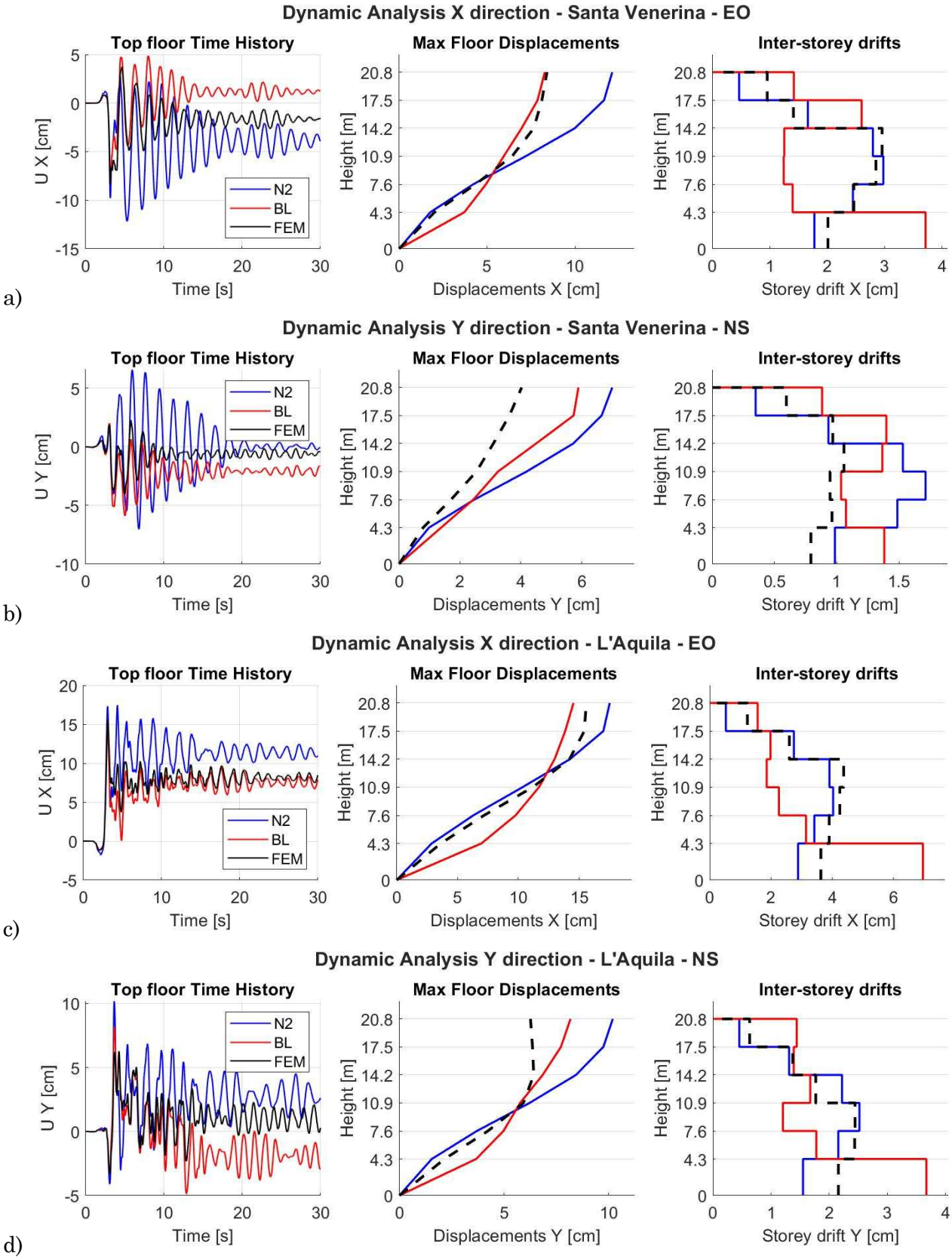

Figure 4.33 - Top displacement time history, maximum floor displacements and inter-storey drifts under Santa Venerina earthquake in a) *x* and b) *y* directions and L'Aquila earthquake in c) *x* and d) *y* directions with non-linear beam-like and N2 SDOF models associated with inverse triangular force distribution

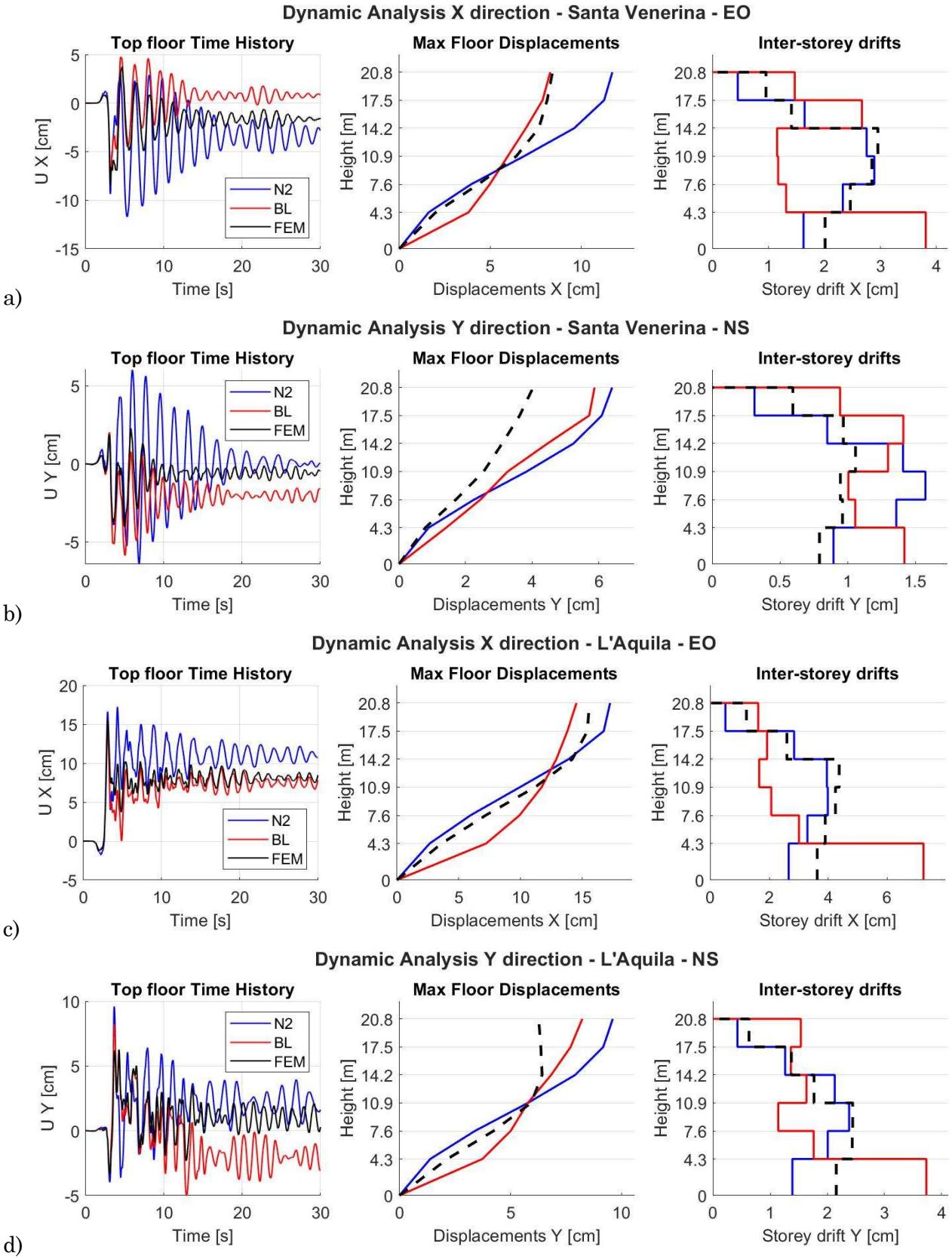

Figure 4.34 - Top displacement time history, maximum floor displacements and inter-storey drifts under Santa Venerina earthquake in a) *x* and b) *y* directions and L'Aquila earthquake in c) *x* and d) *y* directions with non-linear beam-like and N2 SDOF models associated with mode proportional force distribution

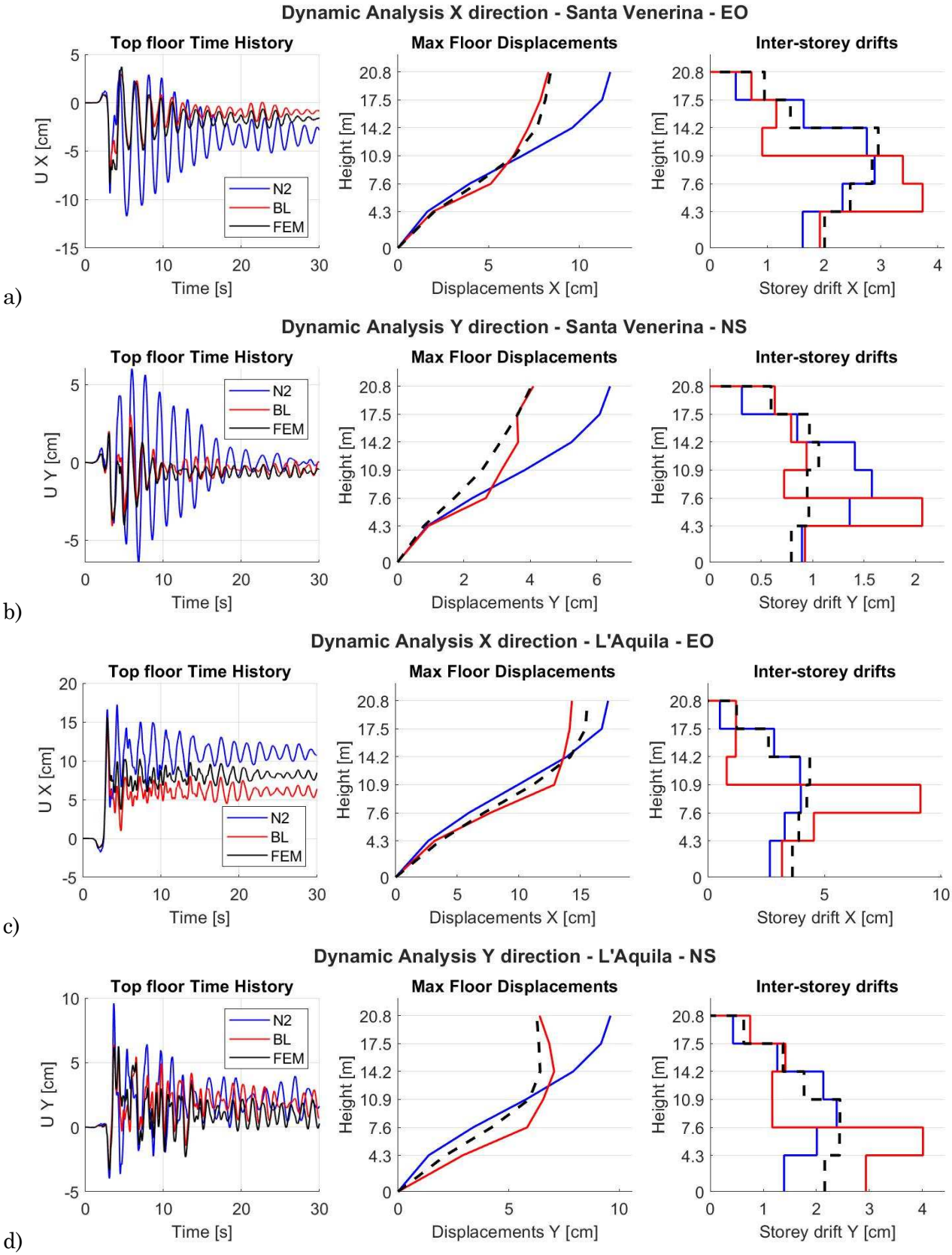

Figure 4.35 - Top displacement time history, maximum floor displacements and inter-storey drifts under Santa Venerina earthquake in a) *x* and b) *y* directions and L'Aquila earthquake in c) *x* and d) *y* directions with non-linear beam-like and N2 SDOF models associated with modal displacement distribution

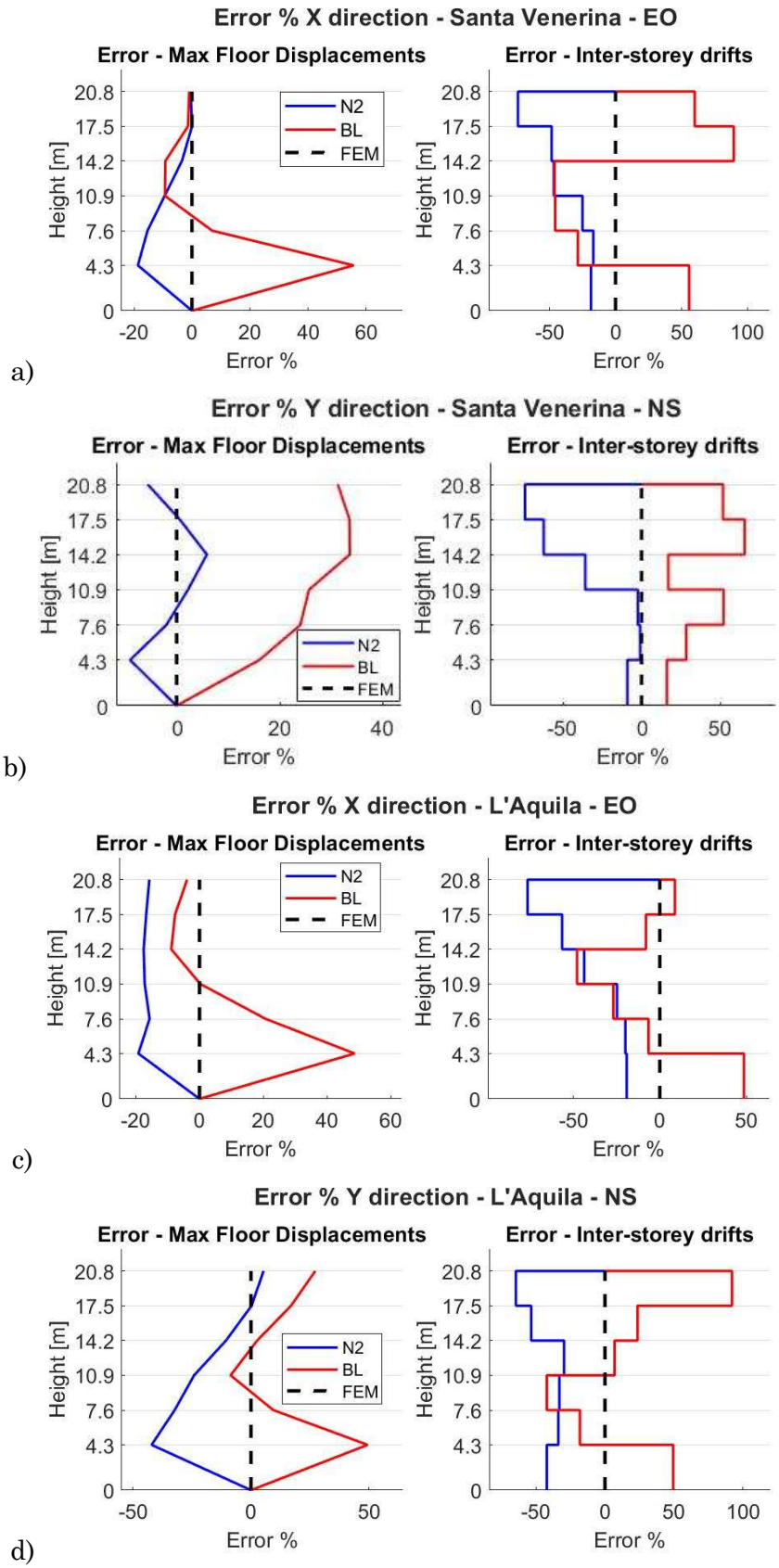

Figure 4.36 - Percentage error on maximum floor displacements and inter-storey drifts under Santa Venerina earthquake in a) *x* and b) *y* directions and L'Aquila earthquake in c) *x* and d) *y* directions with non-linear beam-like and N2 SDOF models associated with mass proportional force distribution

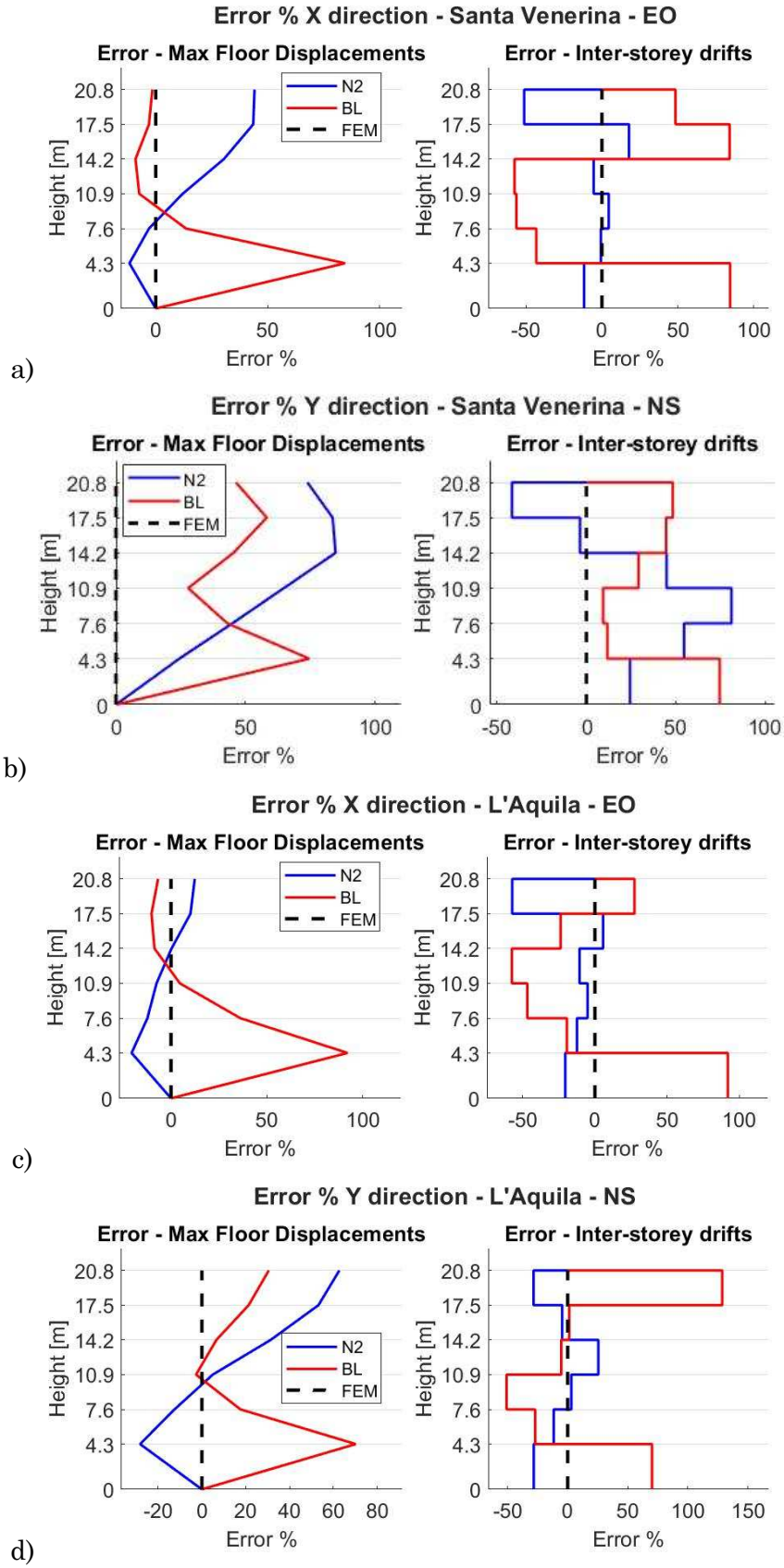

Figure 4.37 - Percentage error on maximum floor displacements and inter-storey drifts under Santa Venerina earthquake in a) *x* and b) *y* directions and L'Aquila earthquake in c) *x* and d) *y* directions with non-linear beam-like and N2 SDOF models associated with inverse triangular force distribution

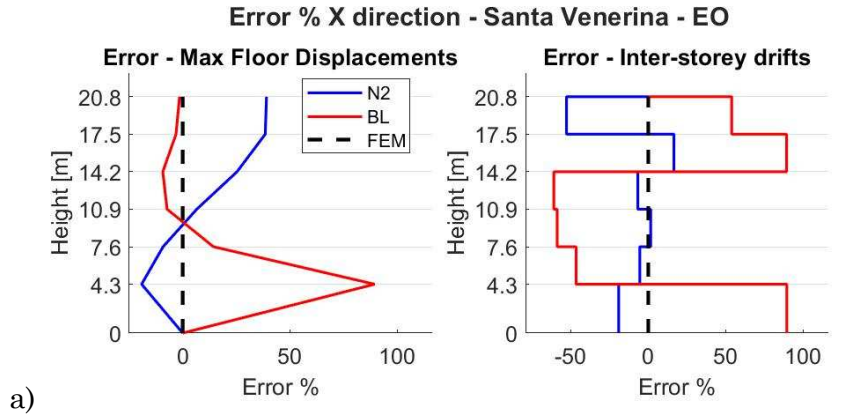

a)

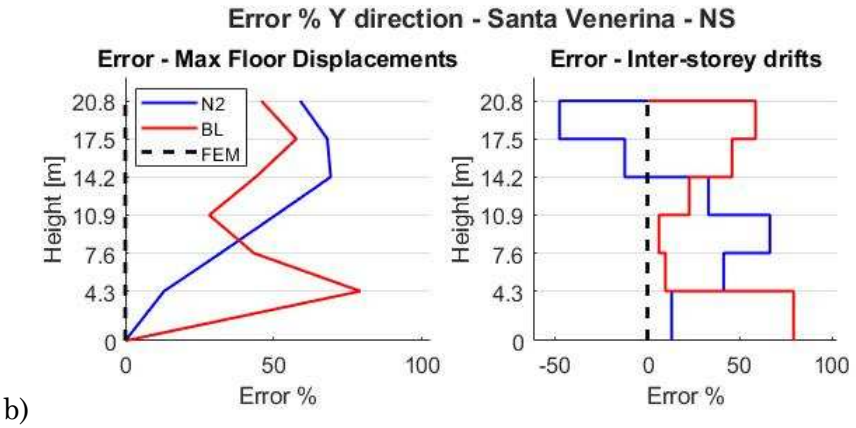

b)

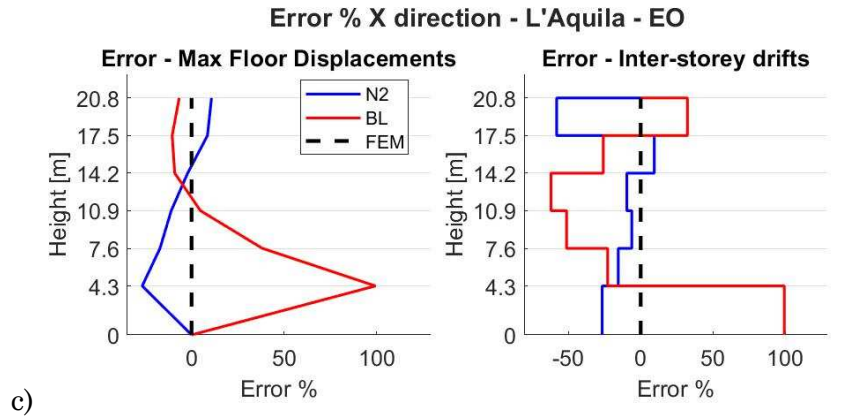

c)

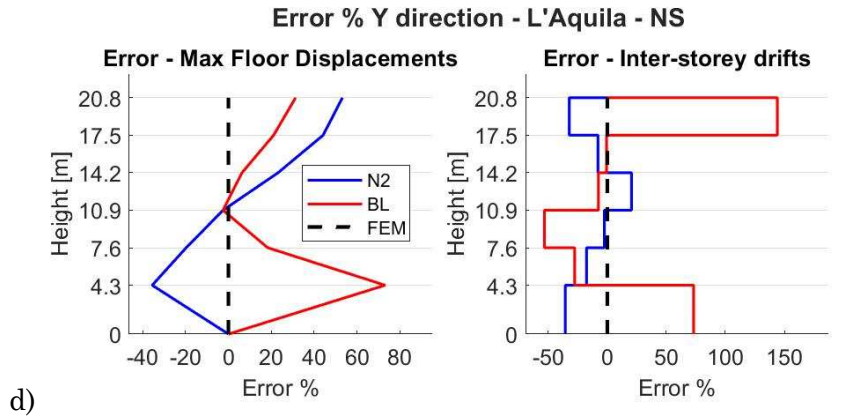

d)

Figure 4.38 - Percentage error on maximum floor displacements and inter-storey drifts under Santa Venerina earthquake in a) *x* and b) *y* directions and L'Aquila earthquake in c) *x* and d) *y* directions with non-linear beam-like and N2 SDOF models associated with mode proportional force distribution

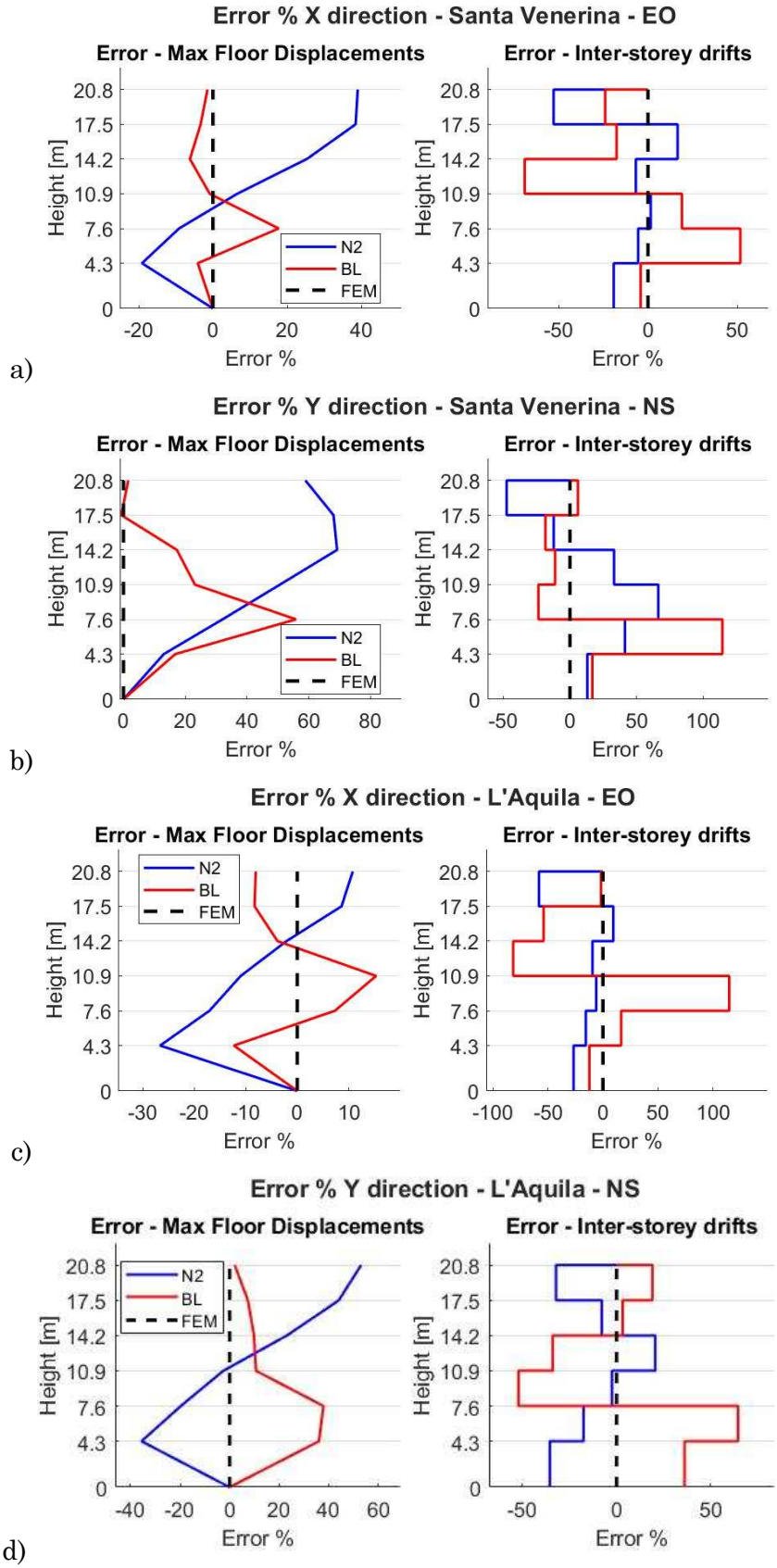

Figure 4.39 - Percentage error on maximum floor displacements and inter-storey drifts under Santa Venerina earthquake in a) *x* and b) *y* directions and L'Aquila earthquake in c) *x* and d) *y* directions with non-linear beam-like and N2 SDOF models associated with modal displacement distribution

4.3.5 Collapse mechanism

Once the dynamic non-linear response has been obtained by means of the beam-like model as shown in paragraph 4.3.3, it is possible to predict the collapse mechanism of the building also if concentrated at a specific floor. In particular, assuming that the collapse is obtained when the inter-storey drift value reaches a fixed threshold, it is possible to determine if collapse floor mechanisms have been achieved or not, and the relative collapsed floor.

The threshold can be defined as the inter-storey drift value which corresponds to a ductile or a brittle failure mechanism. These reference inter-storey drifts can be assigned taking into account typical limit values of the specific building typologies as proposed in several studies in national codes. However, more accurate limit inter-storey drifts can be obtained by considering the results of pushover analyses performed on the 3D FEM model as better specified in what follows.

The ductile failure mechanism, according to Eurocode8 – Part3 and Italian NTC18, is referred to the achievement of the ultimate chord rotation capacity of a column. The brittle collapse mechanism is referred to the achievement of the ultimate shear capacity of a column.

The ultimate chord rotation capacity of each column for the Near Collapse (NC) Limit State has been calculated according to the following two Seismic Codes: Eurocode8 – Part3, Appendix A.3.2.2 [86]; Italian NTC18, Circular C.8.7.2.3.2 [85]. However, it is more convenient to evaluate the ultimate plastic chord rotation capacity of each column for the NC Limit State according to Eurocode8 – Part3, Appendix A.3.2.2.

The ultimate shear capacity of each column for the NC Limit State has been evaluated according to suggestions reported in the Eurocode2-Part1-1 par. 6.2.3 and in the Italian Code NTC18 par. 4.1.2.3.5.2.

In this PhD thesis, in order to evaluate the ultimate plastic chord rotation capacity and the ultimate shear capacity of each column, the values of the internal forces of the structural members have been determined considering the results of a non-linear static analysis performed on the FEM model of the building. In particular, for each floor a non-linear static analysis has been performed for determining the ultimate inter-storey drift, by applying a force on the slab of the considered floor and by fixing equal to zero the x and y displacements of all the nodes below the considered floor, in order to exploit only the non-linear behaviour of the considered floor still accounting for the stiffness contribution of the remaining structure, as qualitatively shown in Figure 4.40.

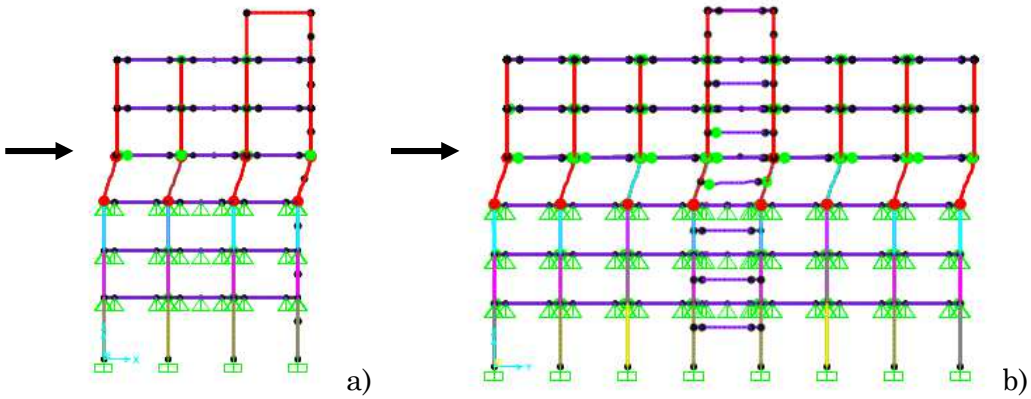

Figure 4.40 - Example of the FEM model adopted for the pushover analysis for the determination of the ultimate inter-storey drifts of the 4th floor, in a) x and b) y directions

An alternative way to evaluate the internal forces of the structural members is to consider the results of a non-linear static analysis performed on the FEM model of the building subjected to a suitable force distribution without any further kinematic constraint. However, this choice would not conduct to an appropriate definition of ultimate inter-storey drift for each floor, since not all the inter-storeys would have shown a structural member reaching the ultimate plastic chord rotation capacity or the ultimate shear capacity.

Ductile or brittle failure floor mechanisms have been associated, respectively, to the achievement of the ultimate plastic chord rotation capacity and the ultimate shear capacity at least in one of the columns of the considered floor. It is worth highlighting that the ultimate plastic chord rotation capacity and the ultimate shear capacity values have been determined for each step of the analysis and for each column of the considered floor. Therefore, the ultimate inter-storey drift value has been determined from the displacement distribution of the building at the step of the pushover analysis in which the first ductile or brittle failure mechanism has been achieved.
The ultimate inter-storey drifts assumed as threshold in *x* and *y* direction are reported in Table 4.10 and in Table 4.11 considering ductile failure mechanism only or ductile and brittle failure mechanisms, respectively.

Table 4.10 - Maximum Inter-storey drift for Limit State Near Collapse considering ductile failure mechanism only

Floor	Height *h* [m]	Maximum Inter-storey Drift (NC) [cm]	
		***x* direction**	***y* direction**
1	4.30	5.76	6.23
2	3.30	5.13	4.83
3	3.30	4.95	5.16
4	3.30	5.43	5.16
5	3.30	6.24	6.06
6	3.30	7.26	6.24

Table 4.11 - Maximum Inter-storey drift for Limit State Near Collapse considering ductile or brittle failure mechanism

Floor	Height *h* [m]	Maximum Inter-storey Drift (NC) [cm]	
		***x* direction**	***y* direction**
1	4.30	0.66	0.66
2	3.30	0.51	0.48
3	3.30	0.57	0.51
4	3.30	0.75	0.27
5	3.30	6.24	0.27
6	3.30	7.26	0.51

Once identified the ultimate inter-storey drift values according to the procedure above described, for each dynamic analysis, it is therefore possible to determine the floor in which the threshold has been firstly reached, the inter-storey drift value and the associated time instant. It is assumed that the building will not collapse if the threshold is not reached in any floor.

As already shown in paragraph 4.3.3, for each seismic record, four dynamic analyses have been performed in each considered direction (x and y), each one assuming the inter-storey shear-displacement relationship corresponding to the load distribution a), b), c) or displacement distribution d).
The results for each considered seismic record, for each direction and for each distribution a), b), c) or d) are shown in Table 4.12 and in Table 4.13, considering the ductile failure mechanism only, and in Table 4.14 and in Table 4.15, considering both the ductile and brittle failure mechanisms, compared to the results obtained from the FEM model. It is worth highlighting that in case of ductile failure mechanisms only, the building does not collapse in most cases since the drift thresholds are very high. While, in the case of ductile or brittle failure mechanisms the results of the beam-like model, especially for the displacement distribution d), are in good accordance with those of the FEM model.
In Figure 4.41 the time histories of the floor displacements and the inter-storey drifts with the associated thresholds (denoted as "Max") are reported, respectively, until the time instant when the conventional collapse has been reached. The percentage of each inter-storey drift value at the collapse time instant with respect to the associated floor threshold is reported in Table 4.16 and in Table 4.17. For the sake of brevity, only the results considering the force-displacement relationship for the displacement distribution d) compared to the FEM results are reported, considering both the ductile and brittle failure mechanisms.
The figures and the tables show that the beam-like model is able to correctly reproduce the displacement distribution and inter-storey drifts time history of each floor until the achievement of the brittle failure mechanism of the building.

Table 4.12 – Ductile collapse mechanism parameters in x direction

Seismic Record	Collapse x direction	BEAM-LIKE				FEM
		Force dist. a)	Force dist. b)	Force dist. c)	Displ. dist. d)	
L'Aquila	Floor	-	1	1	3	-
	Δu [cm]	-	5.8	5.86	5.08	-
	T [s]	-	2.98	2.98	3.08	-
Santa Venerina	Floor	-	-	-	-	-
	Δu [cm]	-	-	-	-	-
	T [s]	-	-	-	-	-

Table 4.13 – Ductile collapse mechanism parameters in y direction

Seismic Record	Collapse y direction	BEAM-LIKE				FEM
		Force dist. a)	Force dist. b)	Force dist. c)	Displ. dist. d)	
L'Aquila	Floor	-	-	-	-	-
	Δu [cm]	-	-	-	-	-
	T [s]	-	-	-	-	-
Santa Venerina	Floor	-	-	-	-	-
	Δu [cm]	-	-	-	-	-
	T [s]	-	-	-	-	-

Table 4.14 - Ductile or brittle collapse mechanism parameters in *x* direction

Seismic Record	Collapse *x* direction	BEAM-LIKE				FEM
		Force dist. a)	Force dist. b)	Force dist. c)	Displ. dist. d)	
L'Aquila	Floor	1	1	1	1	1
	Δu [cm]	0.67	0.68	0.68	0.68	0.66
	T [s]	2.69	2.69	2.69	2.69	2.69
Santa Venerina	Floor	1	1	1	2	2
	Δu [cm]	0.67	0.66	0.67	0.54	0.51
	T [s]	2.95	2.94	2.94	2.94	2.94

Table 4.15 - Ductile or brittle collapse mechanism parameters in *y* direction

Seismic Record	Collapse *y* direction	BEAM-LIKE				FEM
		Force dist. a)	Force dist. b)	Force dist. c)	Displ. dist. d)	
L'Aquila	Floor	4	4	4	4	4
	Δu [cm]	0.28	0.28	0.28	0.27	0.27
	T [s]	2.87	2.87	2.87	2.87	2.83
Santa Venerina	Floor	4	4	4	4	5
	Δu [cm]	0.27	0.28	0.28	0.27	0.27
	T [s]	2.92	2.93	2.93	2.93	2.93

a)

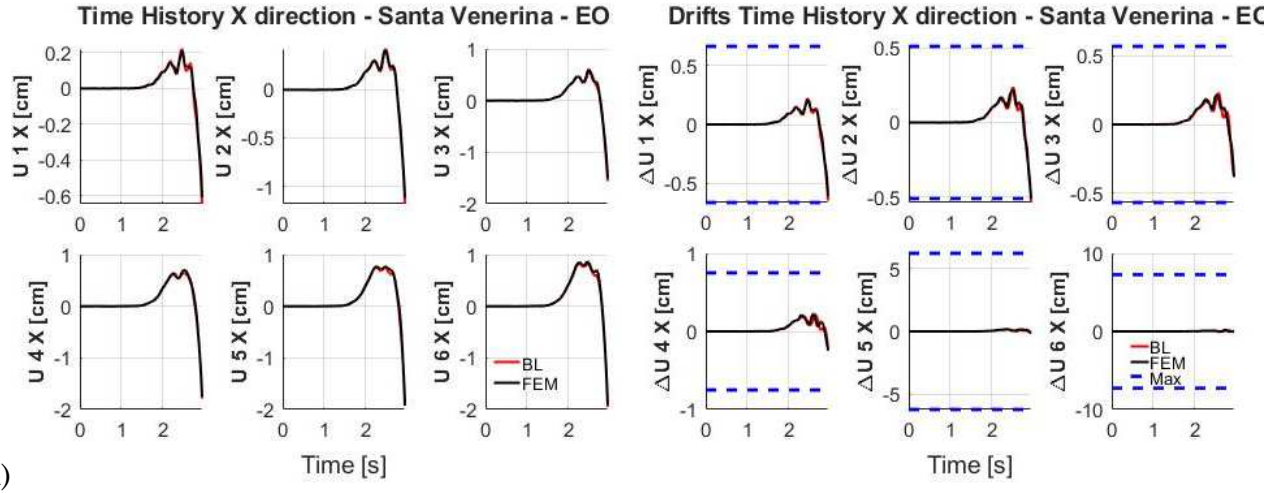

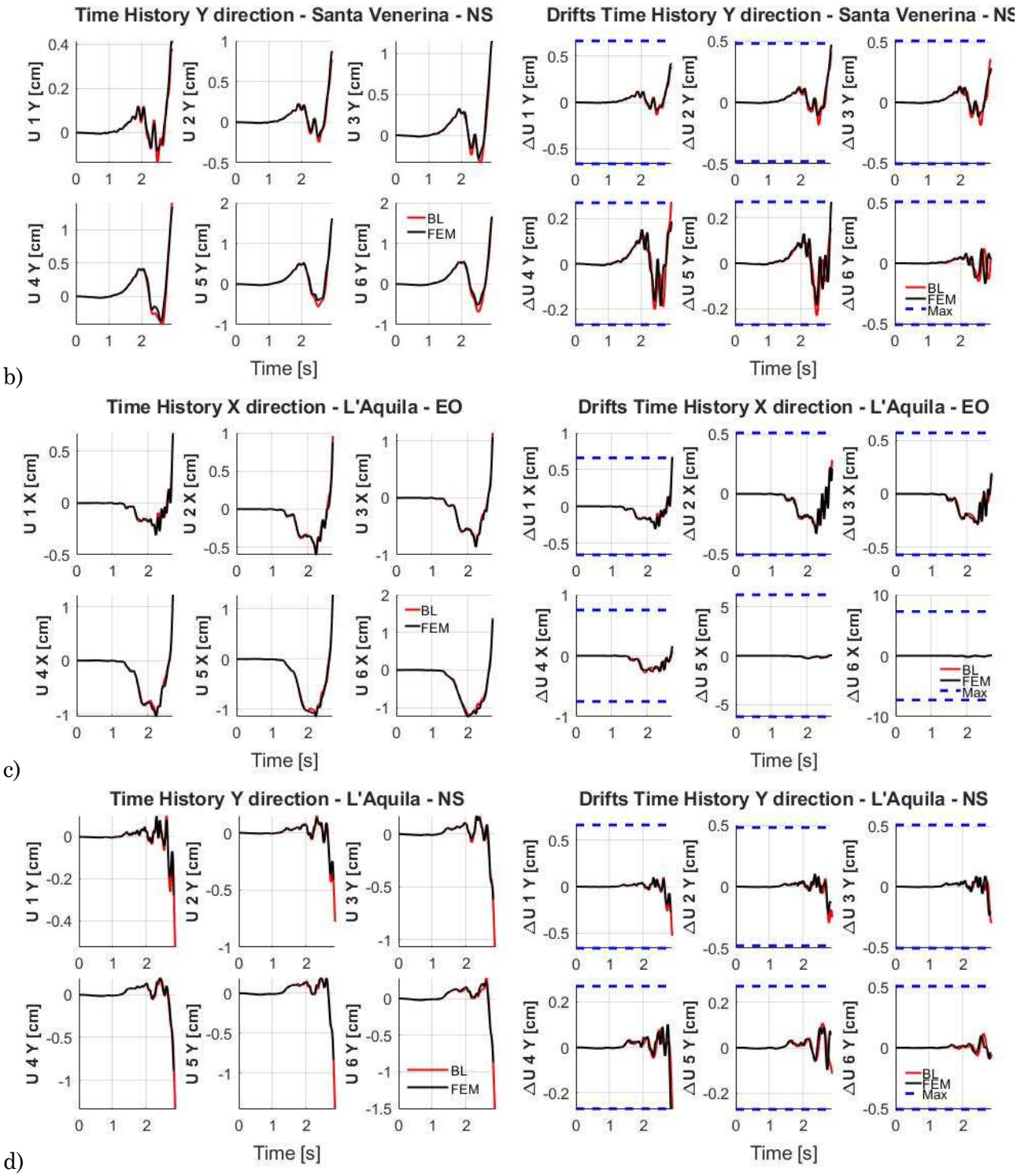

Figure 4.41 - Time histories of the floor displacements and of the inter-storey drifts until the collapse time instant for a-b) Santa Venerina and c-d) L'Aquila earthquake, in *x* and *y* direction respectively considering the force-displacement relationship for load distribution d) and the ductile and brittle failure mechanisms

Table 4.16 - Percentage of each inter-storey drift value at the collapse time instant with respect to the associated floor threshold for Santa Venerina earthquake considering the force-displacement relationship for load distribution d) and the ductile and brittle failure mechanisms

Floor	% $\Delta u/\Delta u_{max}$ – *x* direction		% $\Delta u/\Delta u_{max}$ – *y* direction	
	BEAM-LIKE Displ. dist. d)	FEM	BEAM-LIKE Displ. dist. d)	FEM
1	97.57	91.97	55.79	61.36
2	105.19	100.2	84.68	97.71
3	66.61	67.37	70.4	55.49
4	30.27	32.8	101.69	69.63
5	0.73	2.85	57.2	100.19
6	1.64	0.32	9.27	8.72

Table 4.17 - Percentage of each inter-storey drift value at the collapse time instant with respect to the associated floor threshold for L'Aquila earthquake considering the force-displacement relationship for load distribution d) and the ductile and brittle failure mechanisms

Floor	% $\Delta u/\Delta u_{max}$ – *x* direction		% $\Delta u/\Delta u_{max}$ – *y* direction	
	BEAM-LIKE Displ. dist. d)	FEM	BEAM-LIKE Displ. dist. d)	FEM
1	102.62	100.15	79.67	42.2
2	55.46	41.37	52.25	28.12
3	31.77	33.68	57.29	40.29
4	10.62	20.93	100.47	100.93
5	0.88	0.90	42.08	20.56
6	1.49	0.73	11.24	6.86

4.3.6 Fragility curves

The results of the study reported in the previous paragraph show that the beam-like model is able to correctly reproduce the displacement distribution and inter-storey drifts time history of each floor until the failure mechanism of the building is reached. Therefore, this model can be adopted for an accurate seismic vulnerability assessment of existing buildings, allowing to reduce the computational effort and time with respect to corresponding calculations based on FEM models.
In particular, this paragraph describes how the beam-like model can be used for the construction of the fragility curves of the considered building.
Fragility curves have been obtained following the Multiple Stripe Analysis (MSA) procedure proposed by Baker and briefly described in 3.1.
Two groups of seismic records have been adopted for the dynamic non-linear analyses. The first one considers seven real accelerograms whose response spectra are compatible with the design spectra suggested by the Italian Code NTC18 [85] for the geological site of Catania. The second one considers twenty-three real accelerograms in addition to the seven already mentioned, in order to dispose of thirty seismic records, whose main characteristics are compatible with the Catania site. The characteristics of the considered seismic records and their representation are reported in Appendix E.
The ground motion Intensity Measure (*IM*) used in the following MSA procedure is the PGA. The dynamic non-linear analyses are performed at a discrete set of *IM* levels equal to [0.05 0.1 0.2 0.3 0.4 0.5 0.6] *g*. The same accelerograms (seven or thirty), reported in Appendix E, have been adopted for each *IM* level, therefore the seismic records have been scaled in order to have their PGA equal to the considered *IM* levels.
The construction of the fragility curves has been developed with reference to three Limit States of interest according to the Eurocode8: Damage Limitation (DL), Significant Damage (SD), Near Collapse (NC). These Limit States according to Italian Code NTC18 correspond respectively to: Immediate Occupancy (SLD), Life Safety (SLV) and Collapse Prevention (SLC).
The chosen Damage Parameter (*DP*) is the inter-storey drift. The Damage Threshold (*DT*) can be defined according to the Hazus earthquake technical manual 4-2 of the FEMA [116] or by determining the inter-storey drift values which correspond to a ductile or a brittle collapse mechanism, as described in the previous paragraph.
The ductile collapse mechanism, according to Eurocode8 – Part3 and Italian NTC18, is referred to the achievement of the ultimate chord rotation capacity of a column. The brittle collapse mechanism is referred to the achievement of the ultimate shear capacity of a column.
The ultimate chord rotation capacity of each column for the three Limit States (NC, SD, DL) has been calculated according to the following two Seismic Codes: Eurocode8 – Part3, Appendix A.3.2.2, A.3.2.3, A.3.2.4 [86]; Italian NTC18, Circular C.8.7.2.3.2, C.8.7.2.3.3, C.8.7.2.3.4 [85].
However, it is more convenient to evaluate the ultimate plastic chord rotation capacity of each column for the NC Limit State according to Eurocode8 – Part3, Appendix A.3.2.2. The ultimate plastic chord rotation capacity of each column for the SD Limit State has been set equal to the 3/4 of the value for NC, while equal to zero for DL (which corresponds to the achievement of the first plastic chord rotation and therefore to the end of the linear elastic behaviour).

The ultimate shear capacity of each column for the DL, SD and NC Limit States has been evaluated according to suggestions reported in the Eurocode2-Part1-1 par. 6.2.3 and in the Italian Code NTC18 par. 4.1.2.3.5.2.
Adopting the same procedure described in paragraph 4.3.5, the values of the internal forces of the structural members for the computation of the ultimate plastic chord rotation capacity and for the ultimate shear capacity of each column have been determined considering the results of a non-linear static analysis performed on the FEM model of the building. In particular, for each floor a non-linear static analysis has been performed for determining the ultimate inter-storey drift, by applying a force on the slab of the considered floor and by fixing equal to zero the *x* and *y* displacements of all the nodes below the considered floor, in order to exploit only the non-linear behaviour of the considered floor still accounting for the stiffness contribution of the remaining structure. For each step of the analysis, the ultimate plastic chord rotation capacity and the ultimate shear capacity for the NC, SD or DL Limit State have been determined for each column of the considered floor, and if those values have been reached at least in one of the columns, a ductile or brittle failure mechanism has been achieved, respectively. Therefore, the inter-storey drift values assumed as *DT* have been determined from the displacement distribution of the building at the step of the pushover analysis in which the first ductile or brittle collapse mechanism has been achieved for the NC, SD or DL Limit State.
The ultimate inter-storey drift values assumed as threshold in *x* and *y* direction for each Limit State obtained considering ductile collapse mechanism only or both ductile and brittle collapse mechanisms are reported in Table 4.18 and in Table 4.19, respectively.

Table 4.18 - Damage Thresholds considering ductile collapse mechanisms only

Floor	***DT* = Δu [cm] – *x* direction**			***DT* = Δu [cm] – *y* direction**		
	NC	**SD**	**DL**	**NC**	**SD**	**DL**
1	5.76	4.50	0.72	6.23	4.80	0.69
2	5.13	3.99	0.54	4.83	3.78	0.63
3	4.95	3.90	0.54	5.16	3.99	0.57
4	5.43	4.23	0.63	5.16	4.08	0.57
5	6.24	4.89	0.54	6.06	4.74	0.48
6	7.26	5.61	0.30	6.24	4.83	0.21

Table 4.19 - Damage Thresholds considering ductile and brittle collapse mechanisms

Floor	***DT* = Δu [cm] – *x* direction**			***DT* = Δu [cm] – *y* direction**		
	NC	**SD**	**DL**	**NC**	**SD**	**DL**
1	0.66	0.66	0.66	0.66	0.66	0.66
2	0.51	0.51	0.51	0.48	0.48	0.48
3	0.57	0.57	0.54	0.51	0.51	0.51
4	0.75	0.75	0.63	0.27	0.27	0.27
5	6.24	4.89	0.54	0.27	0.27	0.27
6	7.26	5.61	0.30	0.51	0.51	0.21

It is worth noting that in the ductile or brittle failure mechanism case some values of the inter-storey drift thresholds for the NC, SD or DL Limit States are equal because the ultimate shear capacity of a column is assumed to be the same for the three Limit States.
For the sake of brevity, the fragility curves have been obtained considering in the beam-like model only the inter-storey shear-displacement relationship corresponding to the displacement distribution d), obtained in paragraph 4.3.1.
In the following, the fragility curves obtained adopting the first set of seven accelerograms in *x* and *y* directions and considering the ductile collapse mechanism only or both the ductile and brittle failure mechanisms, are shown in Figure 4.42.a-b, respectively. Then the fragility curves obtained adopting the second set of thirty accelerograms are shown in Figure 4.43.a-b, for the ductile collapse mechanism only or both the ductile and brittle failure mechanisms respectively. In the same figures, the circles represent the "empirical" values of percentage of collapse for each *IM* level obtained by means of the dynamic non-linear analyses performed with the equivalent beam-like model. In Figure 4.43, for the case of thirty accelerograms in *x* direction only, the asterisks represent the "empirical" values of percentage of collapse for each *IM* level obtained by means of the dynamic non-linear analyses performed with the FEM model.
In Table 4.20 an in Table 4.21 the mean μ and standard deviation σ of the obtained fragility curves are reported.

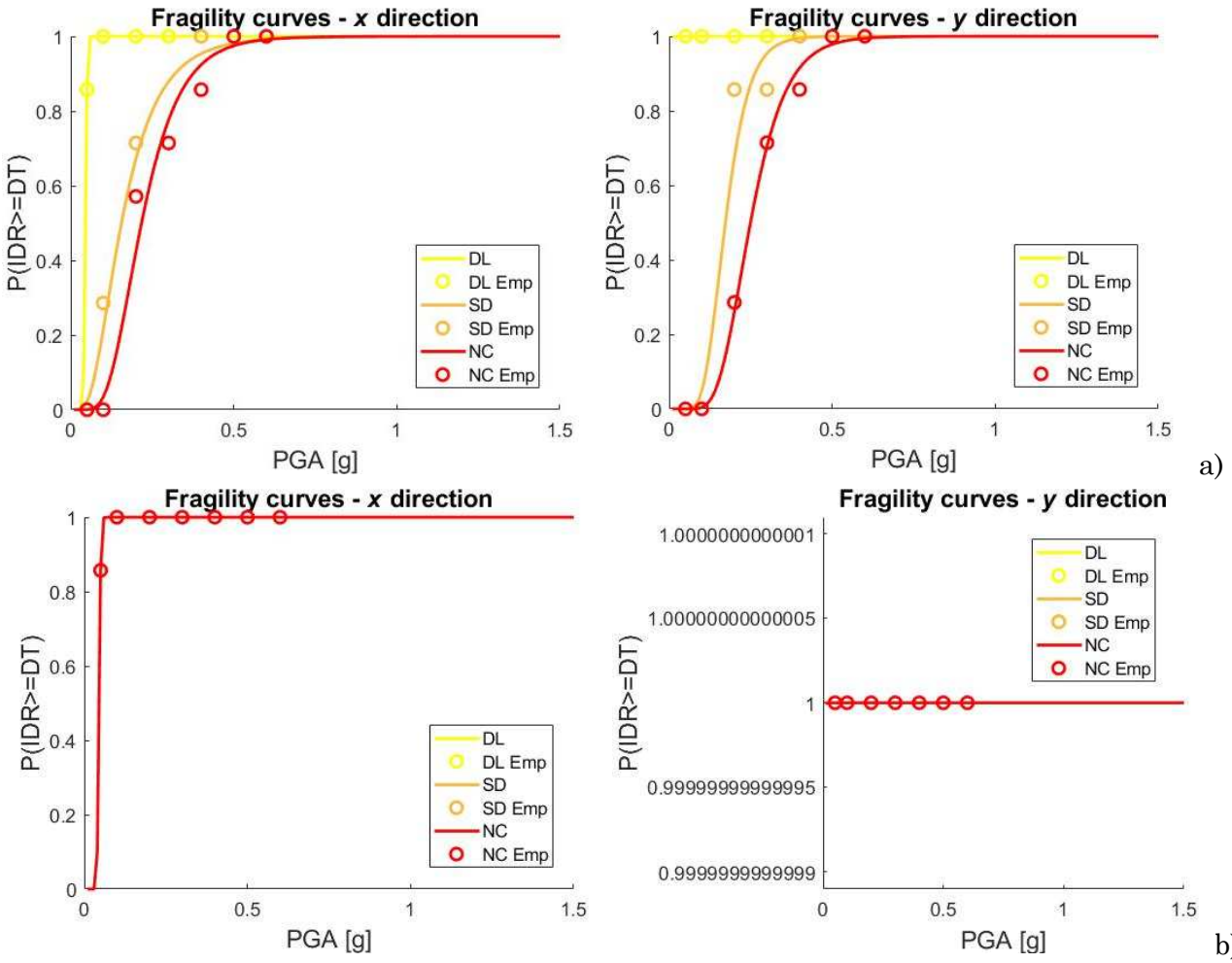

Figure 4.42 - Fragility curves obtained adopting the first set of seven accelerograms in *x* and *y* directions considering the ductile collapse mechanism only a) or both the ductile and brittle failure mechanisms b)

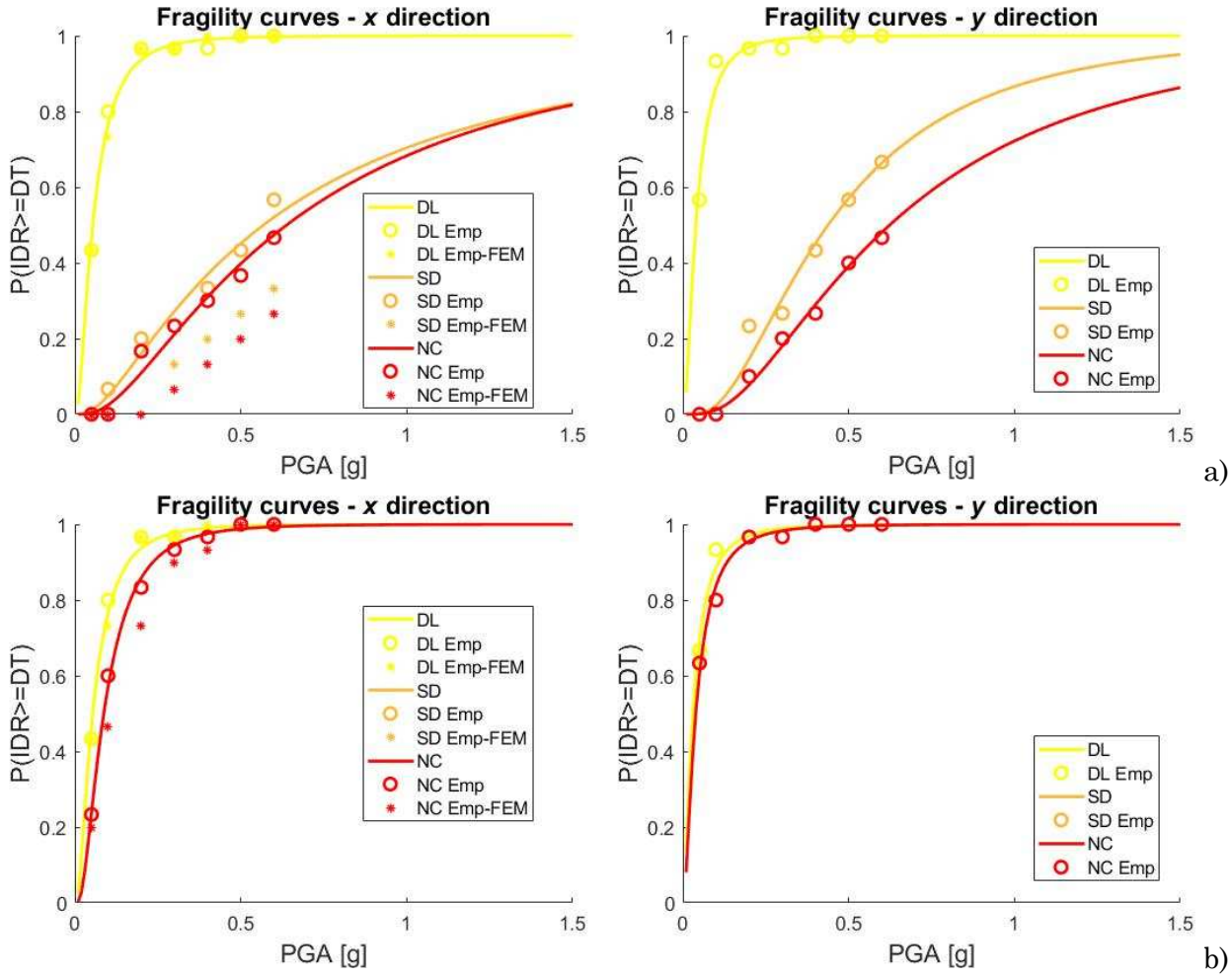

Figure 4.43 - Fragility curves obtained adopting the second set of thirty accelerograms in *x* and *y* directions considering the ductile collapse mechanism only a) or both the ductile and brittle failure mechanisms b)

Table 4.20 - Fragility curves parameters considering the ductile collapse mechanism only

N° seismic records	FC parameter	*x* direction			*y* direction		
		NC	SD	DL	NC	SD	DL
7	μ	-1.527	-1.859	-3.097	-1.389	-1.757	-46.643
	σ	0.426	0.561	0.095	0.344	0.328	5.161
30	μ	-0.449	-0.565	-2.925	-0.472	-0.826	-3.243
	σ	0.942	1.054	0.860	0.801	0.745	0.863

Table 4.21 - Fragility curves parameters considering the ductile and brittle failure mechanisms

N° seismic records	FC parameter	*x* direction			*y* direction		
		NC	SD	DL	NC	SD	DL
7	μ	-3097	-3097	-3.097	-46.643	-46.643	-46.643
	σ	0.095	0.095	0.095	5.161	5.161	5.161
30	μ	-2.440	-2.440	-2.925	-3.252	-3.252	-3.508
	σ	0.775	0.775	0.860	0.964	0.964	1.002

Figure 4.42 and Figure 4.43 clearly show how important is the use of an appropriate number of seismic records for the construction of fragility curves. Of course, the increase in the number of adopted accelerograms improves the obtained results since there is a wider statistical range of experimental collected data. However, nowadays the use of a huge number of seismic records is not allowed for fast seismic vulnerability assessment if a FEM software is adopted for the dynamic non-linear analyses due to the computational effort and time required. For this reason the experimental values of percentage of collapse in this study have been obtained by means of the FEM model only for the x direction. In terms of computational time it is important to highlight that the non-linear dynamic analyses of thirty accelerograms (considering only the first 15 [s] of each seismic record) for seven *IM* levels performed on the FEM model of the considered building require about 120 times the computational time required to perform the same analyses (considering the whole seismic record) by means of the equivalent beam-like model.

It is worth noting that the fragility curves, which consider ductile or brittle failure mechanisms, show a higher percentage of collapse for a fixed IM level with respect to the ones which consider ductile failure mechanism only. This is in accordance with the type of construction of reinforced concrete buildings, which show mainly a brittle behaviour if they have been designed to resist gravity loadings only.

Furthermore, the differences between the experimental values of the percentage of collapse obtained by means of the beam-like and the FEM models are almost negligible in the case of ductile or brittle failure mechanism, as shown in Figure 4.43.b. Therefore, this proves the reliability and great utility of the beam-like model for the construction of the fragility curves of existing buildings considering ductile or failure mechanisms.

4.4 CASE STUDY 2: BEAM LIKE MODEL OF SAC BUILDING - INELASTIC BEHAVIOUR

In this chapter the proposed inelastic beam-like model is applied to another benchmark, known as SAC building, which has been the subject of several numerical investigations in the scientific literature [79, 117, 118, 119, 120]. This case study is a 9-storey steel building, whose detailed description is provided in [121, 79], considered representative of typical medium-rise buildings designed for Los Angeles, California, according to the seismic code requirements of the 1994 UBC. The building has been analysed according to a two-dimensional model which consists of the N-S perimeter moment resisting frame (MRF), representing half of the building in the N-S direction.

The non-linear static and dynamic analyses on a FEM model of the SAC building have been developed by using the well-known software SAP2000 v.22 [122]. Consistently to the numerical investigations already reported in the literature [79], axial deformability of columns and beams and large displacements effects have been neglected. The global non-linear behaviour of the structure has been modelled by introducing plastic hinges at the ends of all the structural elements (beams and columns). In particular, P-M2-M3 hinges have been used for columns and M3 hinges for beams, where shear failure has been neglected, according to the ASCE 41-17 criteria.

First, the calibration procedure was performed in order to identify the equivalent beam-like model. Then the proposed multi-stepped beam was adopted for simulating the static and dynamic inelastic behaviour of the building and the results, in terms of static and seismic response, were compared to those obtained by means of the conventional 3D FEM model.

Since the capacity curves depend on the applied distribution of forces, different loading patterns have been taken into account in order to investigate the differences in predicting the inelastic responses, as better specified in the following.

The complete FEM and the beam-like models of the building have been subjected to a static force vector $\underline{\mathbf{F}}_b$ according to the following relationships:

$$\mathbf{F}_b = \mathbf{M}_b \boldsymbol{\phi} \tag{4.2.5}$$

where $\boldsymbol{\phi}$ is the fixed displacement distribution and $\mathbf{M}_b$ is the diagonal mass matrix which considers lumped masses at the nodes due to the applied seismic masses.

In particular, the following three load distributions have been considered in the numerical applications:

a) mass proportional force distribution (Figure 4.44a);
b) inverse triangular proportional force distribution (Figure 4.44b);
c) force distribution associated with the fundamental natural mode of vibration (Figure 4.44c).

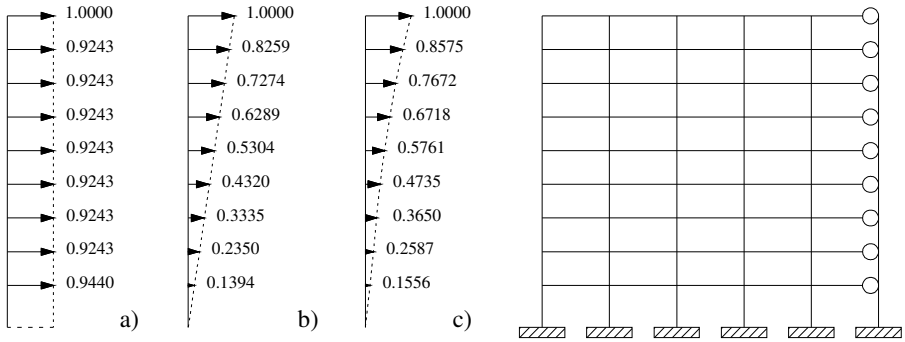

Figure 4.44 - Lateral force distribution types: a) Mass proportional, b) inverse triangular mass proportional and c) associated with fundamental mode

The non-linear dynamic analyses have been performed by considering the N-S component of the earthquake recorded at El Centro in 1940, plotted in Figure 4.45.

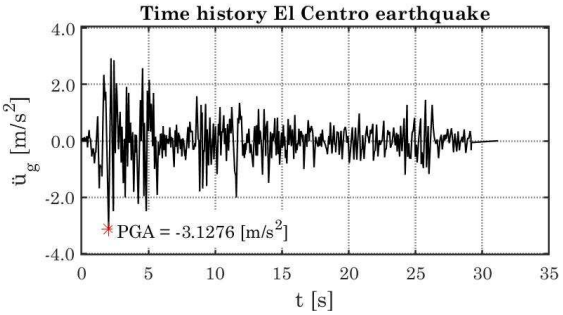

Figure 4.45 - Time history for El Centro earthquake

4.4.1 Calibration procedure

The results of the non-linear static analysis have been reported in terms of inter-storey capacity curves in Figure 4.46 for the three previously described load distributions. It can be observed that the damage is mainly distributed along the first six levels of the building for all the considered load distributions.

The beam-like model has been calibrated by following the procedure described in paragraph 2.2.3. As first step, the inelastic inter-storey responses, reported in Figure 4.46, have been considered for the calibration of the inelastic multi-stepped beam. As second step, the obtained inter-storey capacity curves have been transformed into equivalent bilinear elasto-plastic force-displacement laws with positive kinematic hardening. The equivalence has been obtained by imposing the equality between the areas below the non-linear and bilinear capacity curves and assuming as initial inter-storey stiffness the tangent to the origin of the inter-storey capacity curve. The stiffness values of each beam segment, assumed as initial stiffness in the successive non-linear analyses, are reported in Table 4.22; the latter data, together with the mass distribution, allow to define the linear elastic behaviour of each beam-like model associated with each force distribution. In Table 4.23 the inelastic limits and the hardening parameters for each beam segment are reported; in this case, no limits of the ductile behaviour have been considered. The latter parameters are sufficient for the characterization of the non-linear response of the beam-like model.

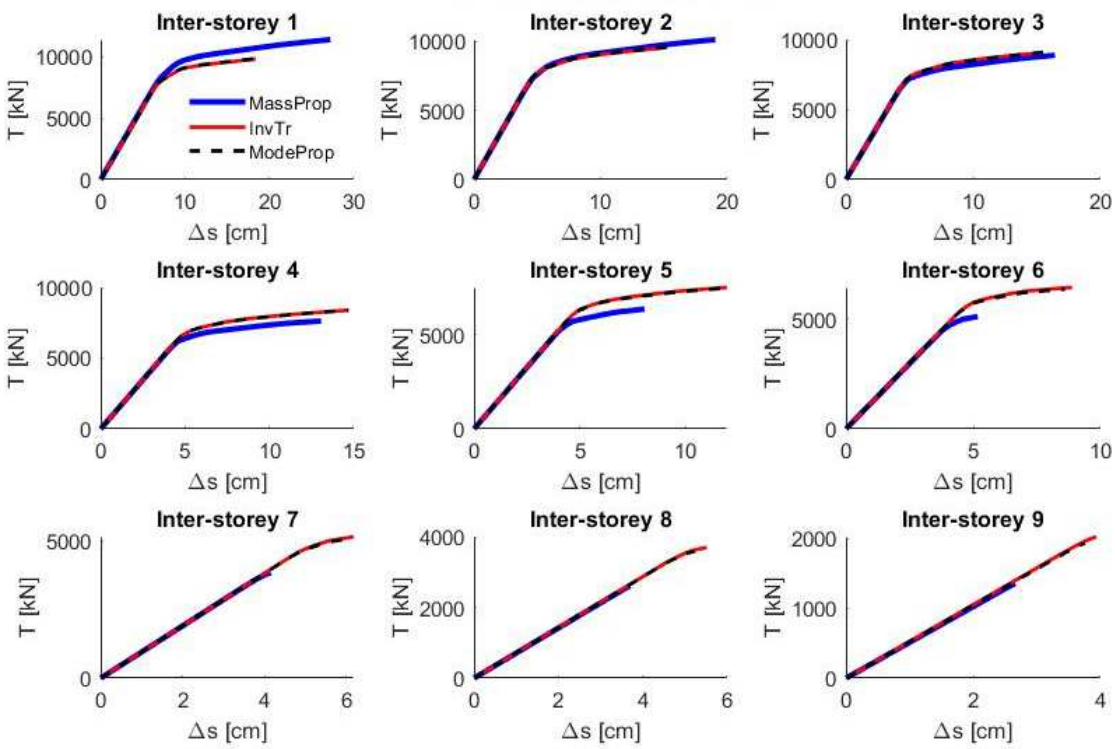

Figure 4.46 - Inter-storey capacity curves for load distribution a (blue), b (red) and c (black)

Table 4.22 - Initial stiffness of each beam segment associated with each different force distribution

Beam segment	Height h [m]	Initial stiffness R [N/m] · 10^8		
		Force dist. a)	Force dist. b)	Force dist. c)
1	5.49	1.188	1.172	1.172
2	3.96	1.621	1.637	1.630
3	3.96	1.535	1.541	1.545
4	3.96	1.386	1.402	1.401
5	3.96	1.301	1.312	1.316
6	3.96	1.193	1.201	1.195
7	3.96	0.963	0.954	0.961
8	3.96	0.705	0.724	0.715
9	3.96	0.510	0.526	0.524

Table 4.23 - Yielding force and hardening parameter of each beam segment associated with each different force distribution

	Yielding force F_y [N] · 10^6			Post yielding stiffness R_T [N/m] · 10^7		
Beam segment	Force dist. a)	Force dist. b)	Force dist. c)	Force dist. a)	Force dist. b)	Force dist. c)
1	9.714	8.756	8.787	0.893	0.981	0.973
2	8.504	8.282	8.322	1.180	1.270	1.248
3	7.601	7.860	7.854	1.116	1.176	1.185
4	6.662	7.272	7.262	1.169	1.180	1.185
5	5.757	6.706	6.647	1.694	1.183	1.228
6	4.723	5.913	5.872	3.249	1.338	1.335
7	2.759	4.928	4.594	8.579	2.381	4.153
8	2.585	3.102	3.550	7.235	4.835	1.339
9	1.343	1.961	-	6.024	3.088	5.240

Three bilinear relationships have been defined, each one representing the monotonic inelastic inter-storey response of the building subjected to the considered force distribution. In Figure 4.47 the inter-storey inelastic equivalent force-displacement laws relative to the mode proportional analysis only are reported as an example. Since the last storey exhibited an elastic response, this has been considered as linear elastic.

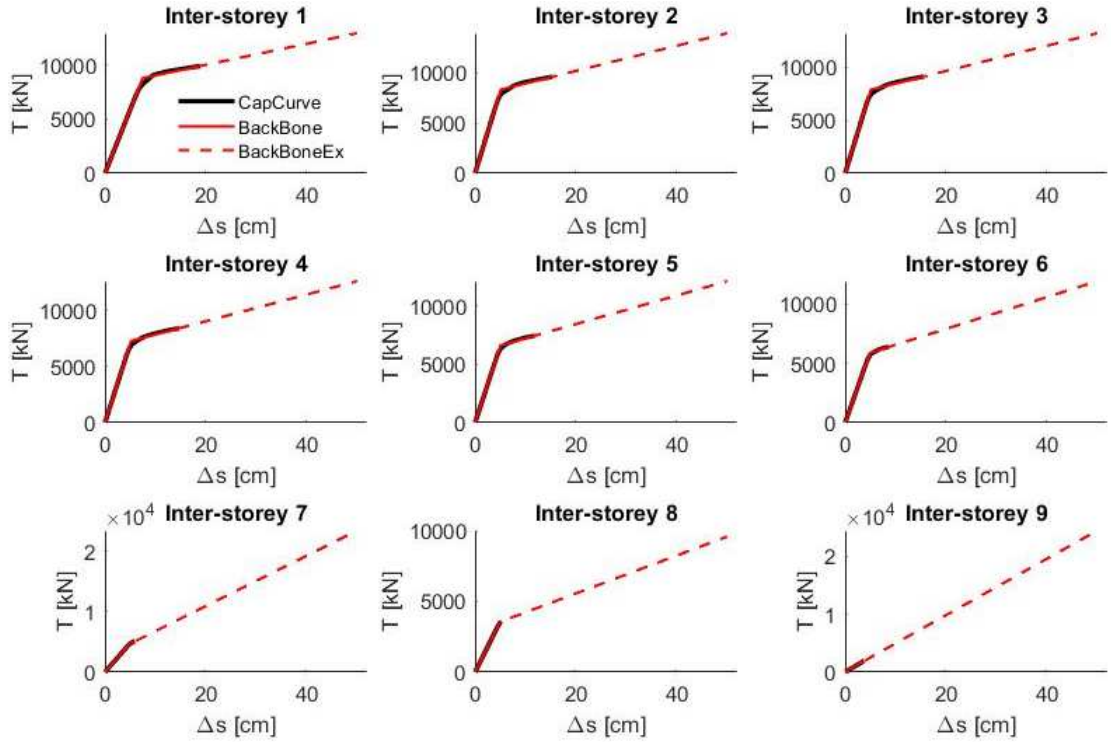

Figure 4.47 - Inter-storey capacity curves (CapCurve in black), the corresponding Back-Bone curves (red) and the ex-tended Back-Bone without limits of the ductile behaviour (BackBoneEx dashed in red) for mode proportional analysis

4.4.2 Non-linear static response

Once each inter-storey non-linear behaviour has been defined, it is possible to perform non-linear pushover analyses by making use of the beam-like model.

The non-linear pushover analyses of the equivalent beam model take into account load distributions equal to the above described initial force distributions adopted for the FEM model. The forces are applied on the beam axis at the floor level and are proportionally increased until a conventional 1 m top displacement is obtained [79].

A Newton-Raphson iterative procedure, described in Appendix C.1, has been applied in order to evaluate the response of the beam-like model to the static non-linear loading process.

For each force distribution, the capacity curves representative of the global behaviour of the building have been retrieved by considering the above described beam-like models. In particular, the static non-linear response has been obtained by means of the two approaches already presented in 2.2 and in 2.3. The first one considers a discretization of the beam-like model according to finite element method, in which the beam element is divided into a number N_f of uniform sub-beam shear deformable elements, as described in 2.2.2. In the second

approach, a unique step-wise shear-torsional beam finite element is adopted for the static non-linear analysis of the entire inelastic beam-like model, as described in 2.3.2. In Figure 4.48.a-c the comparisons between the global capacity curves, obtained by means of the FEM and the beam-like models adopting a sub-beam shear deformable elements discretization (denoted as BEAM-LIKE.b in Figure 4.48) and a unique step-wise shear-torsional beam finite element (denoted as BEAM-LIKE.a in Figure 4.48), are reported and a very good agreement is observed.

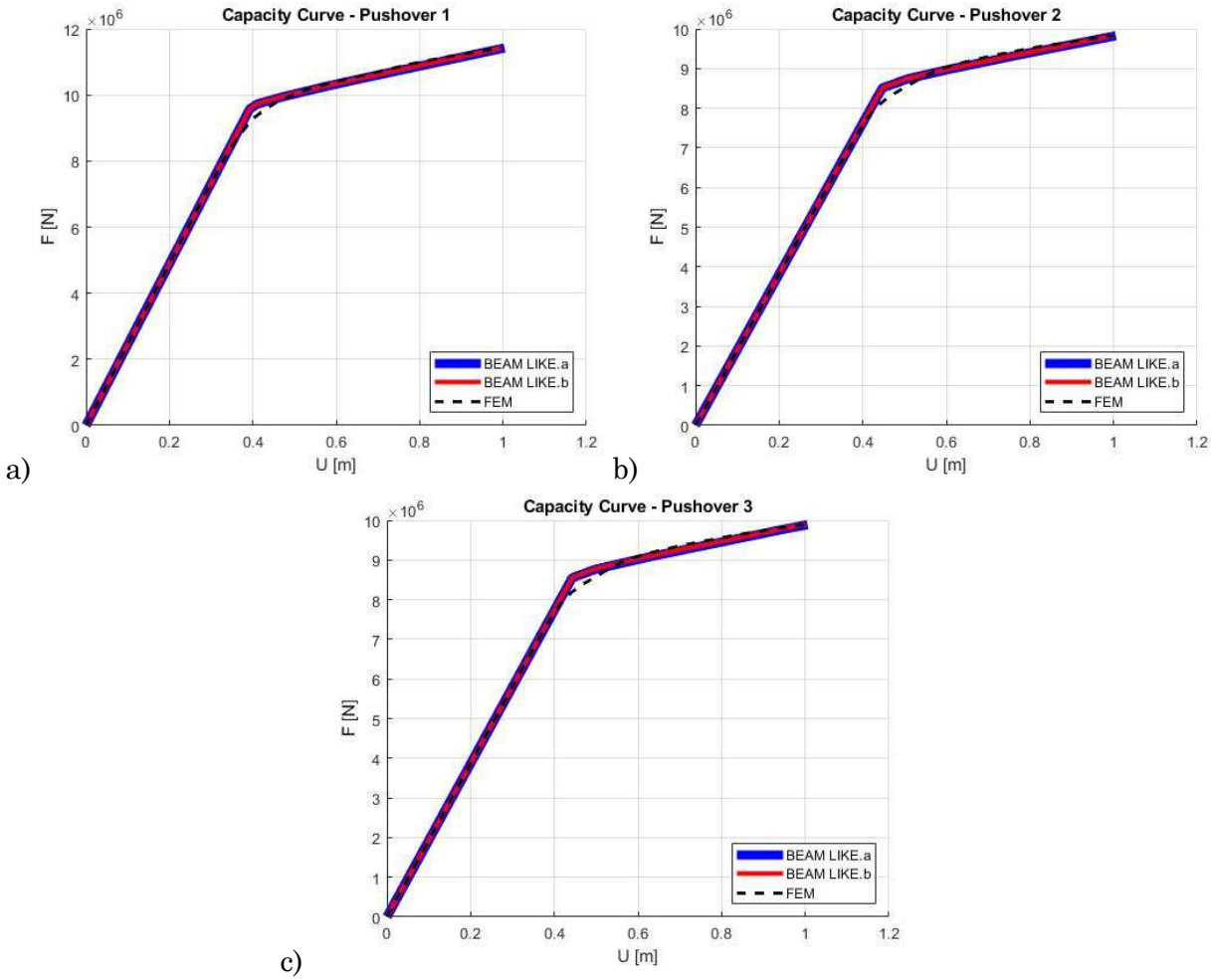

Figure 4.48 - Capacity curves for a) Uniform force distribution; b) Inverse triangular force distribution; c) Fundamental natural mode force distribution

The latter comparisons confirm the ability of the beam-like model to reproduce accurately the non-linear static response of the building even if the inter-storey force-displacement relationships has been replaced by an equivalent bilinear inelastic behaviour with kinematic hardening.

In the following paragraph, the beam-like models have been adopted to predict the non-linear dynamic response of the SAC9 building by means of non-linear dynamic analyses.

4.4.3 Non-linear dynamic response

The dynamic response of the beam-like model was obtained by means of the approach presented in Appendix D. For simplicity, no limits have been considered in the available ductility at each floor level.

Three dynamic analyses have been performed, each one assuming the inter-storey shear-displacement relationship corresponding to the force distribution a), b) or c). The damping matrix $\mathbf{C}$ has been obtained by setting the modal damping ratio equal to 5% for all the nine vibration modes of the beam-like model.

Figure 4.49 reports the time histories, expressed in terms of floor level displacements, for the three beam-like models, compared to the results of the FEM model.

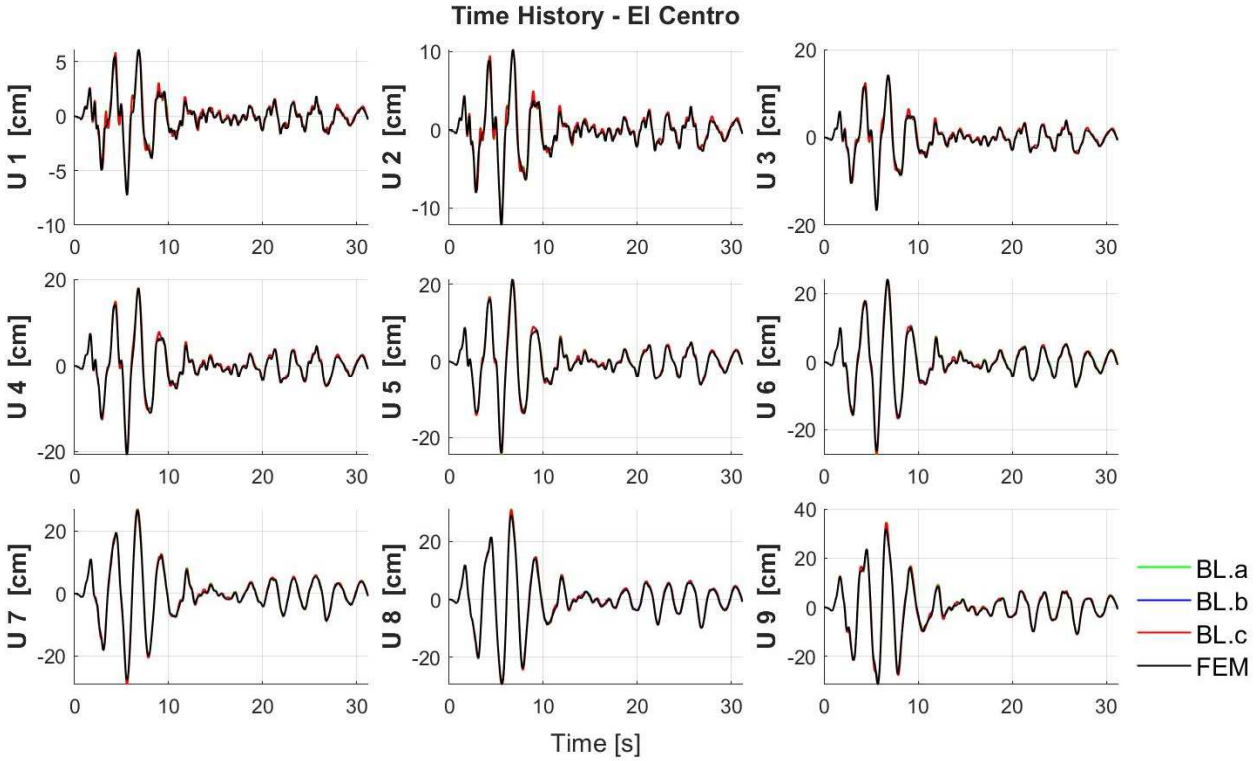

Figure 4.49 - Dynamic response to El Centro earthquake with constitutive law of the Beam-Like model associated with mass proportional (BL.a), inverse triangular (BL.b) and mode proportional (BL.c) force distributions

The results show that all the proposed inelastic beam models are able to reproduce the non-linear dynamic behaviour of the entire building with a very good accuracy.

Differently from the analyses based on the equivalent SDOF system, it is worth noting that the beam-like model allows to compute the non-linear dynamic response at each floor level without introducing any kinematic constraint.

The proposed beam-like model allows to reduce drastically the computational burden being related to a beam-like model characterised by a number of degrees of freedom equal to the number of floors, independently on the complexity of the full FEM model.

4.4.4 Beam-like model versus N2, UMRHA and MPA Approaches

Aiming at comparing the beam-like model with other simplified approaches proposed in the literature, the obtained results for the analysed structure have been compared with those provided by the SDOF-based N2 method and the multi-modal based strategies proposed by Chopra in [79] known as UMRHA and MPA.

The inter-storey drifts provided by the N2 method have been retrieved by the 3D FEM model capacity curve. Precisely, the displacement distributions associated to the ultimate displacement, corresponding to the target point obtained on the equivalent SDOF system, have been identified. This procedure has been applied for each of the three previously described force distributions (mass proportional, inverse triangular, mode proportional). The definition of the equivalent SDOF system has been obtained according to the bilinearization procedure suggested in the Eurocode 8 [86]. The main characteristics of the equivalent SDOF system (conventional notation has been used) are reported in Table 4.24.

The seismic demand for the equivalent SDOF system has been calculated by means of non-linear dynamic analysis, which was performed by considering the El Centro ground motion, already used in the previous paragraph, scaled by a multiplier equal to 1.5 [79]. Consistently to the previously performed analyses, a damping ratio equal to 5% has been assumed.

Table 4.24 - Characteristics of equivalent SDOF system

Characteristic	Force distribution a)	Force distribution b)	Force distribution c)
m* [kg]·10^6	4.59	2.64	2.79
Γ	1.00	1.41	1.36
T* [s]	2.93	2.47	2.52
F_y* [kN] ·10^3	11.42	6.97	7.28
s_y* [cm]	54.28	40.70	41.91

The displacement time history of the top floor Centre of Mass (CM) of the building, assumed as control point in accordance to the N2 method and obtained by means of the N2 equivalent SDOF system, has been compared to: *i*) the top node displacement of the equivalent beam-like model, *ii*) to the displacement of the CM top floor obtained by means of the UMRHA reported in [79] and *iii*) to the FEM displacement time history of the top floor of the building. Furthermore, the maximum floor displacements, as well as the maximum inter-storey drifts, have been compared. The results of the dynamic analyses for each adopted force distribution a), b) and c) in the pushover analysis are shown in Figure 4.50.a-c, respectively. The percentage errors, with respect to FEM results, on the maximum floor displacements and storey drifts have been reported in Figure 4.51.a-c, while the related average percentage errors are reported in Table 4.25.

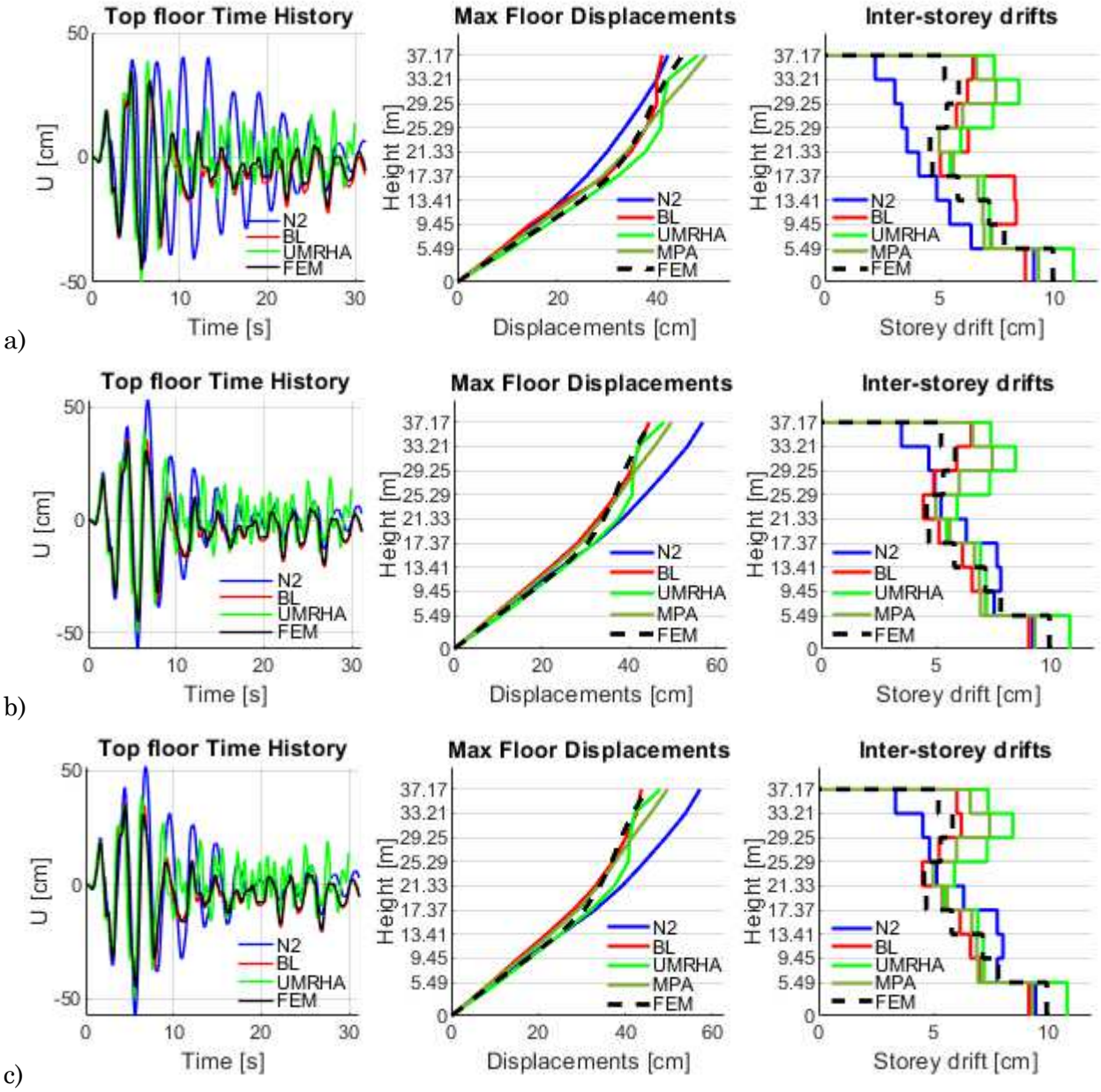

Figure 4.50 - Top displacement time history, maximum floor displacements and inter-storey drifts under 1.5x El Centro earthquake with non-linear beam-like, N2 SDOF models associated with a) mass proportional, b) inverse triangular, c) mode proportional force distribution, UMRHA and MPA

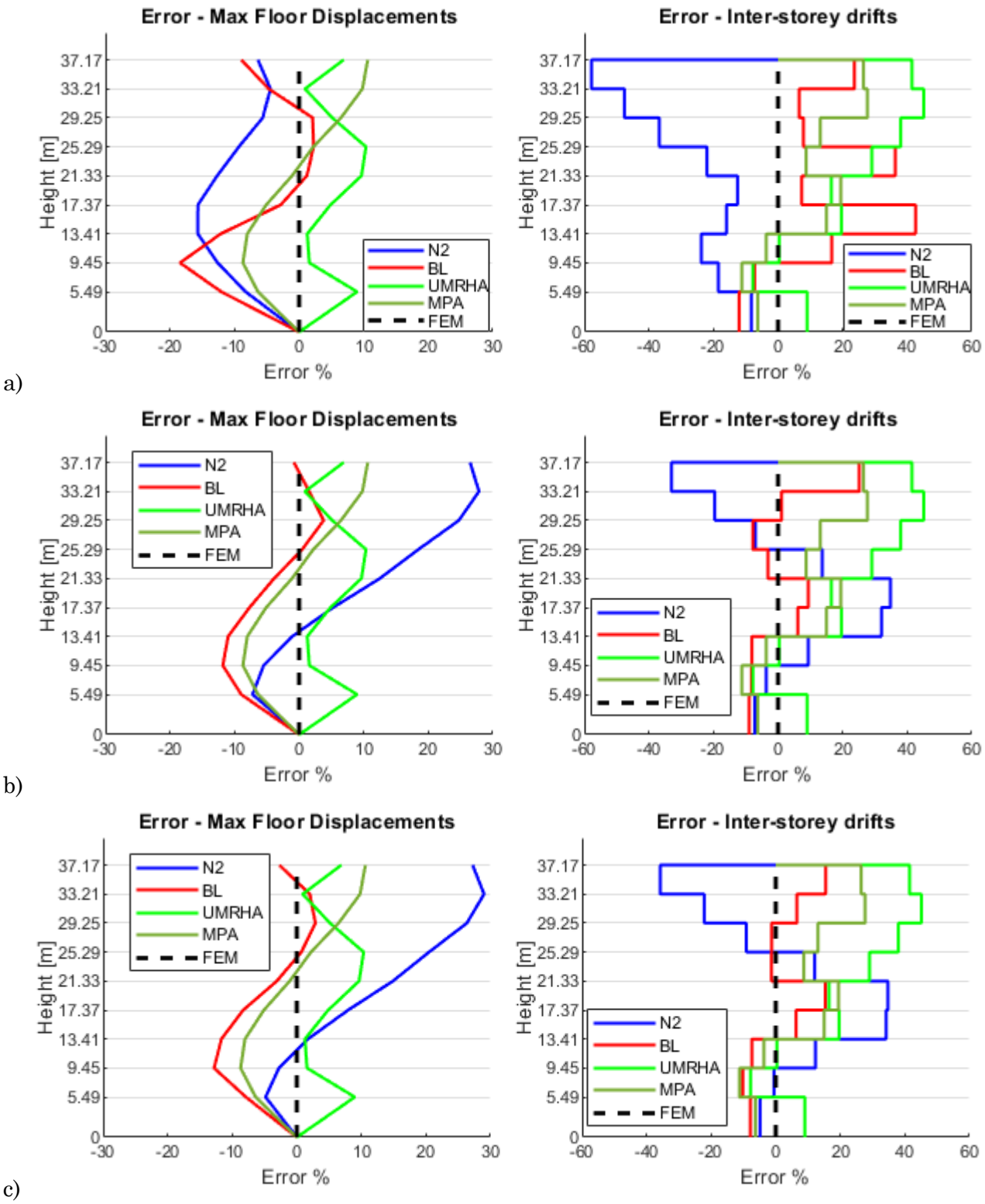

Figure 4.51 - Percentage error on maximum floor displacements and inter-storey drifts under 1.5x El Centro earth-quake with non-linear beam-like, N2 SDOF models associated with: a) mass proportional b) inverse triangular and c) mode proportional force distributions, UMRHA and MPA

Table 4.25 - Average percentage errors on maximum floor displacements and inter-storey drifts under 1.5x El Centro earthquake with non-linear beam-like, N2 SDOF models associated with: a) mass proportional b) inverse triangular and c) mode proportional force distributions, UMRHA and MPA

Strategy	**Average error – Floor Displacements**			**Average error – Storey Drifts**		
	Force dis. a)	Force dis. b)	Force dis. c)	Force dis. a)	Force dis. b)	Force dis. c)
Beam-like	7.19%	5.55%	5.79%	17.80%	8.66%	7.97%
N2 method	10.08%	14.34%	15.02%	27.02%	17.82%	18.42%
UMRHA	5.51%			23.00%		
MPA	6.49%			14.62%		

The analysis of the results expressed in terms of maximum displacements and maximum inter-storey drifts and the data obtained as cumulative and average errors at all floors, reveals that the N2 method is the less accurate one compared to the other considered strategies. The results provided by the proposed procedure based on the beam-like inelastic model seems to be characterised by an accuracy comparable to those obtained by the multi-modal strategies proposed by Chopra, although these latter imply a pushover analysis for each vibration mode whose contribution is considered. On the contrary, the beam-like model-based proposed strategy requires a non-linear static analysis and non-linear dynamic analysis performed in beam-like model whose discretization involves a number of degrees of freedom corresponding to the number of floors. Therefore, the associated computation cost is significantly lower with respect to those required by multi-modal-based approaches. Furthermore, the performance of the beam-like model appears to be even more competitive with regard to the evaluation of the inter-storey drifts.

In order to investigate how the errors in the beam-like model vary with the deformation demands imposed by the ground motion, dynamic analyses have been repeated for the El Centro ground motion scaled by the following multiplier: 0.25, 0.5, 0.75, 0.85, 1, 1.5, 2, 3. For each excitation, identified by the Ground Motion (GM) multiplier λ , the response errors (maximum floor displacements and storey drifts) obtained by means of the beam-like model with respect to the FEM model have been determined for each floor and reported in Figure 4.52.a-c. Furthermore, an envelope curve considering all the numerical investigations has been represented in the same figure.

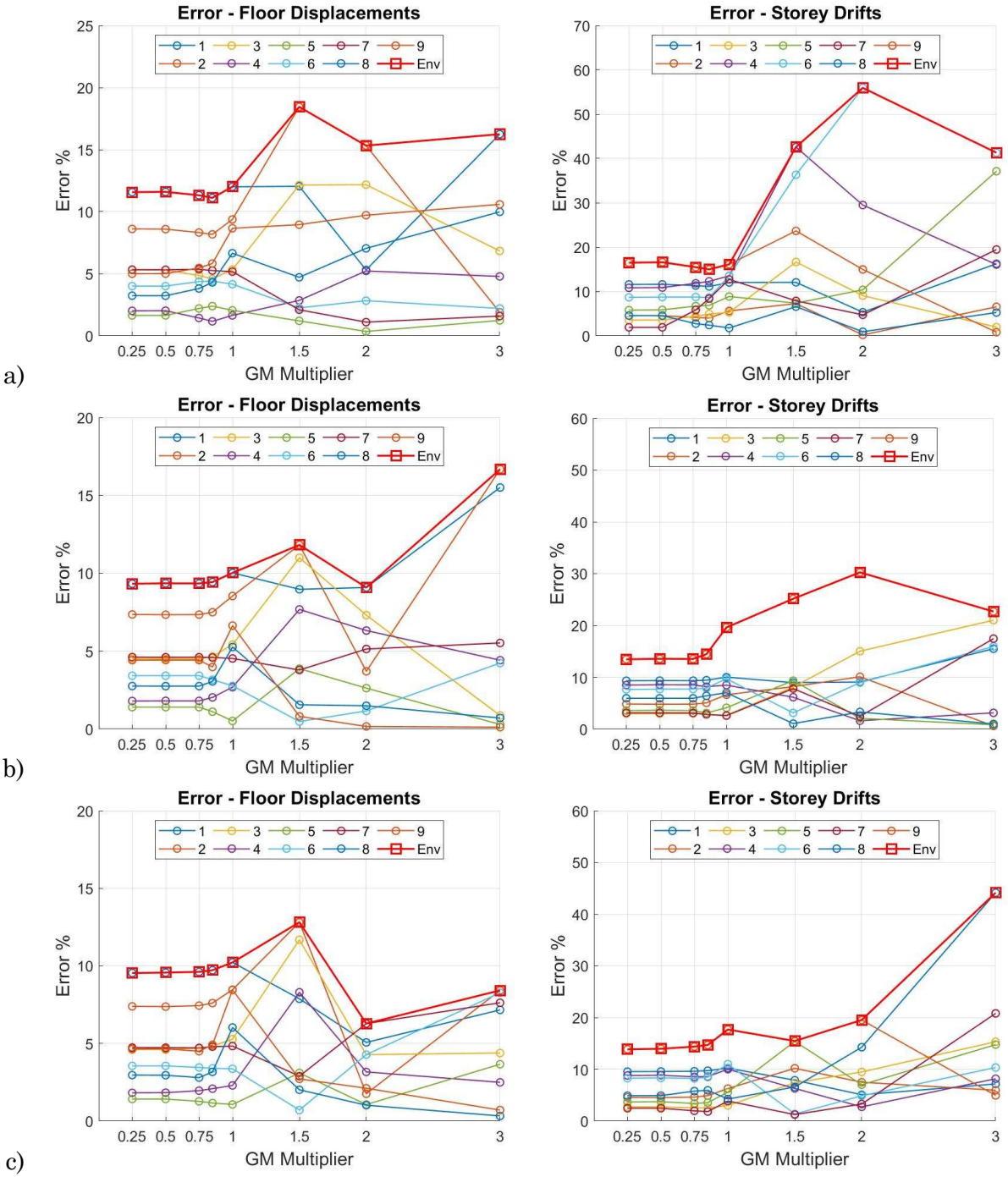

Figure 4.52 - Percentage errors on maximum floor displacements and inter-storey drifts as a function of ground motion intensity obtained with non-linear beam-like model associated with: a) mass proportional, b) inverse triangular and c) mode proportional force distributions

From the observation of the error distribution associated to the three considered load patterns, it appears that the beam-like model based on the mode proportional pushover analysis provides the more accurate results. Furthermore, the errors appear to be always lower than 20% for a ground motion characterised by a multiplier less than 1. The errors progressively increase for a load multiplier in the range $1 \leq \lambda \leq 3$. It is worth noting that these results are very close to those obtained by Chopra in [79].

CONCLUSIONS

In this thesis beam-like models suitable for the evaluation of linear and non-linear static and dynamic behaviour of multi-storey buildings have been proposed. The main goal of the proposed equivalent models is their possible applications in the field of seismic risk assessment of new and existing buildings. The low computational cost of beam-like models suggests their use also for the seismic vulnerability assessment at urban scale.

In fact, modern risk policies within all municipalities aim at identifying the most vulnerable portions of urban areas and therefore to plan opportune strategies for seismic risk reduction.

Nowadays, the seismic vulnerability assessment of the building heritage can be performed either using non-linear 3D FEM models, whose computational effort and time are very high, or adopting simplified SDOF models, which anyway do not provide accurate and exhaustive results about the structure behaviour.

For this reason, the introduction of a continuous beam-like model, more reliable than the SDOF system, able to simplify the analysis of the static and dynamic behaviour of a building could be very useful. Some beam-like models have been presented in the last decades by researchers, anyway they do not sufficiently characterize the existing buildings with vertical or horizontal stiffness irregularities and, almost all of them, do not account for the non-linear behaviour. The new beam-like models here proposed allow to overcome some of the limitations of the existing simplified approaches and have been specifically conceived for their use in the seismic assessment of new and existing buildings.

The proposed beam-like model for a simplified modelling of the linear behaviour of building subjected to earthquake loadings is a three-dimensional step-wise shear-torsional beam, suitable for the static and dynamic analyses of buildings with non-uniform stiffness distribution and eccentricity between the Mass Centre and the Stiffness Centre. The capability of the model to simulate the dynamic behaviour of an entire building makes this model useful for large vulnerability assessment survey that can also be performed at urban scale. Furthermore, since the calibration process is based on the knowledge of a certain number of modes and frequencies of the target building, it could be particularly useful for the dynamic identification of buildings whose geometry is not fully identified.

In the thesis, the elastic beam-like model has been defined starting from geometric and mechanical data of the building, and then it has been calibrated by considering the modal characteristics of the building itself. In order to reduce the number of degrees of freedom of the simplified model, a Rayleigh-Ritz discretization has been adopted using the modes of vibration of a uniform shear cantilever beam as shape functions.

Aiming at extending this model to the non-linear context, it has been upgraded for the simulation of the inelastic behaviour of buildings using different calibration strategies based on the results of pushover analyses performed on a non-linear 3D FEM model of the reference building.

Namely, the inelastic beam-like model has been defined as a step-wise shear only cantilever beam, whose segments are representative of the inter-storey mechanical properties of the building. The inter-storey constitutive laws have been calibrated by means of the results of a static non-linear analysis performed on the 3D FEM model of the building. In particular, the

equivalence between beam and building has been enforced by calibrating the inelastic beam-like model in order to predict the same pushover curve obtained by performing non-linear static analysis on the full 3D FEM model.
It is worth highlighting that, in view of the adopted calibration procedure, the equivalent inelastic beam-like model is related to the considered direction of the base input motion. Once the inelastic beam-like model has been obtained, dynamic non-linear analyses can be performed on this simplified model, thus drastically reducing the required computational effort and time with respect to the more demanding 3D FEM model.
It is worth noting that the proposed beam-like model could provide a more accurate representation of the seismic behaviour of multi-storey buildings both in terms of capacity and demand, particularly if compared to the commonly used SDOF system adopted within the N2 method. In fact, the equivalent SDOF systems-based approaches rely to the simplified hypothesis that the structure vibrates predominantly with a single mode and transfer the results of the pushover analysis to a SDOF system with the aim to identify the seismic demand according to a displacement based approach. The beam-like model instead is able to take into account the higher mode effects, since it is defined as an equivalent MDOF system having one degree of freedom for each floor of the building. This leads to the evaluation of all the floor displacements allowing the identification of partial failure mechanisms, which is not possible by using equivalent SDOF system-based approaches.
Furthermore, the collapse floor mechanism of a building can be evaluated by means of the proposed MDOF model while no inter-storey drifts time histories can be obtained using the N2 method being all the floor displacements related to the target point adopted in the pushover analysis.
The reliability of the proposed beam-like model has been validated through some numerical applications on two considered buildings that represented benchmark in previous research. In particular, the first building is a multi-storey RC frame representative of residential buildings in Catania designed to resist only to gravity loading. The second application refers to the well-known SAC9 building, well-known in scientific literature. For the first considered building, static and dynamic analyses have been performed on the equivalent beam-like model, considering both the linear and non-linear behaviour, and the results have been compared with those obtained by means of a FEM model of the building, confirming the validity of the proposed model. Furthermore, an inelastic beam-like model equivalent to SAC building has been adopted for the evaluation of its static and dynamic response, showing a very good equivalence with the corresponding 3D non-linear FEM model.
The seismic vulnerability assessment of the first case study, relative to a building designed for vertical loads only, has been also investigated by means of fragility curves evaluated by adopting the proposed beam-like model. It is worth noting that the fragility curves, obtained by performing non-linear dynamic analyses on the equivalent beam-like model, allow to express an expeditious and accurate seismic vulnerability assessment of the building. In fact, the required computational time for evaluating a fragility curve for the FEM model is about 120 times the one required for the beam-like one.
The adoption of these simplified beam-like models, endowed with shear deformation only, have been here applied and validated for simulating the dynamic behaviour of low- and mid- rise buildings. Other simplified models, studied in the past but limited to linear behaviour, include

bending deformation too. Future developments, aimed at analyzing tall buildings, could introduce also the flexural deformability leading to inhomogeneous inelastic Timoshenko beam-like models.
Another important development concerns the calibration of the inelastic beam-like model with the adoption of different non-linear constitutive law able to consider the progressive damage and the softening behaviour. These latter features are particularly important for a simplified modelling of masonry buildings or mixed reinforced concrete masonry structures.

REFERENCES

[1] M. Hirosawa, S. Sugano and T. Kaminosono, “Essentials of Current Evaluation and Retrofitting for Existing and Damaged Buildings in Japan,” in *IISEE-JICA*, 1995.

[2] S. Otani, “Seismic Vulnerability Assessment and Retrofit - State of Pratice in Japan,” in *Proc. of fib Conference Concrete Structures in Seismic Regions*, Athens, May, 2003.

[3] G. M. Calvi, “A displacement-based approach for vulnerability evaluation of classes of buildings,” *Journal of Earthquake Engineering,* vol. 3, no. 3, pp. 411-438, 1999.

[4] D. McCallen and K. M. Romstad, “Application of a Continuum Model in Building Analysis,” in *"Buildings Structures" Proceedings Structures Congress*, May 1987.

[5] M. Chajes, K. Romstad and D. McCallen, “Analysis of multiple-bay frames using continuum model,” *Journal of Structural Engineering ASCE,* vol. 119, no. 2, pp. 522-546, 1993.

[6] G. Piccardo, F. Tubino and A. Luongo, “Equivalent nonlinear beam model for the 3-D analysis of shear-type buildings: Application to aeroelastic instability,” *International Journal of Non-Linear Mechanics,* vol. 80, pp. 52-65, 2015.

[7] G. Piccardo, F. Tubino and A. Luongo, “A shear-shear torsional beam model for nonlinear aeroelastic analysis of tower buildings,” *Journal of Applied Mathematics and Physics,* vol. 66, no. 4, pp. 1895-1913, 2014.

[8] G. Potza and L. Kollar, “Analysis of building structures by replacement sandwich beams,” *International Journal of Solids and Structures,* pp. 535-553, 2003.

[9] F. Cluni, M. Gioffrè and V. Gusella, “Dynamic response of tall buildings to wind loads by reduced order equivalent shear-beam models,” *Journal of Wind Engineering and Industrial Aerodynamics,* vol. 123, pp. 339-348, 2013.

[10] K. Bozdogan, “A method for dynamic analysis of frame - hinged shear wall structures,” *Earthquakes and Structures,* vol. 11, no. 1, 2016.

[11] G. Piccardo, F. Tubino and A. Luongo, “Equivalent Timoshenko linear beam model for the static and dynamic analysis of tower buildings,” *Applied Mathematical Modelling,* vol. 71, pp. 77-95, 2019.

[12] C. Boutin and S. Hans, “Homogenisation of periodic discrete medium: Application to dynamics of framed structures,” *Computers and Geotechnics,* pp. 303-320, 2003.

[13] K. Zalka, “A simplified method for calculation of the natural frequencies of wall-frame buildings,” *Engineering Structures,* vol. 23, no. 12, pp. 1544-1555, 2001.

[14] A. Greco, I. Fiore, G. Occhipinti, S. Caddemi, D. Spina and I. Caliò, "An Equivalent Non-Uniform Beam-Like Model for Dynamic Analysis of Multi-Storey Irregular Buildings," *Applied Sciences,* vol. 10, p. 3212, 2020.

[15] A. Basu and G. Dar, "Dynamic characteristics of coupled wall-frame systems," *Earthquake Engineering and Structural Dynamics,* pp. 615-631, 1982.

[16] A. Basu, A. Nagpal and A. Nagar, "Dynamic characteristiccs of frame-wall systems," *Journal of the Structural Division,* vol. 105, pp. 1201-1218, 1982.

[17] A. Basu, "Seismic edsign charts for coupled shear walls," *Journal of Structural Engineering,* vol. 109, no. 2, pp. 335-352, 1983.

[18] A. Basu, A. Nagpai and S. Kaul, "Charts for seismic design of frame-wall systems," *Journal of Structural Engineering,* vol. 110, no. 1, pp. 31-46, 1984.

[19] B. Stafford Smith and E. Crowe, "Estimating periods of vibration of tall buildings," *Journal of structural Engineering ,* vol. 112, no. 5, pp. 1005-1019, 1986.

[20] B. Stafford Smith and Y.-S. Yoon, "Estimating seismic base shears of tall wall-frame buildings," *Journal od Structural Engineering,* vol. 117, no. 10, pp. 3026-3041, 1991.

[21] W. D. Iwan, "Drift spectrum: measure of demand for earthquake ground motions," *Journal of structural engineering,* vol. 123, no. 4, pp. 397-404, 1997.

[22] C.-T. Huang, "Considerations of multimode structural response for near-field earthquakes," *Journal of Engineering Mechanics,* vol. 129, no. 4, pp. 458-467, 2003.

[23] D. B. McCallen and K. M. Romstad, "A continuum model for the nonlinear analysis of beam-like lattice structures," *Computer & Structures,* vol. 29, no. 2, pp. 177-197, 1988.

[24] M. Chajes, W. Finch and J. Kirby, "Dynamic analysis of a ten-story reinforced concrete building using a continuum model," *Computers & Structures,* pp. 487-498, 1996.

[25] M. Chajes, L. Zhang and J. Kirby, "Dynamic analysis of tall building using reduced-order continuum model," *Journal of Structural Engineering ASCE,* pp. 1284-1291, 1996.

[26] E. Miranda, "Approximate seismic lateral deformation demands in multistory buildings.," *Journal of Structural Engineering ASCE,* pp. 417-425, 1999.

[27] E. Miranda and C. Reyes, "Approximate lateral drift demands in multistory buildings with nonuniform stiffness," *Journal of Structural Engineering ASCE,* pp. 840-849, 2002.

[28] E. Miranda and S. Taghavi, "Approximate floor acceleration demands in multistory buildings. I. Formulation," *Journal of Structural Engineering ASCE,* pp. 203-211, 2005.

[29] S. Taghavi and E. Miranda, "Approximate floor acceleration demands in multistory buildings. II. Applications," *Journal od Structural Engineering ASCE,* pp. 212-220, 2005.

[30] P. Gulkan and S. Akkar, "A simple replacement for the drift spectrum," *Engineering Structures,* vol. 24, pp. 1477-1484, 2002.

[31] S. Akkar, U. Yazgan and P. Gulkan, "Drift estimates in Frame Buildings Subjected to Near-Fault Ground Motions," *Journal of Structural Engineering,* vol. 131, no. 7, pp. 1014-1024, 2005.

[32] E. Miranda and S. D. Akkar, "Generalized interstorey drift spectrum," *Journal of Structural Engineering,* vol. 132, no. 6, pp. 840-852, 2006.

[33] Y. Wang, C. Arnaouti and S. Guo, "A simple approximate formulation for the first two frequencies of asymmetric wall-frame multi-storey building structures," *Journal of Sound and Vibration,* vol. 236, no. 1, pp. 141-160, 2000.

[34] S. Ng and J. S. Kuang, "Triply coupled vibration of asymmetric wall-frame structures," *Journal of Structural Engineering,* vol. 126, no. 8, pp. 982-987, 2000.

[35] J. S. Kuang and S. Ng, "Dynamic coupling of asymmetric shear wall structures: an analytical solution," *International Journal of Solids and Structures,* vol. 38, pp. 8723-8733, 2001.

[36] J. S. Kuang and S. Ng, "Coupled vibration of tall building structures," *The structural design of tall and special buildings,* vol. 13, pp. 291-303, 2004.

[37] J. S. Kuang and S. Ng, "Lateral shear-St. Venant torsion coupled vibration of asymmetric-plan frame structures," *The structural design of tall and special buildings,* vol. 18, pp. 647-656, 2009.

[38] Q. S. Li, J. Q. Fang and A. P. Jeary, "Free vibration analysis of cantilevered tall structures under various axial loads," *Engineering Structures,* vol. 22, pp. 525-534, 2000.

[39] R. Rahgozar, H. Safari and P. Kaviani, "Free vibration of tall buildings using Timoshenko beams with variable cross-section," *Structures under shock and impact VIII,* 2004.

[40] P. Kaviani, R. Rahgozar and H. Saffari, "Approximate analysis of tall buildings using sandwich beam models with variable cross section," *The structural design of tall and special buildings,* vol. 17, pp. 401- 418, 2008.

[41] S. Swaddiwudhipong, S.-L. Lee and Q. Zhou, "Effect of axial deformation on vibration of tall buildings," *The structural design of tall buildings,* vol. 10, pp. 79-91, 2001.

[42] S. Swaddiwudhipong, S. Soelarno Sidji and S.-L. Lee, "The effects of axial deformation and axial force on vibration characteristics of tall buidings," *The structural design of tall buildings,* vol. 11, pp. 309-328, 2002.

[43] A. R. Khaloo and H. Kosravi, "Multi-mode response of shear and flexural buildings to pulse-type ground motions in near-field earthquakes," *Journal of Earthquake Engineering,* vol. 12, pp. 616-630, 2008.

[44] K. Zalka, "A simple method for the deflection analysis of tall wall-frame building structures under horizontal load," *The Structural Design of Tall and Special Buildings,* pp. 291-311, 2009.

[45] K. Zalka, "Maximum deflection of asymmetric wall-frame buildings under horizontal load," *Periodica Polytechnica: Civil Engineering,* vol. 58, no. 4, pp. 387-396, 2014.

[46] S. Timoshenko and D. Young, Theory of Structures, McGraw-Hill, 1965.

[47] G. Tarjan and L. P. Kollar, "Approximate analysis of building structures with identical stories subjected to earthquakes," *International Journal of Solids and Structures,* pp. 1411-1433, 2004.

[48] M. Gioffrè, F. Cluni and V. Gusella, "Characterization of an Equivalent Coupled Flexural-Torsional Beam Model for the Analysis of Tall Buildings under Stochastic Actions," *Journal of Structural Engineering,* vol. 146, no. 11, 2020.

[49] F. Cluni, S. Fiorucci, V. Gusella and M. Gioffrè, "Estimation of the Mechanical Parameters for a Reduced Coupled Flexural-Torsional Beam Model of a Tall Building by a Sub-Structure Approach," *Applied Sciences,* vol. 11, p. 4655, 2021.

[50] S. A. Meftah, A. Tounsi and A. B. El Abbas, "A simplified approach for seismic calculation of a tall building braced by shear wall and thin-walled open section structures," *Engineering Structures,* vol. 29, pp. 2576-2585, 2007.

[51] S. A. Meftah and A. Tounsi, "Vibration charateristics of tall buildings braced by shear walls and thin-walled open section structures," *The structural design of tall and special buildings,* vol. 17, pp. 203-216, 2008.

[52] B. Rafezy, A. Zare and W. P. Howson, "Coupled lateral-torsional frequencies of asymmetric, three-dimensional frame structures," *International Journal of Solids and Structures,* vol. 44, pp. 128-144, 2007.

[53] B. Rafezy and W. P. Howson, "Vibration analysis of doubly asymmetric, three-dimensional structures comprising wall and frame assemblies with variable cross-section," *Journal of Sound and Vibration,* vol. 318, pp. 247-266, 2008.

[54] S. Hans and C. Boutin, "Dynamics of discrete framed structures: a unified homogenized description," *Journal of Mechanics of Materials and Structures,* vol. 3, no. 9, pp. 1709-1739, 2008.

[55] C. Chesnais, C. Boutin and S. Hans, "Effects of the local resonance in bending on the longitudinal vibrations of the reticulated beams," *Wave motion,* vol. 57, pp. 1-22, 2015.

[56] A. Kwan, "Simple method for approximate analysis of framed tube structures," *Journal of Structural Engineering ASCE,* pp. 1221-1239, 1994.

[57] R. Rahgozar, A. Ahmadi and Y. Sharifi, "A simple mathematical model for approximate analysis of tall buildings," *Applied Mathematical Modelling,* vol. 34, no. 9, pp. 2437-2451, 2010.

[58] M. Malekinejad and R. Rahgozar, "A simple analytic method for computing the natural frequencies and mode shapes of tall buildings," *Applied Mathematical Modelling,* vol. 36, pp. 3419-3432, 2012.

[59] M. Malekinejad and R. Rahgozar, "An analytical model for dynamic response analysis of tubular tall buildings," *The Structural Design of Tall and Special Buildings,* pp. 67-80, 2014.

[60] A. Carpinteri, G. Lacidogna and S. Cammarano, "Structural analysis of high-rise buildings under horizontal loads: A study on the Intesa Sanpaolo Tower in Turin," *Engineering Structures,* vol. 56, pp. 1362-1371, 2013.

[61] A. Carpinteri, G. Lacidogna and G. Nitti, "Open and closed shear-walls in high-rise structural systems: Static and dynamic analysis," vol. 3, no. 1, pp. 154-171, 2016.

[62] G. Nitti, G. Lacidogna and A. Carpinteri, "Structural analysis of high-rise buildings under horizontal loads: a study on the Piedmont Region Headquarters tower in Turin," *The Open Construction & Building Technology Journal,* vol. 13, pp. 81-96, 2019.

[63] D. Ozturk and K. B. Bozdogan, "Determination of the Dynamic Characteristics of Frame Structures with Non-Uniform Shear Stiffness," *Iran Journal of Science ...,* 2019.

[64] M. Sciomenta and A. Luongo, "Linear dynamic analysis of multistore tower buildings via an equivalent shear-shear torsional beam model," in *XXIII Conference The Italian Association of Theoretical and Applied Mechanics*, 2017.

[65] F. D'Annibale, M. Ferretti and A. Luongo, "Shear-shear-torsional homogenous beam models for nonlinear periodic beam-like structures," *Engineering Structures,* no. 184, pp. 115-133, 2019.

[66] A. Luongo and D. Zulli, "Free and forced linear dynamics of a homogeneous model for beam-like structures," *Meccanica,* 2019.

[67] L. Ragni, A. Zona and A. Dall'Asta, "Analytical expressions for preliminary design of dissipative bracing systems in steel frames," *Journl of Constructional Steel Frames ,* vol. 67, no. 102-113, 2011.

[68] P. Fajfar and M. Fischinger, "N2- A method for non-linear seismic analysis of regular buildings," in *Proceedings of Ninth World Conference on Earthquake Engineering*, Tokyo-Kyoto, 1988.

[69] A. Gaspersic, P. Fajfar and M. Fischinger, "An approximate method for seismic damage analysis of buildings," in *Earthquake Engneering Tenth World Conference*, Rotterdam, 1992.

[70] P. Faifar and P. Gaspersic, "The N2 Method for the seismic damage analysis of RC buildings," *Earthquake Engineering and Structural Dynamics,* vol. 25, pp. 31-46, 1996.

[71] P. Fajfar, "Capacity spectrum method based on inelastic demand spectra," *Earthquake Engineering and Structural Dynamics,* vol. 28, pp. 979-993, 1999.

[72] P. Fajfar and M. Eeri, "A Nonlinear Analysis Method for Performance Based Seismic Design," *Earthquake Spectra,* vol. 16, no. 3, pp. 573-592, 2000.

[73] M. Dolsek and P. Fajfar, "Simplified non-linear seismic analysis of infilled reinforced concrete frames," *Earthquake Engineering and Structural Dynamics,* vol. 34, pp. 49-66, 2005.

[74] P. Fajfar, D. Marusic and I. Perus, "Torsional effects in the pushover-based seismic analysis of buildings," *Journal of Earthquake Engineering,* vol. 9, no. 6, pp. 831-854, 2005.

[75] M. Kreslin and P. Fajfar, "The extended N2 method taking into account higher mode effects in elevation," *Earthquake Engineering and Structural Dynamics,* vol. 40, pp. 1571-1589, 2011.

[76] M. Kreslin and P. Fajfar, "The extended N2 method considering higher mode effects in both plan and elevation," *Bulletin of Earthquake Engineering,* vol. 10, pp. 695-715, 2012.

[77] S. A. Freeman, "The Capacity Spectrum Method as a Tool for Seismic Design," in *Proceedings of the 11th European Conference on Earthquake Engineering*, Paris, 1998.

[78] S. A. Freeman, "Review of the development of the Capacity Spectrum Method," *ISET Journal of Earthquake Technology,* vol. 41, no. 1, pp. 1-13, 2004.

[79] A. K. Chopra and R. K. Goel, "A modal pushover analysis procedure for estimating seismic demands for buildings," *Earthquake Engineering and Structural Dynamics,* vol. 31, pp. 561-582, 2002.

[80] *ASCE/SEI 41-17 Seismic Evaluation and Retrofit of Existing Buildings,* American Society of Civil Engineers, 2017.

[81] *FEMA 356 Prestandard and Commentary for the seismic rehabilitation of buildings,* Washington: Federal Emergency Management Agency, 2000.

[82] A. Standard, *Structural design actions Part 4: Earthquake actions in Australia,* Sidney: Committee BD-006, 2007.

[83] I. Caliò, A. Greco and M. Intelisano, "Analisi push-over multi-modali: applicazione ad un edificio irregolare in c.a.," in *ANIDIS*, Bari, 2011.

[84] B. Gupta and S. Kunnath, "Adaptive spectra-based pushover procedure for seismic evaluation of structures," *Earthquake spectra,* vol. 16, no. 2, pp. 367-392, 2000.

[85] *Norme tecniche per le costruzioni,* Gazzetta Uffuciale della Repubblica Italiana, 2018.

[86] EC8, *Eurocode 8 - Design of structures for earthquake resistance,* UNI EN 1998-1, 2010.

[87] H. Krawinkler and G. D. P. K. Seneviratna, "Pros and cons of a pushover analysis of seismic performance evaluation," *Engineering Structures,* vol. 20, pp. 452- 464, 1998.

[88] C. Chacara, F. Cannizzaro, B. Pantò, I. Caliò and P. Lourenco, "Assessment of the dynamic response of unreinforced masonry structures using a macroelement modeling approach," *Earthquake Engineering and Structural Dynamics,* vol. 47, no. 12, pp. 2426-2446, 2018.

[89] M. Lai, Y. Li and C. Zhang, "Analysis method of multi-rigid-body model for earthquake responses of shear-type structures," in *Earthquake Engineering, X World Conference*, Rotterdam, 1992.

[90] I. Hajirasouliha and A. Doostan, "A simplified model for seismic response prediction of concentrically braced frames," *Advances in Engineering Software,* vol. 41, p. 497–505, 2010.

[91] Y. Lu, I. Hajirasouliha and A. M. Marshall, "Performance-based seismic design of flexible-base multi-storey buildings considering soil-structure interaction," *Engineering Structures,* vol. 108, pp. 90-103, 2016.

[92] M. Nakashima, K. Ogawa and K. Inoue, "Generic frame model for simulation of earthquake responses of steel moment frames," *Earthquake Engineering and Structural Dynamics,* vol. 31, p. 671–692, 2002.

[93] N. Luco, Y. Mori, Y. Funahashi, C. A. Cornell and M. Nakashima, "Evaluation of predictors of non-linear seismic demands using 'fishbone' models of SMRF buildings," *Earthquake Engineering and Structural Dynamics,* vol. 32, p. 2267–2288, 2003.

[94] A. R. Khaloo and H. Kosravi, "Modified fish-bone model: A simplified MDOF model for simulation of seismic responses of moment resisting frames," *Soil Dynamics and Earthquake Engineering,* vol. 55, pp. 195-210, 2013.

[95] Y. Araki, M. Ohno, I. Mukai and N. Hashimoto, "Consistent DOF reduction of tall steel frames," *Earthquake Engineering and Structural Dynamics,* vol. 46, pp. 1581-159, 2017.

[96] R. Soleimani, H. Khosravi and H. Hamidi, "Substitute Frame and adapted Fish-Bone model: Two simplified frames representative of RC moment resisting frames," *Engineering Structures,* vol. 185, pp. 68-89, 2019.

[97] A. Jamšek and M. Dolšek, "Seismic analysis of older and contemporary reinforced concrete frames with the improved fish-bone model," *Engineering Structures,* vol. 212, 2020.

[98] D. B. McCallen and K. M. Romstad, "A continuum model for lattice structures with geometric and material nonlinearities," *Computers & Structures ,* vol. 37, no. 5, pp. 795-822, 1990.

[99] M. J. Chajes, K. M. Romstad and D. B. McCallen, "Inelastic frame analysis using a continuum model," in *Proceedings 1990 Annual Technical Session*, St. Louis, 1990.

[100] M. J. Chajes, K. M. Romstad and D. B. McCallen, "Nonlinear frame analysis using a continuum model," in *Proceedings 8th ASCE Structures Congress*, New York, 1990.

[101] H. Ozdemir, *Nonlinear transient dynamic analysis of yielding structures,* University of California, Berkley: PhD dissertation, 1976.

[102] V. Gicev and M. D. Trifunac, "Transient and permanent shear strains in a building excited by strong earthquake pulses," *Soil Dynamics and Earthquake Engineering,* vol. 29, p. 1358–1366, 2009.

[103] J. S. Kuang and K. Huang, "Simplified multi-degree-of-freedom model for estimation of seismic response of regular wall-frame structures," *The structural design of tall and special buildings,* vol. 20, pp. 418-432, 2011.

[104] B. Biondi and S. Caddemi, "Euler-Bernoulli beams with multiple singularities in the flexural stiffness," *European Journal of Mechanics,* vol. 26, pp. 789-809, 2007.

[105] S. Caddemi, I. Caliò and F. Cannizzaro, "Closed form solutions for stepped Timoshenko beams with internal singularities and along-axis external supports," *Archive of Applied Mechanics,* vol. 83, pp. 559-577, 2013.

[106] J. W. Baker, "Efficient analytical fragility function fitting using dynamic structural analysis," *Earthquake spectra,* vol. 31, no. 1, pp. 579-599, 2015.

[107] D. Vamvatsikos and C. A. Cornell, "Incremental dynamic analysis," *Earthquake Engineering and Structural Dynamics,* vol. 31, no. 3, pp. 491-514, 2002.

[108] L. F. Ibarra and H. Krawinkler, "Global collapse of frame structures under seismic excitations," John, A. , Blume Earthquake Engineering Center, Stanford, CA, 324, 2005.

[109] J. W. Baker and C. A. Cornell, "A vector-valued ground motion intensity measure consisting of spectral acceleration and epsilon," *Earthquake Engineering & Structural Dynamics,* vol. 34, no. 10, pp. 1193-1217, 2005.

[110] I. Caliò, A. Ghersi, E. Marino, P. Rossi, F. Contrafatto, F. Barbagallo, M. Bosco and G. Occhipinti, "Definition of the Pilot Building (ANCE|Catania Project 2016)," ANCE, Catania, 2017.

[111] G. Occhipinti, B. Izzudin, L. Macorini and I. Caliò, "Realistic 3D nonlinear dynamic analysis of existing and retrofitted multi-storey RC buildings subject to earthquake loading," in *Proceedings of the 6th International Conference on Computational Methods in Structural Dynamics and Earthquake Engineering, COMPDYN 2017*, 2017.

[112] G. Occhipinti, B. Izzudin, L. Macorini and I. Caliò, "Realistic seismic assessment of RC buildings with masonry infills using 3D high-fidelity simulations," in *Proceedings of the 6th European Conference on Computational Mechanics: Solids, Structures and Coupled Problems, ECCM 2018 and 7th European Conference on Computational Fluid Dynamics, ECFD*, 2020.

[113] CSI, CSI Analysis Reference Manual for SAP2000, Computers and Structures, 2007.

[114] INGV, "INGVterremoti," [Online]. Available: https://ingvterremoti.wordpress.com/i-terremoti-in-italia/. [Accessed luglio 2018].

[115] M. Pastor, M. Binda and T. Harcarik, "Modal Assurance Criterion," *Procedia Engineering,* vol. 48, pp. 543-548, 2012.

[116] FEMA, Hazus Earthquake Model Technical Manual 4.2, Federal Emergency Management Agency, 2020.

[117] J.-L. Lin, J.-Y. Dai and K.-C. Tsai, "Optimization approach to uniformly distributed peak interstorey drifts along building heights," *Journal of Structural Engineering,* vol. 145, no. 5, 2019.

[118] A. K. Chopra and R. K. Goel, "A modal pushover analysis procedure to estimate seismic demands for buildings: theory and preliminary evaluation," University of California, Berkley, 2001.

[119] D. A. Foutch and S.-Y. Yun, "Modeling of steel moment frames for seismic loads," *Journal of Constructional Steel Research,* vol. 58, pp. 529-564, 2002.

[120] A. Gupta and H. Krawinkler, "Estimation of seismic drift demands for frame structures," *Earthquake Engineering and Structural Dynamics,* vol. 29, pp. 1287-1305, 2000.

[121] A. Gupta and H. Krawinkler, "Seismic demands for performance evaluation of steel moment resisting frame structures," The John A. Blume Earthquake Engineering Center, Department of Civil and Environmental Engineering, Standford University, 1999.

[122] CSI, *CSI Analysis Reference Manual for SAP2000,* Computers and Structures Inc., 2007.

[123] A. K. Chopra, “Dynamics of Structures, Theory and Application to Earthquake Engineering,” in *Dynamics of Structures, Theory and Application to Earthquake Engineering*, Upper Saddle River, Prentice Hall, 2001.

[124] M. Marletta, *Tesi Massimo Marletta,* Catania.

[125] E. Riks, “An incremental approach to the solution of snapping and buckling problems,” *International Journal of Solids and Structures,* vol. 15, pp. 529-551, 1979.

[126] M. A. Crisfield, “A fast incremental/iterative solution procedure that handles "snap-through",” *Computers and Structures,* vol. 13, pp. 55-62, 1981.

[127] I. Iervolino, C. Galasso and E. Cosenza, “REXEL: computer aided record selection for code-based seismic structural analysis,” *Bulletin of Earthquake Engineering,* pp. 339-362, 2009.

[128] I. Iervolino, C. Galasso, R. Paolucci and F. Pacor, “Engineering ground motion record selection in the ITalian ACcelerometric Archive,” *Bulletin of Earthquake Engineering,* vol. 9, no. 6, pp. 1761-1778, 2011.

[129] “Seismic hazard model MPS04-S1,” [Online]. Available: http://esse1-gis.mi.ingv.it/mps04_eng.jsp.

APPENDIX A

SHEAR ONLY BEAM MODEL

Since the proposed research focuses on the definition of an equivalent shear only beam model, it is useful to illustrate the shear only beam theory reported in the scientific literature. This model, although represents a simplification of the more general Timoshenko and the Euler-Bernoulli beam models, is suitable for the schematization of the dynamic behaviour of low- and mid-rise buildings.

The beam model is fundamental in structural mechanics, and it is based on the hypothesis that its behaviour can be described only referring to its axis and cross-sections.

The beam models are analysed as spatial problems, where flexural-shear and torsional behaviour are uncoupled since there is no eccentricity between Mass Centre and Shear Centre.

For the considered shear only beam model, the study of its dynamics allowed to obtain the equations of motion under earthquake loads and then, by neglecting the inertia forces, the equations that govern the static problem have also been determined.

In Figure A.1 a generic beam is represented with the assumed Cartesian reference system. The *z* axis is assumed coincident with the beam axis, while *x* and *y* axes lie on the plan of the cross section with origin on the centre of gravity.

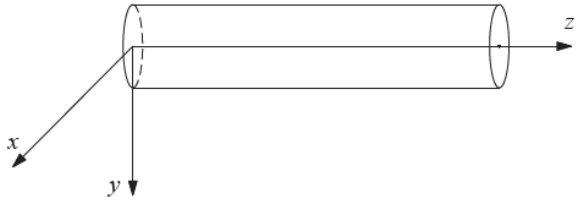

Figure A.1 - Beam model

Shear only beam model takes into account only shear deformability. Plane sections hypothesis is assumed, but orthogonality between cross-section and beam axis in not ensured.

A distributed load *p(z,t)* is considered acting on a beam with shear stiffness *GA(z)* and distributed mass *m(z),* as shown in Figure A.2:

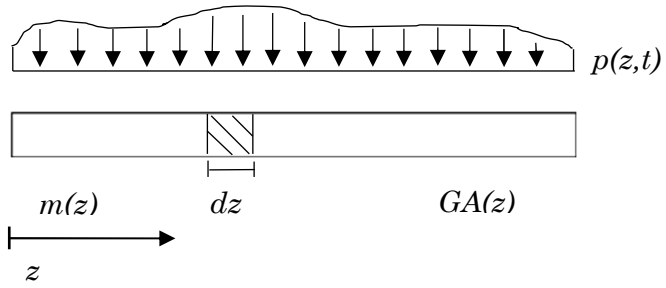

Figure A.2 - Shear only beam model

- Compatibility equation

$$\gamma = \frac{\partial v}{\partial z} = v^{I}(z,t) \tag{A.1}$$

where γ, v denote the shear strain and the transversal displacement, respectively.

- Constitutive equation

$$T = kGA(z)\gamma \tag{A.2}$$

Dynamics

Static and kinematic parameters with reference to a portion *dz* of the beam are shown in Figure A.3.

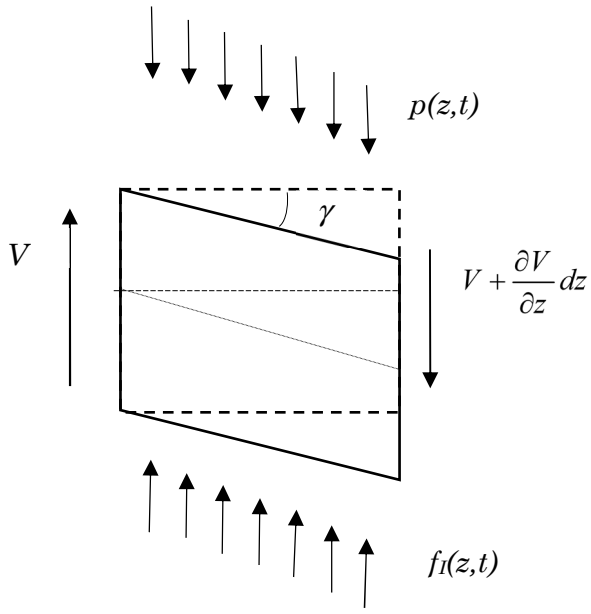

Figure A.3 - Shear only beam model - dynamics

The inertia forces are defined as:

$$f_I(z,t) = \rho A(z)\ddot{v}(z,t) \tag{A.3}$$

where $\rho A(z) = m(z)$.

Equilibrium equation with respect *y* axis translation:

$$V + \frac{\partial V}{\partial z}dz - V - f_I(z,t)dz + p(z,t)dz = 0 \tag{A.4}$$

where the vertical force V is equal to the shear force T:

$$T = V \tag{A.5}$$

Rearranging Equations (A.4)-(A.5) and substituting compatibility and constitutive equations, the equation of motion for shear only beam model is obtained:

$$kGAv^{II} - m\ddot{v} = -p(z,t) \tag{A.6}$$

Equation (A.6), setting $p(z,t) = 0$, allows to find the natural frequencies and mode shapes of a uniform cantilever beam, expressed in dimensionless terms:

$$\omega_n = (2n-1)\frac{\pi}{2}\sqrt{\frac{kGA}{mL^2}} \qquad n = 1,...,+\infty \tag{A.7}$$

$$\phi_n(\zeta) = C_1 \sin\left[(2n-1)\frac{\pi}{2}\zeta\right] \qquad n = 1,...,+\infty \tag{A.8}$$

Static

Static and kinematic parameters with reference to a portion *dz* of the beam are shown in Figure A.4.

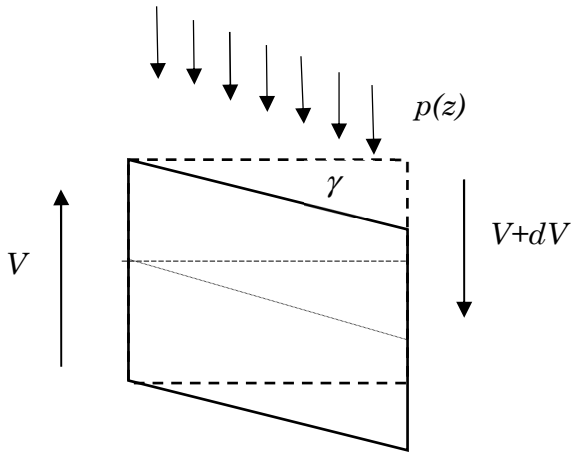

Figure A.4 - Shear only beam model- static

Neglecting the inertia forces in Equation (A.6), the governing equation of the static problem is obtained:

$$kGAv^{II} = -p(z) \tag{A.9}$$

whose solution for $p(z) = p$ is:

$$v(z) = -\frac{p}{2kGA}z^2 + C_1 z + C_2 \tag{A.10}$$

For a cantilever beam, Equation (A.10) becomes:

$$v(z) = -\frac{p}{2kGA}z^2 + \frac{pL}{kGA}z \tag{A.11}$$

APPENDIX B

DERIVATION OF THE INELASTIC BEAM-LIKE MODEL

B.1 Nodal equilibrium equations

For each node, a horizontal equilibrium equation in the fixed direction is written. Each one of these equations involve both the correspondent nodal force and the shear forces which arise in each beam segment connected to the node (Figure B.1).

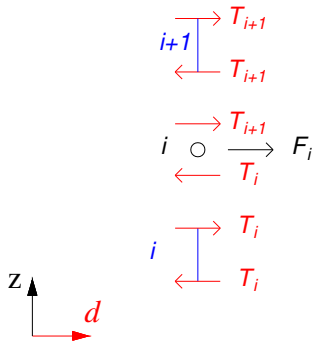

Figure B.1 - Equilibrium of the *i*-th node in *d* direction

Shear force T_i in the fixed direction, is considered in each beam segment.

Equilibrium of the *i*-th node in direction *d*, shown in Figure B.1, is analysed, assuming positive shear forces at the top of the *i*-th and *i+1*-th beam segments.
Equilibrium of the i-th node in direction *d* is given by:

$$F_i = T_i - T_{i+1} \tag{B.1}$$

The vector of the shear forces in the fixed direction of all the beam segments is given by:

$$\mathbf{T} = \begin{bmatrix} T_1 \\ T_2 \\ \vdots \\ T_N \end{bmatrix} \tag{B.2}$$

Therefore, equilibrium equations of all the nodes can be written in matrix form, as shown below:

$$\begin{bmatrix} 1 & -1 & 0 & \cdots & 0 & 0 \\ 0 & 1 & -1 & \cdots & 0 & 0 \\ 0 & 0 & 1 & \cdots & 0 & 0 \\ \vdots & \vdots & \vdots & \ddots & \vdots & \vdots \\ 0 & 0 & 0 & \cdots & 1 & -1 \\ 0 & 0 & 0 & \cdots & 0 & 1 \end{bmatrix} \begin{bmatrix} T_1 \\ T_2 \\ T_3 \\ \vdots \\ T_{N-1} \\ T_N \end{bmatrix} = \begin{bmatrix} F_1 \\ F_2 \\ F_3 \\ \vdots \\ F_{N-1} \\ F_N \end{bmatrix} \tag{B.3}$$

Or:

$$\mathbf{C}^T \cdot \mathbf{T} = \mathbf{F} \tag{B.4}$$

where it is shown the **equilibrium matrix** $\mathbf{C}^T$.

B.2 Compatibility equations

In order to write the compatibility equations, the Principle of Virtual Work is applied. A virtual configuration of the system, described by virtual displacements $\hat{\mathbf{u}}$ of the nodes, is considered:

$$\hat{\mathbf{u}} = \begin{bmatrix} \hat{u}_1 \\ \hat{u}_2 \\ \vdots \\ \hat{u}_N \end{bmatrix} \tag{B.5}$$

The external virtual work L_{ve} is given by:

$$L_{ve} = \mathbf{F}^T \cdot \hat{\mathbf{u}} \tag{B.6}$$

While the internal virtual work L_{vi} is given by:

$$L_{vi} = \int_V tr(\mathbf{TE}) dV \tag{B.7}$$

According to the adopted beam model, taking into account only shear deformability into Equation (B.7):

$$L_{vi} = \int_V tr(\mathbf{TE}) dV = \sum_{i=1}^{N} \int_{V_i} \tau_{zd} \gamma_d dV = \sum_{i=1}^{N} \int_{A_i} \int_{l_i} \tau_{zd} \gamma_d dl\, dA = \sum_{i=1}^{N} T_i s_i = \mathbf{T}^T \mathbf{s} \tag{B.8}$$

where T_i is the shear force on *i*-th beam segment and s_i is the relative displacement due to shear strain between the end nodes of *i*-th beam segment.
Setting $L_{ve} = L_{vi}$:

$$\mathbf{F}^T \cdot \hat{\mathbf{u}} = \mathbf{T}^T \mathbf{s} \tag{B.9}$$

Considering the equilibrium equation:

$$\mathbf{C}^T \cdot \mathbf{T} = \mathbf{F} \qquad \Rightarrow \qquad \mathbf{F}^T = \mathbf{T}^T \cdot \mathbf{C} \tag{B.10}$$

Therefore:

$$\mathbf{T}^T \cdot \mathbf{C} \cdot \hat{\mathbf{u}} = \mathbf{T}^T \mathbf{s} \qquad \Rightarrow \qquad \mathbf{T}^T \left[\mathbf{C} \cdot \hat{\mathbf{u}} - \mathbf{s} \right] = \mathbf{0} \qquad \Rightarrow \qquad \mathbf{C} \cdot \hat{\mathbf{u}} = \mathbf{s} \tag{B.11}$$

The last expression is the compatibility equation which relates displacements and relative displacements by means of the **compatibility matrix** $\mathbf{C}$, which is also equal to the transpose of the equilibrium matrix.

B.3 Constitutive law

The constitutive law relating shear forces and relative displacements between the ends of *i*-th beam segment is expressed as follows:

$$T_i = R_i \cdot s_i \tag{B.12}$$

denoting with R_i the shear stiffness in the fixed direction of the *i*-th equivalent beam segment. The constitutive law for each beam segment can be expressed in matrix form as follows:

$$\begin{bmatrix} T_1 \\ T_2 \\ T_3 \\ \vdots \\ T_{N-1} \\ T_N \end{bmatrix} = \begin{bmatrix} R_1 & 0 & 0 & \cdots & 0 & 0 \\ 0 & R_2 & 0 & \cdots & 0 & 0 \\ 0 & 0 & R_3 & \cdots & 0 & 0 \\ \vdots & \vdots & \vdots & \ddots & \vdots & \vdots \\ 0 & 0 & 0 & \cdots & R_{N-1} & 0 \\ 0 & 0 & 0 & \cdots & 0 & R_N \end{bmatrix} \begin{bmatrix} s_1 \\ s_2 \\ s_3 \\ \vdots \\ s_{N-1} \\ s_N \end{bmatrix} \tag{B.13}$$

or in compact notation:

$$\mathbf{T} = \mathbf{D} \cdot \mathbf{s} \tag{B.14}$$

where $\mathbf{D}$ is the matrix containing the shear stiffness R_i, dependent on the non-linear constitutive behaviour of the structure.

It is worth noting that the shear stiffness R_i of the *i*-th equivalent beam segment, assumes different values depending on the considered constitutive law. In case of non-linear analyses its value can be evaluated for example assuming either an elasto-perfectly plastic constitutive law, an elasto-plastic constitutive law with kinematic hardening or an inelastic multilinear constitutive law (described in Appendix B.7).

B.4 Stiffness matrix

Rearranging the equilibrium and compatibility equations and the constitutive law:

$$\mathbf{F} = \mathbf{C}^T \cdot \mathbf{T} \qquad \Rightarrow \qquad \mathbf{F} = \mathbf{C}^T \cdot \mathbf{D} \cdot \mathbf{s} \qquad \Rightarrow \qquad \mathbf{F} = \mathbf{C}^T \cdot \mathbf{D} \cdot \mathbf{C} \cdot \hat{\mathbf{u}} \tag{B.15}$$

A nodal force – displacement relationship is obtained:

$$\mathbf{F} = \mathbf{K} \cdot \hat{\mathbf{u}} \tag{B.16}$$

where $\mathbf{K}$ denotes the **stiffness matrix** of the structure, equal to:

$$\mathbf{K} = \mathbf{C}^T \cdot \mathbf{D} \cdot \mathbf{C} \tag{B.17}$$

The tangent stiffness matrix of the inelastic beam model can be expressed as follows:

$$\mathbf{K} = \begin{bmatrix} K_{11} & K_{12} & 0 & 0 & \cdots & 0 & 0 & 0 \\ K_{21} & K_{22} & K_{23} & 0 & \cdots & 0 & 0 & 0 \\ 0 & K_{32} & K_{33} & K_{34} & \cdots & 0 & 0 & 0 \\ 0 & 0 & K_{43} & K_{44} & \cdots & 0 & 0 & 0 \\ \vdots & \vdots & \vdots & \vdots & \ddots & \vdots & \vdots & \vdots \\ 0 & 0 & 0 & 0 & \cdots & K_{N-2N-2} & K_{N-2N-1} & 0 \\ 0 & 0 & 0 & 0 & \cdots & K_{N-1N-2} & K_{N-1N-1} & K_{N-1N} \\ 0 & 0 & 0 & 0 & \cdots & 0 & K_{NN-1} & K_{NN} \end{bmatrix} \tag{B.18}$$

being the matrix coefficients related to the state of the beam according to the adopted non-linear inter-storey force-displacement constitutive laws (described in this thesis as "inter-storey constitutive laws"). In the applications reported in this thesis, the inter-storey constitutive law has been assumed as elasto-plastic with or without linear hardening. For specific applications a multilinear inelastic behaviour described in Appendix B.7 has also been assumed.

B.5 Mass matrix

In the applications reported in this thesis, the mass distribution of the whole beam has been assumed to be lumped at the nodes.

Therefore, the mass matrix is given by:

$$\mathbf{M} = \begin{bmatrix} M_1 & 0 & \cdots & 0 \\ 0 & M_2 & \cdots & 0 \\ \vdots & \vdots & \ddots & \vdots \\ 0 & 0 & \cdots & M_N \end{bmatrix} \tag{B.19}$$

where $N = N_f$.

B.6 Damping matrix

Assuming a classical damping associated to a certain number of fixed damping ratio, the related damping matrix can be obtained by the superposition of the corresponding modal damping ratios as follows.

By solving the eigen problem $\left(\mathbf{K}-\boldsymbol{\omega}^2\mathbf{M}\right)\boldsymbol{\phi}=\mathbf{0}$, it is possible to find natural frequencies ω_n and mode shapes, collected in matrix $\boldsymbol{\Phi}$.

By fixing modal damping ratios ξ_n and remembering that $C_{\mathrm{mod},n}=2\xi_n M_{\mathrm{mod},n}\omega_n$, it is possible to define the following modal damping matrix:

$$\mathbf{C}_{\mathrm{mod}}=\begin{bmatrix} 2\xi_1 M_{\mathrm{mod},1}\omega_1 & 0 & \cdots & 0 \\ 0 & 2\xi_2 M_{\mathrm{mod},2}\omega_2 & \cdots & 0 \\ \vdots & \vdots & \ddots & \vdots \\ 0 & 0 & \cdots & 2\xi_N M_{\mathrm{mod},N}\omega_N \end{bmatrix} \tag{B.20}$$

The relation $\boldsymbol{\Phi}^T\mathbf{C}\boldsymbol{\Phi}=\mathbf{C}_{\mathrm{mod}}$ can be rewritten as:

$$\mathbf{C}=\boldsymbol{\Phi}^{-T}\mathbf{C}_{\mathrm{mod}}\boldsymbol{\Phi}^{-1} \tag{B.21}$$

Starting with the orthogonality relationship $\boldsymbol{\Phi}^T\mathbf{M}\boldsymbol{\Phi}=\mathbf{M}_{\mathrm{mod}}$ it is possible to demonstrate:

$$\boldsymbol{\Phi}^{-1}=\mathbf{M}_{\mathrm{mod}}^{-1}\boldsymbol{\Phi}^T\mathbf{M} \qquad \boldsymbol{\Phi}^{-T}=\mathbf{M}\boldsymbol{\Phi}\mathbf{M}_{\mathrm{mod}}^{-1} \tag{B.22}$$

Therefore, remembering that $\mathbf{M}_{\mathrm{mod}}$ and $\mathbf{C}_{\mathrm{mod}}$ are diagonal matrices, it is possible to write:

$$\mathbf{C}=\mathbf{M}\sum_{i=1}^{Nt}\boldsymbol{\phi}_i\boldsymbol{\phi}_i^T\frac{2\xi_i\omega_i}{M_{\mathrm{mod},i}}\mathbf{M} \tag{B.23}$$

If all the mode shapes are not known, it is reasonable to include in Equation (B.23) only the first S modes that are expected to contribute significantly to the response, as shown below.

$$\mathbf{C}=\mathbf{M}\sum_{i=1}^{S}\boldsymbol{\phi}_i\boldsymbol{\phi}_i^T\frac{2\xi_i\omega_i}{M_{\mathrm{mod},i}}\mathbf{M} \tag{B.24}$$

The lack of damping in modes $S+1$ to N does not create numerical problems if an unconditionally stable time-stepping procedure is used to integrate the equation of motion.

Damping matrix can be also defined according to the Rayleigh approach. It is possible to consider Rayleigh damping, which is mass-stiffness proportional:

$$\mathbf{C}=a_1\mathbf{M}+a_2\mathbf{K} \qquad a_1,a_2\in R \tag{B.25}$$

with reference to the initial linear elastic stiffness matrix. The coefficients a_1,a_2 have to be evaluated by imposing the damping ratios corresponding to two different frequencies [123].

B.7 Multilinear constitutive law

In [124] an original formulation of a piecewise linear constitutive law has been proposed. This formulation has been here adopted in order to simulate an inelastic multilinear constitutive law.

A piecewise linear force-displacement relationship can be modelled by using a certain number of parallel springs with elastic-plastic behaviour. Denoting with N the number of linear segments of the piecewise linear force-displacement relationship, u_j the displacement corresponding to the *j*-th change of the stiffness, F_j the corresponding force and K_j the tangent stiffness of the *j*-th linear segment expressed as:

$$K_j = \begin{cases} \dfrac{F_1}{u_1} & for \quad j = 1 \\ \dfrac{F_j - F_{j-1}}{u_j - u_{j-1}} & for \quad 1 < j \le N \end{cases} \tag{B.26}$$

it is possible to schematize the assigned relationship as the superposition of one spring with linear elastic behaviour and $N-1$ springs with elastic-perfectly plastic behaviour. The stiffness K_j are assumed to be decreasing.

This schematization allows to model the piecewise linear force-displacement relationship by means of elastic-plastic elements only with bilinear force-displacement relationship.

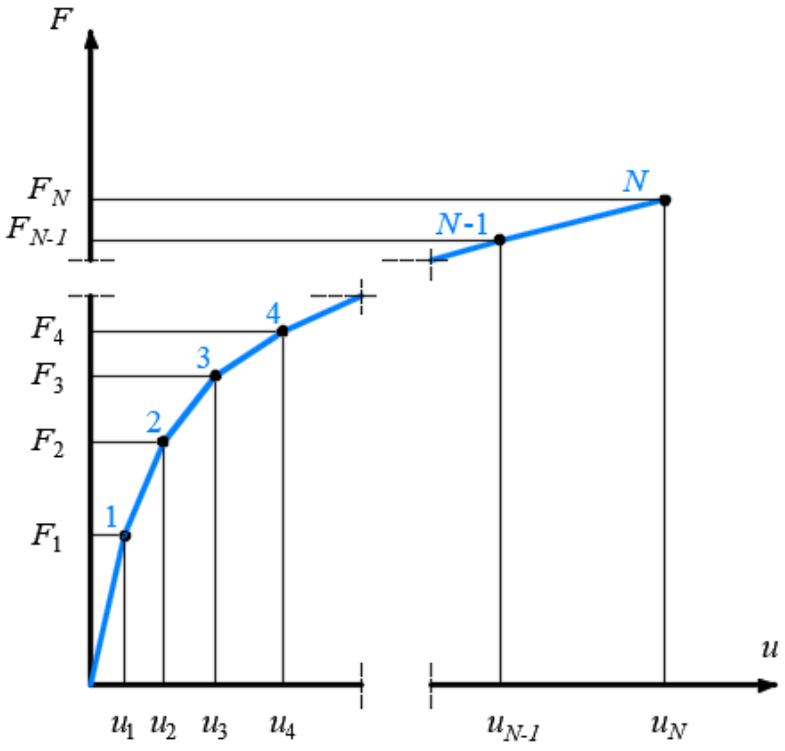

Figure B.2 - Piecewise linear force-displacement relationship

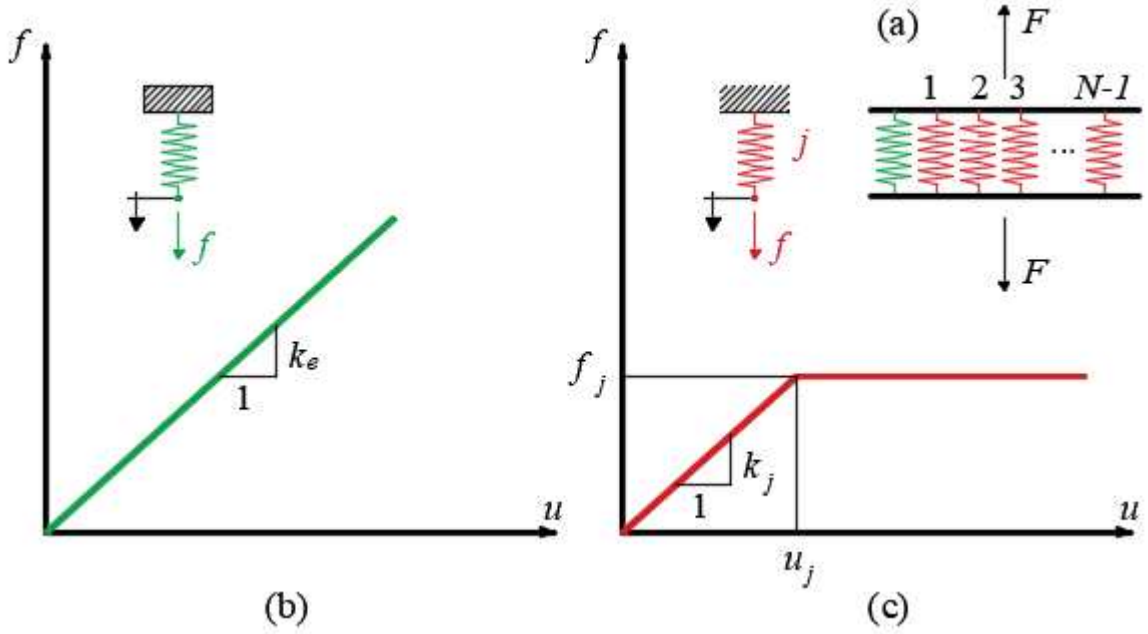

Figure B.3 - (a) parallel springs, (b) elastic spring constitutive law and (c) elastic-plastic j-th spring constitutive law

With reference to Figure B.3, k_j denotes the initial elastic stiffness of the j-th spring with elastic-perfectly plastic behaviour. The yielding displacements of the $N-1$ elastic-plastic spring are equal to the displacements u_j of the assigned piecewise linear constitutive law. Without loss of generality, it is possible to sort the $N-1$ elastic-plastic springs according to the increasing values of u_j. The corresponding yielding forces are denoted with f_j. The stiffness of the unique elastic spring is denoted with k_e.

For a fixed displacement u, the sum of the tangent stiffnesses of the N parallel springs must be equal to the tangent stiffness of the piecewise linear relationship. By imposing such equality for different values of the displacement u, it is possible to obtain the following system of N equations:

$$\begin{cases} k_e + k_1 + k_2 + k_3 + \ldots + k_{N-2} + k_{N-1} = K_1 \\ k_e + k_2 + k_3 + \ldots + k_{N-2} + k_{N-1} = K_2 \\ k_e + k_3 + \ldots + k_{N-2} + k_{N-1} = K_3 \\ \quad \vdots \\ k_e + k_{N-1} = K_{N-1} \\ k_e = K_N \end{cases} \tag{B.27}$$

where the first equation has been obtained for a displacement $0 < u < u_1$, and the j-th equation (with $j > 1$) is obtained by imposing a displacement $u_{j-1} < u < u_j$. It is worth noting that in the system the number of unknowns is equal to the number of equations.

By solving the system in Equation (B.27), the N unknowns are obtained: the stiffness k_e of the linear elastic spring and the initial stiffness of the $N-1$ springs with elastic-perfectly plastic behaviour. The stiffness values are:

$$k_e = K_N$$
$$k_j = K_j - K_{j+1} \qquad j = 1,2,...N-1 \tag{B.28}$$

The yielding force f_1 of the first spring can be determined by considering that the total force of the system corresponding to the yielding displacement u_1 of the first spring is equal to:

$$F_1 = K_1 \cdot u_1 \tag{B.29}$$

while the corresponding force in the first spring is:

$$f_1 = k_1 \cdot u_1 \tag{B.30}$$

Deriving u_1 from Equation (B.29) and substituting in Equation (B.30), remembering Equation (B.28) for k_1, it is possible to obtain:

$$f_1 = \left(1 - \frac{K_2}{K_1}\right) F_1 \tag{B.31}$$

Analogously, in order to define the yielding force of the second spring, the total force of the system corresponding to the yielding displacement u_2 of the second spring is considered:

$$F_2 = F_1 + K_2 \cdot (u_2 - u_1) \tag{B.32}$$

The corresponding force in the second spring is equal to:

$$f_2 = k_2 \cdot u_2 \tag{B.33}$$

Deriving u_2 from Equation (B.32) and substituting in Equation (B.33), remembering Equation (B.28) for k_2 and Equation (B.31) for f_1, after simple algebra it is possible to obtain:

$$f_2 = \left(1 - \frac{K_3}{K_2}\right)(F_2 - f_1) \tag{B.34}$$

Proceeding in a similar way, it is possible to obtain the yielding force of each remaining spring. It is possible to use the following general expression:

$$f_j = \left(1 - \frac{K_{j+1}}{K_j}\right)\left(F_j - \sum_{i=1}^{j-1} f_i\right), \quad j \geq 2 \tag{B.35.a}$$

$$f_j = \left(1 - \frac{K_{j+1}}{K_j}\right)\left(F_j - F_{j-1} + K_j u_{j-1}\right), \quad j \geq 2 \tag{B.35.b}$$

In a numerical implementation it can be convenient to substitute the linear elastic spring and one of the springs with elastic-perfectly plastic behaviour with a spring having elastic-plastic constitutive law with hardening. By assuming, without loss of generality, to combine the linear elastic spring with the first elastic-perfectly plastic spring, the modified stiffness of the springs can be expressed as follows:

$$k_1^e = K_1 - K_2 + K_N$$
$$k_1^p = K_N \tag{B.36}$$
$$k_j = K_j - K_{j+1} \qquad j = 2,3,...N-1$$

denoting with k_1^e and k_1^p the stiffness of the first spring in the elastic and plastic field, respectively. The yielding force f_1^* of the elastic-plastic spring with hardening is equal to:

$$f_1^* = f_1 + k_e \cdot u_1 = \left(1 - \frac{K_2}{K_1} + \frac{K_N}{K_1}\right) F_1 \tag{B.37}$$

The yielding force of the remaining springs is still given by Equation (B.35.b), or by Equation (B.35.a) where f_1^* has been made explicit:

$$f_j = \begin{cases} \left(1 - \dfrac{K_{j+1}}{K_j}\right)\left(F_j - f_1^* + \dfrac{K_N}{K_1} F_1\right) & for \quad j = 2 \\ \left(1 - \dfrac{K_{j+1}}{K_j}\right)\left(F_j - f_1^* + \dfrac{K_N}{K_1} F_1 - \sum_{i=2}^{j-1} f_i\right) & for \quad j > 2 \end{cases} \tag{B.38}$$

APPENDIX C

INCREMENTAL STATIC ANALYSIS

Incremental static analysis is performed by applying on the structure a linear increasing load distribution. The load vector is referred to as $\lambda\mathbf{F}$, where λ is the load multiplier which increases the applied loads proportionally. In order to study the response of the structure during the loading process, the equilibrium between the applied load and the structure reaction must be evaluated at each time instant. Since the structure is a MDOF system, equilibrium is expressed in terms of the following vectors: displacements $\mathbf{u}$, forces $\mathbf{F}$, displacement increments $\Delta\mathbf{u}$, force increments $\Delta\mathbf{F}$.

The resisting forces $\mathbf{f}_{\mathbf{R}}$ depend on the displacement vector $\mathbf{u}$ and therefore the equilibrium at each load step can be expressed as:

$$\lambda\mathbf{F} = \mathbf{f}_{\mathbf{R}}(\mathbf{u}) \tag{C.1}$$

In addition, at each step and for each element, the element state must be evaluated in order to establish whether it has an elastic behaviour or not, consequently updating the corresponding stiffness. The goal is to determine the vector $\mathbf{u}$ at each step.

Several procedures can be applied according to the adopted load or displacement distribution and the force-displacement constitutive laws of the beam-like model. These iterative procedures are the Newton-Raphson method [123] and the Arc-Length method. In the following these procedures, applied in the numerical section, are briefly described.

Finally, the procedure for the static non-linear analysis performed on the beam-like model by applying an increasing displacement distribution instead of a load distribution is illustrated.

C.1 Newton-Raphson Method (force control analysis)

The equilibrium at each n-th step can be expressed as:

$$\lambda_n\mathbf{F} = \mathbf{f}_{\mathbf{R}}(\mathbf{u}_n) \tag{C.2}$$

It is supposed that equilibrium has been satisfied at the $n-1$-th step among applied forces $\lambda_{n-1}\mathbf{F}$ and resisting forces $\mathbf{f}_{\mathbf{R},n-1}$, therefore the system response $\mathbf{u}_{n-1}$ is known.

A force increment $\Delta\mathbf{F}_n = (\lambda_n - \lambda_{n-1})\mathbf{F}$ is therefore considered. The goal is to determine the displacement vector $\mathbf{u}_n$.

Initially, at the first iteration the resisting forces at n-th step coincide with those of the previous step: $\mathbf{f}_{\mathbf{R},n}^{(1)} = \mathbf{f}_{\mathbf{R},n-1}$.

According to the Newton-Raphson method, the response of the structure is determined considering the tangent stiffness matrix at the current iteration $\mathbf{K}_T^{(1)} = \mathbf{C}^T \cdot \mathbf{D}_T^{(1)} \cdot \mathbf{C}$.

The displacement increment associated with the force increment $\Delta\mathbf{F}_n = \Delta\mathbf{R}^{(1)}$ is therefore obtained by:

$$\mathbf{K}_T^{(1)}\Delta\mathbf{u}_n^{(1)} = \Delta\mathbf{R}^{(1)} \tag{C.3}$$

And the approximated total displacement at iteration end is:

$$\mathbf{u}_n^{(1)} = \mathbf{u}_{n-1} + \Delta\mathbf{u}_n^{(1)} \tag{C.4}$$

Then, it is possible to determine the relative displacement increment in the structural elements:

$$\Delta \mathbf{s}_n^{(1)} = \mathbf{C} \cdot \Delta \mathbf{u}_n^{(1)} \tag{C.5}$$

Since the constitutive law of the structural elements are defined, it is also possible to determine the internal shear forces $\mathbf{T}_n^{(1)}$ and therefore to compute the corresponding resisting forces $\mathbf{f}_{\mathbf{R},n}^{(2)} = \mathbf{C}^T \cdot \mathbf{T}_n^{(1)}$. There is a residual equal to:

$$\Delta \mathbf{R}^{(2)} = \lambda_n \mathbf{F} - \mathbf{f}_{\mathbf{R},n}^{(2)} \tag{C.6}$$

If the residual is lower than a fixed tolerance, the convergence is achieved, and a good approximation of the displacement is obtained at the n-th step. Otherwise, iterations go on. Considering the updated tangent stiffness matrix, according to the new stress-strain state of the structural elements $\mathbf{K}_T^{(2)} = \mathbf{C}^T \cdot \mathbf{D}_T^{(2)} \cdot \mathbf{C}$, the new displacement increment is obtained by:

$$\mathbf{K}_T^{(2)} \Delta \mathbf{u}_n^{(2)} = \Delta \mathbf{R}^{(2)} \tag{C.7}$$

And the approximated total displacement at iteration end is:

$$\mathbf{u}_n^{(2)} = \mathbf{u}_{n-1} + \Delta \mathbf{u}_n^{(1)} + \Delta \mathbf{u}_n^{(2)} \tag{C.8}$$

Therefore, it is possible to determine the relative displacement increment in the structural elements:

$$\Delta \mathbf{s}_n^{(2)} = \mathbf{C} \cdot \Delta \mathbf{u}_n^{(2)} \tag{C.9}$$

It is also possible to determine the internal shear forces $\mathbf{T}_n^{(2)}$, the corresponding resisting forces $\mathbf{f}_{\mathbf{R},n}^{(3)}$ and the new residual $\Delta \mathbf{R}^{(3)} = \lambda_n \mathbf{F} - \mathbf{f}_{\mathbf{R},n}^{(3)}$. As done before, if the residual is lower than a fixed tolerance, the convergence is achieved, and a good approximation of the displacement is obtained at the n-th step; otherwise, iterations go on.

When the m-th residual is lower than the fixed tolerance, the convergence is achieved, and the approximation of the displacement at the n-th step end is:

$$\mathbf{u}_n = \mathbf{u}_{n-1} + \sum_{i=1}^{m} \Delta \mathbf{u}_n^{(i)} \tag{C.10}$$

where m obviously depends on the fixed tolerance.

Therefore, the procedure goes on with the next load step, with the same iterative process repeated every load step, until the maximum load or the collapse of the structure is achieved.

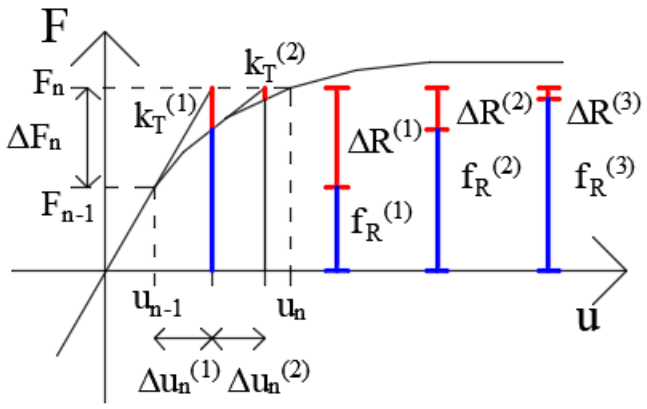

Figure C.1 - Newton-Raphson iterative procedure

In summary, the Newton-Raphson iterative procedure, reported in Figure C.1, is based on the hypothesis that, for each n-th step, the following approximation can be adopted:

$$\mathbf{f}_{\mathbf{R},n}^{(j+1)} \simeq \mathbf{f}_{\mathbf{R},n}^{(j)} + \mathbf{K}_T^{(j)} \Delta \mathbf{u}_n^{(j)} = \lambda_n \mathbf{F} \tag{C.11}$$

where j is the order number of the current iteration, $\mathbf{f}_{\mathbf{R},n}^{(j)}$ the resisting forces at n-th step and j-th iteration, $\mathbf{K}_T^{(j)}$ the tangent stiffness matrix dependent on $\mathbf{u}_n^{(j)}$ displacement.

The non-linear equilibrium equations at each n-th step can be solved by means of the Newton-Raphson iterative procedure starting with the approximation of the displacements from the previous loading step, according to the following procedure:

1.0 Initial state determination:

- $\mathbf{F}_0 = \lambda_0 \mathbf{F} = \mathbf{0}$;
- $\mathbf{u}_0 = \mathbf{0}$, assuming at rest initial conditions (therefore $\mathbf{s}_0 = \mathbf{0}$);
- $\mathbf{f}_{\mathbf{R},1} = \mathbf{0}$ (therefore $\mathbf{T}_0 = \mathbf{0}$);
- $\mathbf{K}_T = \mathbf{K}_e$, initial stiffness matrix - elastic behaviour.

2.0 For each loading step $n = 0,1,2,3,...N_S$, initialize:

- $\Delta \mathbf{F}_{n+1} = \left(\lambda_{n+1} - \lambda_n\right)\mathbf{F}$;
- $\mathbf{F}_{n+1} = \mathbf{F}_n + \Delta \mathbf{F}_{n+1}$;
- $\Delta \mathbf{R}^{(1)} = \Delta \mathbf{F}_{n+1}$; (N.B. $\Delta \mathbf{R}^{(1)} = \mathbf{F}_{n+1} - \mathbf{f}_{\mathbf{R},n} = \mathbf{F}_n + \Delta \mathbf{F}_{n+1} - \mathbf{f}_{\mathbf{R},n} = \Delta \mathbf{F}_{n+1}$)
- $\mathbf{u}_{n+1}^{(1)} = \mathbf{u}_n$ (therefore $\mathbf{s}_{n+1}^{(1)} = \mathbf{s}_n$);
- $\mathbf{f}_{\mathbf{R},n+1}^{(1)} = \mathbf{f}_{\mathbf{R},n}$ (therefore $\mathbf{T}_{n+1}^{(1)} = \mathbf{T}_n$).

3.0 For each iteration $j = 1,2,3,...$ inside the n-th step:

- Check convergence; if the acceptance criteria are not met, implement following steps; otherwise, skip these steps and go to step 4.0;
- Update tangent stiffness matrix $\mathbf{K}_T^{(j)} = \mathbf{C}^T \cdot \mathbf{D}_T^{(j)} \cdot \mathbf{C}$;
- Solve $\mathbf{K}_T^{(j)} \Delta \mathbf{u}_{n+1}^{(j)} = \Delta \mathbf{R}^{(j)}$ to find $\Delta \mathbf{u}_{n+1}^{(j)}$;
- $\mathbf{u}_{n+1}^{(j+1)} = \mathbf{u}_{n+1}^{(j)} + \Delta \mathbf{u}_{n+1}^{(j)}$;
- Compute relative displacement increments in structural elements $\Delta \mathbf{s}_{n+1}^{(j)} = \mathbf{C} \cdot \Delta \mathbf{u}_{n+1}^{(j)}$;
- Update stress state $\mathbf{T}_{n+1}^{(j+1)}$ of structural elements according to relative displacement increment and constitutive law and, therefore, update matrix $\mathbf{D}_T^{(j+1)}$ and strain vector $\mathbf{s}_{n+1}^{(j+1)}$;
- Compute reaction forces $\mathbf{f}_{\mathbf{R},n+1}^{(j+1)} = \mathbf{C}^T \cdot \mathbf{T}_{n+1}^{(j+1)}$;
- Compute residual $\Delta \mathbf{R}^{(j+1)} = \mathbf{F}_{n+1} - \mathbf{f}_{\mathbf{R},n+1}^{(j+1)}$;
- Compute $err = \dfrac{\left\| \Delta \underline{\mathbf{R}}^{(j+1)} \right\|}{\left\| \Delta \underline{\mathbf{F}}_{n+1} \right\|}$ for check convergence;
- Replace $j = j+1$, repeat from step 3.0.

4.0 Save results at step end, replace $n = n+1$ and repeat from step 2.0.

C.2 Modified Newton-Raphson Method (force control analysis)

It is possible to avoid updating the tangent stiffness matrix $\mathbf{K}_T^{(j)}$ at each iteration by means of the Modified Newton-Raphson Method. In this case, the tangent stiffness matrix $\mathbf{K}_T^{(1)}$ is updated only at the first iteration of each loading step and it remains the same for all the iterations inside the current loading step (Figure C.2).

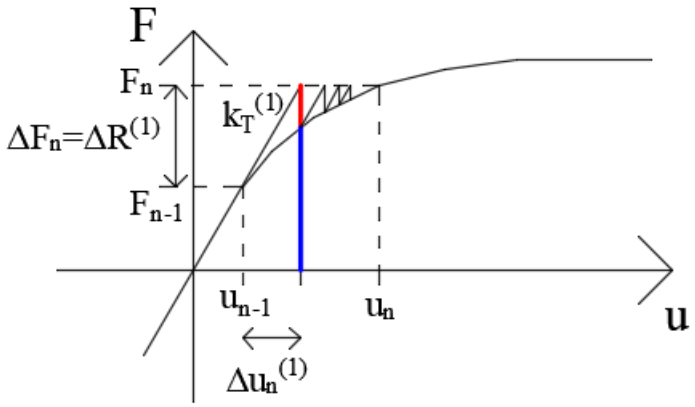

Figure C.2 - Modified Newton-Raphson iterative procedure

C.3 Initial Stiffness Matrix Method (force control analysis)

The "Initial Stiffness Matrix method", indeed, assumes the tangent stiffness matrix $\mathbf{K}_T$ to be constant for each iteration inside the loading step and for each loading step too. In that way, the stiffness matrix $\mathbf{K}_T$ is always equal to the elastic stiffness matrix of the structure.

C.4 Arc Length method

Differently from the Newton-Raphson method, which is a force control analysis and it increases the load distribution according to a prefixed load multiplier, the Arc-Length method is a displacement control analysis and it defines the load distribution increment together with the displacement increment.

This method is very efficient in solving non-linear systems of equations when the problem under consideration exhibits one or more critical points (well-known is their classification into limit points and bifurcation points, geometrical concepts that are connected with the physical concepts of snapping and buckling respectively). In this paragraph, the Riks and Crisfield formulations are described. Riks started from the Newton's method and added a special parameter controlling the progress of the computations along the equilibrium paths [125]. In the geometrical terms the control parameter selected corresponds in good approximation to the "arc length" of the equilibrium path to be computed. In fact, he added, to the standard

equilibrium equations, a constraint equation fixing the length of the incremental load step in load/deflection space.
Crisfield in 1983 published a paper where he presented an alternative formulation for the Arc Length method which could be readily implemented in any commercial finite element software that was able to solve non-linear problems using Newton-Raphson method [126].

Riks formulation

The system of the non-linear equations to be solved is:

$$\mathbf{F}^{ext} - \mathbf{F}^{\text{int}} = 0 \quad \Rightarrow \quad \lambda \mathbf{F} = \mathbf{f}_{\mathbf{R}}(\mathbf{u}) \tag{C.12}$$

where λ is the load multiplier, $\mathbf{F}$ the external load vector and $\mathbf{f}_{\mathbf{R}}$ the internal resisting forces dependent on the displacement vector $\mathbf{u}$.
Assuming that the point $(\mathbf{u}_0, \lambda_0)$ is such to satisfy the system of equations (C.12), thus it belongs to the 'equilibrium path'. Unlike the Newton-Raphson method, the Arc Length method postulates simultaneous variation in both the displacement vector $\Delta\mathbf{u}$ and the load multiplier $\Delta\lambda$. The main difference is that both $\Delta\mathbf{u}$ and $\Delta\lambda$ are unknowns in contrast to Newton-Raphson method where $\Delta\lambda$ is fixed and only $\Delta\mathbf{u}$ have to be determined by means of an iterative procedure. It is possible to write:

$$\Delta\mathbf{R}(\mathbf{u}', \lambda') = (\lambda_0 + \Delta\lambda)\mathbf{F} - \mathbf{f}_{\mathbf{R}}(\mathbf{u}_0 + \Delta\mathbf{u}) = \mathbf{0} \tag{C.13}$$

If Equation (C.13) is satisfied for $(\mathbf{u}_0 + \Delta\mathbf{u}, \lambda_0 + \Delta\lambda)$ then this point also belongs to the 'equilibrium path'. In most cases, however, immediate satisfaction of Equation (C.13) is not achievable. As a result a correction $(\delta\underline{\mathbf{u}}, \delta\lambda)$ is necessary to update the point $(\mathbf{u}_0 + \Delta\mathbf{u} + \delta\mathbf{u}, \lambda_0 + \Delta\lambda + \delta\lambda)$ in order to satisfy Equation (C.13). Hence:

$$\Delta\mathbf{R}(\mathbf{u}'', \lambda'') = (\lambda_0 + \Delta\lambda + \delta\lambda)\mathbf{F} - \mathbf{f}_{\mathbf{R}}(\mathbf{u}_0 + \Delta\mathbf{u} + \delta\mathbf{u}) = \mathbf{0} \tag{C.14}$$

Using a Taylor series expansion and retaining only the linear terms, Equation (C.14) can be written as:

$$(\lambda_0 + \Delta\lambda + \delta\lambda)\mathbf{F} - \left[\mathbf{f}_{\mathbf{R}}(\mathbf{u}_0 + \Delta\mathbf{u}) + \left[\frac{\partial \mathbf{f}_{\mathbf{R}}(\mathbf{u})}{\partial \mathbf{u}}\right]_{\mathbf{u}_0 + \Delta\mathbf{u}} \cdot \delta\mathbf{u}\right] = \mathbf{0} \tag{C.15}$$

where $\dfrac{\partial \mathbf{f}_{\mathbf{R}}(\mathbf{u})}{\partial \mathbf{u}} = \mathbf{K}_T$ is the stiffness matrix of the system. Thus, Equation (C.15) can be written as:

$$\left[\mathbf{K}_T\right]_{\mathbf{u}_0 + \Delta\mathbf{u}} \cdot \delta\mathbf{u} - \delta\lambda\mathbf{F} = (\lambda_0 + \Delta\lambda)\mathbf{F} - \mathbf{f}_{\mathbf{R}}(\mathbf{u}_0 + \Delta\mathbf{u}) = \Delta\mathbf{R}(\mathbf{u}', \lambda') \tag{C.16}$$

It is worth noting that $\delta\mathbf{u}$ and $\delta\lambda$ are unknowns. Therefore, since $\mathbf{u}$ vector has dimension N, the system (C.16) has only N equations to solve N+1 unknowns (N unknowns $\delta\mathbf{u}$ and 1 unknown $\delta\lambda$). Equations (C.16) then are not sufficient to determine $\delta\mathbf{u}$ and $\delta\lambda$. The supplementary equation that completes the system is called the Arc Length Equation and has the following form:

$$(\Delta\mathbf{u} + \delta\mathbf{u})^T \cdot (\Delta\mathbf{u} + \delta\mathbf{u}) + \psi^2 (\Delta\lambda + \delta\lambda)^2 (\mathbf{F}^T \cdot \mathbf{F}) = \Delta l^2 \tag{C.17}$$

where ψ and Δl are user defined parameters. In a sense Δl defines how far to search for the next equilibrium point and its analogous (but not directly equivalent) to the load increment $\Delta\lambda$ used in Newton's method. The Arc-length method constrains the norm of the incremental

displacements to a prescribed value. This is done by simultaneously adapting the size of the increment. It is worth noting that the size of the increment is adapted within the iteration process and is not fixed at the moment the increment starts.
Collecting up equations (C.16) and (C.17), it is possible to write the system of equations in a more compact manner as:

$$\begin{bmatrix} \mathbf{K}_T & -\mathbf{F} \\ 2\Delta\mathbf{u}^T & 2\psi^2\Delta\lambda\left(\mathbf{F}^T\cdot\mathbf{F}\right) \end{bmatrix}\cdot\begin{bmatrix} \delta\mathbf{u} \\ \delta\lambda \end{bmatrix}=\begin{bmatrix} \Delta\mathbf{R} \\ A \end{bmatrix} \tag{C.18}$$

where:

$$\begin{aligned} \Delta\mathbf{R} &= \left(\lambda_0+\Delta\lambda\right)\mathbf{F}-\mathbf{f}_{\mathbf{R}}(\mathbf{u}_0+\Delta\mathbf{u}) \\ A &= -\left(\Delta\mathbf{u}^T\cdot\Delta\mathbf{u}+\psi^2\Delta\lambda^2\left(\mathbf{F}^T\cdot\mathbf{F}\right)-\Delta l^2\right) \end{aligned} \tag{C.19}$$

The system of equations (C.18) is solved for $\delta\mathbf{u},\delta\lambda$ and updates the previous corrections $\Delta\mathbf{u},\Delta\lambda$ to be $\Delta\mathbf{u}'=\Delta\mathbf{u}+\delta\mathbf{u}$ and $\Delta\lambda'=\Delta\lambda+\delta\lambda$ respectively. The method continues to provide such incremental corrections $\delta\mathbf{u},\delta\lambda$ until convergence is achieved in (C.14). When $\psi=1$ the method is also called the Spherical Arc Length Method because Equation (C.17) suggests that the points $\Delta\mathbf{u}',\Delta\lambda'$ belong to a circle with radius Δl. In its most general form for arbitrary ψ, Equation (C.17) can be geometrically interpreted as a hyper-ellipse in the multidimensional displacement-load space $\left(\mathbf{u}-\lambda\right)$. The user decides which value should be assigned to the "radius" and the next converged point is then obtained as the point of intersection between the equilibrium path and that sphere.
This method is widely proven to cope quite well in problems with a snapping behaviour and is implemented in most commercial finite element software (i.e. ABAQUS). This way of formulating the Arc-Length method, however, and in particular the system of equations (C.18) is not the most efficient one and, as a result, many commercial software use a different approach to this method. The reason for this is that Equation (C.18) essentially introduces a completely new system of equations to be solved simultaneously for $\delta\mathbf{u}$ and $\delta\lambda$. Therefore, the techniques commonly used by finite element software such as ABAQUS to solve the system of equations in all other cases (static analysis with Newton-Raphson method, Dynamic analysis etc.) cannot be used in this case where the system of equations is different than the one used in Newton-Raphson method. Despite the capabilities of this method in cases where Newton-Raphson method fails, this particular formulation obstructed the immediate implementation of the method in such software because sacrificing the solver's efficiency and at the same time having to modify all the convergence criteria wasn't an option. It was necessary that the implementation of the method would be based on a different formulation that would ideally include no modifications to the system of equations to be solved.

Crisfield formulation

Crisfield expressed Equation (C.16) as:

$$\delta\mathbf{u}=\left[\mathbf{K}_T\right]^{-1}_{\mathbf{u}_0+\Delta\mathbf{u}}\cdot\left[\left(\lambda_0+\Delta\lambda\right)\mathbf{F}-\mathbf{f}_{\mathbf{R}}(\mathbf{u}_0+\Delta\mathbf{u})\right]+\delta\lambda\left[\mathbf{K}_T\right]^{-1}_{\mathbf{u}_0+\Delta\mathbf{u}}\cdot\mathbf{F} \tag{C.20}$$

or:

$$\delta\mathbf{u}=\delta\hat{\mathbf{u}}+\delta\lambda\delta\mathbf{u}_t \tag{C.21}$$

where:

$$\delta\hat{\mathbf{u}} = \left[\mathbf{K}_T\right]^{-1}_{\mathbf{u}_0+\Delta\mathbf{u}} \cdot \left[\left(\lambda_0 + \Delta\lambda\right)\mathbf{F} - \mathbf{f}_{\mathbf{R}}\left(\mathbf{u}_0 + \Delta\mathbf{u}\right)\right] = \left[\mathbf{K}_T\right]^{-1}_{\mathbf{u}_0+\Delta\mathbf{u}} \cdot \Delta\mathbf{R}$$
$$\delta\mathbf{u}_t = \left[\mathbf{K}_T\right]^{-1}_{\mathbf{u}_0+\Delta\mathbf{u}} \cdot \mathbf{F} \qquad \text{(C.22)}$$

It is worth noting that $\delta\hat{\mathbf{u}}$ and $\delta\mathbf{u}_t$ can be calculated immediately since they only require known information. Once the displacement correction is expressed as in (C.21), it can be substituted in the Arc Length Equation (C.17), leading to:

$$a_1\delta\lambda^2 + a_2\delta\lambda + a_3 = 0 \qquad \text{(C.23)}$$

where the coefficients a_1, a_2 and a_3 are given by:

$$a_1 = \delta\mathbf{u}_t^{\,T} \cdot \delta\mathbf{u}_t + \psi^2\left(\mathbf{F}^T \cdot \mathbf{F}\right)$$
$$a_2 = 2\left(\Delta\mathbf{u} + \delta\hat{\mathbf{u}}\right)^T \cdot \delta\mathbf{u}_t + 2\psi^2\Delta\lambda\left(\mathbf{F}^T \cdot \mathbf{F}\right) \qquad \text{(C.24)}$$
$$a_3 = \left(\Delta\mathbf{u} + \delta\hat{\mathbf{u}}\right)^T \cdot \left(\Delta\mathbf{u} + \delta\hat{\mathbf{u}}\right) + \psi^2\Delta\lambda^2\left(\mathbf{F}^T \cdot \mathbf{F}\right) - \Delta l^2$$

Equation (C.23) can be easily solved to find $\delta\lambda$ and to update the displacement variation with Equation (C.21). With this particular formulation, every iteration, the program has to find $\delta\hat{\mathbf{u}}$ and $\delta\mathbf{u}_t$, which can be done by making use of the existing solver since the stiffness matrix involved is the same as in other methods. Subsequently, using $\delta\hat{\mathbf{u}}$ and $\delta\mathbf{u}_t$ it is possible to solve the quadratic Equation (C.23) with respect to $\delta\lambda$ and to update the variations $\Delta\mathbf{u}$ and $\Delta\lambda$. These steps of the iterative procedure have to be repeated until convergence is achieved.
Crisfield formulation, furthermore, sets $\psi = 0$.

Choice of the appropriate Arc Length equation solution

The quadratic Equation (C.23) would in general lead to two distinct solutions for $\delta\lambda$ which will in turn lead to two distinct solutions for $\delta\mathbf{u}$. Thus, every iteration, the solver determined two sets of solutions, namely $\left(\delta\mathbf{u}_1, \delta\lambda_1\right)$ and $\left(\delta\mathbf{u}_2, \delta\lambda_2\right)$.

The issue that arises, then, is to develop a robust algorithm that would be able to accurately determine the correct set of $\left(\delta\mathbf{u}, \delta\lambda\right)$ to update the solution. In general, the solution which avoids "doubling back" on the original load/deflection path should be chosen.
An efficient rule to follow in order to choose the next point correctly is the following.
It is possible to compute the two displacement corrections $\delta\mathbf{u}_1$ and $\delta\mathbf{u}_2$ corresponding to $\delta\lambda_1$ and $\delta\lambda_2$ respectively. Subsequently, the projections (dot-products) of these generalised correction vectors on the previous corrections are calculated. The $\delta\lambda$, which leads to the largest value of the dot product and thus forms the closest correction to the previous one and therefore the smallest "angle" between the incremental vectors of the previous and current iterations, is chosen. Crisfield, however, suggested to choose the $\delta\lambda$ which leads to a positive value of the dot product; if both the dot products are positive, the appropriate root is that closest to the linear solution $\delta\lambda = -a_3 / a_2$.

The dot product is defined as:

$$DOT^{(i)} = \left(\Delta\mathbf{u} + \delta\mathbf{u}^i, \lambda + \Delta\lambda + \delta\lambda^i\right) \cdot \left(\Delta\mathbf{u}, \lambda + \Delta\lambda\right) \Rightarrow$$
$$DOT^{(i)} = \left(\Delta\mathbf{u} + \delta\mathbf{u}^i\right)^T \cdot \Delta\mathbf{u} + \psi^2\Delta\lambda\left(\Delta\lambda + \delta\lambda^i\right)\left(\mathbf{F}^T \cdot \mathbf{F}\right) \qquad i = 1, 2 \qquad \text{(C.25)}$$

If the initial corrections $(\Delta\mathbf{u}, \Delta\lambda)$ are equal to zero (for example at the beginning of each increment), the corresponding DOT products are zero, therefore the chosen $\delta\lambda$ is the one that has the same sign of the determinant of the stiffness matrix.
The Arc Length method initiation for every increment as well as the iterative loops until convergence is achieved are outlined in the pseudocode that follows:

1.0 Initialization of the variables:

- fix user defined parameters ψ, Δl and tolerance *tol*;
- $\lambda_0 = 0 \quad \Rightarrow \quad \mathbf{F}_0^{ext} = \lambda_0 \mathbf{F} = \mathbf{0}$;
- $\mathbf{u}_0 = \mathbf{0}$, for at rest initial conditions (therefore $\mathbf{s}_0 = \mathbf{0}$);
- $\mathbf{f}_{\mathbf{R},0} = \mathbf{0}$ (therefore $\mathbf{T}_0 = \mathbf{0}$);
- $n = 1$.

2.0 For each load step until $\mathbf{u}_{n-1} \le \mathbf{u}_{\max}$ (for a target point), variables initialization:

- $\mathbf{u}_n^{(0)} = \mathbf{u}_{n-1}$ (therefore $\mathbf{s}_n^{(0)} = \mathbf{s}_{n-1}$)
- $\lambda_n^{(0)} = \lambda_{n-1}$
- $\Delta\mathbf{u}^{(0)} = \mathbf{0}; \qquad \Delta\lambda^{(0)} = 0;$
- determine $\left[\mathbf{K}_T\right]_{\mathbf{u}_n + \Delta\mathbf{u}}$, tangent stiffness matrix
- $\delta\hat{\mathbf{u}} = \mathbf{0}; \qquad \delta\mathbf{u}_t = \left[\mathbf{K}_T\right]^{-1}_{\mathbf{u}_n + \Delta\mathbf{u}} \cdot \mathbf{F}$;
- solve Arc Length equation (C.23), and choose the appropriate solution:

  a) if the two solutions $\delta\lambda_1$ and $\delta\lambda_2$ are equal, then choose either one

  b) else the chosen $\delta\lambda$ is the one that has the same sign of the determinant of the stiffness matrix

- $\delta\mathbf{u} = \delta\hat{\mathbf{u}} + \delta\lambda\delta\mathbf{u}_t$;
- compute $\Delta\mathbf{s}^{(0)} = \mathbf{C} \cdot \left(\Delta\mathbf{u}^{(0)} + \delta\mathbf{u}\right)$ and update $\mathbf{T}_n^{(0)}$, $\mathbf{D}_T$, $\mathbf{s}_n^{(0)}$ and $\mathbf{f}_{\mathbf{R}}(\mathbf{u}_n^{(0)} + \Delta\mathbf{u}^{(0)} + \delta\mathbf{u}) = \mathbf{C}^T \cdot \mathbf{T}_n^{(0)}$
- $\Delta\mathbf{R}^{(0)} = \left(\lambda_n^{(0)} + \Delta\lambda^{(0)} + \delta\lambda\right)\mathbf{F} - \mathbf{f}_{\mathbf{R}}(\mathbf{u}_n^{(0)} + \Delta\mathbf{u}^{(0)} + \delta\mathbf{u})$;
- $err = \dfrac{\left\|\Delta\mathbf{R}^{(0)}\right\|}{\left\|\left(\Delta\lambda^{(0)} + \delta\lambda\right)\mathbf{F}\right\|}$

  a) if $err < tol$: go to step 4.

  b) else go to step 3.

3.0 For each iteration $j = 1, 2, 3, \ldots I_{\max}$ inside *n*-th load step

- $\Delta\mathbf{u}^{(j)} = \Delta\mathbf{u}^{(j-1)} + \delta\mathbf{u}; \qquad \Delta\lambda^{(j)} = \Delta\lambda^{(j-1)} + \delta\lambda$
- determine $\left[\mathbf{K}_T\right]_{\mathbf{u}_n + \Delta\mathbf{u}}$, tangent stiffness matrix
- $\delta\hat{\mathbf{u}} = \left[\mathbf{K}_T\right]^{-1}_{\mathbf{u}_n + \Delta\mathbf{u}} \cdot \Delta\mathbf{R}^{(j-1)}; \qquad \delta\mathbf{u}_t = \left[\mathbf{K}_T\right]^{-1}_{\mathbf{u}_n + \Delta\mathbf{u}} \cdot \mathbf{F}$

- solve Arc Length equation (C.23), and choose the appropriate solution:

a) if the two solutions $\delta\lambda_1$ and $\delta\lambda_2$ are equal, then choose either one

b) else if $\left\|\Delta\mathbf{u}^{(j)}\right\| = 0$, the chosen $\delta\lambda$ is the one that has the same sign of the determinant of the stiffness matrix

c) else the chosen $\delta\lambda$ is the one which leads to the largest value of the dot product, given by Equation (14)

- $\delta\mathbf{u} = \delta\hat{\mathbf{u}} + \delta\lambda\delta\mathbf{u}_t$;

-compute $\delta\mathbf{s}^{(j)} = \mathbf{C}\cdot\left(\delta\mathbf{u}\right)$ and update $\mathbf{T}_n^{(j)}$, $\mathbf{D}_T$, $\mathbf{s}_n^{(j)}$ and $\mathbf{f}_\mathbf{R}(\mathbf{u}_n^{(0)} + \Delta\mathbf{u}^{(j)} + \delta\mathbf{u}) = \mathbf{C}^T\cdot\mathbf{T}_n^{(j)}$

- $\Delta\mathbf{R}^{(j)} = \left(\lambda_n^{(0)} + \Delta\lambda^{(j)} + \delta\lambda\right)\mathbf{F} - \mathbf{f}_\mathbf{R}(\mathbf{u}_n^{(0)} + \Delta\mathbf{u}^{(j)} + \delta\mathbf{u})$

- $err = \dfrac{\left\|\Delta\mathbf{R}^{(j)}\right\|}{\left\|\left(\Delta\lambda^{(j)} + \delta\lambda\right)\mathbf{F}\right\|}$

a) if $err < tol$: go to step 4.

b) else $j = j+1$. Go to step 3.

4.0 Save results: $\mathbf{u}_n = \mathbf{u}_n^{(0)} + \Delta\mathbf{u}^{(j)} + \delta\mathbf{u}$ and $\lambda_n = \lambda_n^{(0)} + \Delta\lambda^{(j)} + \delta\lambda$. $n = n+1$. Go to step 2.

C.5 Static non-linear analysis by applying an increasing displacement distribution

The static non-linear analysis can be performed by applying on the structure an increasing displacement distribution. The applied displacement vector is referred to as $\lambda\mathbf{u}$, where λ is the load multiplier which increases the applied displacements proportionally.
In this case, since the displacements of all the degrees of freedom of the beam-like model are defined for each step of the analysis, there are no unknown displacements, and it is possible to determine the relative displacements (drifts) for each element of the equivalent beam.
Denoting with $\Delta\mathbf{u}_{n+1}$ the *n+1*-th displacement increment, it is possible to determine the corresponding drifts as follows:

$$\Delta\mathbf{s}_{n+1}=\mathbf{C}\cdot\Delta\mathbf{u}_{n+1} \tag{C.26}$$

In addition, by determining the drift at each step and for each element, the element state can be easily evaluated in order to establish whether it has an elastic behaviour or not, consequently updating the corresponding stiffness. It is also possible to determine the vector of shear forces of the elements $\mathbf{T}_{n+1}$. The goal is to determine the vector of the external forces $\mathbf{F}$ at each step. Of course, the external forces will be equal to the resisting forces $\mathbf{f}_{\mathbf{R}}$, therefore they can be determined as:

$$\mathbf{F}_{n+1}=\mathbf{C}^T\cdot\mathbf{T}_{n+1} \tag{C.27}$$

Therefore, no iterations are needed for the solution process, as described in the following procedure.

1.0 Initial state determination:

- $\mathbf{F}_0=\mathbf{f}_{\mathbf{R},1}=\mathbf{0}$ (therefore $\mathbf{T}_0=\mathbf{0}$);
- $\mathbf{u}_0=\lambda_0\mathbf{u}=\mathbf{0}$, assuming at rest initial conditions (therefore $\mathbf{s}_0=\mathbf{0}$);
- $\mathbf{K}_T=\mathbf{K}_e$, initial stiffness matrix - elastic behaviour.

2.0 For each loading step $n=0,1,2,3,...N_S$:

- $\Delta\mathbf{u}_{n+1}=\left(\lambda_{n+1}-\lambda_n\right)\mathbf{u}$
- $\mathbf{u}_{n+1}=\mathbf{u}_n+\Delta\mathbf{u}_{n+1}$;
- $\Delta\mathbf{s}_{n+1}=\mathbf{C}\cdot\Delta\mathbf{u}_{n+1}$;
- Update stress state $\mathbf{T}_{n+1}$ of structural elements according to relative displacement increment and constitutive law and, therefore, update matrix $\mathbf{D}_T$ and strain vector $\mathbf{s}_{n+1}$;
- Compute external forces $\mathbf{F}_{n+1}=\mathbf{C}^T\cdot\mathbf{T}_{n+1}$;
- Update stiffness matrix $\mathbf{K}_T=\mathbf{C}^T\cdot\mathbf{D}_T\cdot\mathbf{C}$.

3.0 Save results at step end, replace $n=n+1$ and repeat from step 2.0.

C.6 Static Pushover Curve

Once the results in terms of force and displacements have been collected for each step by means of one of the procedures described above, it is possible to plot the **capacity curve of the building** or **Pushover Curve**. This curve shows the relation between V and u, where V is the base shear while u is the displacement of the control point. For the considered equivalent beam model, a control point located at the top of the beam has been chosen.

It is worth remembering that the base shear at the n-th step is equal to the sum of the applied nodal forces at the n-th step: $V_n = \sum_{i=2}^{N} F_{n,i}$.

An example of capacity curve has been reported in Figure C.3 for the sake of clarity.

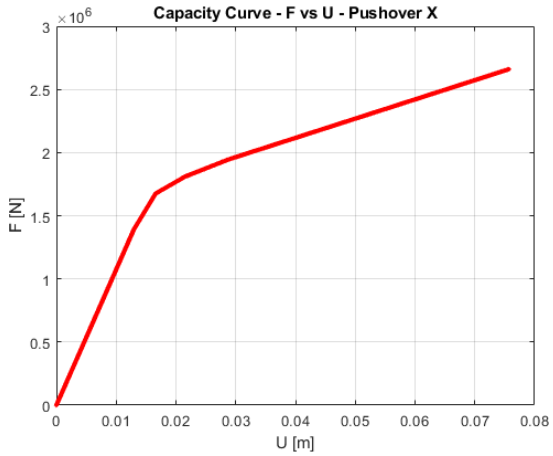

Figure C.3 - Capacity curve

APPENDIX D

DYNAMIC ANALYSIS

The dynamic behaviour of the structure is ruled by the following equation of motion:

$$\mathbf{M}\ddot{\mathbf{u}}(t)+\mathbf{C}\dot{\mathbf{u}}(t)+\mathbf{f_R}\left(\mathbf{u}(t)\right)=-\mathbf{M}\underline{\mathbf{i}}\ddot{u}_g(t) \tag{D.1}$$

where the vector $\underline{\mathbf{i}}$ denotes the spatial distribution of the load.

For non-linear dynamic analyses, the resisting forces depend non-linearly on the displacement vector $\mathbf{u}$ and its increment $\Delta\mathbf{u}$, while in the linear analysis the force displacement relationship is linear. Nevertheless, also in case of linear analysis in presence of non-classical damping the equations of motion turn out to be coupled and must therefore be solved through time-stepping numerical integration methods.

The at rest initial conditions are:

$$\mathbf{u}_0=\mathbf{0} \qquad \dot{\mathbf{u}}_0=\mathbf{0} \tag{D.2}$$

Usually, the applied force is given by a set of discrete values, with a sampling interval equal to $\Delta t_i=t_{i+1}-t_i$, which, although not necessary, is usually assumed to be constant.

Because of that, the equation of motion requires a numerical solution for each time-step $i+1$, starting with the conditions already known at *i*-th step. The equation of motion to be solved numerically is:

$$\mathbf{M}\ddot{\mathbf{u}}_{i+1}+\mathbf{C}\dot{\mathbf{u}}_{i+1}+\mathbf{f_R}(\mathbf{u}_{i+1})=-\mathbf{M}\underline{\mathbf{i}}\ddot{u}_{g,i+1} \tag{D.3}$$

which allows to find: $\mathbf{u}_{i+1},\dot{\mathbf{u}}_{i+1},\ddot{\mathbf{u}}_{i+1}$, the associated resisting forces $\mathbf{f_R}(\mathbf{u}_{i+1})$ and the stress-strain state of the structural elements.

The solution strategy is based on the Newmark's Method [123], which is described below for both linear and non-linear systems.

D.1 Basic procedure

Newmark's method is based on the following equations:

$$\dot{\mathbf{u}}_{i+1} = \dot{\mathbf{u}}_i + \left[(1-\gamma)\Delta t\right]\ddot{\mathbf{u}}_i + (\gamma\Delta t)\ddot{\mathbf{u}}_{i+1} \tag{D.4a}$$

$$\mathbf{u}_{i+1} = \mathbf{u}_i + (\Delta t)\dot{\mathbf{u}}_i + \left[(0.5-\beta)(\Delta t)^2\right]\ddot{\mathbf{u}}_i + \left[\beta(\Delta t)^2\right]\ddot{\mathbf{u}}_{i+1} \tag{D.4b}$$

The parameters β and γ define the variation of acceleration over a time step, whose typical values are: $\gamma = \frac{1}{2}$, $\frac{1}{6} \le \beta \le \frac{1}{4}$.

These two equations, combined with the equilibrium Equation (D.3) at the end of the time step, allow to solve the problem. An iterative procedure is required to implement these computations because the unknown $\ddot{\mathbf{u}}_{i+1}$ at the $i+1$-th step, which is the same step for the determination of $\dot{\mathbf{u}}_{i+1}$ and $\mathbf{u}_{i+1}$, appears in the right side of Equations (D.4), therefore making the problem implicit. However, for linear systems it is possible to modify Newmark's original formulation in order to solve Equation (D.3) and Equations (D.4) without iteration although still implicit.
Two special cases of Newmark's method, which are obtained by fixing appropriately β and γ, are shown in the following.

Constant average acceleration method

Assuming that the acceleration over a time step Δt is constant and equal to its mean value, the acceleration at the instant τ included in Δt is given by:

$$\ddot{\mathbf{u}}(\tau) = \frac{1}{2}\left(\ddot{\mathbf{u}}_{i+1} + \ddot{\mathbf{u}}_i\right) \tag{D.5}$$

Integration of (D.5) allows to obtain the velocity:

$$\dot{\mathbf{u}}(\tau) = \dot{\mathbf{u}}_i + \frac{\tau}{2}\left(\ddot{\mathbf{u}}_{i+1} + \ddot{\mathbf{u}}_i\right) \tag{D.6}$$

Integration of (D.6) allows to obtain the displacement:

$$\mathbf{u}(\tau) = \mathbf{u}_i + \dot{\mathbf{u}}_i\tau + \frac{\tau^2}{4}\left(\ddot{\mathbf{u}}_{i+1} + \ddot{\mathbf{u}}_i\right) \tag{D.7}$$

Velocity and displacement values at the end of the time step are given by:

$$\begin{aligned} \dot{\mathbf{u}}_{i+1} &= \dot{\mathbf{u}}_i + \frac{\Delta t}{2}\left(\ddot{\mathbf{u}}_{i+1} + \ddot{\mathbf{u}}_i\right) \\ \mathbf{u}_{i+1} &= \mathbf{u}_i + \Delta t \cdot \dot{\mathbf{u}}_i + \frac{\Delta t^2}{4}\left(\ddot{\mathbf{u}}_{i+1} + \ddot{\mathbf{u}}_i\right) \end{aligned} \tag{D.8}$$

These expressions can be obtained by imposing in Equations (D.4) $\gamma = \frac{1}{2}$ and $\beta = \frac{1}{4}$.

Linear acceleration method

Assuming that the acceleration varies linearly over a time step Δt, the acceleration at the instant τ included in Δt is given by:

$$\ddot{\mathbf{u}}(\tau) = \ddot{\mathbf{u}}_i + \frac{\tau}{\Delta t}\left(\ddot{\mathbf{u}}_{i+1} - \ddot{\mathbf{u}}_i\right) \tag{D.9}$$

Integration of (D.9) allows to obtain the velocity:

$$\dot{\mathbf{u}}(\tau) = \dot{\mathbf{u}}_i + \ddot{\mathbf{u}}_i\tau + \frac{\tau^2}{2\Delta t}\left(\ddot{\mathbf{u}}_{i+1} - \ddot{\mathbf{u}}_i\right) \tag{D.10}$$

Integration of (D.10) allows to obtain the displacement:

$$\mathbf{u}(\tau) = \mathbf{u}_i + \dot{\mathbf{u}}_i\tau + \ddot{\mathbf{u}}_i\frac{\tau^2}{2} + \frac{\tau^3}{6\Delta t}\left(\ddot{\mathbf{u}}_{i+1} - \ddot{\mathbf{u}}_i\right) \tag{D.11}$$

Velocity and displacement values at the end of the time step are given by:

$$\begin{aligned} \dot{\mathbf{u}}_{i+1} &= \dot{\mathbf{u}}_i + \frac{\Delta t}{2}\left(\ddot{\mathbf{u}}_{i+1} + \ddot{\mathbf{u}}_i\right) \\ \mathbf{u}_{i+1} &= \mathbf{u}_i + \Delta t \cdot \dot{\mathbf{u}}_i + \frac{\Delta t^2}{3}\ddot{\mathbf{u}}_i + \frac{\Delta t^2}{6}\ddot{\mathbf{u}}_{i+1} \end{aligned} \tag{D.12}$$

These expressions can be obtained by imposing in Equations (D.4) $\gamma = \frac{1}{2}$ and $\beta = \frac{1}{6}$.

D.2 Linear systems

For linear systems it is possible to modify Newmark's original formulation to permit solution of Equation (D.3) and Equations (D.4) without iteration although still implicit.

The equation of motion for linear systems is given by:

$$\mathbf{M}\ddot{\mathbf{u}}_{i+1} + \mathbf{C}\dot{\mathbf{u}}_{i+1} + \mathbf{K}\mathbf{u}_{i+1} = -\mathbf{M}\mathbf{i}\ddot{u}_{g,i+1} \tag{D.13}$$

Equation (D.4b) allow to express $\ddot{\mathbf{u}}_{i+1}$ as a function of $\mathbf{u}_{i+1}$:

$$\ddot{\mathbf{u}}_{i+1} = \frac{1}{\beta(\Delta t)^2}(\mathbf{u}_{i+1} - \mathbf{u}_i) - \frac{1}{\beta\Delta t}\dot{\mathbf{u}}_i - \left(\frac{1}{2\beta} - 1\right)\ddot{\mathbf{u}}_i \tag{D.14}$$

Substituting Equation (D.14) in Equation (D.4a) allows to express the velocity as:

$$\dot{\mathbf{u}}_{i+1} = \frac{\gamma}{\beta\Delta t}(\mathbf{u}_{i+1} - \mathbf{u}_i) + \left(1 - \frac{\gamma}{\beta}\right)\dot{\mathbf{u}}_i + \Delta t\left(1 - \frac{\gamma}{2\beta}\right)\ddot{\mathbf{u}}_i \tag{D.15}$$

Substitution of Equations (D.14) and (D.15) in Equation (D.3) allows to obtain:

$$\mathbf{M}\left[\frac{1}{\beta(\Delta t)^2}(\mathbf{u}_{i+1} - \mathbf{u}_i) - \frac{1}{\beta\Delta t}\dot{\mathbf{u}}_i - \left(\frac{1}{2\beta} - 1\right)\ddot{\mathbf{u}}_i\right] + \mathbf{C}\left[\frac{\gamma}{\beta\Delta t}(\mathbf{u}_{i+1} - \mathbf{u}_i) + \left(1 - \frac{\gamma}{\beta}\right)\dot{\mathbf{u}}_i + \Delta t\left(1 - \frac{\gamma}{2\beta}\right)\ddot{\mathbf{u}}_i\right] +$$
$$+\mathbf{K}\mathbf{u}_{i+1} = -\mathbf{M}\mathbf{i}\ddot{u}_{g,i+1} \tag{D.16}$$

Rearranging the terms:

$$\left[\frac{1}{\beta(\Delta t)^2}\mathbf{M} + \frac{\gamma}{\beta\Delta t}\mathbf{C} + \mathbf{K}\right]\mathbf{u}_{i+1} = -\mathbf{M}\mathbf{i}\ddot{u}_{g,i+1} + \left[\frac{1}{\beta(\Delta t)^2}\mathbf{M} + \frac{\gamma}{\beta\Delta t}\mathbf{C}\right]\mathbf{u}_i + \left[\frac{1}{\beta\Delta t}\mathbf{M} + \left(\frac{\gamma}{\beta} - 1\right)\mathbf{C}\right]\dot{\mathbf{u}}_i +$$
$$+\left[\left(\frac{1}{2\beta} - 1\right)\mathbf{M} + \Delta t\left(\frac{\gamma}{2\beta} - 1\right)\mathbf{C}\right]\ddot{\mathbf{u}}_i \tag{D.17}$$

Which can be written in matrix form as:

$$\hat{\mathbf{K}}\mathbf{u}_{i+1} = \hat{\mathbf{F}}_{i+1} \tag{D.18}$$

where:

$$\hat{\mathbf{K}} = \mathbf{K} + \frac{1}{\beta(\Delta t)^2}\mathbf{M} + \frac{\gamma}{\beta\Delta t}\mathbf{C}$$

$$\hat{\mathbf{F}}_{i+1} = -\mathbf{M}\mathbf{i}\ddot{u}_{g,i+1} + \left[\frac{1}{\beta(\Delta t)^2}\mathbf{M} + \frac{\gamma}{\beta\Delta t}\mathbf{C}\right]\mathbf{u}_i + \left[\frac{1}{\beta\Delta t}\mathbf{M} + \left(\frac{\gamma}{\beta} - 1\right)\mathbf{C}\right]\dot{\mathbf{u}}_i + \left[\left(\frac{1}{2\beta} - 1\right)\mathbf{M} + \Delta t\left(\frac{\gamma}{2\beta} - 1\right)\mathbf{C}\right]\ddot{\mathbf{u}}_i$$

It is worth noting that $\hat{\mathbf{K}}$ and $\hat{\mathbf{F}}_{i+1}$ are known and which depend on the system characteristics, β and γ parameters and the quantities $\mathbf{u}_i, \dot{\mathbf{u}}_i, \ddot{\mathbf{u}}_i$. Solving the system $\hat{\mathbf{K}}\mathbf{u}_{i+1} = \hat{\mathbf{F}}_{i+1}$ and therefore computing the quantities $\dot{\mathbf{u}}_{i+1}$ and $\ddot{\mathbf{u}}_{i+1}$ by using Equations (D.14)-(D.15), it is possible to find the system response at the $i+1$-th step. However, in order to ensure the equilibrium at the $i+1$-th step, it is possible to compute the acceleration by using the equation of motion:

$$\mathbf{M}\ddot{\mathbf{u}}_{i+1} = -\mathbf{M}\mathbf{i}\ddot{u}_{g,i+1} - \mathbf{C}\dot{\mathbf{u}}_{i+1} - \mathbf{K}\mathbf{u}_{i+1} \tag{D.19}$$

being known the quantities at the right side.

The procedure to implement the linear dynamic analysis by means of Newmark's method is shown in the following:

1.0 Choose special case:

a) Constant average acceleration method: set $\gamma = \frac{1}{2}$ and $\beta = \frac{1}{4}$;

b) Linear acceleration method: set $\gamma = \frac{1}{2}$ and $\beta = \frac{1}{6}$;

2.0 Initialize variables:

- $\mathbf{u}_0 = \mathbf{0}$, assuming at rest initial conditions (therefore $\mathbf{s}_0 = \mathbf{0}$ and $\mathbf{T}_0 = \mathbf{0}$);
- $\dot{\mathbf{u}}_0 = \mathbf{0}$, assuming at rest initial conditions;
- $\mathbf{M}, \mathbf{C}, \mathbf{K}$ matrices assembling;
- compute $\ddot{\mathbf{u}}_0$ by solving the equation of motion at initial time instant: $\mathbf{M}\ddot{\mathbf{u}}_0 = -\mathbf{M}\mathbf{i}\ddot{u}_{g,0} - \mathbf{C}\dot{\mathbf{u}}_0 - \mathbf{K}\mathbf{u}_0$;
- select Δt, usually equal to the sampling interval of the accelerogram;
- $a_1 = \frac{1}{\beta(\Delta t)^2}\mathbf{M} + \frac{\gamma}{\beta \Delta t}\mathbf{C}$; $\quad a_2 = \frac{1}{\beta \Delta t}\mathbf{M} + \left(\frac{\gamma}{\beta} - 1\right)\mathbf{C}$; $\quad a_3 = \left(\frac{1}{2\beta} - 1\right)\mathbf{M} + \Delta t\left(\frac{\gamma}{2\beta} - 1\right)\mathbf{C}$;
- $\hat{\mathbf{K}} = \mathbf{K} + a_1$.

3.0 For each time instant $i = 0,1,2,3,...N_S$:

- $\hat{\mathbf{F}}_{i+1} = -\mathbf{M}\mathbf{i}\ddot{u}_{g,i+1} + a_1 \cdot \mathbf{u}_i + a_2 \cdot \dot{\mathbf{u}}_i + a_3 \cdot \ddot{\mathbf{u}}_i$;
- Compute $\mathbf{u}_{i+1}$ by solving $\hat{\mathbf{K}}\mathbf{u}_{i+1} = \hat{\mathbf{F}}_{i+1}$;
- $\dot{\mathbf{u}}_{i+1} = \frac{\gamma}{\beta \Delta t}(\mathbf{u}_{i+1} - \mathbf{u}_i) + \left(1 - \frac{\gamma}{\beta}\right)\dot{\mathbf{u}}_i + \Delta t\left(1 - \frac{\gamma}{2\beta}\right)\ddot{\mathbf{u}}_i$;
- $\ddot{\mathbf{u}}_{i+1} = \frac{1}{\beta(\Delta t)^2}(\mathbf{u}_{i+1} - \mathbf{u}_i) - \frac{1}{\beta \Delta t}\dot{\mathbf{u}}_i - \left(\frac{1}{2\beta} - 1\right)\ddot{\mathbf{u}}_i$ or compute $\ddot{\mathbf{u}}_{i+1}$ by imposing the equilibrium at step end: $\mathbf{M}\ddot{\mathbf{u}}_{i+1} = -\mathbf{M}\mathbf{i}\ddot{u}_{g,i+1} - \mathbf{C}\dot{\mathbf{u}}_{i+1} - \mathbf{K}\mathbf{u}_{i+1}$;
- $\mathbf{s}_{i+1} = \mathbf{C} \cdot \mathbf{u}_{i+1}$;
- $\mathbf{T}_{i+1} = \mathbf{D} \cdot \mathbf{s}_{i+1}$.

4.0 Save results at step end, replace $i = i + 1$ and repeat from step 3.0.

D.3 Non-linear systems

For non-linear systems the resisting forces $\mathbf{f_R}(\mathbf{u}_{i+1})$ depend on the unknown displacement $\mathbf{u}_{i+1}$ therefore the equation of motion is solved by means of an iterative procedure. In this case Newton-Raphson Method is adopted, already used for the non-linear static problem.

The equation of motion for non-linear systems is given by:

$$\mathbf{M}\ddot{\mathbf{u}}_{i+1} + \mathbf{C}\dot{\mathbf{u}}_{i+1} + \mathbf{f_R}(\mathbf{u}_{i+1}) = -\mathbf{M}\mathbf{i}\ddot{u}_{g,i+1} \tag{D.20}$$

which can be written as:

$$\hat{\mathbf{P}}_{i+1} = -\mathbf{M}\mathbf{i}\ddot{u}_{g,i+1} \tag{D.21}$$

where $\hat{\mathbf{P}}_{i+1} = \mathbf{M}\ddot{\mathbf{u}}_{i+1} + \mathbf{C}\dot{\mathbf{u}}_{i+1} + \mathbf{f_R}(\mathbf{u}_{i+1})$.

According to the Newton-Raphson method, for each $i+1$-th step it is possible to use the following approximation:

$$\hat{\mathbf{P}}_{i+1}^{(j+1)} \simeq \hat{\mathbf{P}}_{i+1}^{(j)} + \left.\frac{\partial \hat{\mathbf{P}}}{\partial \mathbf{u}}\right|_{\mathbf{u}_{i+1}^{(j)}} \Delta\mathbf{u}_{i+1}^{(j)} = -\mathbf{M}\mathbf{i}\ddot{u}_{g,i+1} \tag{D.22}$$

where j is the current iteration number, $\hat{\mathbf{P}}_{i+1}^{(j)}$ is the force vector known at $i+1$-th step and j-th iteration, $\left.\frac{\partial \hat{\mathbf{P}}}{\partial \mathbf{u}}\right|_{\mathbf{u}_{i+1}^{(j)}}$ is the derivative of $\hat{\mathbf{P}}_{i+1}$ with respect to displacement $\mathbf{u}_{i+1}^{(j)}$, and $\Delta\mathbf{u}_{i+1}^{(j)} = \mathbf{u}_{i+1}^{(j+1)} - \mathbf{u}_{i+1}^{(j)}$ is the displacement increment at $i+1$-th step and j-th iteration.

Making the derivative of $\hat{\mathbf{P}}_{i+1}$ with respect to $\mathbf{u}_{i+1}^{(j)}$:

$$\left.\frac{\partial \hat{\mathbf{P}}}{\partial \mathbf{u}}\right|_{\mathbf{u}_{i+1}^{(j)}} = \mathbf{M}\left.\frac{\partial \ddot{\mathbf{u}}_{i+1}}{\partial \mathbf{u}}\right|_{\mathbf{u}_{i+1}^{(j)}} + \mathbf{C}\left.\frac{\partial \dot{\mathbf{u}}_{i+1}}{\partial \mathbf{u}}\right|_{\mathbf{u}_{i+1}^{(j)}} + \left.\frac{\partial \mathbf{f_R}(\mathbf{u}_{i+1})}{\partial \mathbf{u}}\right|_{\mathbf{u}_{i+1}^{(j)}} = \mathbf{M}\frac{\partial \ddot{\mathbf{u}}_{i+1}}{\partial \mathbf{u}_{i+1}^{(j)}} + \mathbf{C}\frac{\partial \dot{\mathbf{u}}_{i+1}}{\partial \mathbf{u}_{i+1}^{(j)}} + \frac{\partial \mathbf{f_R}(\mathbf{u}_{i+1})}{\partial \mathbf{u}_{i+1}^{(j)}} \tag{D.23}$$

According to Newmark's method, it is possible to express $\dot{\mathbf{u}}_{i+1}$ and $\ddot{\mathbf{u}}_{i+1}$ as already done for linear systems in Equations (D.14) and (D.15):

$$\dot{\mathbf{u}}_{i+1} = \frac{\gamma}{\beta\Delta t}\left(\mathbf{u}_{i+1} - \mathbf{u}_i\right) + \left(1 - \frac{\gamma}{\beta}\right)\dot{\mathbf{u}}_i + \Delta t\left(1 - \frac{\gamma}{2\beta}\right)\ddot{\mathbf{u}}_i \tag{D.24}$$

$$\ddot{\mathbf{u}}_{i+1} = \frac{1}{\beta\left(\Delta t\right)^2}\left(\mathbf{u}_{i+1} - \mathbf{u}_i\right) - \frac{1}{\beta\Delta t}\dot{\mathbf{u}}_i - \left(\frac{1}{2\beta} - 1\right)\ddot{\mathbf{u}}_i \tag{D.25}$$

Deriving these expressions:

$$\frac{\partial \dot{\mathbf{u}}_{i+1}}{\partial \mathbf{u}_{i+1}^{(j)}} = \frac{\gamma}{\beta\Delta t} \tag{D.26}$$

$$\frac{\partial \ddot{\mathbf{u}}_{i+1}}{\partial \mathbf{u}_{i+1}^{(j)}} = \frac{1}{\beta\left(\Delta t\right)^2} \tag{D.27}$$

It is worth noting that $\frac{\partial \mathbf{f_R}(\mathbf{u}_{i+1})}{\partial \mathbf{u}_{i+1}^{(j)}} = \mathbf{K}_{T,i+1}^{(j)}$ is equal to the tangent stiffness matrix at $i+1$-th step and j-th iteration. Therefore Equation (D.23) can be written as:

$$\hat{\mathbf{K}}_{T,i+1}^{(j)} = \left.\frac{\partial \hat{\mathbf{P}}}{\partial \mathbf{u}}\right|_{\mathbf{u}_{i+1}^{(j)}} = \frac{1}{\beta\left(\Delta t\right)^2}\mathbf{M} + \frac{\gamma}{\beta\Delta t}\mathbf{C} + \mathbf{K}_{T,i+1}^{(j)} \tag{D.28}$$

Substituting Equations (D.24) and (D.25) in $\hat{\mathbf{P}}_{i+1}^{(j)}$, it allows to obtain:

$$\hat{\mathbf{P}}_{i+1}^{(j)} = \mathbf{M}\ddot{\mathbf{u}}_{i+1}^{(j)} + \mathbf{C}\dot{\mathbf{u}}_{i+1}^{(j)} + \mathbf{f}_{\mathbf{R}}(\mathbf{u}_{i+1}^{(j)}) =$$

$$= \mathbf{M}\left[\frac{1}{\beta(\Delta t)^2}\left(\mathbf{u}_{i+1}^{(j)} - \mathbf{u}_i\right) - \frac{1}{\beta\Delta t}\dot{\mathbf{u}}_i - \left(\frac{1}{2\beta} - 1\right)\ddot{\mathbf{u}}_i\right] + \mathbf{C}\left[\frac{\gamma}{\beta\Delta t}\left(\mathbf{u}_{i+1}^{(j)} - \mathbf{u}_i\right) + \left(1 - \frac{\gamma}{\beta}\right)\dot{\mathbf{u}}_i + \Delta t\left(1 - \frac{\gamma}{2\beta}\right)\ddot{\mathbf{u}}_i\right] +$$

$$+\mathbf{f}_{\mathbf{R},i+1}^{(j)} =$$

$$= \left[\frac{1}{\beta(\Delta t)^2}\mathbf{M} + \frac{\gamma}{\beta\Delta t}\mathbf{C}\right]\left(\mathbf{u}_{i+1}^{(j)} - \mathbf{u}_i\right) - \left[\frac{1}{\beta\Delta t}\mathbf{M} + \left(\frac{\gamma}{\beta} - 1\right)\mathbf{C}\right]\dot{\mathbf{u}}_i - \left[\left(\frac{1}{2\beta} - 1\right)\mathbf{M} + \Delta t\left(\frac{\gamma}{2\beta} - 1\right)\mathbf{C}\right]\ddot{\mathbf{u}}_i + \mathbf{f}_{\mathbf{R},i+1}^{(j)} \tag{D.29}$$

Therefore, Equation (D.22) can be written as follows:

$$\hat{\mathbf{K}}_{T,i+1}^{(j)}\Delta\mathbf{u}_{i+1}^{(j)} = -\mathbf{M}\mathbf{i}\ddot{u}_{g,i+1} - \left[\frac{1}{\beta(\Delta t)^2}\mathbf{M} + \frac{\gamma}{\beta\Delta t}\mathbf{C}\right]\left(\mathbf{u}_{i+1}^{(j)} - \mathbf{u}_i\right) + \left[\frac{1}{\beta\Delta t}\mathbf{M} + \left(\frac{\gamma}{\beta} - 1\right)\mathbf{C}\right]\dot{\mathbf{u}}_i +$$
$$+\left[\left(\frac{1}{2\beta} - 1\right)\mathbf{M} + \Delta t\left(\frac{\gamma}{2\beta} - 1\right)\mathbf{C}\right]\ddot{\mathbf{u}}_i - \mathbf{f}_{\mathbf{R},i+1}^{(j)} \tag{D.30}$$

which can be written in matrix form:

$$\hat{\mathbf{K}}_{T,i+1}^{(j)}\Delta\mathbf{u}_{i+1}^{(j)} = \Delta\mathbf{R}^{(j)} \tag{D.31}$$

where:

$$\Delta\mathbf{R}^{(j)} = -\mathbf{M}\mathbf{i}\ddot{u}_{g,i+1} - \left[\frac{1}{\beta(\Delta t)^2}\mathbf{M} + \frac{\gamma}{\beta\Delta t}\mathbf{C}\right]\left(\mathbf{u}_{i+1}^{(j)} - \mathbf{u}_i\right) + \left[\frac{1}{\beta\Delta t}\mathbf{M} + \left(\frac{\gamma}{\beta} - 1\right)\mathbf{C}\right]\dot{\mathbf{u}}_i +$$
$$+\left[\left(\frac{1}{2\beta} - 1\right)\mathbf{M} + \Delta t\left(\frac{\gamma}{2\beta} - 1\right)\mathbf{C}\right]\ddot{\mathbf{u}}_i - \mathbf{f}_{\mathbf{R},i+1}^{(j)} \tag{D.32}$$

By solving Equation (D.31), it is possible to determine $\mathbf{u}_{i+1}^{(j+1)} = \mathbf{u}_{i+1}^{(j)} + \Delta\mathbf{u}_{i+1}^{(j)}$. Therefore, it is possible to check the convergence and, if it is not satisfied, to go on with the next iteration. When the convergence is achieved, it is possible to determine $\dot{\mathbf{u}}_{i+1}$ and $\ddot{\mathbf{u}}_{i+1}$ from Equations (D.24) and (D.25), respectively, or by imposing the equilibrium at step end:

$$\mathbf{M}\ddot{\mathbf{u}}_{i+1} = -\mathbf{C}\dot{\mathbf{u}}_{i+1} - \mathbf{f}_{\mathbf{R}}(\mathbf{u}_{i+1}) - \mathbf{M}\mathbf{i}\ddot{u}_{g,i+1} \tag{D.33}$$

being known the quantities at the right side.

The procedure to implement the non-linear dynamic analysis by means of Newmark's method is shown in the following:

1.0 Choose special case:

a) Constant average acceleration method: set $\gamma = \frac{1}{2}$ and $\beta = \frac{1}{4}$;

b) Linear acceleration method: set $\gamma = \frac{1}{2}$ and $\beta = \frac{1}{6}$;

2.0 Initialize variables:

- $\mathbf{u}_0 = \mathbf{0}$, assuming at rest initial conditions (therefore $\mathbf{s}_0 = \mathbf{0}$ and $\mathbf{T}_0 = \mathbf{0}$);

- $\dot{\mathbf{u}}_0 = \mathbf{0}$, assuming at rest initial conditions;

- $\mathbf{M}, \mathbf{C}, \mathbf{K}_e$ matrices assembling;

- compute static resisting forces $\mathbf{f}_{\mathbf{R},0} = \mathbf{K}_e \mathbf{u}_0$;

- compute $\ddot{\mathbf{u}}_0$ by solving the equation of motion at initial time instant: $\mathbf{M}\ddot{\mathbf{u}}_0 = -\mathbf{M}\mathbf{i}\ddot{u}_{g,0} - \mathbf{C}\dot{\mathbf{u}}_0 - \mathbf{f}_{\mathbf{R},0}$;

- select Δt, usually equal to the sampling interval of the accelerogram;

- $a_1 = \dfrac{1}{\beta(\Delta t)^2}\mathbf{M} + \dfrac{\gamma}{\beta \Delta t}\mathbf{C}$; $\quad a_2 = \dfrac{1}{\beta \Delta t}\mathbf{M} + \left(\dfrac{\gamma}{\beta} - 1\right)\mathbf{C}$; $\quad a_3 = \left(\dfrac{1}{2\beta} - 1\right)\mathbf{M} + \Delta t\left(\dfrac{\gamma}{2\beta} - 1\right)\mathbf{C}$.

3.0 For each time instant $i = 0,1,2,3,...N_S$, initialize variables:

- $\mathbf{u}_{i+1}^{(1)} = \mathbf{u}_i$ (therefore $\mathbf{s}_{i+1}^{(1)} = \mathbf{s}_i$);
- $\mathbf{f}_{\mathbf{R},i+1}^{(1)} = \mathbf{f}_{\mathbf{R},i}$ (therefore $\mathbf{T}_{i+1}^{(1)} = \mathbf{T}_i$);
- $\mathbf{K}_{T,i+1}^{(1)} = \mathbf{K}_{T,i}$;
- $\hat{\mathbf{F}}_{i+1} = -\mathbf{M}\mathbf{i}\ddot{u}_{g,i+1} + \left[\dfrac{1}{\beta(\Delta t)^2}\mathbf{M} + \dfrac{\gamma}{\beta \Delta t}\mathbf{C}\right]\mathbf{u}_i + \left[\dfrac{1}{\beta \Delta t}\mathbf{M} + \left(\dfrac{\gamma}{\beta} - 1\right)\mathbf{C}\right]\dot{\mathbf{u}}_i +$
$+\left[\left(\dfrac{1}{2\beta} - 1\right)\mathbf{M} + \Delta t\left(\dfrac{\gamma}{2\beta} - 1\right)\mathbf{C}\right]\ddot{\mathbf{u}}_i$

4.0 For each iteration $j = 1,2,3,...$ inside the i-th time step:

- Check convergence; if the acceptance criteria are not met, implement following steps; otherwise, skip these steps and go to step 5.0;
- Update tangent stiffness matrix $\mathbf{K}_{T,i+1}^{(j)} = \mathbf{C}^T \cdot \mathbf{D}_{T,i+1}^{(j)} \cdot \mathbf{C}$;
- $\Delta \mathbf{R}^{(j)} = \hat{\mathbf{F}}_{i+1} - a_1 \cdot \mathbf{u}_{i+1}^{(j)} - \mathbf{f}_{\mathbf{R},i+1}^{(j)}$;
- $\hat{\mathbf{K}}_{T,i+1}^{(j)} = a_1 + \mathbf{K}_{T,i+1}^{(j)}$;
- Solve $\hat{\mathbf{K}}_{T,i+1}^{(j)} \Delta \mathbf{u}_{i+1}^{(j)} = \Delta \mathbf{R}^{(j)}$ in order to find $\Delta \mathbf{u}_{i+1}^{(j)}$;
- $\mathbf{u}_{i+1}^{(j+1)} = \mathbf{u}_{i+1}^{(j)} + \Delta \mathbf{u}_{i+1}^{(j)}$;
- Compute relative displacement increments in structural elements $\Delta \mathbf{s}_{i+1}^{(j)} = \mathbf{C} \cdot \Delta \mathbf{u}_{i+1}^{(j)}$;
- Update internal shear forces $\mathbf{T}_{i+1}^{(j+1)}$ of structural elements according to relative displacement increment and constitutive law, therefore update elastic matrix $\mathbf{D}_{T,i+1}^{(j+1)}$ and relative displacement vector $\mathbf{s}_{i+1}^{(j+1)}$;
- Compute resisting forces $\mathbf{f}_{\mathbf{R},i+1}^{(j+1)} = \mathbf{C}^T \cdot \mathbf{T}_{i+1}^{(j+1)}$;
- Compute residual $\Delta \mathbf{R}^{(j+1)} = \hat{\mathbf{F}}_{i+1} - a_1 \cdot \mathbf{u}_{i+1}^{(j+1)} - \mathbf{f}_{\mathbf{R},i+1}^{(j+1)}$;

- Compute $err = \dfrac{\left\|\Delta \mathbf{R}^{(j+1)}\right\|}{\left\|\Delta \mathbf{F}_{i+1}\right\|}$ for check convergence;

- Replace $j = j+1$, repeat from step 4.0.

5.0 Time step end:

- $\dot{\mathbf{u}}_{i+1} = \dfrac{\gamma}{\beta \Delta t}\left(\mathbf{u}_{i+1} - \mathbf{u}_i\right) + \left(1 - \dfrac{\gamma}{\beta}\right)\dot{\mathbf{u}}_i + \Delta t\left(1 - \dfrac{\gamma}{2\beta}\right)\ddot{\mathbf{u}}_i$;

- $\ddot{\mathbf{u}}_{i+1} = \dfrac{1}{\beta\left(\Delta t\right)^2}\left(\mathbf{u}_{i+1} - \mathbf{u}_i\right) - \dfrac{1}{\beta \Delta t}\dot{\mathbf{u}}_i - \left(\dfrac{1}{2\beta} - 1\right)\ddot{\mathbf{u}}_i$ or compute $\ddot{\mathbf{u}}_{i+1}$ by imposing the equilibrium at step end: $\mathbf{M}\ddot{\mathbf{u}}_{i+1} = -\mathbf{C}\dot{\mathbf{u}}_{i+1} - \mathbf{f}_{\mathbf{R},i+1}(\mathbf{u}_{i+1}) - \mathbf{M}\mathbf{i}\ddot{u}_{g,i+1}$;

- Save results at step end, replace $i = i+1$ and repeat from step 3.0.

APPENDIX E

The seismic records considered in the non-linear dynamic analyses used for the construction of the fragility curves have been chosen among the real accelerograms collected in the European Strong Motion (ESM) database.

The first seven earthquake records have been selected by means of the REXELite online tool [127, 128], which allows to search for a suite of waveforms compatible with a target spectrum, generated according to Italian Code NTC18 for the Catania site (SLV). The search has been limited to the records whose main characteristics are in agreement with those of the Catania site according to the Seismic hazard model MPS04-S1 [129] (mean Mw = 5.34, mean distance = 9.28 km). In Table E.1 are reported the inputs given to the tool, while in Figure E.1 the response spectra of the selected records are shown with the target spectrum.

The other twenty-three records have been chosen maintaining the characteristics of the Catania site according to the Seismic hazard model MPS04-S1, therefore having Mw or M_L inside the range [4.5 6.0] and epicentral distance lower than 50 km.

Table E.1 - Inputs for REXELIte

Target spectrum		**Preliminary record search**	
Latitude [°]	37.52	Station site classification	B,B*,C,C*
Longitude [°]	15.07	Magnitude Mw or M_L range	[4.5 6.0]
Site classification	C	Epicentral distance range	[0 50] [km]
Topography	1	Period range [T1 T2]	[0.15 2.0] [s]
Nominal life	50 [y]	Tolerance below	10%
Building functional type (Cu)	1.0	Tolerance above	30%
Limit state	SLV		

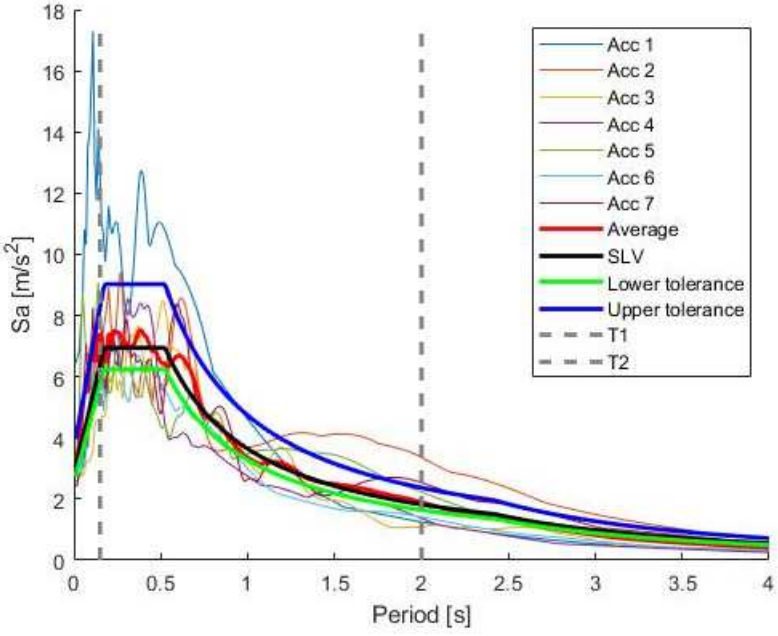

Figure E.1 - Response and target spectra - 5% damping

In Table E.2 and Table E.3 the selected earthquake records with dates, corresponding station IDs and main characteristics (PGAs, Mw, M_L, epicentral distance, etc.) are reported. In Figure E.2 the representation of the selected earthquake records is shown.

Table E.2 – Selected earthquake records with dates

Acc. ID	Event Name	Event Date	Event Time	Event Latitude [°]	Event Longitude [°]	Event Depth [km]
1	L_Aquila	06/04/2009	01:32:40	42,3420	13,3800	8,3
2	Emilia_2nd_shock	29/05/2012	07:00:02	44,8417	11,0657	8,1
3	Turkey	27/06/1998	13:55:53	36,8451	35,3250	46,6
4	Emilia_1st_shock	20/05/2012	02:03:50	44,8955	11,2635	9,5
5	L_Aquila	06/04/2009	01:32:40	42,3420	13,3800	8,3
6	Northern_Italy	29/05/2012	10:55:56	44,8652	10,9795	4,3
7	Emilia_2nd_shock	29/05/2012	07:00:02	44,8417	11,0657	8,1
8	Central_Italy	24/08/2016	01:36:32	42,6983	13,2335	8,1
9	Central_Italy	24/08/2016	01:36:32	42,6983	13,2335	8,1
10	Central_Italy	24/08/2016	01:36:32	42,6983	13,2335	8,1
11	Central_Italy	24/08/2016	01:36:32	42,6983	13,2335	8,1
12	Greece	31/03/2015	15:48:41	38,33	20,49	13
13	Central_Italy	18/01/2017	10:14:12	42,531	13,2838	9,6
14	Central_Italy	18/01/2017	10:14:12	42,531	13,2838	9,6
15	Central_Italy	18/01/2017	10:25:26	42,5033	13,277	9,4
16	Central_Italy	18/01/2017	10:25:26	42,5033	13,277	9,4
17	Emilia_1st_shock	20/05/2012	02:03:50	44,8955	11,2635	9,5
18	Emilia_2nd_shock	29/05/2012	07:00:02	44,8417	11,0657	8,1
19	Emilia_2nd_shock	29/05/2012	07:00:02	44,8417	11,0657	8,1
20	Northern_Italy	15/10/1996	09:56	44,797	10,662	5
21	L_Aquila	06/04/2009	01:32:40	42,3420	13,3800	8,3
22	Central_Italy	18/01/2017	10:16:39	42,5375	13,2677	8,2
23	Cosenza	25/10/2012	23:05:24	39,8747	16,0158	9,7
24	Central_Italy	24/08/2016	02:33:29	42,7922	13,1507	8
25	Central_Italy	24/08/2016	02:33:29	42,7922	13,1507	8
26	Central_Italy	24/08/2016	02:33:29	42,7922	13,1507	8
27	Central_Italy	24/08/2016	02:33:29	42,7922	13,1507	8
28	Sicily_Italy	26/12/2018	02:19:17	37,644	15,116	
29	Sicily_Italy	26/12/2018	02:19:17	37,644	15,116	
30	Western_Turkey	26/06/2020	07:21:11	38,78	27,81	10

Table E.3 - Selected earthquake records with corresponding station IDs and main characteristics

Acc. ID	Station Code	Epicentral Distance [km]	Stream	PGA [cm/s²]	M_L	M_W
1	AQV	4,9	HNE	644,25	5,9	6,1
2	MRN	4,1	HNN	-288,63	5,8	6
3	0105	48,2	HNE	271,95	5,9	6,2
4	MRN	16,1	HNE	-257,23	5,9	6,1
5	AQK	1,8	HNN	-346,78	5,9	6,1
6	T0819	6,8	HNE	253,12	5,3	5,5
7	MIR08	8,6	HNN	-242,97	5,8	6
8	AMT	8,5	HGE	-850,80		6
9	CLF	45,5	HGN	128,78		6
10	FEMA	32,9	HNE	242,34		6
11	NRC	15,3	HGN	366,77		6
12	LXRA	15,2	HNE	-95,05		4,7
13	ASP	46,2	HGE	105,18		5,5
14	PCB	5,4	HGN	-584,33		5,5
15	ACT	31,8	HGN	-101,97		5,4
16	MSCT	6,6	HGN	-279,88		5,4
17	MRN	16,1	HNN	-258,80		6,1
18	MIR01	0,5	HNE	411,37		6
19	MIR04	13	HNE	392,11		6
20	NVL	7,5	HNE	-195,09		5,4
21	AQV	4,9	HNN	-535,20		6,1
22	PCB	6,2	HGE	92,79	4,6	
23	0PAP	8,9	HGN	-234,94		5,2
24	AMT	20,9	HGE	105,58		5,3
25	FEMA	20,6	HNE	54,15		5,3
26	GUMA	33,6	HNN	65,45		5,3
27	NRC	4,4	HGN	190,80		5,3
28	SVN	4,5	HGE	-547,93		4,9
29	SVN	4,5	HGN	-277,60		4,9
30	AKS	10,9	HNN	-364,93	5,2	

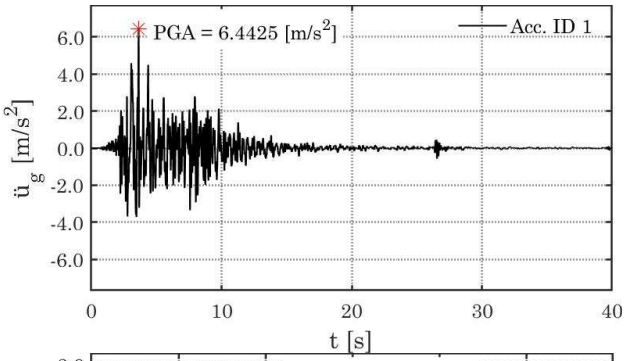
PGA = 6.4425 [m/s^2]
Acc. ID 1
$\ddot{u}_g$ [m/s^2]
t [s]

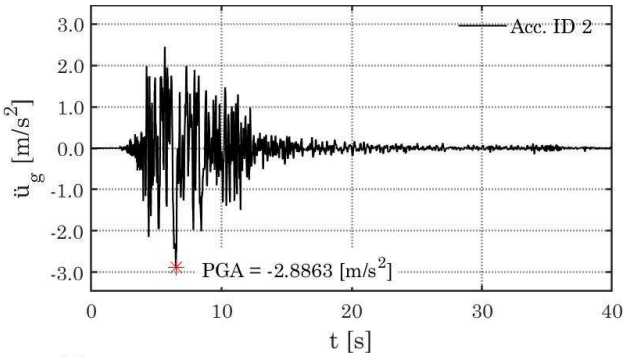
Acc. ID 2
PGA = -2.8863 [m/s^2]
$\ddot{u}_g$ [m/s^2]
t [s]

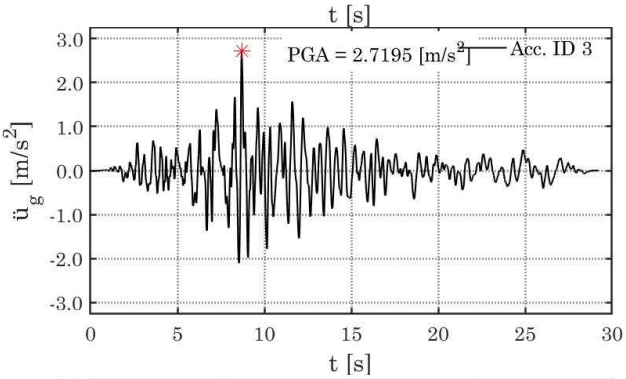
PGA = 2.7195 [m/s^2]
Acc. ID 3
$\ddot{u}_g$ [m/s^2]
t [s]

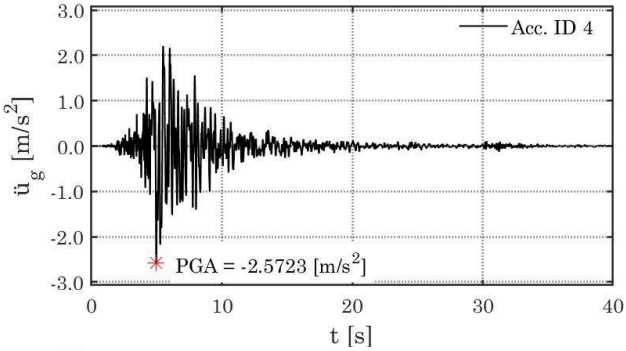
Acc. ID 4
PGA = -2.5723 [m/s^2]
$\ddot{u}_g$ [m/s^2]
t [s]

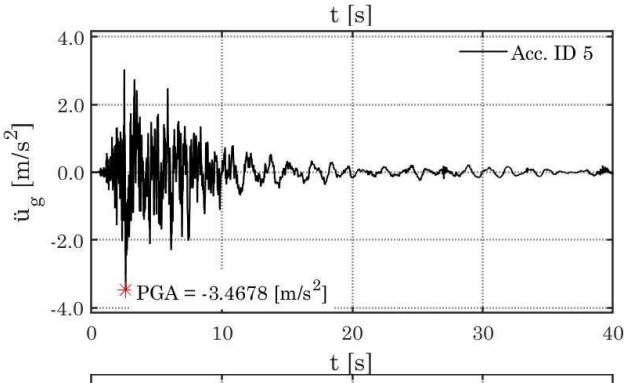
Acc. ID 5
PGA = -3.4678 [m/s^2]
$\ddot{u}_g$ [m/s^2]
t [s]

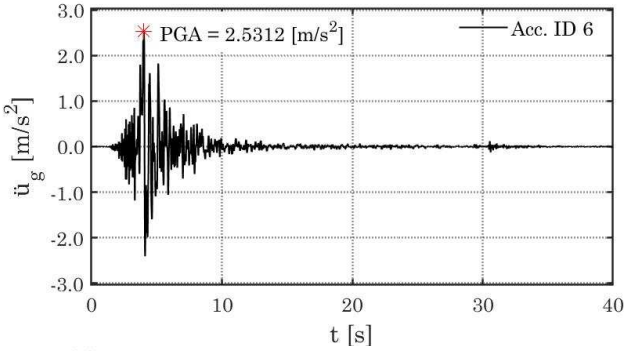
PGA = 2.5312 [m/s^2]
Acc. ID 6
$\ddot{u}_g$ [m/s^2]
t [s]

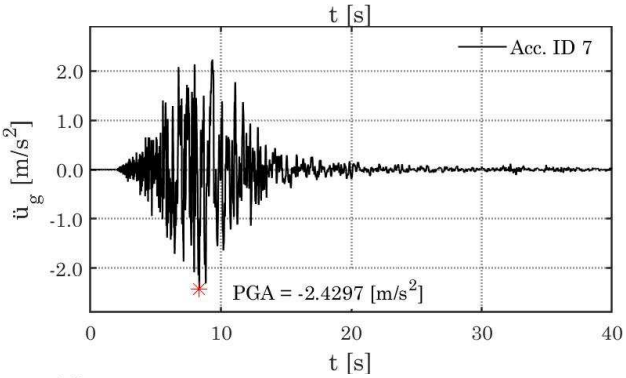
Acc. ID 7
PGA = -2.4297 [m/s^2]
$\ddot{u}_g$ [m/s^2]
t [s]

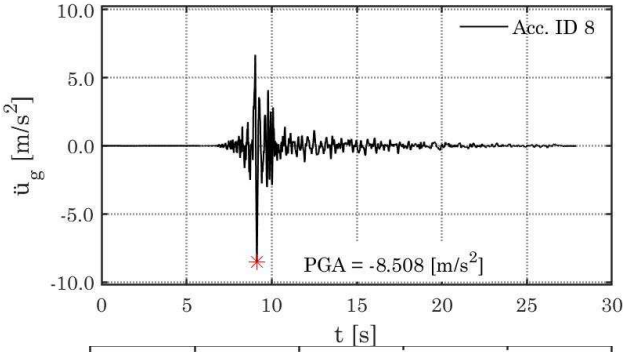
Acc. ID 8
PGA = -8.508 [m/s^2]
$\ddot{u}_g$ [m/s^2]
t [s]

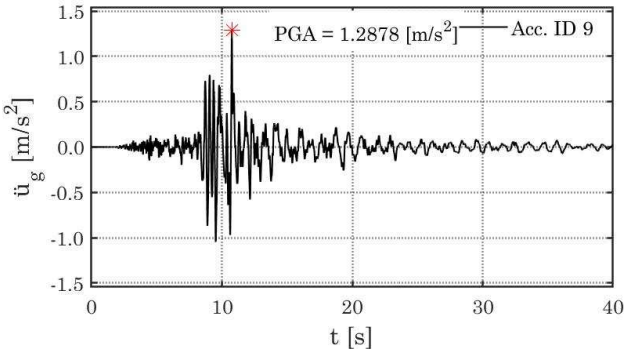
PGA = 1.2878 [m/s^2]
Acc. ID 9
$\ddot{u}_g$ [m/s^2]
t [s]

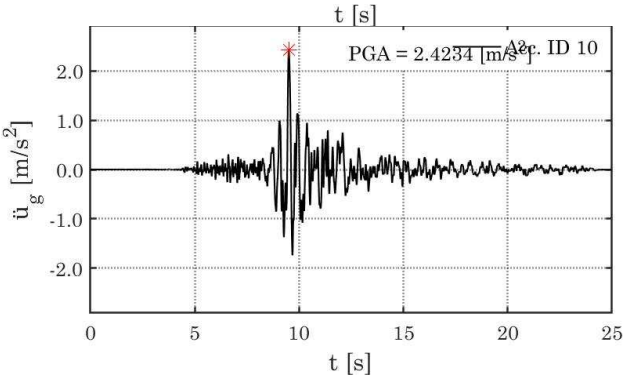
PGA = 2.4234 [m/s^2]
Acc. ID 10
$\ddot{u}_g$ [m/s^2]
t [s]

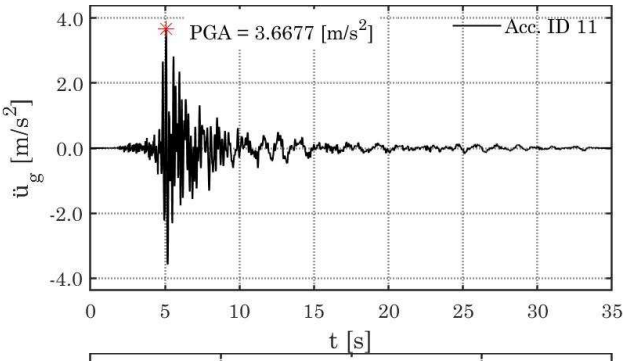
PGA = 3.6677 [m/s^2]
Acc. ID 11
$\ddot{u}_g$ [m/s^2]
t [s]

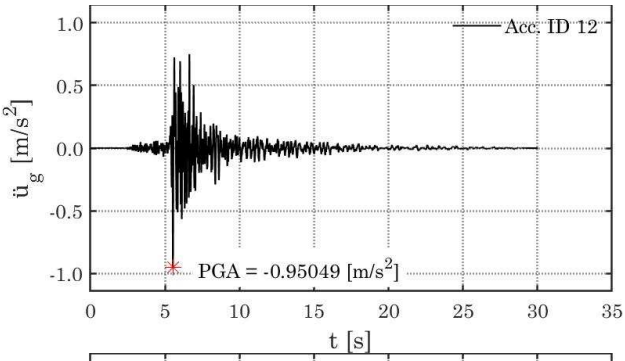
Acc. ID 12
PGA = -0.95049 [m/s^2]
$\ddot{u}_g$ [m/s^2]
t [s]

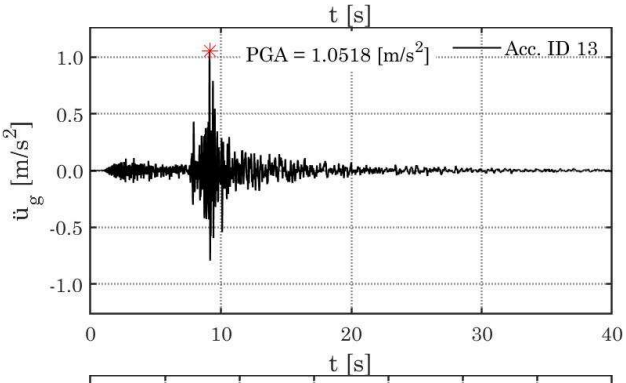
PGA = 1.0518 [m/s^2]
Acc. ID 13
$\ddot{u}_g$ [m/s^2]
t [s]

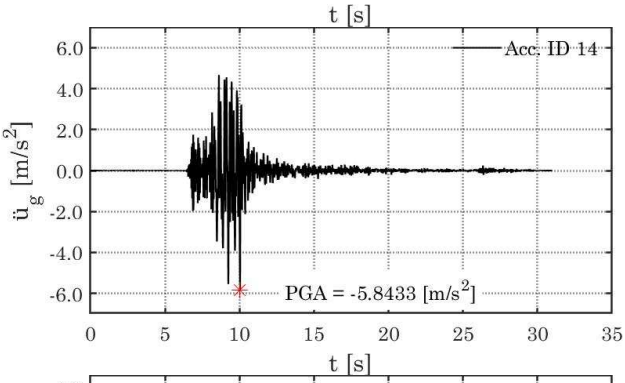
Acc. ID 14
PGA = -5.8433 [m/s^2]
$\ddot{u}_g$ [m/s^2]
t [s]

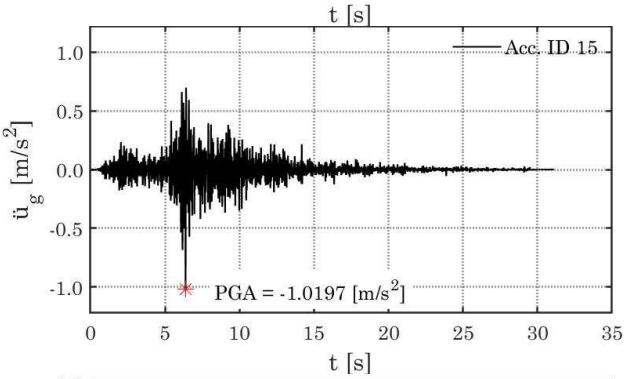
Acc. ID 15
PGA = -1.0197 [m/s^2]
$\ddot{u}_g$ [m/s^2]
t [s]

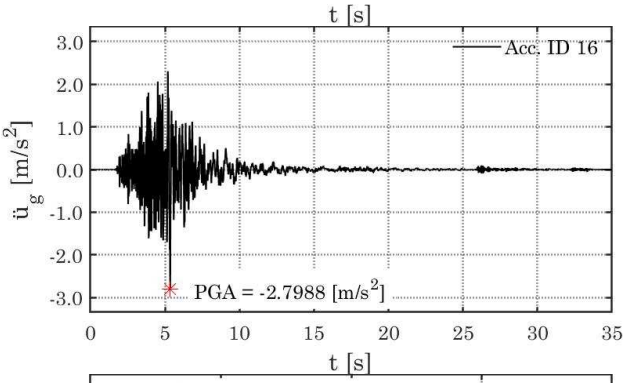
Acc. ID 16
PGA = -2.7988 [m/s^2]
$\ddot{u}_g$ [m/s^2]
t [s]

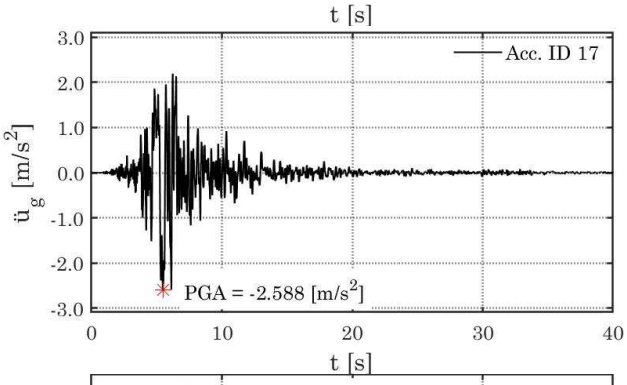
Acc. ID 17
PGA = -2.588 [m/s^2]
$\ddot{u}_g$ [m/s^2]
t [s]

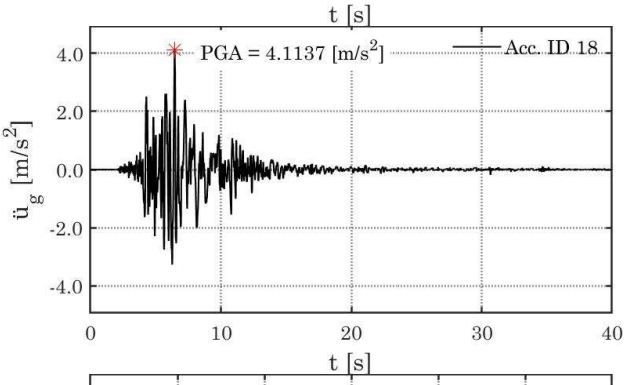
PGA = 4.1137 [m/s^2]
Acc. ID 18
$\ddot{u}_g$ [m/s^2]
t [s]

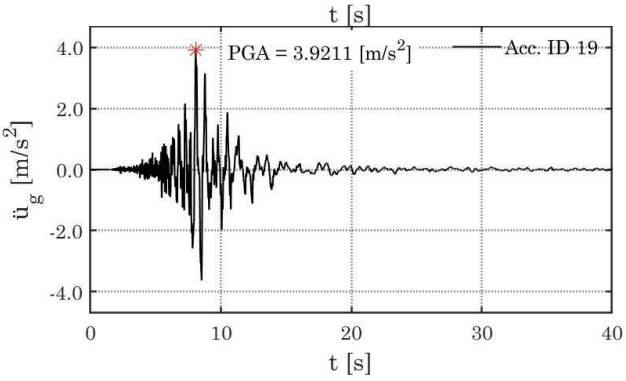
PGA = 3.9211 [m/s^2]
Acc. ID 19
$\ddot{u}_g$ [m/s^2]
t [s]

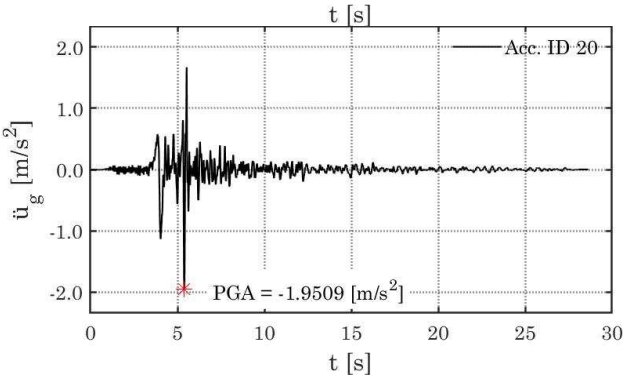
Acc. ID 20
PGA = -1.9509 [m/s^2]
$\ddot{u}_g$ [m/s^2]
t [s]

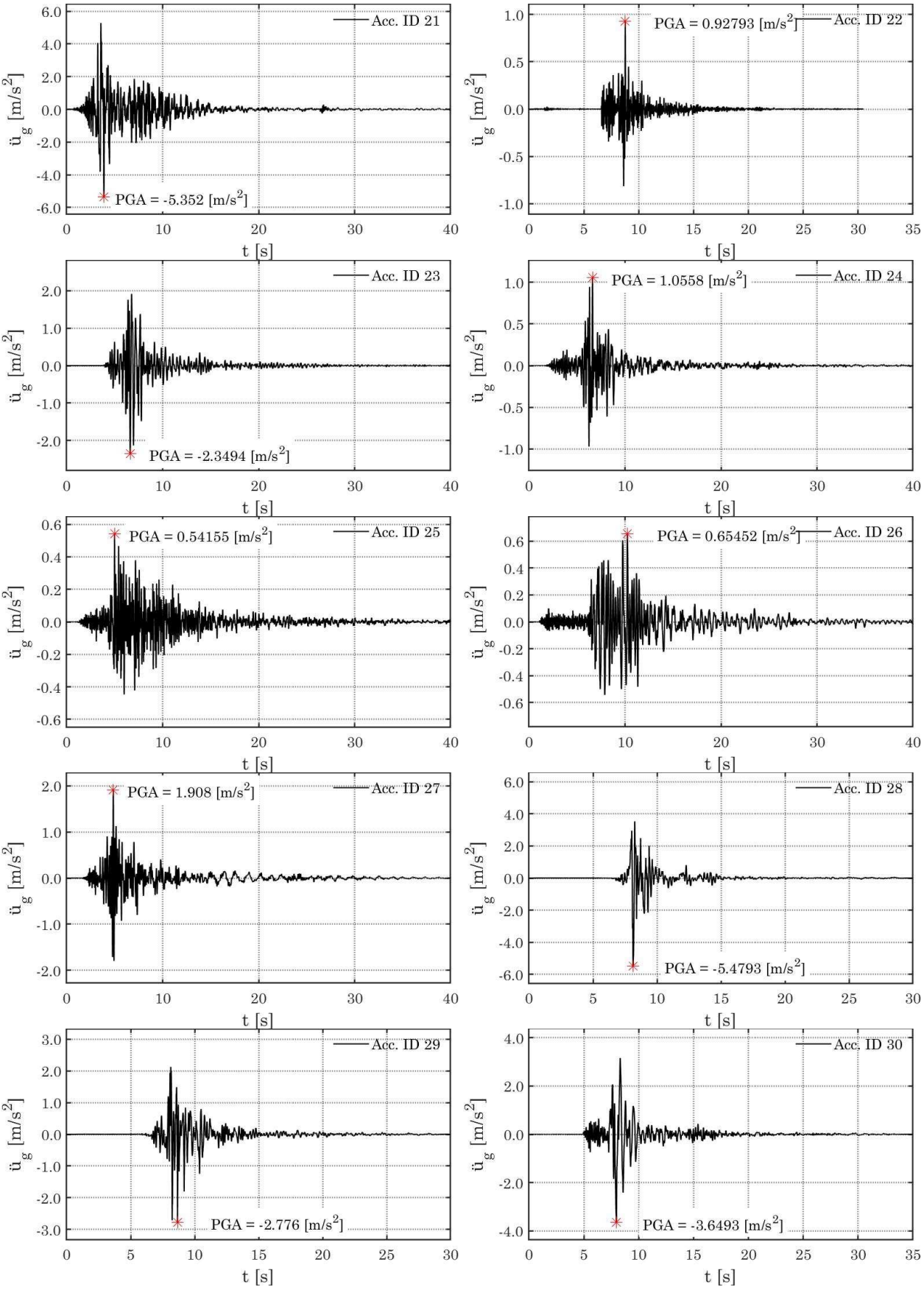

Figure E.2 - Representation of the earthquake records